INFORMATION TO USERS

This manuscript has been reproduced from the microfilm master. UMI films the text directly from the original or copy submitted. Thus, some thesis and dissertation copies are in typewriter face, while others may be from any type of computer printer.

The quality of this reproduction is dependent upon the quality of the copy submitted. Broken or indistinct print, colored or poor quality illustrations and photographs, print bleedthrough, substandard margins, and improper alignment can adversely affect reproduction.

In the unlikely event that the author did not send UMI a complete manuscript and there are missing pages, these will be noted. Also, if unauthorized copyright material had to be removed, a note will indicate the deletion.

Oversize materials (e.g., maps, drawings, charts) are reproduced by sectioning the original, beginning at the upper left-hand corner and continuing from left to right in equal sections with small overlaps.

Photographs included in the original manuscript have been reproduced xerographically in this copy. Higher quality 6" x 9" black and white photographic prints are available for any photographs or illustrations appearing in this copy for an additional charge. Contact UMI directly to order.

Bell & Howell Information and Learning
300 North Zeeb Road, Ann Arbor, MI 48106-1346 USA
800-521-0600

FLUORESCENCE PROBING AND SIZE EXCLUSION CHROMATOGRAPHIC STUDIES OF POLYMER-SURFACTANT INTERACTIONS

by

Andrew Paul Rodenhiser

Submitted in partial fulfillment of the requirements
for the degree of Doctor of Philosophy

at

Dalhousie University
Halifax, Nova Scotia
September 1998

DALHOUSIE UNIVERSITY

FACULTY OF GRADUATE STUDIES

The undersigned hereby certify that they have read and recommend to the Faculty of Graduate Studies for acceptance a thesis entitled "Fluorescence Probing and Size Exclusion Chromatographic Studies of Polymer-Surfactant Interactions"

by Andrew Paul Rodenhiser

in partial fulfillment of the requirements for the degree of Doctor of Philosophy.

Dated: October 30, 1998

External Examiner

Research Supervisor

Examining Committee

DALHOUSIE UNIVERSITY

DATE. 4 November 1998

AUTHOR: Andrew Paul Rodenhiser

TITLE: Fluorescence Probing and Size Exclusion Chromatographic Studies of Polymer-Surfactant Interactions

DEPARTMENT OR SCHOOL: Chemistry

DEGREE: Ph.D. CONVOCATION: May YEAR: 1999

Permission is herewith granted to Dalhousie University to circulate and to have copied for non-commercial purposes, at its discretion, the above title upon the request of individuals or institutions.

Signature of Author

TABLE OF CONTENTS

LIST OF FIGURES

LIST OF TABLES

ABSTRACT

Fluorescence probing and size exclusion chromatographic (SEC) techniques were applied to study complexes formed in several polymer-surfactant systems. Fluorescence probing techniques measure the size, micropolarity and microviscosity of the micellar aggregates bound to the polymer. The use of the time resolved fluorescence quenching technique required writing software for data analysis. Size exclusion chromatography was adapted to measure the size of the overall polymer-surfactant complex. A multiangle laser light scattering detector and a refractometer allowed molecular weight determination without reference to elution volume.

The methods were tested on mixtures of sodium dodecyl sulfate (SDS) with poly(ethylene oxide) (PEO) and poly(vinyl pyrrolidone) (PVP). Micelle aggregation numbers were lower in the bound micelles than in free micelles. The PVP-SDS micelles were more rigid and more polar than PEO-SDS micelles. The SEC study revealed three types of SDS binding as a function of PEO degree of polymerization (DP): no interaction for the smallest glycols, partitioning in and out of micelles for the intermediate oligomers (DP 5 to $\approx$ 20), and binding of one or more micelles to the longer polymer chains.

Micelles of dodecyltrimethylammonium bromide bound to poly(acrylamide-*co*-sodium acrylate) polyelectrolytes were similar in size to free micelles, increasing slightly with degree of binding and polymer charge density. The use of cationic quenchers in these systems perturbed the binding, as predicted by ideal mixing theory, and should be avoided.

Formation of interpolymer complexes in hydrophobically modified polyacrylamide-surfactant mixtures was enhanced by shear in SEC. Fluorescence measurements suggest a stepwise growth and division of the micelles bound to the polymer hydrophobes, and a rigid micellar surface.

LIST OF ABBREVIATIONS AND SYMBOLS USED

α	degree of hydrolysis of polyacrylamide
β	binding ratio of surfactant to polymer
β_c	binding ratio per polymer charge units
β_h	binding ratio per mole HPAM hydrophobes
δ	NMR chemical shift
ε	porosity ratio of packed bed
η	viscosity
η_0	viscosity of the solvent
η_{sp}	specific viscosity
θ	angle of scattered light
Λ	raw skewness of the size distribution
λ_g	Gaussian standardized skewness of the size distribution
λ	wavelength of light in the medium
λ_0	wavelength of light in vacuum
λ_{max}	wavelength of maximum UV absorption
ν	Simha shape factor
Π	$=[Q]_m/[S]_m$
π	osmotic pressure
ρ	rotational relaxation time
σ^2	variance of the distribution
τ	observed lifetime of fluorescence
τ_0	observed lifetime of fluorescence in the absence of quencher
τ_r	radiative lifetime
Φ_f	quantum yield
Φ°_f	quantum yield in the absence of quencher
ϕ	volume fraction of solute
φ	phase difference of light between reference and sample
χ^2	chi squared value of the fit
a	mole fraction of quencher in bulk solution
a_k	preexponential factors of lifetime distribution function
A	amplitude of transmitted polarized light
A_0	amplitude of incident polarized light
A_i (A_1, A_2, A_3, A_4)	fit parameters of micellar quenching equation
δA_i	adjustments made to parameters A_i during fitting to micellar quenching equation
A_2, A_3	second and third virial coefficients
AA	acrylic acid
ADC	analog to digital converter
AM	acrylamide
ANS	8-anilino-1-naphthalenesulfonic acid, ammonium salt
AP	associative polymer

APCI	atmospheric pressure chemical ionization
B	random background level in fluorescence decay curve
BzPh	benzophenone
c	polymer concentration
C*	critical overlap concentration
$C_{10}TA^+$	decyltrimethylammonium ion
C10	decyl sidechain
C12	dodecyl sidechain
C14	tetradecyl sidechain
cac	critical aggregation concentration
CFD	constant fraction discriminator
ch	channel of fluorescence decay histogram
cmc	critical micelle concentration
C_nAM	N-n-alkylacrylamide, where n = 10, 12, 14
C_nP^+	alkylpyridinium ion
CPC	cetylpyridinium chloride
Cryo-TEM	cryogenic transmission electron microscopy
C_nTA^+	alkyltrimethylammonium ion
C_nTAB	alkyltrimethylammonium bromide
CTAB	cetyltrimethylammonium bromide
CTAC	cetyltrimethylammonium chloride
D	difference between cac of surfactant and cac of quencher surfactant
D	Slope of probe mobility plot of A_2 versus A_3
DMSO	dimethylsulfoxide
dn/dc	differential refractive index increment with respect to concentration
DP	degree of polymerization
d_p	diameter of particles in a packed bed
DP^+	dodecylpyridinium cation
DPC	dodecylpyridinium chloride
DS^-	dodecyl sulfate anion
DSP	digital signal processing
DTA^+	dodecyltrimethylammonium cation
DTAB	dodecyltrimethylammonium bromide
DTAX	dodecyltrimethylammonium halide
$[DTAB]_f$	concentration of free DTAB monomer in solution
dv/dr	shear rate in a channel
E	$[S]_t + [Q]_t - D$
EG	ethylene glycol
EO	ethylene oxide
ESI	electrospray ionization
ESM	exponential series method

ESR	electron spin resonance
f	modulation frequency
f	frictional coefficient
$F_{calc}(t)$	calculated convoluted decay curve
$F_{meas}(t)$	measured convoluted decay curve
FTIR	Fourier transform infrared spectrometry
FWHM	full width at half maximum
GFC	gel filtration chromatography
GPC	gel permeation chromatography
$\Delta_{tr}G°$	Gibbs energy of transfer of surfactant ions from bulk solution into the complex
$\Delta G°$	standard Gibbs energy difference
$\bar{h}$	average number of hydrophobes per polymer chain
$\Delta H°$	standard enthalpy difference
HMP	hydrophobically modified polymer
HPAM	hydrophobically modified polyacrylamide
HPLC	high performance liquid chromatography
HPSEC	high pressure size exclusion chromatography
I	intensity of fluorescence
$I_{\parallel}$	measured intensity parallel to the direction of partial polarization
$I_{\perp}$	measured intensity perpendicular to the direction of partial polarization
I(t)	intensity as a function of time
I_e	intensity of excimer emission
$I_{fit}(t)$	proposed model of fluorescence decay curve
I_{HH}, I_{VV}, I_{HV}, I_{VH}	fluorescence intensities at different horizontal and vertical orientations of the excitation and emission polarizers
I_m	intensity of monomer emission
IR	infrared
K	partition coefficient
K	constant for isolated binding
K*	optical constant in light scattering
K, a	Mark-Houwink coefficients
K_e	parameter representing the effect of polymer end groups on dn/dc
K_{MW}	micelle-water distribution coefficient
K_{SEC}	distribution coefficient for SEC
K_{SW}	stationary phase-water distribution coefficient
Ku	constant for binding adjacent to a bound site
k_+	rate constant of quencher entry
k_-	rate constant of quencher exit from micelle
k_0	fluorescence decay rate of an excited probe molecule in the absence of

	quenching
kD	kilo Dalton
k_E	rate constant of excimer formation
k_f	rate constant for fluorescence decay
k_{IC}	rate constant for internal conversion
k_{ISC}	rate constant for intersystem crossing
k_q	rate constant for quenching
L	length of capillary
L(t)	instrumental response function
LS	light scattering
M	molecular weight
M	micelle
[M]	concentration of micelles
M	mass of a molecule
m/z	mass to charge ratio
m_0	slope of the Zimm plot
MALDI	matrix assisted laser desorption ionization
MALLS	multi angle laser light scattering
MCA	multichannel analyzer
MEM	maximum entropy method
MLC	micellar liquid chromatography
$\bar{m}$	average number of micelles bound per polymer
M_m	average monomer molecular weight
M_n	number-average molecular weight
m_p	mass of polymer injected
M_p	molar mass of polymer repeat unit
MS	mass spectrometry
M_s	molar mass of surfactant
$m_{s,b}$	mass of bound surfactant
M_v	viscosity-average molecular weight
M_w	weight-average molecular weight
M_z	z-average molecular weight
n	refractive index
n_0	refractive index of the solvent at λ_0
N_A	Avogadro's number
NaPA	sodium polyacrylate
N_h	hydrophobe aggregation number
NMR	nuclear magnetic resonance
N_q	quenching-average aggregation number
N_s	mean aggregation number of micelles
N_t	total aggregation number of surfactants and HPAM hydrophobes
N_w	weight-average aggregation number

OO	two empty adjacent sites on the polymer
OS	isolated bound site on the polymer
p	residual degree of polarization of light
p_0	principal polarization
P	probe
P(θ)	light scattering form function
P-S	polymer-surfactant
ΔP	pressure drop over the length of a capillary
PAA	polyacrylic acid
PAM	polyacrylamide
PAM-*co*-NaPA	acrylamide-sodium acrylate copolymer
PEG	polyethylene glycol
PEO	polyethylene oxide
PMT	photomultiplier tube
P_n	micelle containing one probe molecule and n quencher molecules
P^*_n	micelle containing one excited probe molecule and n quencher molecules
P_n	Poissonian probability that a micelle contains n solubilizates
ppm	parts per million
PPO	polypropylene oxide
PVC	poly(vinylchloride)
PVP	poly(vinylpyrrolidone)
<P>	average number of probe molecules per micelle
<Q>	average number of quenchers per micelle
Q	quencher
Q_w	aqueous quencher molecule
[Q]	quencher concentration
$[Q]_b$	concentration of quencher contained in polymer-bound aggregates
$[Q]_{cac}$	cac of the quencher surfactant
$[Q]_{cmc}$	cmc of the quencher surfactant
$[Q]_m$	concentration of quencher contained in micelles
$[Q]_t$	total bulk quencher concentration
r	radius from the center of gravity of a molecule
r_c	radius at the channel wall
R_θ	excess Rayleigh ratio
R_f	TLC retention factor
$\langle r_e^2 \rangle^{1/2}$	root mean square end-to-end distance
R_g	root mean square radius
R_h	hydrodynamic radius
RI	refractive index
R_n	number-average radius
R_w	weight-average radius

R_z	z-average radius
$\Delta S°$	standard entropy difference
S	surfactant
S^+	surfactant cation
$[S]_b$	concentration of surfactant contained in polymer-bound aggregates
$[S]_{cac}$	cac of surfactant
$[S]_{cmc}$	cmc of surfactant
$[S]_f$	concentration of surfactant monomer free in solution
$[S]_m$	concentration of surfactant contained in micelles
$[S]_t$	total concentration of surfactant in solution
S_0, S_1, S_2	singlet states
SANS	small angle neutron scattering
SAXS	small angle x-ray scattering
SDS	sodium dodecyl sulfate
SEC	size-exclusion chromatography
SS	two adjacent bound sites on the polymer
TAC	time to amplitude converter
TLC	thin layer chromatography
TPB	tetradecylpyridinium bromide
TPC	tetradecylpyridinium chloride
TRFQ	time resolved fluorescence quenching
TTA^+	tetradecyltrimethylammonium cation
TTAB	tetradecyltrimethylammonium bromide
TTAC	tetradecyltrimethylammonium chloride
u	cooperativity parameter
$\bar{v}$	partial molar volume
$\bar{v}°$	partial molar volume of polymer at infinite dilution
<v>	flow velocity
V	molar volume of the molecule
V_0	volume outside the pores of the SEC packing
V_e	SEC elution volume
V_h	hydrodynamic volume
V_i	volume inside the pores of the SEC packing
V_m	mobile phase volume of the SEC column
v_{max}	maximum velocity in a channel
V_s	stationary phase volume of the SEC column
V_t	total volume of the mobile phase
W_P	weight fraction of polymer in a complex
W_S	weight fraction of surfactant in a complex

x	bulk average number of solubilizates per micelle
X_q	mole fraction of quencher in mixed micelles
y	feed mole ratio of C_nAM in HPAM
z	feed mole ratio of AA in HPAM

ACKNOWLEDGEMENTS

I must first thank Dr. Jan C.T. Kwak for much support and encouragement over eight years spent as a member of the Colloid Science Group. My many associates in the Group, past and present, are thanked for companionship and stimulating discussions, in particular Dr. D. Gerrard Marangoni and Dr. Ian McLennan on both counts. I also wish to thank my supervisory committee (Dr. Guy, Dr. Pincock, Dr. Stephens, Dr. Wasylishen) for their guidance and Dr. Paul L. Dubin (Indiana University Purdue University at Indianapolis) for acting as my external examiner and for his comments on this thesis. Funding for this research came from NSERC and Dalhousie.

For various measurements performed during this study, I thank Brent Jewett and Beata Kolakowski (mass spectra); Melanie O'Neill and Dr. Karen Crouse-Badri (dipyme synthesis and characterization); Calvin Howley and Dr. Jochem Effing (HPAM synthesis and characterization); Jill Thomas and Dr. Sumita Sanjeevi-Ranganathan (PAM-*co*-NaPA synthesis and characterization).

For other assistance I thank Jürgen Müller (custom glassware and financial advice); Brian Millier and Chris Wright (MCA construction and computer and spectrometer maintenance); Rick Conrad, Bud Eisener and Ross Shortt (machining and mechanical repairs); Dr. Kevin McMahon and Dr. Peter Redden (lifetime instrument training); Dr. Ram Palepu, StFX (use of spectrofluorometer); Dr. Jean Sturm, Dr. Jacques Lang and Dr. Raoul Zana, U. de Strasbourg (Convol software); Dr. Paul Presunka and Dr. John Coxon (FORTRAN assistance); Dr. Darren Andrews, Dr. Peter Wentzell, Sean Brennan at Stanford U. and The Mathworks Inc. (MATLAB assistance); Wyatt Technology Corporation (SEC detector servicing and technical support).

Finally I must thank my family for much needed support, and my wife Lana for editing and layout assistance, and much patience and suffering.

CHAPTER 1. INTRODUCTION

The interactions of polymers with surfactants have attracted interest for industrial applications such as in tertiary oil recovery and in detergents and cosmetics. The high solubilizing power of these mixtures at low concentrations and the rheological properties of the solutions are of key industrial interest, and also of intellectual interest, as they are the result of the microscopic structure of these complexes. Studies of these systems have focused on characterizing both bulk properties such as viscosity and microscopic properties such as the precise arrangement of the bound surfactant molecules. A clear picture of the structure of these aggregates and the factors which affect that structure is desirable both for the design of better industrial formulations and for a better fundamental understanding of the interaction.

A vast number of combinations of polymers and surfactants remain to be investigated, and new methods continue to be proposed and refined. Fluorescence probing methods exist which are used to measure various properties of the immediate environment of the probe molecule, providing excellent ways to elucidate the structure of polymer-surfactant aggregates on a molecular level. Chromatographic methods have seen little use in this field, but have the potential to measure the size of complexes, the degree of surfactant binding, and kinetic aspects of the polymer-surfactant interaction. It is the aim of this research to study a variety of polymer-surfactant systems by luminescence probing methods and to develop ways to use size exclusion chromatography to explore these systems. For this study we have chosen polymer-surfactant systems which have been widely investigated as well as unique systems which were the focus of studies by other methods in our laboratory.

1.1. Surfactants and Micelles

Surfactants are molecules which contain both polar and nonpolar moieties. Their amphiphilic structure causes them to be soluble in both polar and nonpolar phases and to tend to adsorb at interfaces between two such phases. At low concentrations surfactants will exist as free monomers in aqueous solution. Above the Krafft temperature and the critical micelle concentration (cmc) the solution becomes saturated with monomers and

any excess surfactant molecules, rather than forming a precipitate, aggregate together to form micelles. These are typically spherical structures with the hydrophilic headgroups distributed over the surface and the hydrophobic tails within, shielded from water contact. The nonpolar core and polar surface provide a range of environments suitable for the solubilization of a wide variety of molecules, a property of surfactants which has resulted in their most recognized application: as detergents.

A characteristic property of a surfactant is the average number of molecules which gather to form a micelle, called the aggregation number (N_s). A typical surfactant has a mean aggregation number of about 50, which can be affected by many factors including the surfactant molecular structure, concentration, solution pH, temperature, and the presence of electrolyte or organic solubilizates. The surfactant headgroup may be anionic, cationic, zwitterionic or nonionic, and the tail may be linear, branched, or two tailed, and may contain olefinic or aromatic groups. These various molecular structures exhibit a wide range of cmcs and aggregation numbers. Certain surfactants, particularly nonionic surfactants, are extremely hydrophobic and form micelles at micromolar concentrations, while some short-tailed molecules are soluble as monomers up to molar concentrations. Some surfactants, because of the way their structures affect the interactions and packing of the molecules, form larger aggregate structures such as rods, vesicles and bilayers with aggregation numbers in the hundreds and thousands.

The driving force for micellization is the hydrophobic effect, the entropy increase which occurs on removing the free monomers from their rigid "iceberg" hydration structures and allowing the surrounding water molecules to adopt a less ordered, more fluid structure [1]. This is often misunderstood as being a repulsion of the tails from water contact and/or an attraction between the tails, but these interactions are relatively weak. It has been demonstrated for hexane and octane that the free energies of formation of hydrocarbon-water and hydrocarbon-hydrocarbon surfaces are favourable and approximately equal, but substantially smaller than the water-water free energy [2]. The driving force for micellization is the water-water hydrogen bonding interaction between the surrounding water molecules, and the spherical geometry a maximization of the number of possible water-water contacts.

The micelles are in equilibrium with the free monomers (as is often described by mass action or pseudo-phase separation models) and such variables as temperature, pressure, and concentration of surfactant and of other species such as electrolytes or solubilizates all affect this equilibrium. The equilibrium affects the cmc and the aggregation number (N_s). Both of these properties are commonly used to characterize surfactants of different structures and trends are monitored to provide information about the structure of the aggregates.

A clear knowledge of the structure of aggregates, how they affect solution properties, and how they are themselves affected by solution conditions, is necessary for the design of practical applications. For example, low cmcs can be desirable for the production of detergent solutions with a minimum of materials. This keeps costs down and allows solutions to be greatly diluted during rinsing without desolubilization of dirt. Understanding surfactant interactions is thus useful in the design of new surfactants with desired properties.

1.2. Water-Soluble Polymers [3,4]

Polymers are large molecules formed by the repeated coupling of smaller molecules referred to as monomers. The monomers may be all the same (homopolymer), or two or more monomers may be incorporated in random sequence or by the joining together of homopolymeric blocks. The polymerization generally yields molecules with a distribution of molecular weights; this will be discussed in more detail in Chapter 4. The polymers of interest in this research are linear, though polymers may also have branched or crosslinked structures, which affects several properties including interpolymer interactions and solubility. Some water-soluble polymers when crosslinked form gel structures which absorb many times their original volume of water without dissolving, leading to applications in agriculture as groundwater reservoirs as well as the more familiar uses of superabsorbent materials in disposable diapers and other personal products. The water solubility of a polymer depends on the balance between the hydrophobicity of the generally hydrocarbon polymer backbone and the hydrophilicity of polar and especially hydrogen-bonding functional groups on the polymer. Most synthetic polymers are not water

soluble, allowing such uses as structural materials, piping, and storage vessels.

The effects of polymer structure on solubility are exemplified by the properties of various naturally occurring polysaccharides. Amylose, the linear fraction of starch, is a water soluble polymer of D-glucose with an intramolecularly hydrogen bonded helical structure. Cellulose, the structural material of plants, is a water-insoluble polymer of D-glucose which differs from amylose only in the stereochemistry at the linkages between the monomers, resulting in an extended, rigid conformation which forms intermolecularly hydrogen bonded sheets. Chitin, the structural material in the exoskeletons of insects and crustaceans, is a polyglucose with one hydroxyl group replaced by an N-acetylamino group. Chitin is soluble only in N,N-dimethylacetamide-LiCl, however deacetylation by strong acid or base produces the water soluble derivative chitosan. Water soluble cellulose derivatives may be made by additions of various polar groups (e.g. hydroxyethyl, hydroxypropyl, carboxymethyl) [5].

Polymers in solution typically have a random, open coil conformation, unless as in the case of many proteins some intramolecular interactions exist which impart a stable tertiary structure. While a random walk model predicts a coil dimension in dilute solution proportional to the square root of the degree of polymerization (DP), in a good solvent the coil swells to avoid intrapolymer contacts, to a theoretical upper limit of radius proportional to $DP^{3/5}$. At theta conditions of temperature and solvent compositions, the swelling is exactly compensated by poor solvation (the Gibbs energies of polymer-polymer and polymer-solvent interaction are equal) and the dilute solution exhibits theoretically ideal behaviour. For example, water at room temperature is a good solvent for polyethylene oxide, with theta conditions reached at 108.3 °C [6] or by addition of electrolyte (for example 0.39 M $MgSO_4$ at 45 °C [7]). The virial coefficients A_2, A_3, etc. describe the nonideality, and may be measured via the dependence of osmotic pressure π on polymer concentration c expressed as a series expansion

$$\pi = \frac{RT}{M_n} c + A_2 c^2 + A_3 c^3 + \ldots \qquad (1.1)$$

or the dependence of intensity of light scattering on concentration in the Rayleigh equation, which will be discussed in Chapter 4. At theta conditions $A_2 = 0$.

Polymers which bear a net electrostatic charge are called polyelectrolytes; an example is sodium polyacrylate (NaPA), investigated in this thesis. In solution a polyelectrolyte binds only a fraction of its counterions, like an ionic micelle, and maintains a net charge. Due to electrostatic repulsions between neighbouring charge groups, polyelectrolytes in dilute solution are more swollen than neutral polymers. This is affected by the charge density on the polymer, with highly charged polymers being more swollen and more conformationally rigid. Addition of supporting electrolyte reduces this effect.

A water soluble polymer may be modified by the addition of hydrophobic side chains to produce what is called a hydrophobically modified polymer (HMP), or hydrophobic endgroups to produce an associative polymer (AP). Polysoaps are hydrophobically modified polyelectrolytes so named due to their resemblance to charged surfactants polymerized at the headgroup. Due to their charge, polysoaps can accommodate high degrees of hydrophobic substitution while retaining solubility, and are usually alternating copolymers of charged and hydrophobic monomers. HMPs can usually only accommodate a few percent of hydrophobic monomers, either randomly distributed along the chain or in blocks. All of these types of modified polymers can aggregate in micelle-like fashion. Since APs bear only two hydrophobes, they tend to form interpolymer aggregates. HMPs and polysoaps of sufficient molecular weight can form many intrapolymer micelles per chain, and do so at extreme dilution, with no evidence of a critical concentration.

1.3. Polymer-Surfactant Interactions

The binding of surfactants to polymers is highly dependent on the structures of the molecules. The strongest binding is observed between ionic surfactants and oppositely charged polyelectrolytes, due mainly to the electrostatic interaction between the charged groups. With neutral water soluble polymers, anionic surfactants show the strongest binding, with the hydrophobicity of both surfactant and polymer being important. Cationic surfactants only bind to neutral polymers which are very hydrophobic [8]. Interaction of nonionic surfactants with polymers or polyelectrolytes is relatively rare and highly dependent on the structures of the molecules. Hydrophobically modified polymers can

bind surfactants of any charge type into their existing hydrophobic domains, and at varying surfactant/hydrophobe ratios can form inter- or intrapolymer aggregates. Generalizations are difficult to make, however, due to the structural variety of available species and thus the many systems which remain uninvestigated.

The precise structure of a polymer-surfactant complex will also depend on the structures of the molecules involved. A general model has emerged which consists of micelle-like surfactant clusters bound within the random coil of the polymer. Early investigators [9,10] suggested that surfactant molecules were bound individually, with their headgroups bound to polar sites on the polymer and their tails parallel to the polymer chain. Further observations, including the presence of a critical aggregation concentration (cac) lower in magnitude than the surfactant cmc but similarly manifested in various solution properties, and the influence of surfactant chain length and polymer molecular weight and hydrophobicity on the binding, led to the consideration of the importance of hydrophobic effects and micellization. In this section the key papers in the development of the currently accepted model will be discussed.

Shinoda and coworkers [11] were the first to note the cooperativity of polymer-surfactant binding. They measured cmcs and cacs for sodium alkyl sulfates in the absence and presence of poly(vinylpyrrolidone) (PVP). Based on these data, they calculated the same free energy of transfer of a CH_2 group between the aqueous phase and the aggregate for both the polymer-free micelle and the polymer-surfactant complex. They thus concluded that even at the initial stages of absorption, bound surfactant molecules were in contact with each other rather than uniformly distributed along the PVP chain. They implied but did not explicitly state that the aggregates were micelle-like.

Shirahama *et al.* [12] investigated the free-boundary electrophoresis of sodium dodecyl sulfate (SDS)-polypeptide and SDS-PVP complexes. The authors determined the electrophoretic mobility to be largely independent of polymer molecular weight, as is the case in polyelectrolytes. Contrary to the earlier model of a compact, prolate ellipsoid in SDS-polypeptide complexes [13], they realized that as with polyelectrolytes, the structure must be an open coil, free-draining with respect to water and counterions. They proposed that the electrophoretic mobility of the complex is the same as that of charged SDS

clusters bound to the polymer, and is dependent on the polymer structure or molecular weight only in any small way that the cluster size and charge is. As the clusters are like pearls strung on a tangled chain, they referred to this as a "necklace" model.

Cabane and Duplessix clearly demonstrated the validity of this model with NMR [14] and neutron scattering [15] observations of the complexes formed between PEO and SDS. They applied the contrast variation technique, which involves deuterating either the solvent or one of the solutes in order to match their densities of scattering length (related to the index of refraction at the neutron wavelength of interest). This eliminates the scatter from that solute, so that the observed scattering is due only to the other solute(s). The scattering was fit to theoretical curves for models of spherical and rodlike particles, and it was determined that the PEO-SDS complex contained spherical SDS aggregates similar in size to free micelles, even at high salt concentrations where SDS alone forms rodlike micelles. There was only one polymer chain per aggregate, and as in the absence of surfactant the polymer radius was proportional to $M^{0.62}$. They referred to the complex structure as a "beads and string" model [16] similar to the "necklace" of Shirahama *et al.* [12].

This model has since been elaborated upon and is generally accepted. The polymer chain is in most studies believed to be coiled around the surfactant aggregate which is often smaller than a free micelle. Long polymers may bind several micelles separated by lengths of free chain. The polymer is generally considered to be bound at the micellar surface, especially for polyelectrolytes and the more hydrophilic neutral polymers, although recent NMR paramagnetic relaxation measurements [17] of partitioning of PEO into SDS [18] have indicated that the polymer penetrates into the micellar core. The charge, hydration, hydrophobicity and stiffness of the polymer chain are important in considerations of its conformation and location of solubilization within the aggregates.

1.4. Object and Scope of the Thesis

The goal of this thesis is to develop and apply methods to investigate the size and structure of complexes formed in various polymer-surfactant systems of interest to our research group. The polymers include several widely studied commercial polymers and

several novel copolymers which had been synthesized by other members of our group. Fluorescence probing techniques were used to monitor changes in the size, micropolarity and microviscosity of the surfactant aggregates with changes in component concentrations. The conversion of the data files output by our time resolved fluorescence apparatus for input into a nonlinear least squares fitting program obtained from another research group, and the later development of our own, more adaptable software, were important parts of this research. Size-exclusion chromatography (SEC) was applied to the PEO-SDS system to measure the size of the entire complex and the bound amount of surfactant. Among the new developments in this technique was the use of a multi-angle laser light scattering detector for the direct measurement of complex molecular weight, which had not been applied in earlier SEC studies of polymer-surfactant complexes.

The systems studied include mixtures of anionic surfactants with nonionic polymers, cationic surfactants with anionic polyelectrolytes, and ionic surfactants with hydrophobically modified polymers. The differences in size, polarity and fluidity of the micelles bound in these various systems may be explained in terms of the different interactions involved: charge effects and hydrophobic effects. To study these effects, the charge density of the anionic polyelectrolyte and the degree of hydrophobe substitution of the hydrophobically modified polymers are varied. The size exclusion chromatographic technique offers insight into the extent of surfactant binding, the polymer size necessary to bind a surfactant micelle, and the balance between inter- and intrapolymer aggregation in hydrophobically modified polymers. The application of these techniques expands our understanding of the broad range of interactions manifested in polymer surfactant systems.

CHAPTER 2. REVIEW OF MAJOR EXPERIMENTAL METHODS USED IN STUDIES OF POLYMER-SURFACTANT INTERACTIONS

The interaction of polymers with surfactants is an interesting aspect of both polymer and surfactant chemistry, is also of interest as a model system in protein chemistry, and for various reasons has technological applications [19]. This provides a meeting ground for discussion and study by researchers from a wide variety of fields. The obvious participants are polymer chemists and surfactant chemists, though there have also been avenues for input from protein chemists, photochemists, theoreticians, engineers and others. Regardless of the backgrounds of the researchers, the methods with which they approached their studies can be loosely classified into three groups. Classical physical chemical methods provided the means for many of the early studies, demonstrating that complexes existed, but in general describing only macroscopic properties of the solution. Spectroscopic work has been performed in nearly every range of the electromagnetic spectrum, and generally provides information about the structure of the complex at the molecular level. Finally, there is the theoretical work, including thermodynamic [20,21] and statistical mechanical models [22], and more recently Monte Carlo simulations [23,24]. Given the recent success of molecular dynamics calculations in predicting intricate structures in surfactant systems [25,26], and the continual advances in computer technology, we can also expect to see this method of simulation extended to polymer-surfactant systems in the near future. We will not discuss theoretical treatments and simulations in detail here, but refer the reader to several recent reviews [27,28,29].

In this chapter we review the major experimental methods which have been applied to the study of polymer-surfactant interactions. The methods are discussed in terms of the sort of information which may be derived from such a study, and how this information complements other techniques. We make note of existing reviews, and further discussions later in this thesis of techniques involved in our own research. The literature is too vast to present an exhaustive review here; chosen examples are either of direct relevance to our research or early studies which significantly contributed to the growth of the field. The format resembles Goddard's more extensive review of the early literature [30], except that that review focused on complexes of ionic surfactants with neutral polymers, and did not

categorize the various methods as is done here. The book by Zana reviewing the use of many of the techniques in surfactant systems is also highly applicable [31].

2.1. Classical Physical Chemical Methods.

The first, and rather loosely defined, classification is classical physical chemical methods. This is truly a catch-all category which comprises any work which is neither spectroscopic nor theoretical, but for the most part these are older methods with their roots in the determination of basic solution properties like viscosities and cloud points, or molecular physical properties like mobility and self-diffusion, and thus the classification is sufficient. This category also tends to encompass most of the methods used in the early work (pre-1980's) which led to the proposal of the "necklace" model. These methods are by no means obsolete, however, and continue to be applied in new ways and to new polymer-surfactant systems.

Binding Isotherms

Binding isotherms may be determined by several rather different methods. In equilibrium dialysis methods, a polymer solution on one side of a membrane in a cell, or within a membrane bag, is equilibrated with a solution of a surfactant which penetrates the membrane. The concentration of free surfactant in the solution outside the membrane is measured and used to calculate the bound concentration. This generally requires a large number of samples, prepared either consecutively in the same cell or concurrently in many similar cells, and left to equilibrate for long times. More recently, special surfactant-selective electrodes have been developed [32], applicable to most charged surfactants, which permit relatively fast titration experiments where the free surfactant monomer concentration may be measured directly in the presence of the polymer-surfactant aggregates, and even at higher concentrations where free micelles coexist.

Binding isotherms provide a quantitative measure of how much surfactant is bound to the polymer under given conditions of bulk concentration (and pH, ionic strength, temperature etc.). This is crucial information, for example, when trying to derive micelle aggregation numbers from fluorescence probing measurements. The surfactant concentration at the onset of binding (cac) is a measure of the binding affinity. The

steepness of the isotherm also provides information on how cooperative the binding process is, which tells us about the tendency of the surfactant to bind in clusters. The measurement and use of binding isotherms is discussed further in Chapter 6, and has been recently reviewed [22]. Binding isotherms have demonstrated the strong cooperativity of interactions between oppositely charged surfactant and polyelectrolyte, the increase in binding affinity with surfactant chain length and polyelectrolyte charge density, and the increase of cooperativity and cac with added electrolyte.

An early example is the determination by Shirahama & Ide [33] of binding isotherms of a series of sodium alkyl sulfates to PEO by dialysis. Based on the cac values, they calculated the free energy of transfer of a methylene group in the surfactant chain from an aqueous environment into the complex. The value of -1.4kT is greater than that of free micelles (-1.1kT) which suggests that the bound micellar environment is slightly more hydrophobic than in a free micelle. The measurements lead them to propose that the PEO binds at the surface of small aggregates, which are scattered along the chain.

Conductivity and Potentiometry

Conductivity and potentiometry are two techniques which have long been used to give evidence of micellization of ionic surfactants and determine critical aggregation concentrations in polymer-surfactant systems. Both methods suffer reduced sensitivity in salt-added systems. The conductivity of a solution increases with increasing concentration of charged surfactant, but upon the formation of aggregates the increase becomes less rapid since the binding of counterions reduces the number of dissociated charged species present. In the presence of a polymer, complex formation is evidenced by the shifting of the break point to a lower concentration of surfactant. A second and sometimes third change in slope are often observed, corresponding to saturation of binding and formation of free micelles (or vice versa [34]). Jones [10] used this method to determine the cac and saturation of binding in PEO-SDS as a function of polymer concentration, and thus determined the stoichiometry of the saturated binding.

Potentiometric titrations to measure the activity coefficient of the surfactant counterion (e.g. Na^+) also show a break point at the cac and are used to quantify the

degree of counterion binding. Both methods were combined in the early study of Botré *et al.* [35] as evidence of complexation of the water insoluble polymer poly(vinyl acetate) and the protein bovine serum albumin with SDS. They postulated micellar clusters bound to the polymers, resulting in polyelectrolyte-like properties, and noted stronger binding of counterions of greater valence.

Surface Tension

The measurement of surface tension is a fundamental technique of colloidal chemistry which found application early on in the study of polymer-surfactant complexes. It has mainly been employed to demonstrate the cac and saturation of binding, and may be employed in salt solutions where conductivity measurements cannot. The early study of Jones [10] showed that a plot of surface tension versus surfactant concentration changes slope at the cac, and at saturation the surface tension coincides with that measured in the absence of polymer. The displacement of the curve has been used to calculate the amount of surfactant bound and construct a binding isotherm in good agreement with that measured by dialysis [11].

Viscometry

Rheology is an indispensable method for the study of polymer solutions. The viscosity of P-S solutions may be determined by capillary viscometry of dilute samples, or by rotating viscometers in highly viscous systems or when the effect of shear rate is of interest. Viscometric measurements evidence changes in interpolymer interactions caused by the polymer-surfactant complexation. Binding of surfactant can cause conformational changes in the polymer coil. This may reduce interpolymer interactions by creating a more compact complex than the native polymer, or the viscosity may increase as a result of the expansion of polymer coils and crosslinking by bound micelles.

Previous rheological investigations of hydrophobically modified polyacrylamides (HPAM)s in our laboratory are discussed in further detail in Chapter 7. Effing *et al.* [36] observed a rapid, nearly linear increase in viscosity of an HPAM solution with concentration of added SDS, followed by a highly viscous gel region at SDS/hydrophobe ratios around 3, and by a less viscous region at higher SDS levels. This behaviour is

believed to be the result of crosslinking of the chains by bound micelles at low SDS/hydrophobe ratios, followed by a breakup of interpolymer structure as the number of hydrophobe chains per bound micelle decreases. The viscosity is dependent on shear rate, thickening rapidly at low shear rates and then decreasing slowly at higher shear [37]. The shear is believed to uncoil the polymer chains, allowing increased interpolymer interactions of the hydrophobes.

Clouding and Phase Separation

Phase diagrams and cloud point measurements are two representations of phase separation phenomena. Phase diagrams, generally in ternary representations for three-component polymer-surfactant-water systems, are depictions of phase boundaries as a function of component concentrations at a constant temperature. Cloud point measurements monitor the temperature of phase separation as a function of component concentration, usually of surfactant concentration at constant polymer concentration.

Phase behaviour in P-S systems has been reviewed by Lindman and coworkers [38,39]. Associative phase separation is generally observed in mixtures of ionic surfactants with oppositely charged (and in some cases neutral) polymers. The two-phase region is closed, meaning that the separation occurs only at intermediate concentrations of the polymer and surfactant, and sufficient addition of either component will shift the equilibrium back to the one-phase region. Segregative phase separation is common with like-charged polymers and surfactants, and also in mixtures of neutral polymers with nonionic surfactants. When interaction between the two components is unfavourable, a separation into a polymer-rich phase and a surfactant rich phase occurs. In nonionic systems, the tendency to segregate increases with increased polymer molecular weight, or with increased micelle size of the surfactant.

Separation Techniques

Separation methods applicable to the study of aggregates include electrophoresis, ultrafiltration, ultracentrifugation and chromatography (in particular size exclusion chromatography). These techniques measure changes in polymer molecular weight, hydrodynamic volume, charge, etc. on surfactant binding. Several methods which are

routinely used to study protein-surfactant complexes have only occasionally been applied to mixtures of surfactants and synthetic polymers. Studies using size exclusion chromatography (including gel filtration and HPLC methods) are discussed in Chapter 4.

The use of electrophoresis techniques has been recently reviewed by Shirahama [22]. Electrophoretic mobility provides information about the complex charge as well as its size. Electrophoresis measurements were vital in the study where the "necklace" model of polymer-bound micelles was proposed [12]. The mobility of numerous protein and PVP complexes with SDS was almost totally independent of the molecular weight of the macromolecule. Thus they concluded that the complexes are free-draining with respect to the solvent, and the electrophoretic mobility of the complex is dependent only on the size of the surfactant clusters, which are similar in size to free SDS micelles. More recently, Shirahama *et al.* [40] observed that complexes both rich and poor in bound surfactant coexist in mixtures of dodecylpyridinium bromide with sodium dextran sulfate. The high cooperativity of the binding causes individual chains to saturate while other chains appear to be almost totally uncomplexed. The binding of surfactant at saturation is greater than 1:1, so that the bound and unbound chains are of opposite net charge and migrate in opposite directions. This is contrary to the usual picture of a relatively uniform binding of surfactant to all chains.

Ultracentrifugation is a classical method for measuring the mass of proteins. François *et al.* [41] applied the technique to monitor the growth of the PEO-SDS complex relative to the unbound polymer, and measure the binding ratio at saturation. The complex displayed hydrodynamic behaviour typical of an expanded polymer coil.

Ultrafiltration employs a porous membrane of a chosen cutoff size to separate aggregates from smaller molecules in solution. It is typically used to purify macromolecules or to recover them from solution. The use of P-S complexes in ultrafiltration for the extraction and removal of chlorophenol contaminants from aqueous waste streams has been investigated [42]. The addition of polyelectrolyte can be used to precipitate and filter a surfactant contaminant, or the formation of P-S complex at low concentrations provides a potentially economic route to remove ionic or hydrophobic contaminants [43]. Ultrafiltration was used by Dubin *et al.* [44] to separate free micelles

from polymer-bound micelles in a system of cationic polyelectrolyte and mixed anionic/nonionic surfactant micelles. The free micelles were of lower anionic content than the bulk mixed surfactant, suggesting a minimum critical surface charge density for binding of the mixed micelles to the polyelectrolyte.

Micellar Relaxation

Several techniques have been used to monitor the kinetics of the relaxation of the micelle size distribution after a sudden disturbance of the system [45]. The data are generally applied to a mass action or other model of micelle formation, to estimate the critical concentrations and aggregation numbers in the system. Often the relaxation is monitored by the absorbance or fluorescence of a dye added to the system, as in the study by Tondre using a temperature jump technique in the PEO-SDS system [46]. The cac and saturation concentration predicted by a mass action model agreed with literature values, and the binding was seen to require a minimum molecular weight of the polymer. D'Aprano *et al.* recently applied ultrasonic relaxation to the PVP-SDS system, measuring sound absorption across a range of incident frequencies [47]. A plateau in the relaxation time was observed in the region between the cac and the formation of free micelles. Application of a mass action model yielded an aggregation number of 19 ± 3 for the bound micelles, much smaller than free micelles but in keeping with literature values from fluorescence quenching measurements.

Calorimetry

The relatively few examples of the use of calorimetry in P-S systems have been recently reviewed by Olofsson and Wang [48]. As the formation of micelles or of polymer-surfactant complexes is driven by thermodynamics, calorimetry can reveal much about the strength and nature of the interactions. Modern advances in methods and instrumentation have improved sensitivity, allowing more reliable investigations of the relatively small heat effects in micellar systems. Isothermal titration calorimetric methods can be used not only to measure critical aggregation concentrations, but to assess the relative strengths of interaction between a series of different polymers or surfactants. Differential scanning calorimetry measures heat capacity as a function of temperature and

can be used to determine phase changes and conformational transitions.

2.2 Spectroscopic Methods

Spectroscopic methods spanning the whole electromagnetic spectrum have been applied to polymer-surfactant systems. These methods provide information about the local environment of a component of the system or a probe molecule, or measure distances which provide information about the size of the bound micelles and the complexes. Kinetic parameters, partition coefficients and diffusion coefficients can also be derived. The methods are discussed in order of increasing frequency of incident radiation.

Nuclear Magnetic Resonance (NMR)

The wide variety of experiments which have been developed in NMR spectroscopy (chemical shift, relaxation, and multinuclear NMR of ^{1}H, ^{2}H, ^{13}C, ^{23}Na and other nuclei) have lead to numerous applications in polymer-surfactant systems. The subject has been reviewed extensively [49,50,51]. Chemical shifts provide an averaged measurement of all the environments experienced by a particular nucleus over all the molecules in a sample. Changes in chemical shift with polymer-surfactant ratio indicate changes in the fractions of surfactant in the free, bound and micellar states. Proximity of one component of the sample to an aromatic ring on another molecule may be evidenced by ring current shifts. Isotopic labeling may be used to study the environment of a particular site on a molecule. Relaxation experiments reveal the mobility or order of surfactant chains or counterions. Self-diffusion experiments reveal large differences between the diffusion coefficients of bound and free surfactants.

The paramagnetic relaxation measurements of Gao *et al.* [18] revealed that 85% of the PEO monomers are solubilized within a PEO-SDS complex, but that value decreases below a PEO molecular weight of 4000 and reaches zero for tetraethylene glycol. The binding ratio at saturation was in good agreement with that determined by other methods. Further results in the presence of electrolyte suggest that most of the bound PEO is in the micellar interior. A recent application of a 2-D NMR technique (nuclear Overhauser enhancement spectroscopy) indicated that the protons of the PEO segments were located near all the methylene groups of the SDS hydrophobe except those nearest the headgroup,

supporting this conclusion [52].

Electron Spin Resonance (ESR)

ESR methods involve probing the aggregate with a stable free radical molecule. The spectra may be interpreted in terms of the distances between probes, indicating aggregate size, and their rotational relaxation, yielding microviscosity measurements. Shirahama *et al.* [53] added a hydrophobic tail to a spin probe and used it to study interactions of SDS with several polymers including PEO and PVP. ESR lines are broadened by spin-spin interactions which depend on the average distance between probes. The greater probe separation in bound aggregates than in the absence of polymer indicated more compartments and thus smaller aggregates. The linewidth in polymer solutions at the limit of zero surfactant was still broader than in pure surfactant samples, indicating a more viscous microenvironment. Wang *et al.* [54] used a similar probe and also found a higher microviscosity in PEO-bound micelles than in free micelles for SDS and LiDS, but not for CsDS. Conversely, Witte *et al.* [55] employed a different spin probe which rotated more freely in SDS/polymer complexes than in free micelles.

Infrared and Raman

Infrared and Raman spectroscopic techniques have seen little use in the study of polymer-surfactant interactions. As infrared spectra are the result of vibrational transitions in molecules, changes in spectra with concentration of system components, temperature, etc. reflect changes in conformation and hydrogen bonding interactions. The strong IR absorption bands of water have limited this technique to the study of P-S complexes as films [56,57] or adsorbed layers [58,59], while the weakness of Raman scatter necessitates high sample concentration. With the continually improving sensitivity of IR measurements, particularly Fourier Transform instruments, sum frequency vibration, and total internal reflectance techniques, application to complexes in solution may be realized.

Fluorescence

A variety of fluorescence techniques have been applied to polymer-surfactant systems. They must be carefully applied, as photophysical probe molecules are relatively

large and hydrophobic, and when added (either as solubilizates or covalently bound to the polymer) they can potentially perturb the system. Time-resolved fluorescence quenching techniques yield surfactant mean aggregation numbers and micelle size polydispersity measurements, and information about the mobility of the solubilized dyes. The quantities of surfactant, probe and quencher present in the aggregates must be known from other techniques such as binding isotherms. Steady state spectra can also be used to measure aggregation numbers, but the quenching kinetics should be known in order to validate the assumptions of the method. The micropolarity and microviscosity of the micellar environment are also measured by steady state techniques, and have been used to measure the cac and as evidence of structural differences between related P-S systems. The application of these techniques in polymer-surfactant systems has been recently reviewed [60,61] and an in depth discussion is presented in Section 4.

UV-Visible

As with fluorescence techniques, UV-visible spectroscopic methods mainly involve observation of a probe solubilized in the complex or covalently bound to the polymer. Exceptions include the use of circular dichroism [62] or optical rotation [63] measurements to determine polymer helicity in complexes. The measurement of the solubilization of water-insoluble dyes by micellar aggregates to yield cac values has been reviewed recently [64]. In some cases, the dye may interact cooperatively with the aggregate and thus perturb the cac of the system. Some dyes show substantial changes in molar absorptivity upon entering a hydrophobic environment. Shifts in the UV maximum wavelength of a dye with the polarity of the solvent are known as solvatochromism [65]. This method has been applied to measure the polarity of mixed solvents, micelles, vesicles, and polymer solutions, but has been rarely applied in P-S systems. In a study of surfactant binding to poly(N-acryloylpyrrolidine), the polymer was labeled with a solvatochromic zwitterionic pyridinium dye [66]. A significant shift in the wavelength of maximum absorbance was observed in the presence of SDS or sodium decyl sulfate, indicating the formation of a P-S complex, while the negligible shift in the presence of DTAB indicated little or no binding of cationic surfactant.

Microscopy

Visible microscopy is not suitable for the observation of nm-scale structures in bulk solution. However, microscopic techniques have been applied to polymer-surfactant structures at the air-solution interface [67], in solid films [68], or in thin liquid samples which have been rapidly frozen, a recent technique known as cryogenic transmission electron microscopy (Cryo-TEM) [69]. The dimensions of rodlike, vesicular and lamellar structures may be quantitatively resolved by Cryo-TEM, with spherical micelles visible but at the limit of resolution. A variety of structures were observed under different solution conditions in samples of SDS with a cationic cellulose [70]. Addition of nonionic surfactant was seen to break up the long threadlike intermolecular micelles of anionic polysoaps [71], while addition of mixed anionic/nonionic micelles resulted in the formation of interpolymer complexes of a cationic polyelectrolyte [72].

Light-Scattering

Light scattering techniques have long been used to measure sizes of micelles and polymers in solution, and are similarly applied to P-S systems. Dubin and co-workers have applied several light scattering techniques (static, dynamic or quasi-electric, and electrophoretic, as well as turbidimetry) in studies of surfactant interactions with cationic [73], anionic [74,75] and nonionic [76] polymers. As well as providing information about the radii and molecular weights of the complexes, diffusion coefficients [77], phase boundaries, cac values, and the number of micelles per polymer chain were determined. The effect of micelle surface charge density was studied using mixed micelles of charged surfactants with nonionic or zwitterionic surfactants. A critical charge density is necessary for micelle binding to polyelectrolytes, which varies with ionic strength, surfactant chain length, etc. With increasing micelle size and decreasing polymer molecular weight, complexes of one or more polymer molecules bound to a single micelle were formed [78].

Neutron Scattering (SANS)

Neutron scattering is a powerful technique used to determine the size of the bound micelles and the polymer coil. The contrast matching technique allows the scattering due

to one sample component to be eliminated (by adjusting the scattering index of the solvent with D_2O) so that the scattering from the micelles or the polymer may be observed alone in separate experiments. The measurements provide very detailed size information when fit to an appropriate model. The theory and techniques have been reviewed by Cabane, including a review of results in polymer-surfactant systems [79]. Cabane and Duplessix [15] used this technique to give a detailed description of the "beads and string" [16] structure of the PEO-SDS complex. The measured micellar radius is similar to that of a normal free micelle. The size distribution for free or bound micelles is very sharp. Long sections of polymer chain are free in the space between micelles, with several bound micelles per polymer chain if the polymer is of sufficient molecular weight (>10000). The aggregates are distributed throughout the polymer coil in a homogeneous manner at low ionic strength. At high ionic strength the spatial distribution becomes Gaussian, higher at the centre, and the complex is slightly more compact, but the micelles remain spherical even though SDS alone forms elongated rodlike micelles at such salt levels.

X-Ray Scattering (SAXS)

X-ray scattering reports on ordered structure, and can be used to determine the diameters of micelles and the distances between them. It is sensitive to electron rich parts of the structure, such as the headgroup region of the micelles, and can be used to determine the thickness of that layer. It has been most commonly applied to gels [80] and films [81]. The scattering curves must be fit to a model equation for particles of spherical, rodlike, threadlike or other shape. Süss *et al.* [82] used visual observations of SDS-PEO and SDS-gelatin structures by Cryo-TEM to select the correct model for fitting of SAXS measurements in order to determine the micellar dimensions. Bound SDS micelles were spheroidal and, in the PEO-SDS case, smaller than free micelles. Threadlike micelles were observed for SDS alone in high concentrations of added salt, but were not formed in the presence of salt and PEO.

2.3. Summary

A wide variety of techniques have been applied to the study of polymer-surfactant interactions. The wide applicability and interdisciplinary nature of the field has broadened

the approach, as techniques from physical and analytical chemistry, spectroscopy, biology, applied science, and other fields have contributed to our growing body of knowledge. Some properties are measurable by multiple techniques which may be compared, and most studies in the literature combine different types of information from several techniques. Often the data from one technique are required in order to fully interpret the data from another, for example the necessity of binding data in order to calculate aggregation numbers from fluorescence quenching measurements. Some techniques (e.g. viscosity and phase separation) measure macroscopic properties of the solution, while others probe the microscopic properties (aggregation number, fluidity, polarity, proximity of two molecules) of the aggregate. These different types of data are often complementary.

Researchers are continually improving experimental methods and finding new ways to probe these systems. Certain techniques have been applied only rarely or not at all, mainly due to technological difficulties, but with further development have the potential for future use. In this thesis we have adapted a size exclusion chromatographic technique previously little-used in polymer-surfactant systems. The usual refractometric detection is augmented by a multi angle laser light scattering detector for more reliable measurement of the size and molecular weight of the P-S complex. We use the chromatographic information to complement our fluorescence probing investigations of the properties of the micellar aggregates bound within the complex.

CHAPTER 3. FLUORESCENCE PROBING STUDIES

In this chapter, an overview is presented of the various photophysical probing methods which have been applied in the literature to the study of micellar aggregates and polymer-surfactant complexes. Particular attention is given to the time-resolved fluorescence quenching method and the model equation for the decay observed in a compartmentalized system. This will be followed by a description of the equipment used to collect such data, and the procedures used to fit the data to the decay equation. Then various improvements made to our instrument, including new hardware and software, are discussed. Finally, we describe the synthesis and characterization of a special fluorescence probe molecule, dipyme.

3.1. Photophysical Probing of Aggregates

The dependence of the photophysical properties of many molecules on the properties of their immediate environment has lead to the development of several techniques for the probing of micellar solutions [83,84]. Some of these techniques will be discussed in the following sections. One must be aware when designing such experiments that the introduction of foreign molecules may perturb the system such that the property of interest is affected by the presence of the probe. Keeping this in mind, such techniques allow one to measure many properties and changes in those properties with variations in concentration, temperature, molecular structure of the system components, etc., which is crucial in understanding the structure of the medium at a molecular level.

3.1.1. Overview of Photophysical Processes of Interest

In singlet-singlet excitation, an electron is raised to a higher orbital by absorption of a photon of UV or visible light; in the $S_0 \rightarrow S_1$ case the molecule is raised from the ground state to the first excited singlet state. The $S_0 \rightarrow S_1$ excitation of pyrene is forbidden by symmetry, such that the $S_0 \rightarrow S_2$ transition at ~338 nm is the experimentally observed lowest energy absorbance band of pyrene in solution. The decay of a singlet excited state may proceed by radiative (fluorescence) or nonradiative (internal conversion, intersystem crossing) processes [85]. In the case of pyrene, the S_2 state decays rapidly by

internal conversion to the S_1 state, which is quite stable with respect to both internal conversion to the S_0 state and intersystem crossing to the triplet (T_1) state. This accounts for the relatively high fluorescence quantum yield and long fluorescence lifetime of pyrene, both of which contribute to its usefulness as a probe molecule.

The excited state energy may also be transferred to another molecule in a process called quenching [86]. Quenching may occur by several mechanisms including collisional energy transfer or transfer of electrons between the excited probe and the quencher molecule. For example, pyrene accepts an electron from the quencher N,N-dimethylaniline [87], but donates an electron to free radical quenchers [88]. In isotropic solution, quenching occurs at a constant rate, such that the decay of the excited state is exponential. In the presence of a quencher, the observed lifetime τ is given by

$$1 / \tau = k_f + k_{ISC} + k_{IC} + k_q[Q] \qquad (3.1)$$

where [Q] is the quencher concentration and the rate constants k are those for the available decay processes; fluorescence, intersystem crossing, internal conversion and quenching, respectively. The quantum yield of fluorescence, or fluorescence efficiency, is the ratio of absorbed to emitted photons and is given by the ratio of the observed lifetime to the purely radiative lifetime $\tau_r = 1 / k_f$

$$\Phi_f = \tau / \tau_r \qquad (3.2)$$

In the absence of quencher the observed lifetime is denoted $\tau_0 = 1 / k_0$, and the quantum yield is

$$\Phi^0_f = \tau_0 / \tau_r \qquad (3.3)$$

The Stern-Volmer quenching equation gives the relationship between the loss of quantum yield and the quencher concentration [83]

$$\Phi^0_f / \Phi_f = 1 + k_q\tau_0[Q] \qquad (3.4)$$

In a micellar solution, the compartmentalization of probes and quenchers into hydrophobic regions perturbs these kinetics, such that the decay is no longer a simple exponential. The kinetics and resulting decay equation will be discussed in Section 3.2.3.

3.1.2. Pyrene Vibronic Spectra and Micropolarity

Pyrene is an aromatic hydrocarbon whose interesting fluorescence properties have been much studied. Pyrene exhibits a vibronic structure in its emission spectrum, shown in Figure 3.1, which is not seen in many fluorescent molecules [89,90]. The series of well-defined peaks arises from transitions between the lowest vibrational level of the excited state to various vibrational levels of different energies and transition moments in the ground state. The relative efficiency of the various transitions is affected by the environment of the molecule, and has been related to solvent polarity. In a polar medium, the intensity of the band at ~373 nm is enhanced, while that of the other bands is lowered by varying degrees. The third peak at ~383 nm is relatively unaffected, and thus shows the maximum variation relative to the first peak, so that the ratio I_1/I_3 (or the hydrophobicity ratio I_3/I_1 in some references) provides the most sensitive scale of polarity.

The solvent effect is mainly due to solute-solvent dipole-dipole interactions between the polar excited state of pyrene and the surrounding solvent molecules, which affects the relative transition probabilities between the excited state and the many vibronic levels of the ground state. The intensities are not precisely correlated with either the dipole moment or dielectric constant of the solvent [91]. Still, this property may be used as a qualitative scale of the micropolarity of the probe surroundings.

Values of I_1/I_3 vary from roughly 0.5 to 2.0. These values depend on the spectrometer used and especially on the monochromator resolution and slit widths, which must be the same in order to confidently compare these values, but are otherwise reproducible. One study reported values of 1.89 in dimethylsulfoxide, 1.59 in water, 1.14 in benzene, 0.60 in hydrocarbons and 0.50 in fluorocarbons [90]. On our instrument, aqueous pyrene has an I_1/I_3 ratio of 1.88. The ratios are independent of excitation wavelength and of pyrene concentration.

Figure 3.1: Pyrene Emission Spectrum, Showing Vibronic Structure.

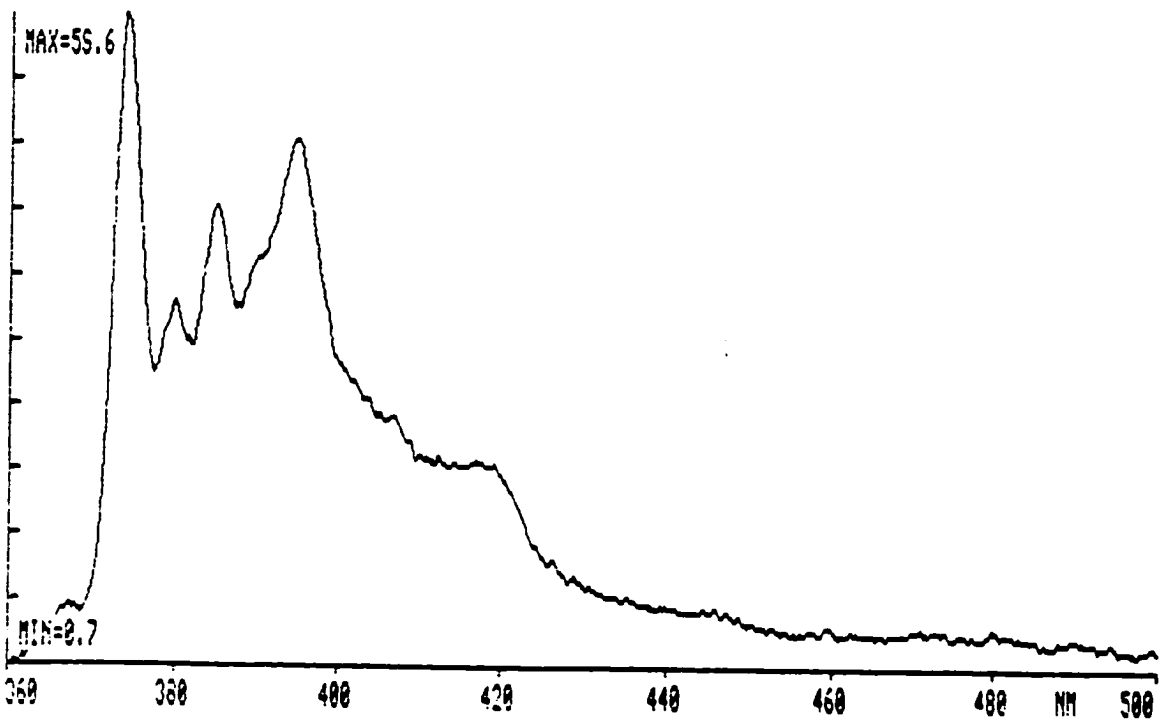

In micellar solutions, values of I_1/I_3 range approximately from 1.0 to 1.6, which is sufficient range to indicate changes in the immediate environment of the probe. A high value is often interpreted as indicating intrusion of water into the micelle, while a low value indicates a probe strongly shielded from water contact. However, a change in the depth of solubilization of the probe molecule or solubilization of polar moieties at the interface could produce similar changes in the observed peak structure. The spectrum is of course an average of the various environments experienced by all probe molecules, including any aqueous probes. Since the value never approaches that measured in saturated hydrocarbons, it is apparent that the pyrene molecules are not fixed deep within the micellar core, but on average are relatively near the polar headgroups and surrounding/penetrating water.

Measurements of I_1/I_3 ratios can be used to determine the cmc of a surfactant, by varying the surfactant concentration from premicellar to postmicellar levels and observing the change of the I_1/I_3 from aqueous pyrene to solubilized pyrene. However, the concentration range over which the ratio changes can be very broad [92], especially in surfactants which contain impurities, solubilizates, or are mixtures of isomers or alkyl chain lengths. Changes in I_1/I_3 may also be observed with changes in polymer-surfactant aggregate structure, such as increasing abundance of free micelles, or change in the amount of polymer bound to the micelles.

3.1.3. Microviscosity Measurement by Fluorescence Polarization [86,93]

The rate of rotation of a molecule depends on temperature, the size and shape of the molecule, and the local friction or "microviscosity" imposed by its solvent environment. If the rate of rotational motion of a fluorescent molecule is of the same order of magnitude as its fluorescence decay rate, the rotational rate can be determined by measuring the residual polarization of the fluorescence of a probe excited with polarized light [94]. A fluorescent molecule has transition moments for excitation and emission which can be represented as vectors. The probability of absorption of a photon depends on the orientation of the electric vector of the incident photon relative to the excitation transition moment of the molecule, and is maximum when they are parallel. The

orientation of the emission transition moment is in general independent of that of the excitation moment, but in S_0 — S_1 transitions they are often nearly parallel. The most probable direction of propagation of the emitted photon is perpendicular to the emission transition moment.

If a solution of probes is excited by plane polarized light, in which all the electric vectors have the same orientation, then the emitted light can still be partially polarized. The degree of polarization of a light beam is defined as

$$p = \frac{I_{\parallel} - I_{\perp}}{I_{\parallel} + I_{\perp}} \tag{3.5}$$

where $I_{\parallel}$ and $I_{\perp}$ are the measured intensities parallel and perpendicular to the direction of partial polarization. To compensate for any geometric differences in the instrument, one can take measurements with the excitation and emission polarizers in all four permutations of their two orthogonal positions (0° or horizontal electric vector and 90° or vertical electric vector). Then the polarization is given by [95]

$$p = \frac{I_{HH}I_{VV} - I_{HV}I_{VH}}{I_{HH}I_{VV} + I_{HV}I_{VH}} \tag{3.6}$$

where the subscripts denote the horizontal and vertical orientations of the excitation and emission polarizers respectively.

If all the fluorescent molecules in a medium were immobile and precisely aligned, their emission would be plane polarized even from unpolarized exciting light. Since probes in solution are randomly oriented at the time of excitation and rotate during the lifetime of the excited state, some of the polarization of the incident light is lost on fluorescence. If the molecule has a very long lifetime and very rapid rotation, any correlation of the emission transition moments to the orientation of the incident plane-polarization is lost through the random rotation of the molecules, and $p = 0$. Otherwise, the observed polarization of the emitted light and the fluorescence lifetime τ can be used to calculate the rotational relaxation time ρ by the Perrin equation [96]

$$1 + \frac{3\tau}{\rho} = \left(\frac{1}{p} - \frac{1}{3}\right) \Big/ \left(\frac{1}{p_0} - \frac{1}{3}\right) \tag{3.7}$$

where p_0 is the principal polarization measured in the absence of all depolarization factors (in practice, in a dilute, rigid solution, often in glycerol). The value of p will range from zero up to a theoretical maximum of 0.5.

For a spherical molecule of molar volume V the rotational relaxation time is related to the viscosity of the medium η by [86,93]

$$\rho = V\eta/RT \qquad (3.8)$$

Thus one can relate the microviscosity of the probe environment measured by this polarization method to a bulk solution viscosity. Inferences about the structure of the probe environment may be made based on these measurements of its rigidity. However, since the method measures the rotation of the probe molecule, it depends on the orientation of the probe with respect to its nearest neighbour molecules and to their sizes and shapes. As probe molecules are not truly spherical, viscosity values thus measured may depend significantly on the shape of the probe used. For example, in an oriented rodlike medium like a liquid crystal, a rodlike probe would find less resistance to rotation than a disklike probe, and thus would measure a lower viscosity. Thus microviscosities measured in this manner need not match bulk viscosities, but at the same time can reveal local structural changes.

3.1.4. Microviscosity Measurement by Intramolecular Excimer Formation

The fluorescence of an excited state molecule may be quenched by formation of a complex with another molecule in the ground state. If the two molecules are the same, the complex is called an excited dimer, or excimer [97], while complexes between unlike molecules are called exciplexes. Excimer formation is observed in many fluorescent molecules, including pyrene. The complex usually has a sandwich-like structure with a charge interaction between the two aromatic planes [98]. Excimer formation of pyrene offers a stabilization of 42 kJ/mol. The resulting complex may fluoresce, relax in a nonradiative fashion to give two ground state molecules, or dissociate to give back the excited and ground state molecules.

Excimer formation is also seen in molecules containing two aromatic groups which are separated by some linkage which allows them to enter a suitable conformation for

bonding. Such complexes are called intramolecular excimers. The length of the linkage affects whether or not excimer formation can occur. Hirayama [99] found that in diphenyl and triphenyl alkanes, only those structures in which two phenyl groups were separated by three carbon atoms permitted excimer formation. Excimer formation of benzene or toluene is only seen in neat or highly concentrated solutions, due to the low stabilization energy of the excimer, but is seen in solutions of polystyrene independent of the polymer concentration. This suggests that the propyl linkage stabilizes the sandwich conformation needed for excimer formation.

Zachariasse and Kühnle [100] examined excimer formation in α,ω-di(1-pyrenyl) alkanes ($Py(CH_2)_nPy$). For a wide range of alkyl linkages (n = 2..16, 22), intramolecular excimers were formed in all cases except n = 2, 7 and 8, with n = 3 as expected exhibiting the most prominent excimer emission. At -110 °C none of the molecules exhibited excimer emission. This indicates that the association is not a ground state process, but occurs by a conformational change in the alkyl linkage, and is dependent on the diffusion of the pyrene moieties through the surrounding media. The presence of preformed ground state pyrene dimers before excitation is uncommon, and may be easily detected via changes in the excitation and excimer emission spectra [98].

The intensity of excimer emission relative to monomer emission I_e/I_m is thus a measure of microviscosity. This method is not valid for intermolecular excimer formation between free pyrene molecules, because of the effect of the distribution of individual pyrene molecules between micelles. The observed intensity ratios I_e/I_m in a micellar solution can be compared to those observed in solvents of varying viscosity, however the anisotropic environment of a micelle may have a different effect on the molecular motion than a bulk hydrocarbon. Microviscosity and bulk viscosity are not necessarily the same property. As well, the microviscosities measured by the fluorescence depolarization due to rotational motion of a probe need not agree with those measured by intramolecular excimer formation, as these are two different types of motion. In a recent study on micelles of SDS bound to ethyl hydroxyethyl cellulose, the two measurements agreed qualitatively, indicating higher microviscosity in the bound aggregates than in free SDS micelles, and a maximum at low binding ratio which coincided with a maximum in bulk

viscosity [101].

For our study, we have synthesized and utilized a molecule which exhibits intramolecular excimer formation. Bis(1-pyrenylmethyl) ether (dipyme) [102] has been used in the literature to investigate the microviscosity of block copolymer surfactants [103] and HMP-SDS aggregates [104,105]. It has the added benefit that the pyrene moieties provide simultaneous micropolarity measurements from the vibronic peaks, which are normally broadened in substituted pyrenes. The dipyme I_1/I_3 scale follows the same qualitative trends, but does not yield the same quantitative values as pyrene. The synthesis and characterization of dipyme are described in Section 3.4.

3.1.5. Aggregation Numbers from Steady-State Fluorescence Quenching

The aggregation numbers of micellar systems may be determined using an ordinary spectrofluorometer. A simple model of fluorescence quenching in micellar solutions was derived by Turro and Yekta [106]. The distribution of probe P and quencher Q among the micelles M is described by Poisson statistics. The model assumes "static" sphere quenching of probe and quencher both contained within the same micelle at the time of probe excitation, with no migration of probes or quenchers in or out of the micelles and 100% probability of quenching an excited probe if one or more quenchers is present in the micelle at the time of excitation. These assumptions can be shown to be reasonable in simple systems with small micelles and hydrophobic probes and quenchers, but it is important to verify these assumptions before using this method [107].

This model may be applied to measurements of the steady-state fluorescence spectra of surfactant solutions containing a probe and varying concentrations of quencher. The intensity I of fluorescence at a chosen wavelength from a sample containing a known quencher concentration is related to the intensity I_0 from a sample containing no quencher by the equation

$$I = I_0 e^{-\langle Q \rangle} \quad \text{or} \quad \ln (I_0 / I) = \langle Q \rangle \tag{3.9}$$

where $\langle Q \rangle$ is the concentration of quencher per micelle [Q]/[M]. A similar result is possible for pyrene excimer quenching under appropriate conditions, with $\langle P \rangle$ representing the concentration of probe per micelle:

$$I = I_0 e^{-\langle P \rangle} \tag{3.10}$$

This is known as the steady-state or static fluorescence quenching equation, and is an extreme limit of the time-resolved fluorescence quenching equation to be discussed in Section 3.2.

These steady-state experiments yield a value for the average occupancy of quencher (or probe, in excimer studies) in micelles. This allows direct measurement of the concentration of micelles in solution. Given the total concentration of surfactant in solution $[S]_t$ and an estimate of the concentration of free monomer $[S]_f$ (which is normally well approximated by the cmc) the mean aggregation number of the micelles may be calculated as

$$N_s = ([S]_t - [S]_f) / [M] \tag{3.11}$$

A plot of $\ln(I_0/I)$ versus [Q] will have an intercept of zero and a slope of $[M]^{-1}$. Thus the mean aggregation number is simply the slope multiplied by $[S]_m$, the concentration of surfactant molecules which are contained in micelles. This method yields a number-average aggregation number, since the measurement is based on the number of micelles in solution [108]. If the micelles are polydisperse in size, the figure will be lower than that measured by methods which derive a weight average, such as light scattering.

These measurements can be made rather quickly and easily on any steady-state fluorescence spectrophotometer. The static method has proven very useful in systems of small micelles, with the choice of a probe and quencher which are strongly solubilized and show high quenching efficiency. The most commonly used probes, pyrene and tris(2,2'-bipyridyl)-ruthenium (II) ($Ru(bipy)_3^{2+}$) have very long lifetimes, and efficient quenchers can normally be found. However, in more complex systems such as polymer-surfactant aggregates the assumptions may not always be valid, leading to inaccurate results. Often the characteristics of a probe-quencher pair in a particular surfactant are assumed to be valid for a complex of that surfactant with a polymer, but this may not be so, particularly if the micelle size or fluidity is significantly different. Prior time resolved measurements in the system of interest are desirable to ensure that the probe and quencher are immobile and that the ratios of quenching rate to fluorescence rate k_q/k_0 and quenching to quencher exit from micelles k_q/k_- are high (at least 10). Otherwise, the slope of the plot tends to

underestimate N_s but remains deceptively linear [84]. The best results are obtained by keeping <Q> less than unity, as the deviation from ideality increases with the quencher concentration.

3.2. Time-Resolved Fluorescence Quenching [84]

The fluorescence probing methods discussed in the previous section can all be performed on a standard fluorescence spectrometer. The time resolved fluorescence quenching method requires more specialized equipment, but provides more reliable measurement of aggregation numbers and also informative rate constants. The use of time resolved fluorescence quenching in micellar systems has become widespread since the development of models to describe the fluorescence decay [109-112] which we discuss in this section.

As the population of an excited state decays exponentially by fluorescence with a rate constant k_0, the intensity of the observed fluorescence also diminishes exponentially. Quenching interactions with other molecules depopulate the excited state and thus reduce the emission intensity. In isotropic solutions, quenching merely reduces the observed lifetime of the molecule, as the probability of an excited probe encountering a quencher is constant in time (recall the Stern-Volmer equation, (3.4)). When the probes and quenchers are solubilized into micelles, quenching is observed to occur mainly during the early stages of fluorescence decay. Since the quenching process requires close proximity of probe and quencher, an excited probe molecule is very likely to be quenched if a quencher molecule is present in the same micelle at the time of excitation, and is much less likely to interact with any quenchers located outside the micelle. Thus at long times after excitation, almost all of the surviving excited state probes are located in micelles which do not contain quenchers. The resulting decay curve is not exponential, but has an initial faster decay as the excited state population is being depleted by quenching, followed by a smooth exponential decay at longer times. This function is not adequately described by a sum of exponentials.

The form of the micellar decay function was first proposed in 1974 by Infelta *et al.* [109], then rigorously derived by Tachiya [110]. The equation is normally written in the

form

$$I(t) = A_1 \exp(-A_2 t - A_3 (1 - \exp(-A_4 t))) \qquad (3.12)$$

where the coefficients A_i are functions of the rates of the various kinetic processes involved. The complexity of the coefficients depends on what processes are considered applicable to the model. Tachiya assumed the following reactions:

$$P_n^* \xrightarrow{k_0} P_n \qquad n = 0, 1,... \quad \text{(fluorescence)}$$

$$P_n^* + Q_w \underset{(n+1)k_-}{\overset{k_+}{\rightleftharpoons}} P_{n+1}^* \qquad n = 0, 1,... \quad \text{(aqueous transfer of quenchers)}$$

$$P_n^* \xrightarrow{nk_q} P_n \qquad n = 1, 2,... \quad \text{(quenching)} \qquad (3.13)$$

where P_n^* and P_n represent micelles containing one probe molecule, in the excited state for the former case, and n quencher molecules. The fluorescence decay rate of an excited probe molecule in the absence of quenching is k_0. Q_w represents an aqueous quencher molecule with a rate constant k_+ for transfer into the micelle which is independent of the number of quenchers in the micelle. The quencher is assumed to partition between the aqueous and micellar phases, and due to this dynamic equilibrium, its aqueous concentration is constant. The rate of exit of quenchers from a micelle containing n quenchers is assumed to be dependent on n, and is expressed as nk_-. The rate of quenching is assumed to be dependent on the number of quenchers in the micelle and is expressed as nk_q.

All probes are assumed to be solubilized within the micelles and immobile, though knowledge of the partition coefficient of the probe between the aqueous and micellar pseudophases allows a correction for this. The distribution of solubilizates among micelles is governed by Poisson statistics [113], assuming that there is no limit to the number of solubilizates which may be contained in a micelle. This is obviously not the case, as there must be some upper limit to the capacity of a micelle, which leads to a binomial distribution. However, it is difficult to estimate this upper limit, and as one rarely requires a micelle occupation of more than two solubilizates in an experiment, the limit is rarely approached. At solubilizate occupancy well below the limit, the binomial distribution may

be approximated by a Poisson distribution. The probability P_n of a micelle containing n solubilizates is

$$P_n = \frac{x^n e^{-x}}{n!} \tag{3.14}$$

where x is the bulk average number of solubilizates per micelle.

No micelle is permitted to contain more than one probe (for quenching studies: obviously this is not the case for excimer formation) which is reasonably satisfied if the bulk probe concentration is 1% of the micelle concentration. Poisson statistics predict that only one in 20000 micelles will contain multiple probes in this case. The Tachiya model assumes no exchange of probes between a given micelle and the aqueous phase or other micelles over the duration of the decay, but this case has since been modeled [114,115]. The model also assumes that all micelles are of the same size. Size dispersity would affect the statistics of solubilization and transfer of probes and quenchers: this will be discussed in Chapter 6.

Quenching will occur rapidly in micelles containing a probe and a quencher, while probes in micelles containing no quencher have essentially zero encounter probability and decay at the normal fluorescence rate. However, it is important that neither the presence nor the number of quenchers in a micelle affect the probability of exciting that particular probe molecule. In other words, there can be no static quenching of the ground state probes, where static quenching describes quenching of the fluorescence of a probe molecule by complexation with another molecule before excitation occurs, as opposed to dynamic quenching which occurs when the probe molecule is first excited and then interacts with a quencher molecule.

From these assumptions the following expressions for A_i are derived [110]:

$A_1 = I(0)$ (peak fluorescence intensity immediately after the excitation)

$$A_2 = k_0 + [Q]_w \frac{k_+ k_q}{k_- + k_q}$$

$$A_3 = [Q]_w \frac{k_+ k_q^2}{k_-(k_- + k_q)^2}$$

$$A_4 = k_- + k_q \tag{3.15}$$

Infelta *et al.* [109] derived an identical expression, though Tachiya contends that their derivation was incorrect [116,117].

The average number of quenchers per micelle $\langle Q \rangle = [Q]_m / [M]$ is related to the aqueous quencher concentration by the partition coefficient $K = k_+ / k_-$, so that

$$\langle Q \rangle = k_+[Q]_w / k_- \tag{3.16}$$

This simplifies the expressions for A_2 and A_3 such that they may be solved for $\langle Q \rangle$ [118].

$$A_2 = k_0 + \langle Q \rangle \frac{k_- k_q}{k_- + k_q}$$

$$A_3 = \langle Q \rangle \frac{k_q^2}{(k_- + k_q)^2} \tag{3.17}$$

As there are five variables to be determined from only four fit parameters, either the value of k_0 must be fixed based on measurements without quencher, or the results from trials at many quencher concentrations must be combined, as will be discussed in Chapter 6.

A further simplification is possible if the rates of quencher exit and entry are slow relative to quenching and decay ($k_- << k_q$ and $k_+[Q]_w << k_0$). Then the quencher is considered to be "immobile" [119] and the coefficients reduce to

$$\begin{aligned} A_1 &= I(0) && \text{(maximum intensity just after excitation)} \\ A_2 &= k_0 = 1/\tau_0 && \text{(fluorescence rate constant, or 1 / lifetime)} \\ A_3 &= \langle Q \rangle = [Q]_m/[M] && \text{(average number of quenchers per micelle)} \\ A_4 &= k_q && \text{(quenching rate constant)} \end{aligned} \tag{3.18}$$

In this form, the data from a single experimental decay curve can be easily fit to this equation to yield the values of the fluorescence and quenching rates and the value of $\langle Q \rangle$. As $\langle Q \rangle = [Q]_m / [M]$, the concentration of micelles [M] can be calculated. One must assume that all quenchers are micellized ($[Q]_m = [Q]_t$, the total bulk quencher concentration) or measure the partitioning of the quencher to determine $[Q]_m$ exactly. Knowing the concentration of micelles, the average number of surfactant molecules per micelle or aggregation number is simply $N_s = [S]_m/[M]$. Again, one can either assume that all surfactant molecules are micellized ($[S]_m = [S]_t$) or measure the concentration of free

aqueous surfactant $[S]_f$. Generally the critical micelle concentration (or, in polymer-surfactant aggregates, the critical aggregation concentration) is used as an estimate of $[S]_f$ in lieu of measurement. However, it is not necessarily a good estimate, as $[S]_f$ can be significantly lower than the cmc (or higher than the cac). Though the time-resolved technique is not restricted to the use of highly efficient quenching, as k_q/k_0 can in theory be less than unity, a good probe/quencher pair is still preferred to give a sharp initial decay and a definite exponential tail.

One further assumption leads to an equation which contains no rate constants or time dependence at all. If it is assumed that the rate of quenching is much faster than the rate of fluorescence, then after integration with respect to time the model equation may be reduced to Equation 3.9, the steady-state fluorescence equation [106] discussed in Section 3.1.5.

In some cases a relatively high concentration of probe may be used and quenching occurs by excimer formation. This mechanism has been used extensively with pyrene and its derivatives as probe molecules. Obviously for this to occur the concentration of probe must be such that there is more than one probe in a significant number of micelles. In general the average occupancy used $\langle P \rangle = [P]/[M]$ is on the order of one probe per micelle, at which point according to Poisson statistics over 26% of micelles contain more than one probe. For excimer quenching, the constants in Equation 3.18 are replaced by $A_3 = \langle P \rangle$ and $A_4 = k_E$, the rate constant for excimer formation. These constants may be complicated by contributions from the rates of excimer dissociation and excimer decay, but under appropriate conditions these processes are insignificant. As pyrene is quite hydrophobic, it can be difficult to solubilize such high concentrations of pyrene in aqueous micellar solution. Common techniques include deposition of a thin film of pyrene onto the walls of the vessel before addition of solution, and injection of a few microlitres of concentrated pyrene in a water-miscible solvent which does not perturb the system or rapidly evaporates from aqueous solution.

3.3. The Fluorescence Lifetime Instrument

Unlike the other fluorescence probing methods which may be performed on

ordinary fluorescence spectrometers, the time resolved fluorescence quenching method requires special instrumentation. Fortunately, commercial instruments, or electronic and optical components for construction of decay spectrophotometers [120] are readily available, experimental techniques are well documented, decay equations have been derived for all typical situations and mathematical techniques [121] and computer algorithms are available for solving the equations. In this section we discuss the design of the single photon counting fluorescence lifetime instrument used to perform the measurements reported in this thesis, followed by a review of the available data treatment methods used to fit fluorescence decay curves to the model equations. Finally, we report our software and hardware adaptations which allowed us to use this instrument to measure aggregation numbers of surfactant and polymer-surfactant aggregates.

3.3.1. Detection Instruments [122]

Speed is an inherent difficulty in making direct measurements of the decay of fluorescence intensity as a function of time on a nanosecond timescale. Such a detector needs a response time on the order of a nanosecond, as does the data recording device. The various instruments which have been developed to carry out such measurements will be briefly introduced below.

The development of microsecond flash photolysis in 1949 was an important advance in the investigation of photophysical events which occur on timescales faster than the eye can perceive. Transient species produced in a sample exposed to a brief flash of light were observed either by monitoring a particular wavelength as a function of time with a photomultiplier and a storage oscilloscope, or by measuring the entire spectrum with a photographic detector after a short delay. Lasers can now provide intense pulses of nanosecond duration for flash photolysis.

Picosecond and even femtosecond laser pulses can be generated for high resolution spectroscopy, but a detector of similar time resolution is required. Until recently, oscilloscopes this fast were unavailable. Resolution higher than 2 ps is possible with a streak camera, which uses a photocathode to convert a light pulse into an electron pulse. The electrons are accelerated and passed between electrodes across which a rapidly

increasing voltage is applied. The earliest arriving electrons are less deflected than the later ones, which spreads out the pulse across the width of the tube. The electrons strike a phosphor screen, with the intensity of the phosphor emission at a given position along the streak being proportional to the intensity of the incident light at a given time.

In phase modulation fluorometry, the source intensity is sinusoidally modulated rather than pulsed, at a frequency comparable to the sample decay rate. The phase shift ϕ between the incident and emitted light is dependent on the decay rate $1/\tau$ and the modulation frequency f by $\tan \phi = 2\pi f\tau$. The modulation of the fluorescence relative to that of the incident light is also used as a measure of the lifetime. This equation requires the assumption of a singly exponential decay, which limits its usefulness. Multiexponential decays require more complex equations and multiple measurements at different modulation frequencies [123]. The application of this method to micellar quenching would require development of appropriate equations to relate the observed phase shift and modulation to the kinetic model. A model-independent application of this technique to micellar systems has recently been reported [124] which distinguished three different environments for pyrene (hydrophobic, hydrophilic, and excimer) but does not yield aggregation numbers.

The method normally used in the fluorescence probing of micelles is the single photon counting method. As the name suggests, this instrument counts individual fluorescence photons. At the heart of the instrument is a time to amplitude converter (TAC) which converts the time delay between start and stop signals produced by excitation and emission PMTs to a voltage. An analog to digital converter (ADC) then assigns this signal a discrete value between 0 and 2^n-1 where n is the bit resolution of the ADC, typically 8, 9 or 10 (256 to 1024 channels). A memory array is used to accumulate a count of the number of times each value has been output by the ADC by incrementing the count in the selected memory channel. After thousands of counts have been collected, the array contains a histogram of events as a function of channel number, proportional to the fluorescence intensity as a function of time.

The benefit of this method is that only the measurement of the elapsed time, and not the recording of the data, requires very fast equipment, and the necessary timing

electronics are easily available. There is sufficient delay between excitation pulses (33 μs in the instrument used here) that the ADC can record the data without having to operate at the same speed as the photochemical process. The data are stored in computer memory and can be analyzed by any of several available fitting procedures. The slow rate of data collection can be a disadvantage, but the counting rate can be optimized in several ways, and the ability to count at very low levels of emission is of great advantage for weakly emitting or low concentration samples, as noise is averaged over many thousands of counts. The single photon counting apparatus will be fully described in the next section.

3.3.2. The Single Photon Counting Apparatus [120,122,123,125,126]

The instrument at Dalhousie is a model FLI 3000 from Photochemical Research Associates, London, Ontario. The optical and electronic components are typical of the instruments described in the literature, except that some researchers use pulsed lasers as excitation sources instead of the flashlamp which will be described. The lasers offer a shorter pulse duration, higher and more stable intensity, and higher pulse rate, which assists in the collection of data at faster rates and to higher precision.

A schematic of the optics and electronic modules of the apparatus is shown in Figure 3.2. The excitation source is a thyratron-gated flashlamp. Two tungsten electrodes are separated by a gap of a few millimetres in a lamp body which is evacuated and then filled with a suitable gas (either H_2 or N_2). The thyratron is a capacitance device which stores a high voltage (adjustable up to 8 kV) and discharges it across the short electrode gap at high frequency (adjustable up to 50 kHz). The voltage is much greater than that needed to jump the gap, which results in an intense, short duration (1-10 ns) spark discharge between the electrodes.

A variety of gases may be used to fill the lamp. Air will do but the lamp stability tends to degrade and deposits form on the lamp body, electrodes, and quartz windows. Hydrogen gas produces a broad but relatively weak continuum band which is useful for general work throughout the UV-visible range. Nitrogen gas produces a series of sharp, intense lines in the UV, the line at 337 nm being perfectly suited for excitation of pyrene. However, the nitrogen pulse is of longer duration (6 ns FWHM as compared to about 2 ns

for H_2) and has a significant tail, resulting in greater convolution of the decay curve (This problem will be discussed in Section 3.3.3.). For either gas, a pressure of about 1/2 atm (we typically used 10" Hg for N_2 and 14" for H_2), a 2 mm electrode gap, 5 to 6 kV high voltage and 30 kHz pulse repetition rate will produce a stable pulse.

Figure 3.2: Schematic of a Photon Counting Instrument.

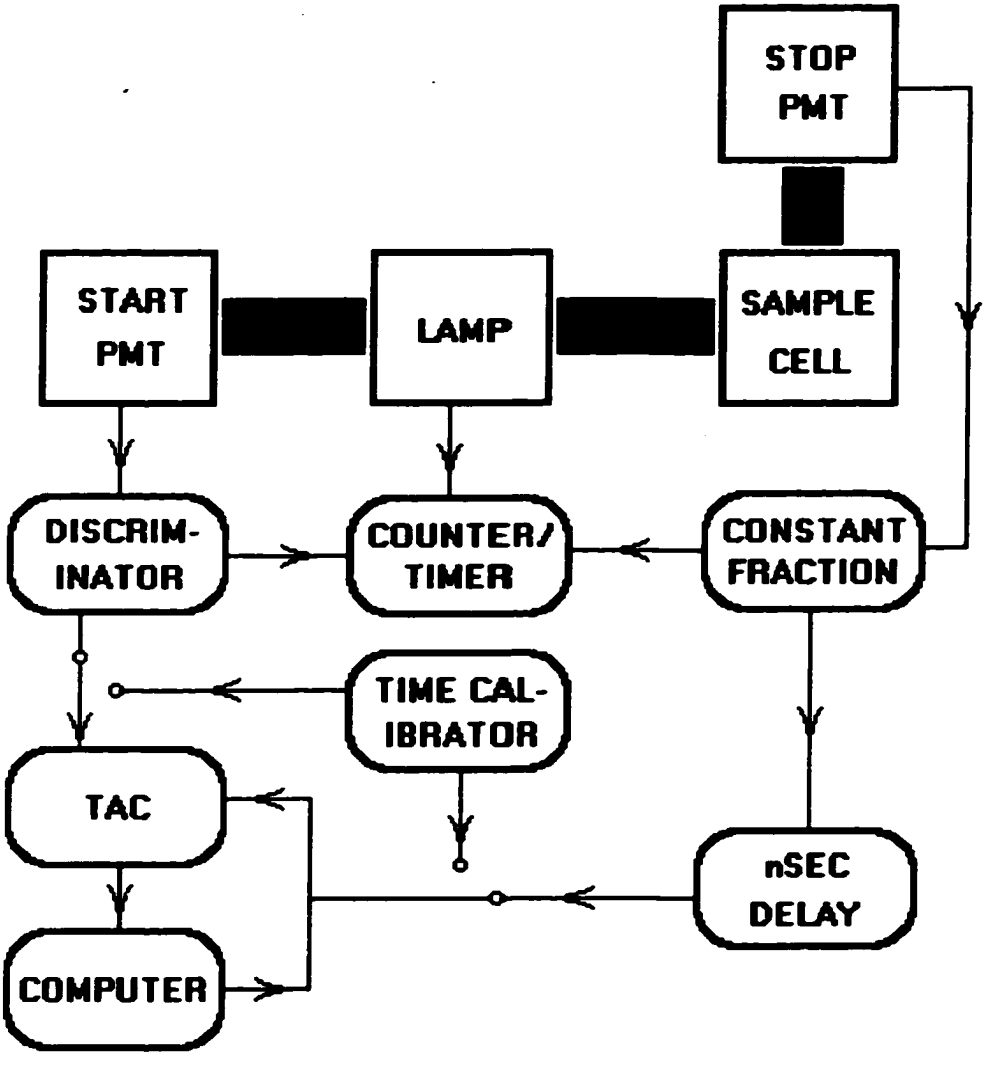

The lamp has a photomultiplier tube (PMT) at the rear which outputs a start signal to the discriminator, indicating the time of the lamp pulse. The lamp has an iris which can be used to reduce the amount of light reaching the sample. The light travels to the excitation monochromator (Modele H.10, Jobin Yvon, Longjumeau, France), which has a slit height adjustment (2 mm - 8 mm) which may be used to further reduce the amount of light reaching the sample. With the removable 2 mm slits in place, the bandpass of the monochromator is 16 nm. The selected band of light enters the sample chamber and is focused through a lens onto the sample cell.

Emitted photons are observed at a 90° angle. An emission shutter protects the very sensitive emission PMT from overexposure if the sample chamber is opened. The emission monochromator (same model) is used to select the desired bandpass such that scattered light does not reach the PMT. The emission PMT is cooled to about -20 °C to reduce dark counts, which occur at a frequency of less than 10 per second under operating conditions. The emission PMT outputs a stop signal to the constant fraction discriminator (CFD).

The iris and slit height adjustment are used to reduce the incident light (if necessary) to ensure that no more than one fluoresced photon is received at the stop PMT per lamp pulse. This is necessary because the TAC can only respond to one stop pulse per start pulse, and by design will respond to the first stop pulse received. Thus if two stop signals are received, the longer delay is always ignored, and the data will become skewed toward the lower end of the timescale. One can calculate by Poisson statistics that if one counts at 2% of the lamp flash rate (for a 30 kHz lamp, 600 counts/sec), approximately 1% of the measured events will be multi-photon events. Some researchers are confident using higher count rates (5% of the flash rate), or use a mathematical correction for this so-called "pulse pileup" error. A detector modification which rejects the first stop pulse if a second stop pulse arrives can be employed to count at rates approaching the flash rate of the lamp. Other modifications to the instrument can allow counting of several stop signals from the same start pulse, but these have not been implemented. All data in the current research were collected at less than 600 counts/sec.

The start PMT signal is sent to a discriminator which rejects any low intensity

pulses from noise or stray light and only passes true lamp pulse signals. The discriminator output signal is sent to the start input of the TAC. This start pulse triggers the charging of a capacitor (as selected by the range multiplier control) by a charging voltage (as selected by the range control).

The stop PMT signal passes through a constant fraction discriminator (CFD), which improves the precision of the measurement of the time at the peak of the pulse. The CFD takes the input pulse and divides the intensity in half to give two signals. One peak is inverted and slightly time-shifted, then the two are added. Now the point in time corresponding to the peak of the input pulse is given by the zero crossing point of the output pulse. The zero cross is a more precise trigger for the TAC than the maximum or some threshold level of the input peak.

The stop pulse passes through a delay system, which allows the TAC capacitor to charge to a significant voltage before the stop pulse is accepted. This is necessary since the time delay between start and stop pulses is often only a few nanoseconds and the early part of the TAC ramp is "decidedly non-linear" [126]. A typical delay time is of the order of one fluorescence lifetime (for pyrene, delays of 120-350 ns were used depending on the MCA and the timescale). The stop pulse triggers the discharge of the capacitor, and the voltage of the TAC output is thus proportional to the time interval between receipt of the start and stop signals.

The TAC output voltage is sent to a multichannel analyzer (MCA) which uses an analog to digital converter circuit to convert the voltage into a channel number, with typical resolution of 8, 9, or 10 bits (256, 512 or 1024 channels). The value stored at the corresponding position in a memory array is incremented by one, thus maintaining a count of how many fluorescence events over the duration of the experiment were recorded with that particular time delay.

3.3.3. Single Photon Counting Data Treatment

The single photon counting apparatus collects a data histogram of photon events counted versus data channel number, which represents the intensity of fluorescence as a function of time. These data must be fit to an appropriate model equation to calculate the

aggregation number and the various rate constants of interest. In this section we will discuss the complexity of this fitting, and several interesting methods of performing the fit.

Deconvolution [127,128]

The data histogram collected by a single photon counting experiment does not precisely represent the true decay profile of the fluorescence. Timing errors do occur, partly due to fluctuations in the electronics, especially in the response times of the PMTs. The main source of distortion is the shape of the flashlamp pulse. All photons in a pulse are not emitted by the lamp at precisely the same time, so that the start time of an observed fluorescence event is not precisely the time reported by the start signal from the lamp PMT. The error in the timing results in a broadening of the measured decay profile. This can be envisioned as the sum of a series of identically shaped decays of different peak intensities which are slightly time shifted relative to each other. This broadening effect is called convolution.

In order to deconvolute the data, a measurement of the shape of the convolution, or the timing errors, is needed. This is accomplished by measuring the profile of the lamp, which will include both the natural pulse shape of the lamp and any inherent timing errors of the instrument. The lamp profile is measured by setting both monochromators to the same wavelength (generally excitation) and using a sample which scatters lamp light directly to the PMT. A rather dense suspension of starch in water is used to scatter light from the less intense H_2 lamp, while a dilute starch suspension or a slightly turbid aqueous solution of about 1% PEO of 5,000,000 molecular weight is a sufficient scatterer of the stronger N_2 signal. An alternate reference reconvolution method, which involves measuring the decay curve of a standard and calculating the convolution based on the known lifetime of the standard, was not used in our study.

The measured decay curve $F_{meas}(t)$ is thus not the true fluorescence intensity as a function of time I(t) but is given by the convolution integral:

$$F_{meas}(t) = \int_0^t L(T)\,I(t-T)\,dT + B \qquad (3.19)$$

where L(t) is the instrumental response function, incorporating the lamp profile and the timing errors in the electronics, and B is the random background level from stray light and

dark counts from the PMT. The background level is measured by delaying the appearance of the peak of the fluorescence to some point after the first 20 or so channels and using those early channels to record the light intensity just before the lamp pulse. Since over 100 probe lifetimes pass between lamp pulses, there is no residual fluorescence intensity from the previous pulse. The observed decay also contains Poisson noise due to the random sampling of the fluoresced photons, the standard deviation of the noise in any channel being equal to the square root of that value.

This integral may be solved by a Fourier or Laplace transform, which turns the integral into a simple multiplication

$$f(s) = l(s)\, i(s) \tag{3.20}$$

where s is the transform coordinate. It is thus easy to solve for i(s), however, the reverse transformation is difficult when one is dealing with discrete data points as in the photon counting experiment. In order to integrate to infinity for the reverse transformation some assumptions must be made about the form of the decay law and a cutoff correction added. Random noise tends to be magnified by the Fourier transform method, though fast Fourier transforms have been applied with more success.

A method more suited to the discrete data of the count histogram is to reconvolute rather than deconvolute. A decay law is proposed for the true fluorescence intensity $I_{fit}(t)$, adjustable parameters are estimated, and this function is convoluted by the measured L(t) to give a proposed $F_{calc}(t)$. This is compared to the measured $F_{meas}(t)$, parameters are adjusted, and the process repeated iteratively until the fit is satisfactory. This is particularly well suited to the discrete data histogram collected by the photon counting method because the integration can be easily performed by a summation over the N data channels

$$F_{calc}(ch) = \sum_{i=0}^{N-1} L(i)\, I_{fit}(ch - i) \tag{3.21}$$

Assessment of the quality of the fit may be performed by several means. Generally the sum of the squares of the residuals are calculated to give a Poisson-weighted chi-squared value.

$$\chi^2 = \sum_{i=0}^{N-1} \frac{[F_{meas}(i) - F_{calc}(i)]^2}{F_{meas}(i)} \qquad (3.22)$$

Plots of these weighted residuals as well as of the autocorrelation function [129] are used as visual assessments of the "goodness of fit".

Nonlinear Least Squares Fitting

The iteration is normally performed by some form of least squares procedure. The most common is the Marquardt algorithm [121], which interpolates between two simple search methods, the steepest descent or gradient method and the Taylor series expansion method, to provide a faster and more reliable convergence. The Taylor series expansion converges rapidly if given good estimates of the fitting parameters, but fails if it has to search for the neighbourhood of the minimum from a distant region which gives little indication as to the direction to the minimum. The gradient method finds the direction of maximum slope (in the multi-dimensional space of the fit parameters) and alters the values of the parameter estimates accordingly to proceed in that direction toward the minimum from a distant starting point. However, since the minimum tends to be contained in a long, curving trough in this problem, the gradient method proceeds in a rather zigzag path with many iterations in order to find the precise minimum. The Marquardt algorithm optimizes the best qualities of these two methods. The gradient search is employed to find the neighbourhood of the minimum, and then the Taylor series method is used to move in smaller steps toward the minimum.

The interpolation is accomplished by a factor λ added to the diagonal elements of the curvature matrix (so named because it represents the curvature of the χ^2 surface in the multi-dimensional search space) which switches the weighting of calculation between the two methods. A high λ favours the gradient equations, while a small λ favours the series expansion. The method calculates χ^2 for the supplied parameter estimates A_i, computes adjustments δA_i to these estimates and then computes a new χ^2. The value of λ is increased or decreased depending on whether χ^2 has increased or decreased, the trial solution A_i is updated if χ^2 decreases (i.e. the new result is better than the old) and a new χ^2 is calculated. The procedure continues until a set number of iterations have been made

(which indicates a failure to find a precise minimum) or until the value of χ^2 is constant within a set error.

An extension of this fitting procedure known as global analysis has been developed by Boens *et al.* [130]. It involves the simultaneous analysis of several decay curves at different quencher concentrations. In this method the quenching, fluorescence, and migration rates are considered to be independent of the quencher concentration, and thus may be optimized simultaneously for the whole series of curves. Results from simulated and real data have been published and demonstrate the effectiveness of the method [131]. Mobilities of both probes and quenchers have been measured [132]. The mechanism of intermicellar migration (which we will discuss further in Chapter 6) is explored [133]. Global analysis appears to be very useful in the study of more complex kinetic systems where these rates of solubilizate entry and exit are significant. However, we have not implemented this capability in our fitting software.

Another interesting approach to fitting fluorescence decay curves measures the distribution of fluorescence lifetimes. In micellar systems, all probes do not experience identical environments at a given time. The micellar size, penetration of water, counterion occupancy and even the orientation and depth of solubilization of each probe molecule is expected to differ. Since the lifetime of the probe is so sensitive to many environmental factors, it is reasonable that in even relatively simple systems a distribution of lifetimes will exist [134]. Siemiarczuk and Ware [135] modeled such systems with a sum of up to 200 exponentials in which the lifetimes are fixed, evenly distributed on a logarithmic scale, and the preexponential factors a_k are solved. Solution by minimization of χ^2 is known as the exponential series method (ESM). The maximum entropy method (MEM) is an alternate procedure in which χ^2 is constrained to be approximately unity and the entropy function

$$S = -\sum a_k \ln\left(\frac{a_k}{\sum a_k}\right) \tag{3.23}$$

is maximized in order to reduce the correlation between the calculated preexponential factors. Data are counted to at least 10^5 counts in the peak channel, to reduce Poisson noise and allow clear resolution of closely spaced multimodal distributions.

Recently this method has been applied to the measurement of micellar size distributions in polydisperse systems [136]. The lifetime distribution is analyzed to recover the micelle size distribution function without any assumptions as to the nature of the size distribution. The experiments studied the transition from spherical to rod-shaped micelles which occurs in SDS or CTAC on addition of salt. The recovered size distributions reveal that the micelles first grow to about double their salt-free size, then form a bimodal distribution of what are likely small spheres and elongated rods. This is an innovative way to analyze the data in such systems, and offers much more information than the earlier method of treating data from polydisperse systems which will be described in Chapter 6. However, many skeptics do not agree that so many preexponential factors may be fit from 256 or even 1024 data points with good reliability, so the method has not gained wide acceptance.

3.3.4. Instrumental Improvements

In this section, we discuss improvements made to our single photon counting instrument, including hardware and software development, to allow measurement of aggregation numbers. The instrument had to be reassembled and tested, and a multichannel analyzer of higher resolution was later added. We first obtained a data fitting program from other researchers, for which we wrote software to convert data files to readable format. Later, we wrote our own software to improve the background correction and allow future customization.

Initial Testing

Before this research project began, the single photon counting apparatus had been disassembled and stored during building renovations. Thus the first task was to reassemble and test the instrument. It took quite some time to discover and correct or optimize many instrumental problems. Light leaks in the optical system which gave rise to high dark count levels were isolated and sealed. A leak in the emission monochromator persists which is corrected by a dark cloth covering the monochromator and light path. The fact that the N_2 line at 337 nm would offer a much more intense excitation than the H_2 continuum was not known at the beginning of the experiments, which meant that many

early trials were counted at low light levels over very long times. The quality of the instrument response function as a function of lamp gas, pressure, electrode spacing and tip shape, and iris and slit height settings was investigated and optimized. The importance of leaving the early data channels open for background subtraction, counting over several probe lifetimes, and avoiding pulse pileup while still accumulating a high number of peak counts to reduce noise were all made clear during the preliminary trials. The setting of time scales and precise calibration using the time calibrator module were learned by trial and error.

Data Fitting Software

The data acquisition computer is equipped with BASIC and FORTRAN software written by Brian Millier for collecting and viewing the data (MCACGA.exe) and for fitting to single (CurvFit.exe) or double exponentials (BiExpo.exe). The fitting software employs the Marquardt algorithm, using the subroutines published by Bevington [137]. These programs do not have the option of fitting to the four-parameter micellar quenching equation to determine micelle aggregation numbers.

Our original solution to this problem was to obtain fitting software (Convol.exe) from Dr. Raoul Zana and Dr. Jean Sturm at the University of Strasbourg, France. This program allows fitting to single or double exponentials as well as the micellar equation, and uses the Marquardt algorithm. It offers the option of deconvolution against the measured lamp profile or input of a zero time channel, as well as input of a fixed value for the fluorescence lifetime. The data plotting routines were incompatible with our available printers, but plots could be generated by a Microsoft Windows screen dump and saved as .PCX graphic files for laser printing by Windows Paintbrush. Sample plots are shown in Figure 3.3. The first plot is a monoexponential fit while the second is an Infelta-Tachiya fit to excimer quenched decay at higher pyrene concentration. Insets A and B are the non-weighted residuals and autocorrelation function respectively.

Figure 3.3: Sample Convol.exe Output Plots.

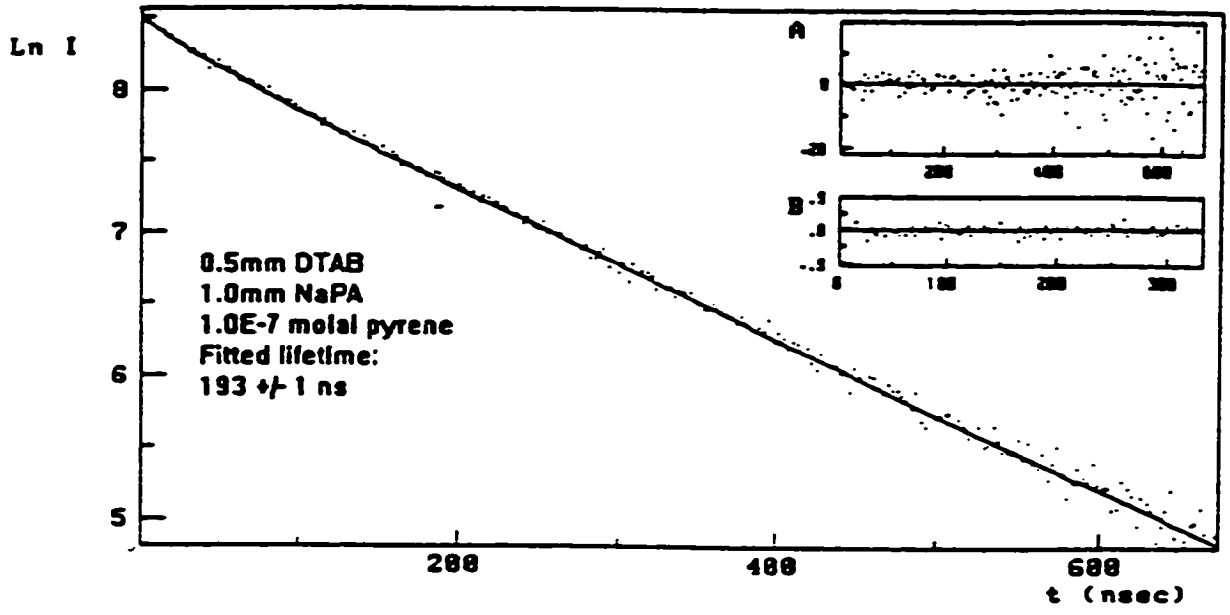

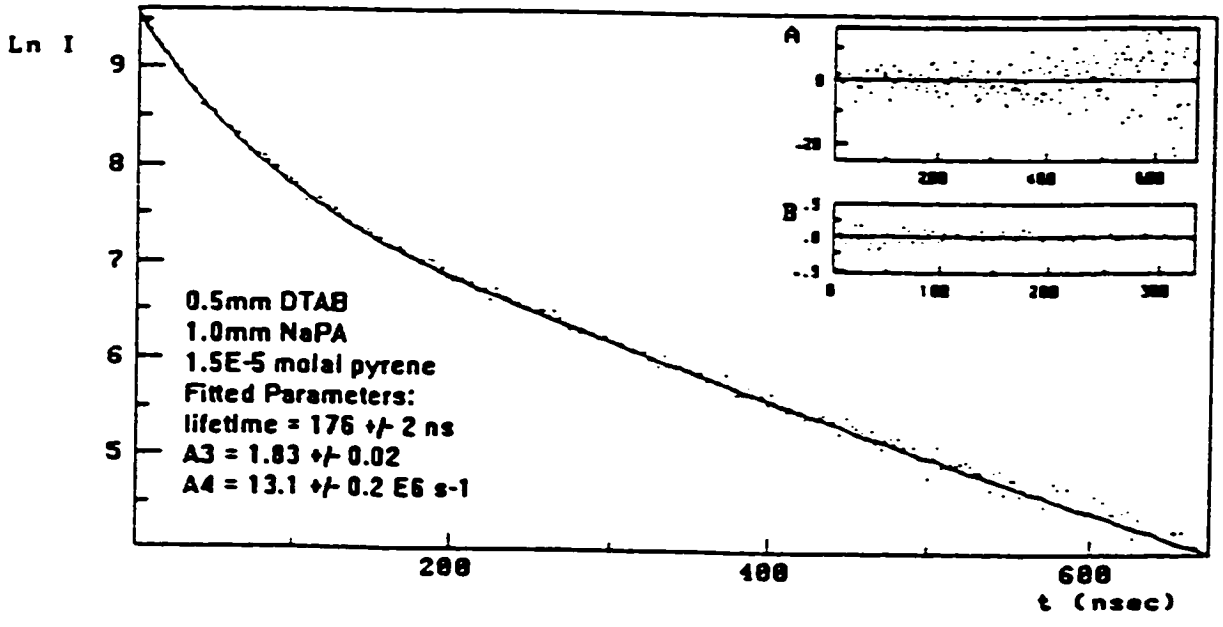

The data acquisition program MCACGA.exe is written in BASIC and outputs two text files, one for the decay curve (Decay.) and one for the lamp profile (Flamp.) and other pertinent data (title, scale in ns/channel, etc.). The text files are then easily input to the FORTRAN fitting routines Curvfit.exe or BiExpo.exe. The Convol software is also written in FORTRAN but requires a precisely formatted input file rather than plain text. A FORTRAN program had to be written to read the text output of the data acquisition program and output a suitable data file for Convol. This program (FileConv.exe) also requests input of the initial estimates of the A_i fitting parameters for the reconvolution, which Convol requires but does not contain a routine to accept them as keyboard input. Making reasonable initial estimates for these variables is rather important in order to achieve proper fits. Several revisions and some communication with Dr. Sturm concerning the variable declarations were required to get the software fully compatible, including the input of the lamp profiles for deconvolution. The fact that the onscreen menus, output and even the variable names are written in French made the "translation" of the data files a twofold problem.

The Convol software supplies clear graphic and text output, and displays a variety of statistical information, of which the χ^2, residuals and autocorrelation function are of greatest use. This software allows fitting to the micellar quenching equation to determine aggregation numbers and rate constants for fluorescence, quenching, and probe migration. In general, this software was able to converge to fit, but in some instances would crash or would not converge after a limiting number of iterations, with little indication of what went wrong. Eventually it was decided that more adaptable software was necessary to add flexibility to the data fitting. In particular, the background noise level measured by the early channels before the fluorescence decay peak was in some data files significantly higher than the total signal in the tail of the decay, calling into question the validity of using these data as a background noise estimate. The ability to fit the background as a variable, as well as to add other correcting terms to the model equation or to fix any of the parameters as a constant was desirable in order to obtain more reliable fits.

The MATLAB programming environment was chosen for the new software for several reasons. MATLAB (The Mathworks, Inc.) is a matrix-based language which lends

itself to easy programming of array and matrix algebra problems. The convolution integral, for example, is a standard MATLAB command, rather than the nested loop which would have to be written in FORTRAN. A tested, robust nonlinear least squares optimization routine, employing the Marquardt algorithm (leasqr.m), as well as the function dfdp.m which estimates the partial derivatives of the trial function with respect to each fitting parameter, were available from the archives of the company website (www.mathworks.com). The author of the most recent updates to the routine, Sean Brennan of Stanford University, brought the existence of the file to our attention and answered several queries regarding the specifics of its use. Thus all that was needed was to write a program (flifit.m) to read the data files, allow input of estimates and setting of fixed parameters, call the leasqr.m subroutine to perform the fit while employing the convolution operation, and produce suitable statistical and graphical output. Sample flifit.m decay curves of similar samples as in Figure 3.3 are presented in Figure 3.4.

The program code is presented in the Appendix. A small modification was necessary to the plotting functions of leasqr.m, also included in the Appendix. The program is run in the form of uncompiled text statements, and thus future users may easily make modifications to improve the input and output, or to add more complicated fitting functions. The fitting functions are present as separate function files, but the main program must be altered in order to handle the estimation of initial parameters for each new file. Currently monoexponential (monoexpo.m), biexponential (biexpntl.m), micellar (micellar.m) and micellar including mobility (mobility.m) decay functions are incorporated into the software. The mobility function was difficult to implement and generally fails to converge because of high covariance of two or more of the fit parameters, so that we in the end employed the graphical fit procedure discussed in Chapter 6. It should generally be simple to create new functions, for example to add an extra exponential term to the micellar function as has been done by several researchers to correct for fluorescent impurities, or to implement a new model equation which may better describe a more complex system.

Figure 3.4. Sample Flifit Decay Curves.

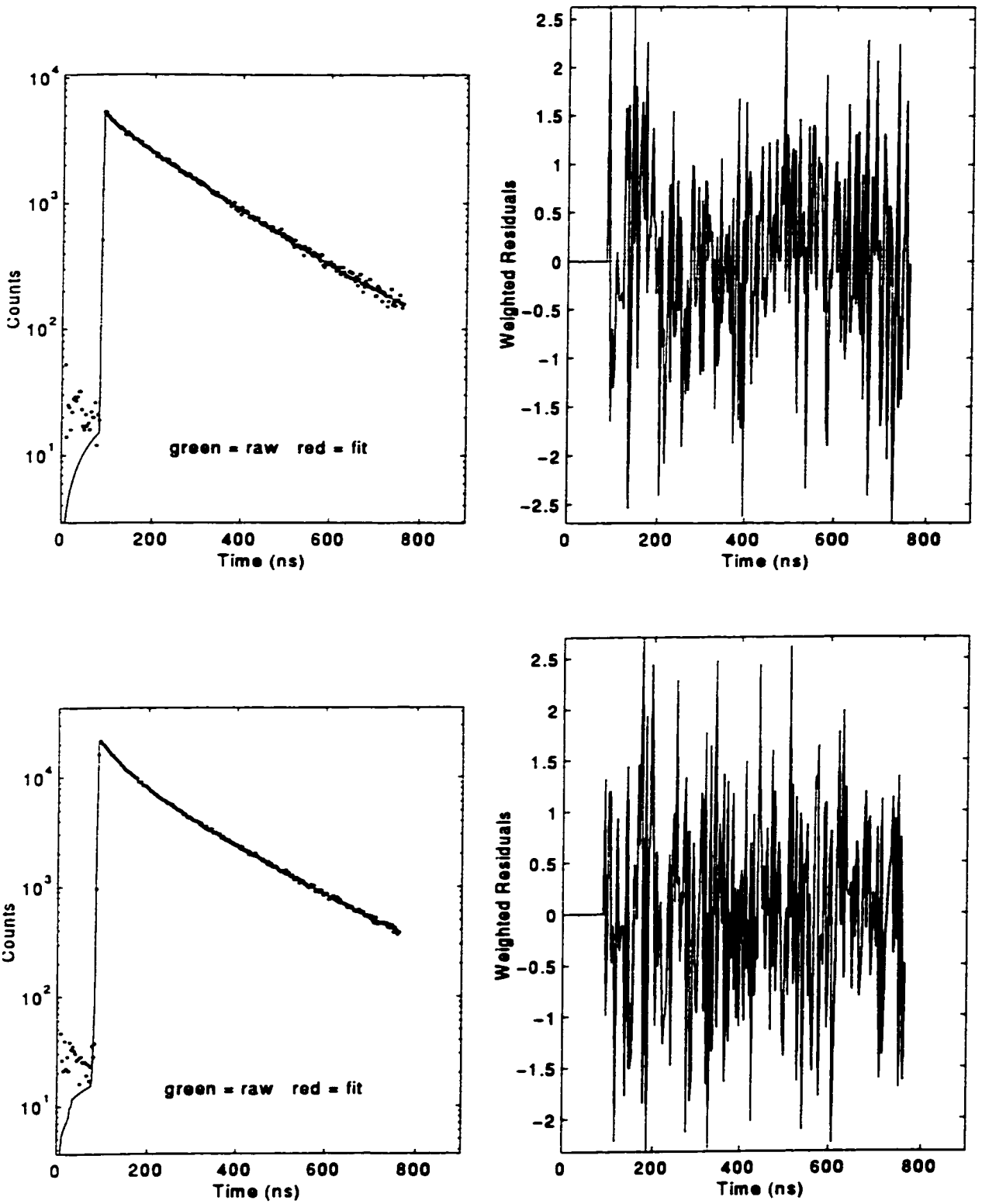

Design and Testing of New MCA Hardware

The instrument at Dalhousie currently has two available MCAs, both designed and built in our electronics shop. There is a 256-channel MCA on a board inside the data acquisition computer, and a 1024-channel MCA in a separate module. The newer, higher resolution MCA requires much longer data collection times to reduce noise and the data transfer to the computer is relatively slow, so that updating the computer display once a second as with the internal MCA is impractical. The higher resolution allows counting to very long timescales to look for the nonlinearity at long times which indicates probe migration. Most of our data were collected on the 256-channel MCA even after construction of the 1024-channel MCA in the interest of speed.

The original MCA used with this instrument is no longer functional. It was replaced by a 256-channel MCA designed and built by Brian Millier and installed on a circuit board in the data acquisition computer. Start, stop, and true start pulses from the timing equipment are sent via three BNC cables to a port at the rear of the computer. An ADC converts the input to a value from zero to 255 and a special processor accumulates the counts and allows fast (9600 baud) reading and writing of data by the host computer. The ADC operates at 30 kHz, which matches the lamp pulse rate.

During our research, a 1024-channel MCA in an external module was built. More channels were desired for better data quality, in particular for counting over longer timescales to observe deviations of the fluorescence lifetime attributable to probe migration or polydispersity effects (see Chapter 6). The MCA receives data from the timing equipment by the same three BNC cables. Communications with the data acquisition computer are via a serial RS-232 cable. The internal circuitry is different than that of the 256-channel MCA because the same components were not available for 10-bit conversion. Unfortunately, the new components and their communication with the host computer suffer for speed, such that data updates both in the computer memory and onscreen are slower. Minor software modifications increased the user-friendliness of the new module. With four times as many data channels, achieving the same number of counts in the peak channel takes four times as long, which is the major drawback to the added resolution. The 10-bit ADC unfortunately is slower than the 30 kHz lamp flash

rate, so that if successive lamp flashes produce stop pulses, the second time delay cannot be assessed. At a 600 Hz count rate, this is not common, so little data is lost, and since there is no correlation between the delay times of fluorescence events from successive pulses, this does not affect the shape of the measured decay.

The new MCA performs well. Some nonlinearity is apparent in the time calibration, but the deviation is less than the resolution of the 256-channel MCA could detect, so it is likely that it is not the fault of the MCA and may even be the fault of the time calibrator. Some SDS and PEO-SDS samples were run on both MCAs with good agreement. In the PEO-SDS data reported in Section 5.2.1, some trials were recorded with each MCA. As there was no apparent need to read the PVP-SDS samples to such detail, the 256-channel MCA was used in order to accumulate data more quickly. In general, the 256-channel MCA was preferred for ease of use and shorter collection times.

3.4. Dipyme Synthesis

In this section we report on the synthesis of a fluorescent molecule which may be used to measure the microviscosity and the micropolarity of micellar environments. This probe is used in our studies reported in Chapters 5 and 7.

Bis(1-pyrenylmethyl) ether (dipyme) [102] was synthesized from 1-pyrenemethanol ($PyCH_2OH$, Aldrich, 98%), adapting the procedure published by Nivaggioli *et al.* [103]. The ether is formed by a Williamson synthesis, a nucleophilic substitution reaction of an alkyl halide with an alkoxide

$$RX + R'O^- Na^+ \rightarrow ROR' + Na^+X^-$$

A portion of $PyCH_2OH$ was converted to 1-(chloromethyl)pyrene ($PyCH_2Cl$) by reaction with thionyl chloride in dichloromethane. The product was evacuated to dryness and after further drying in a vacuum oven was dissolved in dimethylsulfoxide (DMSO). Another portion of $PyCH_2OH$ was converted to the sodium alkoxide ($PyCH_2O^-Na^+$) by reaction with sodium hydride in DMSO, and the $PyCH_2Cl$ solution was added to form the dipyme ether. The resulting solution was mixed with benzene and washed with water to remove DMSO, and dipyme was isolated by dry-column flash chromatography [138] on silica gel with benzene eluent. The synthesis was performed in distilled, dried solvents under

nitrogen atmosphere. The best yield obtained among several trials was 50%.

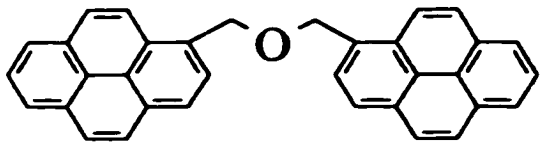

dipyme

Presence of the desired product was evidenced by its strong yellow-green colour due to intramolecular excimer formation, and by electron ionization mass spectroscopy, which showed a strong molecular ion peak at the expected m/z = 446. Major observed fragments included the base peak at m/z = 232 ($PyCH_2OH^{\bullet+}$) and lesser abundances of m/z = 215 ($PyCH_2^+$), 202 ($pyrene^{\bullet+}$), and 216 ($PyCH_3^{\bullet+}$, which was observed by other researchers as the base peak [139]). The odd-electron species are reportedly formed via molecular rearrangement with transfer of a proton while the molecular ion is in an excimer-like conformation [140]. The product was also characterized by ^1H NMR ($\delta \approx$ 8.2 ppm, 18H; δ = 5.4 ppm, 4H, in good agreement with Nivaggioli *et al.* [103]) and purity was evidenced by a narrow melting range (172-173 °C) and a single spot TLC (R_f = 0.81, benzene eluent on silica gel).

3.5. Summary

Numerous fluorescence methods are available which can be used to measure the size, micropolarity and microviscosity of micellar aggregates. While several techniques may be implemented on an ordinary spectrofluorometer, the time resolved fluorescence quenching method requires special instrumentation and fitting procedures. In this chapter, we have discussed the theoretical model of quenching in a micellar system, and the equipment and software necessary for the measurement and fitting of decay curves. We also report the synthesis of an interesting fluorescent probe, dipyme, which we have applied in our studies reported in Chapters 5 and 7.

CHAPTER 4. SIZE EXCLUSION CHROMATOGRAPHY

Size exclusion chromatography is a technique widely used in polymer and protein chemistry to characterize the size of molecules, determine molecular weights and their distributions, and investigate associative and dissociative interactions between molecules. Our interest in size exclusion chromatography was sparked by the need to characterize the molecular weights of new hydrophobically modified polyacrylamides being developed by others in our laboratory. However, we also recognized that this technique could be used to gain new insights on the self-associative interactions between these polymers, as well as the interactions of these and other polymers with surfactants. In this chapter our development of methods toward these goals is discussed. First, some background information is presented on size exclusion, the mechanisms of analyte retention, and the relationships between polymer size and molecular weight. Previous studies of polymer-surfactant interactions by size exclusion techniques in the literature are surveyed. We discuss common modes of detection used in SEC, with special attention to the refractive index and light scattering detectors employed in our own study and how the data are used to calculate radius and molecular weight averages. Then our experimental setup, including adaptation of the method to study polymer-surfactant interactions in surfactant eluent is described. Experimental results on polymers and P-S systems are presented in Chapters 5 and 7.

4.1. Introduction

The theories and techniques of size exclusion chromatography have been the subject of numerous books and reviews [141-147]. When a sample is passed through a column filled with a porous material, analytes of greater size are excluded from the pores and elute more rapidly than analytes small enough to enter the pores. The effect was first reported by Porath and Flodin [148] who referred to the separation as gel filtration, as the gel was eluted by gravity in a vertical column. Their gels, known as Sephadex, were crosslinked dextrans suitable for use with aqueous solutions, and became commonly used to separate proteins from smaller molecules or to separate mixtures of proteins by molecular weight. Later, crosslinked polystyrene gels suitable for use with organic

solvents were developed [149] and a similar method known as gel permeation chromatography (GPC) became widely used to determine molecular weight distributions of industrial polymers. These gels were more rigid, allowing the use of HPLC pumps and closed columns, which gave a speed advantage over the gel filtration chromatography (GFC) columns which were open and eluted slowly under hydrostatic pressure. The resolution of GFC was insufficient to give good characterization of molecular weight distributions of water soluble synthetic polymers. High pressure size exclusion chromatography (HPSEC) in aqueous media did not appear until about twenty years ago, as a result of the development of rigid hydrophilic gels based on silica or crosslinked polymers. Media have been improved over the years such that today's packings are of much smaller particle size (less than 10 μm), sufficiently rigid to withstand pressures of 300 to 3000 psi, and offer separation efficiencies exceeding 50,000 plates per meter.

The mobile phase in a size exclusion column is divided into two types, the imbibed or internal volume inside the pores (V_i) and the void or external volume outside the pores (V_o). The internal volume is the source of the size separation and is equivalent to the stationary phase volume of regular HPLC. A very large solute will have an elution volume V_e equal to V_o whereas a very small solute will elute at the total mobile phase volume $V_t = V_o + V_i$. Depending on the detection method, various calibrants have been used to determine these volumes, in particular D_2O has proven effective as a small noninteractive solute amenable to RI detection [150]. The distribution coefficient K_{SEC}, which may be defined as the ratio of the concentrations of solute in the pore volume and the interstitial volume, determines the elution volume of the solute by the relation

$$V_e = V_o + K_{SEC} V_i \tag{4.1}$$

Interactions of the solute with the packing surface (whether adsorptive or repulsive) add additional terms to this relation and are referred to as secondary or nonideal retention mechanisms. Under normal conditions, the distribution approaches thermodynamic equilibrium and may be related to the standard Gibbs energy difference $\Delta G°$ between the phases

$$\Delta G° = \Delta H° - T\Delta S° = -RT \ln K_{SEC} \tag{4.2}$$

As the enthalpy difference between the two phases is small, solute distribution is mainly

entropy driven, and

$$K_{SEC} = e^{\Delta S^{\circ}/R} \tag{4.3}$$

Solutes in the pores experience a restriction in mobility and thus a decrease in entropy, making it unfavourable for larger molecules to enter the pores. The mean pore radius of column packings is typically given in Angstrom units and is determined by electron microscopy, or from measurements of pore volume (from mercury penetration experiments or the SEC calibration curve) or pore surface area (determined by gas adsorption via the Brunauer, Emmet and Teller equation). The characteristics of the gel when swollen in solution can differ substantially from measurements made on dry gels. Solutes of sizes more than an order of magnitude smaller than the mean pore radius still exhibit some exclusion, for entropic reasons as well as due to the shapes of the pores and breadth of their size distribution.

4.2. Polymer Size and Molecular Weight Relationships

The dimensions of polymer molecules in solution may be expressed in several ways. The root mean square radius or "radius of gyration" R_g is the integration over all mass elements dm of a molecule of mass M at a distance r from the centre of gravity of the molecule

$$R_g^2 = \frac{1}{M}\int r^2 dm \tag{4.4}$$

The radius of gyration reflects the conformation and the density of the molecule, as a more swollen coil will have a larger radius. The radius of gyration may be determined from the variation of light scattering intensity with scattering angle. Another measure of radius is the root mean square end-to-end distance $\langle r_e^2 \rangle^{1/2}$ which measures the average separation between the two ends of the polymer chain, and is greater than R_g by a factor of $\sqrt{6}$ for unperturbed coils and $\sqrt{7}$ for macromolecules in a good solvent [151]. The hydrodynamic radius R_h, determined by diffusion measurements, is the equivalent radius of a sphere with the same frictional coefficient f as the particle [152] according to the Stokes equation

$$f = 6\pi\eta_o R_h \tag{4.5}$$

where η_o is the viscosity of the solvent. The hydrodynamic radius of a randomly coiled

linear polymer is smaller than R_g by a factor of about 0.77 [153].

As species are separated according to their sizes, it would be reasonable to assume that in the absence of other effects, the elution volume of any polymer molecule of any structure would be the same as that of any other molecule of the same volume (and for similar shapes, the same radius). In order to derive the desired molecular weight values from size measurements, a relationship between molecular weight and radius is needed. Traditionally, viscosity measurements have been employed. Measurement of the specific viscosity η_{sp} of a solution of a spherical colloid yields the volume fraction ϕ of solute [154] from the Einstein relation

$$\eta_{sp} = (\eta/\eta_o) - 1 = 2.5\phi \tag{4.6}$$

where η is the viscosity of the solution. The volume fraction may be expressed in terms of the partial molar volume $\bar{v}$ as shown

$$\phi = \frac{c\bar{v}}{M} \tag{4.7}$$

where c is the polymer concentration in mass per unit volume and M is the polymer molecular weight. Then in the limit of infinite dilution an expression for the intrinsic viscosity $[\eta]$ is derived

$$\lim_{c\to 0}\frac{\eta_{sp}}{c} = [\eta] = 2.5\frac{\bar{v}^\circ}{M} \tag{4.8}$$

where $\bar{v}^\circ$ is the partial molar volume of polymer at infinite dilution, and is equivalent to the product of Avogadro's number N_A and hydrodynamic volume V_h

$$V_h = \frac{4}{3}\pi R_h^3 \tag{4.9}$$

The intrinsic viscosity of solutions of a given polymer is logarithmically related to the molecular weight of the polymer by the empirical Mark-Houwink equation

$$\log [\eta] = \log K + a \log M \qquad \text{or} \qquad [\eta] = K M^a \tag{4.10}$$

where K and a are experimentally determined constants characteristic of the polymer. Combining equations, we find that the radius of the polymer coil (whether expressed as R_h or R_g) is proportional to $M^{(a+1)/3}$. For a randomly coiled polymer in a theta solvent (where the free energies of solvent-solvent, solvent-polymer and polymer-polymer interactions are

the same) a has a value of 0.5, and experimental values of a usually range from 0.5 to 1.0. The exponent relating radius to molecular weight is thus typically 0.5 to 0.6.

From this derivation we see that the product $[\eta]M$ is proportional to the hydrodynamic volume

$$[\eta]M = \nu N_A V_h \tag{4.11}$$

Here N_A is Avogadro's number and ν is known as the Simha shape factor, which has the value 2.5 for spherical molecules and larger values for elongated molecules. Thus if the elution volume (or K_{SEC}) of a polymer depends solely on the polymer size, then a plot of $[\eta]M$ versus V_e or K_{SEC} should be identical for any spherical polymer on a particular column under identical conditions. This is commonly used in SEC and referred to as universal calibration [155,156], "universal" because a column calibrated using a series of polymers of known molecular weights can then be used along with viscometric measurements to characterize the molecular weights of essentially any other polymer. However, secondary interactions of the polymer with the column such as adsorption, ion exclusion, or other non-size-exclusion effects may render this calibration invalid.

The assumption of an identical relationship of radius to molecular weight for both the calibration polymer and the samples also may not hold in aggregating systems such as polymer-surfactant systems. A surfactant micelle is compact; it contains almost no water and is much smaller than the same mass of well solvated, randomly coiled polymer. The expansion of the polymer coil by bound surfactant depends on the repulsions between the charged micelles, and for example screening by added salt may even result in a smaller radius for the complex than for the native polymer, as seen in the neutron scattering study of Cabane and Duplessix on PEO-SDS in 0.4 M NaBr [16]. Thus the size of a P-S complex will not necessarily be the same as the size of a polymer coil of the same total molecular weight. In the next section, we discuss previous examples of the application of size exclusion chromatography to the study of P-S interactions, none of which have been able to use elution volumes as a quantitative measure of complex size.

4.3. Application to Polymer-Surfactant Systems

Size exclusion chromatography (SEC) is widely used to characterize the size and

size polydispersity of macromolecules. Aggregation phenomena have also been studied by SEC, particularly the binding of ligands to proteins [157] and surfactant micellar equilibria [158]. Hummel and Dreyer [159] introduced the use of a low-pressure gel column equilibrated with the ligand in the eluent for the study of protein-ligand binding. A sample of macromolecule (or macromolecule and ligand) was injected onto the column, with elution of a peak for the complex and a void for the bound ligand. Using a concentration-sensitive detector, integration of the void yielded a quantitative measure of the amount of bound ligand.

Despite the long history of application of this technique to other associating systems, little work has been done on polymer-surfactant (P-S) interactions. Sasaki *et al.* [160] applied PEO-SDS samples to a low-pressure Sephadex G-100 column and eluted with water. Conductometric detection was used to obtain elution curves which showed broad plateaus, whose heights were interpreted as the fractions of SDS present as free monomers, bound micelles, and free micelles in the original sample. From these data the authors constructed a phase diagram for the system which resembles that later reported by Cabane and Duplessix [15], showing a critical aggregation concentration (cac), then bound complexes, followed by a second critical concentration for the formation of coexisting free micelles. They calculated a binding ratio which increased with decreasing polymer concentration to a maximum of about 0.4 molecules SDS per EO unit of the polymer, comparable to that measured by other methods (See Table 5.1). The group of Wyn-Jones used the same method to study interactions of SDS with poly(vinylpyrrolidone) [161] and with poly(propylene oxide) [162]. These authors observed peaks rather than the plateaus reported by Sasaki *et al.* [160]. However, we note that Sasaki *et al.* used very large volumes of sample relative to the total mobile phase volume of the column. As well, commercial PVP samples tend to be highly polydisperse, and would elute as broader peaks than the relatively monodisperse 6000 g/mol PEO used by Sasaki *et al.*, and the PPO sample used [162] was of low molecular weight (1000 g/mol) and thus may behave more like a solubilizate than a bound polymer. Based on the appearance of two and then three peaks at increasing surfactant concentrations, Wyn-Jones and co-workers estimated the critical concentrations for polymer-surfactant binding

and the appearance of free micelles.

Szmerekova *et al.* [163] were the first to apply high pressure size exclusion chromatography (HPSEC) with refractive index (RI) detection to a P-S system. They studied complexation of PEO of very low molecular weight (1200 g/mol) with SDS and with a nonylphenol polyglycol surfactant. Although their peaks and troughs appear poorly separated, they reported saturated binding with 0.29 mol SDS per mole EO unit and 0.12 mol per mole EO unit for the nonionic surfactant.

Veggeland and Austad [164] investigated HPSEC of complexes of PEO 20000 with SDS as a model for comparison with a xanthan-anionic surfactant complex used in tertiary oil recovery. They used refractive index detection, and from the area of the surfactant void determined a saturation binding ratio of 0.31 mol SDS per mole EO unit in 0.5 wt% SDS and 0.49 mol SDS per mole EO unit in 0.5 wt% SDS with 0.1 wt% NaCl, in good agreement with other methods. They also observed a small void when using NaCl mobile phase which they attributed to binding of 0.2 mol NaCl per mole SDS bound to the complex, due to the Donnan effect. Veggeland and Nilsson [165] used HPSEC to demonstrate the associative and dissociative interactions of different anionic surfactants with PEO 20000 and xanthan. Complexation with PEO ceased for alkylethoxysulfonates containing more than two EO groups, and no alkylethoxysulfonates would complex with xanthan. The separation of a surfactant peak rather than a trough from an anionic xanthan was ascribed to an osmotic effect. Dissociative behavior was also observed by Taugbøl *et al.* [166] between xanthan and an alkyl propoxyethoxysulfate surfactant.

The few studies in the literature show the potential of this method for characterizing polymer-surfactant interactions, both associative and dissociative, and for screening unknown P-S systems for possible interactions. Binding ratios have been calculated from the void peak area, however only qualitative information about the size or molecular weight of the complexes has been deduced from elution volumes.

4.4. Detector Systems

Some of the more traditional modes of detection in SEC are UV, light scattering, and viscometry, while more recently membrane osmometry, FTIR, MALDI MS and others

have been adapted for certain applications [167]. The detector most amenable to the majority of samples and solvents is a refractometer. The refractive index n of a medium is defined as the ratio of the speed of light in vacuum to the speed of light in that medium. As any medium impedes the propagation of light waves relative to vacuum, the refractive index is always greater than unity. For example, the refractive index for water as calculated from the empirical formula of Schiebener *et al.* [168] is 1.328376 ± 0.000015 at 40°C and 690 nm incident light.

The refractive index of a solution depends linearly on the concentration of the solute, so long as neither absorbs light significantly at the wavelength of interest. The refractive index increment dn/dc (units mL/g when concentration is expressed as g/mL) of a solute depends on the solvent, temperature, the wavelength of incident light, and in the case of polymers may also depend on molecular weight. Measured values for polymers, proteins, and other solutes in a variety of solvents have been tabulated at several commonly used wavelengths [169].

The refractive index change for a dilute solution is quite small (~ 10^{-6} RI units), less than the precision of devices such as the Abbé refractometer used to measure refractive indexes of solvents or concentrated solutions. Greater precision is possible by several interferometric methods which measure the relative refractive index difference between a sample and reference cell. The Optilab detector used in this work uses the shearing interferometer principle [170-172]. Light from a filament lamp passes a plane polarizer oriented at -45° to the horizontal. This incident light of amplitude A_o is split by a Wollaston prism into two beams polarized at 90° relative to one another, which pass through the sample and reference cells. For light passing through any medium, the frequency of oscillation of the waves remains constant but the wavelength λ of the light in the medium of refractive index n differs from the wavelength in vacuum λ_o by the relation

$$\lambda = \lambda_o / n \tag{4.12}$$

Any difference in refractive index Δn between the sample and reference cells thus results in a phase difference φ between the two beams

$$\varphi = 360\ (l / \lambda_o)\ \Delta n \tag{4.13}$$

where l is the pathlength of the cell. The out of phase beams are recombined by another

Wollaston prism followed by a quarter wave plate, producing two circularly polarized beams of opposite rotations, which interfere to give a linearly polarized beam oriented at an angle $\varphi/2$ relative to the original source beam. This beam passes a plane polarizer oriented at $90° - \beta$ to the first, then a filter which selects the desired wavelength of light (in our case, 690 nm), and finally strikes a photomultiplier which reads a resulting amplitude A given by

$$A = A_o \sin(\beta + \varphi/2) \tag{4.14}$$

This response, relative to the instrument calibration constant, is used to measure the refractive index change Δn. The refractometer was calibrated using solutions of optical grade NaCl (99.99%, Aldrich) with a known refractive index increment (dn/dc) of 0.172 mL/g at 690 nm and 40 °C.

The increasingly popular use of multiple detectors in SEC improves polymer characterization by combining two or more types of complementary data. The coupling of a light scattering detector with a concentration detector (RI, UV etc.) or a viscometer has been used to provide measurement of molecular weights and radii without reference to elution volume. In our research we couple a miniDAWN three-angle laser light scattering detector with an Optilab DSP interferometric refractometer, both from Wyatt Technology Corporation. We will now briefly discuss light scattering theory and the equations used by the ASTRA version 4.2 software (also from Wyatt) to determine the radius and molecular weight averages of the polymer samples [171,173,174].

The horizontal angular dependence of the intensity of vertically polarized light scattered by a polymer solution was described by Zimm [175,176] by the equation

$$\frac{R_\theta}{K^* c} = M_w P(\theta) - 2A_2 c M_w^2 P^2(\theta) + \ldots \tag{4.15}$$

where R_θ is the excess Rayleigh ratio, a measure of the intensity of scattered light at angle θ, c is the polymer concentration in solution, M_w is the weight-average molecular weight of the polymer, and A_2 is the second virial coefficient. The optical constant K^* is defined as

$$K^* = \frac{4\pi^2 n_0^2}{\lambda_0^4 N_A}\left(\frac{dn}{dc}\right)^2 \tag{4.16}$$

where n_0 is the refractive index of the solvent at the incident radiation wavelength λ_0, N_A is Avogadro's number, and dn/dc is the differential refractive index increment with respect to concentration of polymer in the solution. The form factor $P(\theta)$ may be represented as a truncation of a simple power series in $\sin^2(\theta/2)$ [177]

$$P(\theta) = 1 - \frac{R_g^2}{3}\left(\frac{4\pi n_0}{\lambda_0}\right)^2 \sin^2(\theta/2) + \ldots \tag{4.17}$$

where R_g^2 is the z-average mean square radius of the polymer molecules. The radius can thus be calculated from the slope of a plot of the scattering versus $\sin^2(\theta/2)$.

The method used to fit the miniDAWN data involves a "Zimm plot" of K^*c/R_θ versus $\sin^2(\theta/2)$, which is the inverse of Equation 4.15. The Rayleigh-Gans-Debye approximation in the limit of small polymer concentrations (as is the case for eluted SEC samples) yields the equation

$$\frac{K^*c}{R_\theta} = \frac{1}{M_w P(\theta)} + 2A_2c \tag{4.18}$$

To determine polymer molecular weight, the scattering intensities at several angles are extrapolated to give the Rayleigh ratio at zero angle R_0.

$$\frac{1}{M_w} = \frac{K^*c}{R_0} - 2A_2c \tag{4.19}$$

The value of A_2 may be determined by a batch measurement (direct sample injection without chromatographic separation) over a range of polymer concentrations. However, in SEC detection the polymer concentration is so small that the effect of A_2 on the molecular weight determination is usually negligible. The mean square radius is determined from the slope m_0 of the Zimm plot (whose value is negative).

$$R_g^2 = -\frac{3\lambda^2}{16\pi^2} M_w m_0 \tag{4.20}$$

The miniDAWN detector measures the intensity of scattered light at three angles (nominally 45°, 90° and 135°; the true angles differ slightly due to the difference between the refractive indices of the solvent and the glass cell) at a data collection rate of 8 Hz. When used as an SEC detector, only one data point is kept every 1-2 seconds in order to

reject noise. As the noise in scattering intensity is mostly positive, the lowest signal voltages are recorded. The weight average molecular weight M_i and the mean square radius R_i^2 of the sample at each data point are determined by the Zimm method. The concentration of polymer c_i (in g/mL) at that data point is determined using the refractive index detector. By summing the data over hundreds of points collected across an eluted peak, the number-, weight- and z-average molecular weights and radii are calculated.

$$M_n = \frac{\sum c_i}{\sum \frac{c_i}{M_i}}, \quad M_w = \frac{\sum (c_i M_i)}{\sum c_i}, \quad M_z = \frac{\sum (c_i M_i^2)}{\sum (c_i M_i)} \tag{4.21}$$

$$R_n^2 = \frac{\sum \left(\frac{c_i}{M_i} R_i^2 \right)}{\sum \frac{c_i}{M_i}}, \quad R_w^2 = \frac{\sum \left(c_i R_i^2 \right)}{\sum c_i}, \quad R_z^2 = \frac{\sum (c_i M_i R_i^2)}{\sum (c_i M_i)} \tag{4.22}$$

The miniDAWN must be calibrated in order to calculate the excess Rayleigh ratios from the raw detector voltages. We used HPLC grade toluene (99.8%, Sigma-Aldrich) which shows strong isotropic scattering and for which the known value of R_{90} (9.7801×10^{-6} at 690 nm) is stored in the ASTRA software. The responses of the 45° and 135° photodiodes were then normalized relative to the 90° signal by injecting a sample of radius less than 10 nm, sufficiently low to scatter isotropically, typically a poly(ethylene glycol) of MW 2000 to 8000 or monomeric bovine serum albumin (98%, Sigma). The volume delay of the tubing connections between the two detector cells must be calibrated in order to synchronize the data. Since the RI signal is proportional to concentration and the light scattering signal proportional to the product of concentration and molecular weight, the maximum response will occur at different elution volume except for a highly monodisperse polymer ($M_w \approx M_n$). Special PEO standards of low polydispersity ($M_w/M_n < 1.1$) were used for this calibration.

4.5. Experimental

In this section we give further details about the equipment used in our size exclusion studies, including a homebuilt eluent reservoir. Typical experimental conditions and details of sample filtration are included.

Eluent Reservoir

The adaptation of the chromatography system included a homebuilt reservoir specially designed to allow degassing and fine filtration of surfactant mobile phases. A commercially available multivalve chromatography reservoir might be similarly adapted to meet these specifications. Helium sparging, bulk prefiltration and solvent pick-up adapters commonly used in chromatography cause foaming of the eluent. The design shown in Figure 4.1 permits vacuum degassing without loss of foam. When the vacuum valve is opened to degas the eluent, foam fills the headspace of the vessel. The valve is closed, helium is applied through another valve to break the foam, and the cycle is repeated until the foam produced is open and fragile. The eluent is blanketed with helium during use, with the excess pressure vented through a trap (not shown) which prevents air from entering the vessel. Solvents for light-scattering detection, especially polar solvents such as water, must be meticulously filtered, so the eluent is drawn from the reservoir through up to three disposable syringe tip filters in series, usually a 0.2 μm nylon filter followed by 0.1 and/or 0.02 μm Anotop Plus 25 mm inorganic membranes. Several litres of eluent at flow rates up to 1 mL/min can be supplied before fouling the 0.02 μm filters. A bubble trap at the top of the reservoir helps to prevent gases from entering the pump. In some experiments a 0.2 μm Aqueous IFD (Whatman) was used between the reservoir and the pump to provide backup filtering, degassing and bubble-trapping.

Figure 4.1. Design of a Reservoir for Chromatography with Surfactant Eluent.

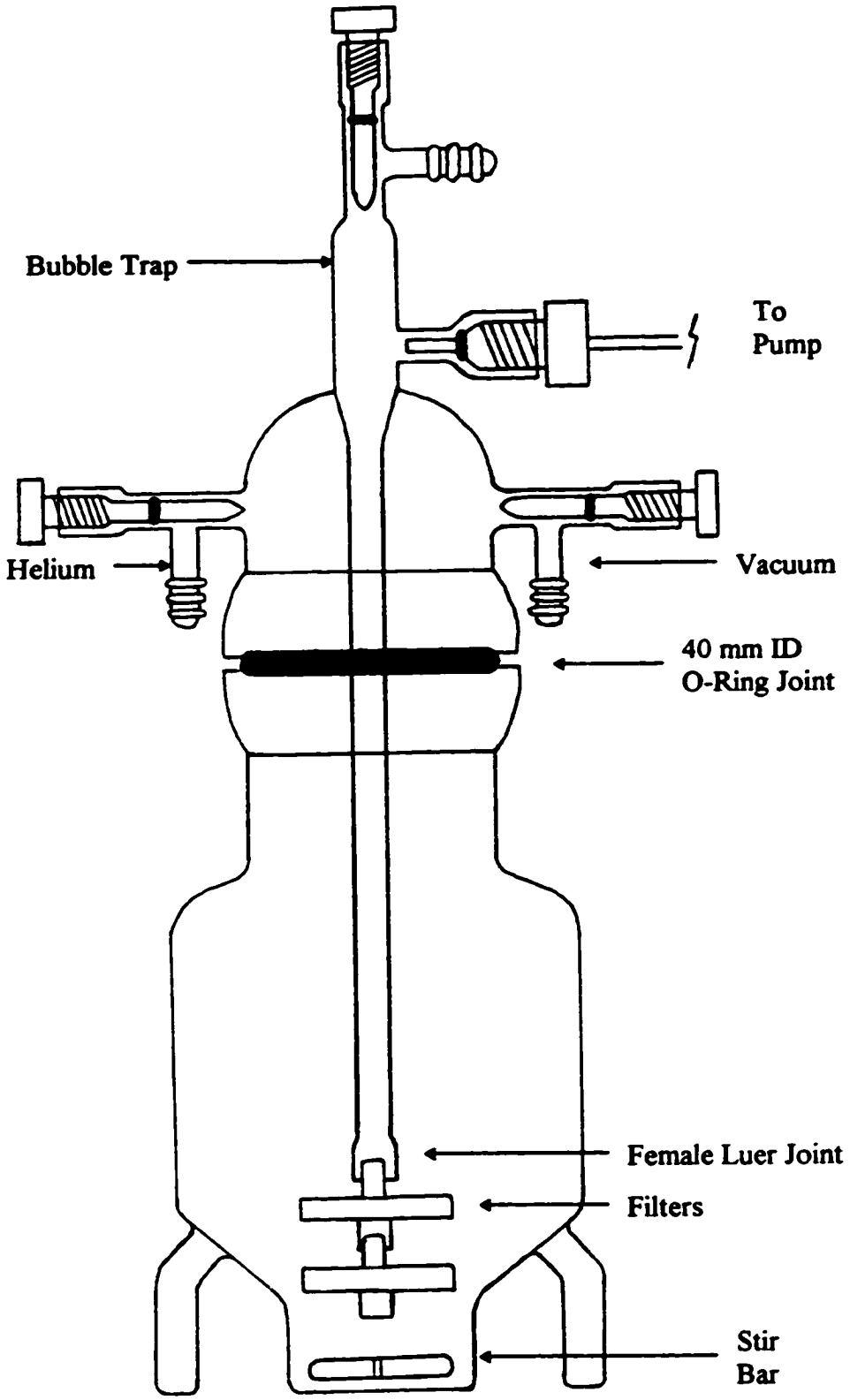

Size Exclusion Chromatography

The eluent was drawn by a Tracor 995 or Waters 600E HPLC pump and passed through an SSI pulse dampener and 0.5 μm injector prefilter. Samples were loaded via a Rheodyne 7125 injector using Hamilton gastight luer-tip syringes of at least twice the loop volume and, where appropriate, Whatman Anotop 13 mm syringe tip filters (0.1 or 0.2 μm pore size). Sample concentration and loop size were varied over the range of polymer molecular weights in order to optimize the response of both detectors. A typical injection was 100 μL of a 3 mg/mL polymer sample.

Progel-TSK PW_{XL} size exclusion columns (300 × 7.8 mm, Supelco) were used; the typical configuration was an ultra-low dead volume 0.5 μm precolumn filter (Upchurch) followed by a PW_{XL} guard column, a G3000 column (200 Å pores, rated for separation of PEO MW < 50 kD) and a G5000 column (1000 Å, rated for MW of 4-1000 kD). Trials were also run with either column alone. Flowrate was maximized while keeping column backpressure below the manufacturer's recommendation (600 psi with the low MW column in use, 300 psi if only the high MW column was used); the typical flowrate was 0.6 mL/min.

The detector system was a miniDAWN three-angle laser light scattering detector, followed by an Optilab DSP interferometric refractometer (Wyatt Technology Corporation), both equipped with 690 nm light sources. Data were collected and processed using ASTRA for Windows version 4.2 software from Wyatt Tech. The chromatography columns and the miniDAWN operated at room temperature (about 20 °C), while the refractometer was thermostatted at 40 °C. We recognize variation in column temperature as a possible source of random error in elution volumes.

Refractometry

Refractive index increments of several polymers and SDS were measured by routing the injector directly to the Optilab detector. A large sample loop (0.99 mL) was used to inject up to 20 samples at increasing concentrations into the system at a typical flowrate of 0.7 mL/min, producing a series of plateaus. DNDC for Windows version 5.00

software (Wyatt) was used to measure plateau values of the relative refractive index of each sample and to compute dn/dc values.

4.6. Data Treatment in P-S Systems

The adaptation of SEC to polymer-surfactant systems required some additional considerations of the data. In particular, the effect of bound surfactant on the value of dn/dc of the polymer had to be accounted for. These calculations are discussed briefly below.

Binding ratios (β, expressed as moles surfactant bound per mole repeat unit of polymer) were determined from the masses of bound surfactant $m_{s,b}$ and polymer m_P using the following formula:

$$\beta = \left(\frac{m_{s,b}}{m_P}\right)\frac{M_P}{M_s} \tag{4.23}$$

where M_P and M_s are the molar masses of the polymer repeat unit and of the surfactant. The mass of polymer was determined from the concentration and loop volume of the injected sample, requiring the assumption of 100% polymer elution. The mass of bound surfactant could be determined by integrating the area of the surfactant void, or in cases where this was not possible, from the difference between the mass of complex (determined by integrating the complex peak) and the mass of injected polymer.

The dn/dc of a given molecular weight of polymer usually differs significantly from that of the surfactant, so that the dn/dc of the polymer-surfactant complex is expected to have an intermediate value between that of the free polymer and the surfactant micelles. We did not measure the dn/dc of the complexes because of the difficulty in correcting for the surfactant background, which would not be constant at increasing polymer concentration. An average dn/dc based on the weight fractions W_P and W_S of the two components in the complex, as has been used in estimating the dn/dc of copolymers [178], was used to measure the mass of complex from the RI peak, and the molecular weight by light scattering.

$$dn/dc_{complex} = W_P\, dn/dc_P + W_S\, dn/dc_S \tag{4.24}$$

For this calculation, the weight fractions of polymer and surfactant in the complex peak

are estimated based on the known amount of polymer injected and the measured amount of bound surfactant. Any variation in this figure due to variation of complex stoichiometry across the peak is not expected to be significant and was not accounted for. This correction was applied in the calculations of complex molecular weights, as well as binding ratios determined from the mass of complex eluted.

4.7. Summary

In this chapter size exclusion chromatography has been discussed in the context of our adaptations to the method for the study of polymer-surfactant complexes. As the separation mechanism is based on size, not molecular weight, values of polymer molecular weight are best determined without reference to elution volume. This is especially true for a polymer-surfactant complex, whose radius is not expected to be the same as that of a randomly coiled polymer of the same molecular weight. No study in the literature of polymer-surfactant complexes by a size exclusion technique has reported quantitative molecular weight information about the complexes based on elution volumes. We therefore applied a multi angle laser light scattering detector in series with a differential refractometer in order to better characterize the complexes. We also designed a special eluent reservoir to provide efficient degassing and very fine filtration of a surfactant mobile phase without the problems of foaming or loss of eluent. This technique was applied to the PEO-SDS system as discussed in Chapter 5, and to the HPAM-SDS systems discussed in Chapter 7.

CHAPTER 5. INTERACTIONS OF SDS WITH PEO AND PVP

The interactions of sodium dodecyl sulfate (SDS) with polyethylene oxide (PEO) have probably been more widely studied than any other polymer-surfactant system. This makes the PEO-SDS system a good choice for testing new methods and for verifying the performance of known methods. However, much is still uncertain about the nature of the interactions in this system; in particular there is some debate about the role of the counterion and the balance of forces which cause the uncharged polymer to be so strongly bound. The relative lack of interaction of nonionic polymers with cationic surfactants suggests that there is something specific taking place in this system, which has resulted in such postulates as crown ether-like cation complexes or slight positive charges on ether oxygens. We chose to investigate this system mainly to test and verify our methods, but also in order to improve our understanding of the structure of these aggregates. The well-known polyvinylpyrrolidone (PVP)-SDS system was also studied as a comparison.

This chapter will begin with some background information on what is known about the structure of PEO-SDS and PVP-SDS aggregates, in particular aggregation numbers, the "phase diagrams" of the binding interactions, and molecular weight effects, as well as proposed explanations of the driving forces involved. We will then discuss our investigations by fluorescence spectroscopy which provide information about the aggregation number, micropolarity and microviscosity of these aggregates, followed by a study of the binding interaction as a function of PEO molecular weight using size exclusion chromatography. Finally, we will combine these results to make some conclusions about the overall nature of the complexes.

5.1. Background

The study of polymer-surfactant interactions was preceded by much research into the interactions of proteins with surfactants, especially sodium dodecyl sulfate which had been found to denature proteins [179]. This and the common industrial use of sodium alkyl sulfates as alternatives to alkanoate soaps have led to SDS being considered the typical anionic surfactant for studies of many aspects of surfactant chemistry including P-S complexes. The earliest studies of polymer-surfactant complexes involved anionic

surfactants (including SDS) and nonionic polymers which were insoluble in water, and in some cases, insoluble in most solvents [68,180]. Solubilization was found to persist on dilution below the surfactant cmc, indicating that the interaction was unlike the solubilization of small organic molecules into micelles. The polymers behaved as anionic polyelectrolytes in electrophoresis measurements, migrating toward the anode. The adsorption of surfactant increased with polymer hydrophobicity, suggesting that hydrophobicity rather than ionic interaction was the driving force for binding. Botré et. al [35] noted the ability of the bound complex to sequester Ca^{2+} counterions like a polyelectrolyte, and proposed that micellar clusters might be formed as had been suggested for protein-surfactant complexes [181,182]. The electrophoretic mobility of PVP-SDS complexes was found to be independent of polymer molecular weight, and comparable to that of SDS micelles, suggesting that the complex is a "necklace" of bound micelles [12].

Further evidence for the micellar nature of the complexes is the existence of critical concentrations for the start of binding, and for saturation of binding and/or formation of free micelles. Jones [10] determined by conductance measurements that the formation of bound micelles in the PEO-SDS system commences at a critical concentration which is lower than the cmc of SDS and decreases slowly with polymer concentration. A second transition point was observed which increased with polymer concentration, which was postulated to be due to the formation of free SDS micelles. The concentration of SDS at the second transition corresponded roughly to the sum of the cmc and a stoichiometric amount of bound surfactant. Numerous researchers detected similar transitions by conductance as well as other methods, including surface tension [183], gel filtration [160], and binding isotherms from dialysis measurements [11]. Fadnavis and Engberts [34] reported three break points in conductivity curves of PVP-SDS solutions, corresponding to onset of binding, onset of free micelle formation, and finally saturation of binding. François *et al.* [41] made a similar observation of a third break point for PEO-SDS, but considered the intermediate point to be a step in the binding isotherm beyond which the aggregation number of the micelles increased. The break points are not sharp, allowing for differing interpretations. There has been some debate over whether free micelle

formation or polymer saturation takes place first in a given polymer surfactant system.

The studies by Cabane and Duplessix clearly laid out the "beads and string" model [16] of small spherical surfactant aggregates distributed within a random polymer coil. Cabane and Duplessix [15] used neutron scattering measurements to determine the size of the individual aggregates in complexes of SDS with various molecular weights of PEO. By using the appropriate amount of D_2O (18%) in the solvent the polymer produced no coherent scatter at small angles and only the scatter from the bound micelles was measured. They measured a micellar radius similar to that of a normal free micelle (22.5Å for pure SDS in .1M NaBr), so the aggregation number was considered to be roughly the same (within a stated error of 30%). The size distribution for free or bound micelles was very sharp. Long lengths of free polymer chain stretch between micelles, and several micelles are bound per polymer chain if the polymer is of sufficient molecular weight (>10000). Only one polymer chain contacts a particular micelle; thus the polymer chains are not crosslinked by the micelles. The aggregates are distributed throughout the polymer coil in a homogeneous manner at low ionic strength. At high ionic strength the spatial distribution becomes Gaussian, higher at the centre, and the complex is slightly more compact, but the micelles remain spherical even though free SDS micelles elongate at such salt levels. The water-hydrocarbon interface was seen to be well-defined, which suggests little water penetration through the layer of polymer bound at the micelle surface. In an earlier paper [14], Cabane reported NMR data which indicated that the surfactant tails are segregated from water, with the polymer at the surface.

Most other studies suggest that bound micelles are smaller than free micelles. Free SDS micelles have an aggregation number of about 60 at low concentration, increasing with concentration of SDS and added salts, and decreasing with temperature [184]. Shirahama [185] measured the binding isotherm for PEO-SDS in 0.1 N NaCl and fit the shape of the isotherm to give a micelle size of about 25 monomers, corresponding to six micelles dispersed along the chain. Smith and Muller [186] studied complexes of ω-trifluoro SDS with PEO by NMR and dialysis, and modeled the complex as aggregates of about 15 SDS molecules with polymer segments of mass 1800 g/mol attached at the micelle surface. Gilányi and Wolfram [187] calculated aggregation numbers of 50 for

PEO-SDS and 44 for PVP-SDS in 0.1 M $NaNO_3$ based on activity data from potentiometric measurements. D'Aprano *et al.* [47] reported an aggregation number for PVP-SDS of 19 ± 3 based on ultrasonic relaxation measurements. Several groups have measured PEO-SDS aggregation numbers by fluorescence quenching [41,188-193], reporting an increase with SDS concentration and a decrease with PEO concentration. These data will be compared with our fluorescence results in Table 5.3.

The binding reaches a saturation level, which has been measured by numerous techniques. A summary of literature values for PEO and PVP, reported in various ways in the literature but converted here to moles SDS bound per total moles polymer repeat unit, is given in Table 5.1. Some of these values were derived from published figures, others were explicitly stated in the text. The range of reported values is surprisingly large, including several apparent outliers, though the polymer concentration dependence reported by Sasaki *et al.* [160] is a possible explanation of the observed range. Representative values of 0.34 (0.42 in 0.1 M salt) for PEO-SDS and 0.41 for PVP-SDS may be chosen. The smaller size and greater hydrophilicity of the PEO monomer relative to the PVP monomer unit may both contribute to the lower degree of binding.

A minimum molecular weight of the polymer is required in order to bind surfactant. Jones [10] first noted that a PEO of low molecular weight (1000 g/mole) showed abnormal behaviour. Schwuger [183] saw no effect of PEO 600 on surface tension of SDS solutions, but typical three-region behaviour for higher molecular weights. Tokiwa and Tsuji [194] determined that below a degree of polymerization of 10-15 (about 600 g/mol) there was no change in the concentration of the first transition, but increased solubilization of dye suggested that complexation did occur above the normal cmc (i.e. oligomeric PEG was bound to micelles but did not induce micelle formation). Smith and Muller [186] studied the binding of ω-trifluoro SDS with PEO and saw little binding at a polymer molecular weight of 1500 g/mol. Tondre [46] used a temperature-jump technique to monitor the relaxation kinetics of micelle formulation-dissolution of SDS in the presence of low molecular weight PEO (MW 10000, 1000 and p-dioxane) and found that the two lower molecular weights did not bind micelles.

Table 5.1. Literature Values of Saturation Binding Ratios (moles SDS bound per mole polymer repeat unit).

Binding Ratio	Conditions	Method	Reference
		PEO-SDS	
0.26 to 0.40	decreasing [PEO]	gel filtration	Sasaki *et al.* [160]
0.29 to 0.33		NMR	Gao *et al.* [18]
0.30		NMR	Cabane [14]
0.31	ω-trifluoro SDS	NMR	Smith & Muller [186]
0.34	ω-trifluoro SDS	dialysis	Smith & Muller [186]
0.35		capillary self-diffusion	Kamenka *et al.* [195]
0.36		calorimetry	Olofsson *et al.* [196]
0.43		flow microcalorimetry	Ballerat-Busserolles *et al.* [197]
0.38	0.1 N NaCl	ultracentrifugation	François *et al.* [41]
0.40	0.1 N NaCl	surface tension	Murata & Arai [198]
0.41	0.1 N NaCl	dialysis	Shirahama [185]
0.48	0.1 M $NaNO_3$	potentiometry	Gilányi & Wolfram[187]
0.3 to 0.9	0 to 0.8 M salt	compiled data	Cabane & Duplessix [15]
		PVP-SDS	
0.33		surfactant electrode	Kale *et al.* [199]
0.20 to 0.35	decreasing [PVP]	dialysis	Fishman & Eirich [200]
0.39	10^{-4} M NaBr	SDS electrode	Wan-Badhi *et al.* [161]
0.44		conductivity	Kamenka *et al.* [195]
0.48		capillary self-diffusion	Kamenka *et al.* [195]
1.11		light scattering	Norwood *et al.* [201]
0.35	0.1 M $NaNO_3$	potentiometry	Gilányi & Wolfram [187]
0.89	0.1 N NaCl	surface tension	Arai *et al.* [11]

The binding of cationic surfactants to neutral polymers such as PEO and PVP is much weaker than that of anionic surfactants. Several theories have been proposed to explain this surprising specificity of a nonionic polymer for surfactants of a particular charge. Saito [202] noted that the binding of anionic surfactant to PVP was disrupted when the surfactant hydrophilicity was increased by the addition of ethylene oxide groups to the alkyl sulfate headgroup, demonstrating that surfactant hydrophobicity is as important as polymer hydrophobicity. Ruckenstein *et al.* [203] theorized that binding of polymer to micelles would only lower the hydrophobe-water interfacial tension if the surfactant headgroup were sufficiently small, which explains the observed behaviour without reference to surfactant charge. Schwuger [183] postulated hydrophobic

interactions as the main driving force, and a slight positive charge on the PEO ether oxygens which would permit binding of anionic surfactants but repel cationic surfactants. This mechanism was supported by the observed decrease in amount bound with increasing pH, but has not been widely accepted.

More recently, several researchers have noted effects of cations on binding between PEO and anionic surfactants. Binana-Limbele and Zana [192] noted an increased aggregation number in the presence of Ca^{2+}. Kamenka *et al.* [195] found that compared to SDS binding, $Cu(DS)_2$ gave a higher saturation binding ratio to PVP but a lower binding ratio to PEO, though both $Cu(DS)_2$ complexes had low degrees of ionization. Maltesh and Somasundaran [204] reported larger aggregation numbers in the presence of Li^+ or Mg^{2+} than for Cs^+ or Na^+, while increasing ionic strength decreased the number of bound micelles but did not change their size. Dubin *et al.* [76] showed that relative to Na^+, Li^+ increased the micelle size and the cmc in the presence of PEO while NH_4^+ had a somewhat weaker lowering effect. They proposed that the PEO chain may bind cations to form a pseudopolycation which then binds anionic surfactant [77]. Since the binding of cations to PEO saturates at a ratio of only one cation to six ether oxygens [205], half that for the binding of SDS, this effect does not predict the observed stoichiometry, but does provide an explanation for the unusually strong binding relative to other systems.

The polarity of the micellar environment is a property of interest. From the effects on the kinetics of hydrolysis of a solubilized probe, Fadnavis and Engberts [34] deduced that the surface of the PVP-SDS aggregate is more polar than a bare SDS micelle. Increased polarity on binding of PEO has been evidenced by pyrene I_1/I_3 ratios [190].

The microviscosity in the micellar environment has been studied by several methods. Shirahama *et al.* [53] used a hydrophobic nitroxide radical spin probe in an ESR study of the interactions of SDS with PEO and PVP in 0.1M NaCl. The ESR linewidth was broader in polymer solutions at the limit of zero surfactant as compared to pure surfactant samples, indicating a more viscous microenvironment for the probe in the polymer-surfactant aggregates than in normal micelles. Witte *et al.* [55] later found the opposite. They conclude from analysis of ESR measurements of a smaller spin probe molecule that it rotates more freely in the SDS/polymer complexes than in free micelles.

Decreased microviscosity was also evidenced by decreased fluorescence polarization of diphenylhexatriene and by decreased pyrene excimer formation rates in PEO-SDS aggregates [190].

The literature data generally support the theory of small micelles bound to polymer with some length of free polymer chain separating the micelles. The polymer is coiled and, if of sufficient length, contains many aggregates. The polymer appears to bind at the micellar surface where it shields the micellar interior from water contact. The hydrophobicities of both the polymer and the surfactant increase the interaction. The fluidity of the micelle is determined by a combination of the looseness of packing of small aggregates and the rigidity imposed on the surface by the adsorbed polymer chain.

5.2. Experimental

Materials

Sodium dodecyl sulfate (Sigma) and poly(vinyl pyrrolidone) (Aldrich, MW 40,000) were used as received. Pyrene (Eastman, or K&K Laboratories, Hollywood, CA) was recrystallized from ethanol and sublimed before use. Anthracene (Fisher) was recrystallized from benzene. Benzophenone (Fisher) was recrystallized from an acetone/ethanol mixture. Dodecylpyridinium chloride monohydrate (Aldrich) was recrystallized from an acetone/diethyl ether mixture. Molecular weight assay by Mohr titration ($AgNO_3$ with chromate indicator) to determine the Cl^- content confirmed that the recrystallized product was anhydrous (Calculated MW 284 g/mol anhydrous, 302 g/mol hydrated, 288 found by assay). Type II deionized water (resistivity 1.5-2.5 MΩ·cm) from a Millipore Milli-R/Q purifier, was used throughout the research, with water for SEC samples filtered through 0.02 μm Anotop Plus 25 mm inorganic membrane syringe tip filters (Whatman).

The commercial glycol, PEG and PEO samples used in size exclusion chromatography were from a number of sources, as listed in Table 5.2, and were used as received. Highly monodisperse standards were purchased from American Polymer Standards Corp. (Mentor, OH) and Polymer Source Inc. (Dorval, PQ). The nominal

Table 5.2: Molecular Weights of PEO Samples

		Nominal	Experimental			
Sample Name	Supplier	M_n or M_v	M_n	%RSD	M_w	M_w/M_n
ethylene glycol	Anachemia	62				
diethylene glycol	MCB	106				
triethylene glycol	J. T. Baker	150				
tetraethylene glycol	Aldrich	194				
POGOL 200	CCC	200	229	*	246	1.07
POGOL 300	CCC	300	361	*	375	1.04
POGOL, PEG 400	CCC,BDH,Fisher	400	423	*	441	1.04
PEG 600	Aldrich	600	541	*	563	1.04
PEG 900	Aldrich	900	928	*	946	1.02
PEG 1000	Aldrich	1000	983	*	1007	1.02
PEG 1050	APS	1000	1042	*	1068	1.03
PEG 1500	Aldrich	1500	1542	*	1582	1.03
PEG 2010	APS	1965				
PEG 2000	Aldrich	2000	2400	19	2600	1.10
PEG 3000-3700	Fisher	3350				
PEG 3300-4000	BDH	4000	3400	5	4000	1.16
PEG 5000	APS	4850	4600	10	5200	1.12
PEG 6000	BDH	6000				
PEG 8000	Aldrich	8000	7600	7	8500	1.12
PEG 10000	Aldrich	10,000				
PEG 10730	APS	10,300				
P445-EO	Polymer Source	48,200				
P277-EO	Polymer Source	100,100	100,000	16	110,000	1.10
PEO 200000	Aldrich	200,000	137,000	36	315,000	2.31
P284-EO	Polymer Source	210,500	210,000	9	228,000	1.09
PEOX270K	APS	240,000	246,000	19	272,000	1.11
P344-EO	Polymer Source	292,400	285,000	6	305,000	1.07
PEO 900000	Aldrich	900,000	119,000	26	1,010,000	8.49
PEO 5000000	Aldrich	5,000,000	1,200,000	31	3,900,000	3.33

Experimental values marked * are from mass spectral data, estimated error 4%; others by SEC.
Abbreviations: APS: American Polymer Standards; BDH: The British Drug Houses;
CCC: Canada Colours and Chemicals; MCB: Matheson Coleman Bell.

molecular weights listed are either the formula weights of the pure oligomers from ethylene glycol (EG) to tetraethylene glycol (4EG), number averages for the PEGs and the monodisperse standards, or viscosity averages for the broad Aldrich PEOs. Also tabulated are our measured M_n, M_w and M_w/M_n values for selected samples, with the estimated precision of M_n as percent relative standard deviation (%RSD). Whereas all PEG samples used (molecular weights up to 10 kD) have -OH endgroups, the PEO samples have a variety of endgroups, some unspecified. All samples for fluorescence measurements were prepared using the 200k Aldrich PEO.

Fluorescence

Aggregation numbers were measured by time-resolved fluorescence using a single photon counting apparatus (Photochemical Research Associates FLI 3000, London, ON). Samples were prepared as moles solute per kilogram solution for ease of dilutions by weight, and concentrations are reported in molal (m) units. In dilute solution, the differences between molar, molal, and moles per kilogram solution are insignificant. A sample of pyrene stock in ethanol was weighed into a flask and the solvent evaporated with nitrogen. Aqueous SDS and PEO stocks were added and the sample mixed for several days to ensure solubilization of pyrene. When using benzophenone as quencher, a sample of ethanolic stock was weighed into a second flask and evaporated. Half of the SDS/PEO/pyrene stock was added and the sample mixed for several days. The dissolved concentration of benzophenone was usually only about 80% of the amount weighed, and was therefore verified by the UV absorption (λ_{max} = 252 nm, ε = 17,400 L/mol·cm [206]) of a sample diluted 20-fold with ethanol. For trials with DPC, an aqueous stock was added to half of the SDS/PEO/pyrene stock and the quencher-free stock was equivalently diluted with distilled water. For trials with PVP, the polymer was generally added as a dry powder. Some samples were deaerated by several freeze-pump-thaw cycles.

Steady-state spectra of selected samples were recorded on a Perkin-Elmer MPF-66 fluorescence spectrometer. The peak intensities at ~373 and 384 nm were read to calculate I_1/I_3 ratios. Samples for fluorescence depolarization measurements were prepared as follows. A sample of a 4 mm stock of anthracene in acetone was placed in a

flask and the solvent evaporated. A 50 mm SDS stock was added and stirred for several days to solubilize the anthracene. Polymers were added to SDS samples as dry powders to give a 2% solution. The excitation and emission polarizers were rotated between the 0° and 90° positions and spectra read at all four permutations. The intensities at four maxima in the emission band (~ 383, 405, 428, 455 nm) were read and the polarization calculated at each wavelength. As no trend was observed in the polarization as a function of wavelength, the average of the four values is reported.

Size Exclusion Chromatography

The size exclusion chromatography equipment is described in detail in Chapter 4. Sample concentration and loop size were varied over the range of polymer molecular weights in order to optimize the response of both the MALLS and RI detectors. A typical injection was 100 μL of a 3 mg/mL polymer sample. Progel-TSK PW_{XL} size exclusion columns (300 × 7.8 mm, Supelco) were used; the typical configuration was an ultra-low dead volume 0.5 μm precolumn filter (Upchurch) followed by a PW_{XL} guard column, a G3000 column (200 Å pores, rated for separation of PEO MW < 50 kD) and a G5000 column (1000 Å, rated for MW of 4-1000 kD). Trials were also run with either column alone. Flowrate was maximized while keeping column backpressure below the manufacturer's recommendation (600 psi with the low MW column in use, 300 psi if only the high MW column was used); the typical flowrate was 0.6 mL/min.

Refractometry

Refractive index increments of the polymers and the surfactant were measured by routing the injector directly to the Optilab detector. A larger sample loop (0.99 mL) was used to inject up to 20 samples at increasing concentrations into the system at a typical flowrate of 0.7 mL/min, producing a series of plateaus. DNDC for Windows version 5.00 software (Wyatt) was used to measure plateau values of the relative refractive index of each sample and to compute dn/dc values.

Mass Spectrometry

The molecular weight distributions of several PEG samples were verified by mass

spectrometry (MS) on a Fisons VG Quattro (I) triple quadrupole instrument with a Quattro (II) atmospheric pressure chemical ionization (APCI) / electrospray ionization (ESI) interface. Data acquisition and processing was performed using MassLynx version 2.1 software. Samples were prepared in 50% (v/v) aqueous acetone or acetonitrile, with addition of acetic acid or ammonium acetate for APCI, at a typical polymer concentration of 5 mg/mL. For APCI sampling, a Rheodyne 7125 valve was used to inject the sample into the flow stream. Samples for ESI were delivered by direct infusion using a Cole Parmer model 74900 syringe pump and 10 mL Hamilton gastight syringe at a flowrate of 1.8 mL/hr. Oligomers were detected in positive ion mode (APCI(+) or ESI(+)) as series of $(M + H^+)$, $(M + NH_4^+)$ or $(M + Na^+)$ ions. Numerous experiments on the PEG 1000 sample using the different ionization modes under different conditions gave reproducible molecular weight averages with a relative standard deviation of 4%. Further details on the methods are available elsewhere [207,208].

5.3. Fluorescence Probing Studies

In this section we describe our results from fluorescence studies of the interactions of the anionic surfactant sodium dodecyl sulfate (SDS) with the neutral polymers poly(ethylene oxide) (PEO) and poly(vinyl pyrrolidone) (PVP). The PEO-SDS system has been widely studied in the literature by a variety of methods including fluorescence, and is thus a good system on which to test our methods. To calculate the aggregation numbers, a free surfactant concentration of 4.5 mm was assumed in all samples. Our results are compared to numerous published values of aggregation numbers derived from fluorescence measurements on samples of various compositions. After testing of the fluorescence methods on the PEO-SDS system, the PVP-SDS system was chosen for comparison. The only fluorescence study of aggregation numbers in this system in the literature was limited to a single polymer concentration [188,189]. We estimated the concentration of free surfactant in the samples, which varied from 4.0 to 2.8 mm with increasing PVP concentration, using the binding isotherms published by Wan-Badhi *et al.* [161].

Results

Aggregation numbers measured in several PEO-SDS samples of different compositions are shown (underlined) in Table 5.3 along with compiled literature data from time resolved and static measurements. Two reported average values at less specific P-S concentrations are not included in the table: N_s = 35 ± 5 at saturation, and increasing above saturation, for PEO = 30 to 120 mM [191], and 24 ± 5 below saturation, independent of salt concentration for several sodium salts [204]. The shaded area of the table indicates samples above the saturation of the polymer with surfactant (0.34 surfactant molecules bound per EO repeat unit) where free micelles coexist. There was no significant difference between N_s values measured using benzophenone and dodecylpyridinium chloride quenchers in the 50 mm SDS samples.

Table 5.3. Experimental and Literature Aggregation Numbers in PEO-SDS Complexes at 20-25 °C

[SDS] mm*	[PEO] mm*							
	0	10	45	50	100	114	227	454
7		30[e]						
10	62[209],65[41]		31[189],41[41]	23[b]		22[193],34[189]	24[189]	
15			43[41]			29[193]		
20	53[193],63[209]		48[189],53[41]	32[b]	25[b]	34[193]	30[192]	23[189]
25			50[190]			40[189]	34[190]	30[190]
30	60[193]					38[193]	36[192]	31[189]
40	64[193]					50[193]	40[192]	
50	52[b],60[c],66[d] 55[210],67[193]		45[d],51[b] 59[189]			44[b],52[d] 52[193],53[189]	37[d],37[b] 45[189]	34[192],42[189]
100	66[190],72[41]		67[189]			63[189]	63[189]	60[189]
130	70[211]							57[192]
200	64[209]					72[189]		
250							77[189]	
300	64[209]					79[189]		
500	79[212]		91[189]			90[188]	90[189]	86[189]

Underlined values are our results, quenched by b) benzophenone, c) CPB, d) DPC, e) excimer.
*Literature values are often mM or converted from weight% polymer

Our aggregation numbers increase with increasing surfactant concentration or decreasing polymer concentration, as do the literature data. Our results tend to be about 20% lower than the literature values. We believe this to be due to micelle polydispersity, discussed in greater detail in Chapter 6. When measurements were made at several

quencher concentrations, the aggregation number tended to decrease with quencher concentration. When the micelles are polydisperse in size, the average number of quenchers per micelle is greater in the larger micelles. This perturbation of the quencher distribution results in less quenching than is predicted by Poisson statistics. Thus the method overestimates the number of micelles, and underestimates the average aggregation number, unless as discussed in Chapter 6 the results are extrapolated to zero quencher concentration. We did not perform measurements at enough quencher concentrations to allow reliable extrapolation in order to quantify the dispersity. Since we expect a bimodal micelle size distribution when bound micelles ($N_a \approx 30$) coexist with free micelles ($N_a \approx 60$), significant polydispersity is to be expected.

Samples of 50 and 100 mm SDS with varying concentrations of PVP were prepared for aggregation number determinations. The aggregation numbers measured by quenching of pyrene by DPC (except as noted) are shown in Table 5.4 along with the measurements of Zana *et al.* [188,189] at 1% (90 mm) PVP. The numbers show the same general trends of decreasing with polymer concentration and increasing with surfactant concentration as in the PEO-SDS samples. Again our numbers are low for the few cases where literature values are available for comparison, however the literature values rise rather rapidly, and seem to favour the free micelles present. We again note a dependence on quencher concentration suggestive of significant polydispersity.

Table 5.4. Experimental and Literature Aggregation Numbers in PVP-SDS Complexes at 20 - 25 °C

[SDS] mm	[PVP] mm 0	14	18	45	90	180	450
20	53 , 63				31		
50	66 55 , 67		38	31	36 59	29	23
90			55				
100	66 , 72	46[b]		32	35 , 81	35	
500	79				88		

Literature values at 90 mm PVP from [188,189], others as in Table 5.4.
Our results underlined, quenched by DPC except b) quenched by benzophenone.

The average lifetime of the fluorescence in aerated samples of SDS was 175 ns, in PVP-SDS complexes 185 ns, and in PEO-SDS complexes 189 ns. The lifetime in

unsaturated PEO and PVP complexes where no free micelles are present was 191 ns, slightly higher than average. The average rate constant for DPC quenching of pyrene was 30×10^6 s^{-1} in SDS and 29×10^6 s^{-1} in PEO-SDS complexes, but was significantly reduced (given a 10-20% error) to 22×10^6 s^{-1} in PVP-SDS complexes. The quenching rate constant of benzophenone was higher in the unsaturated PEO-SDS complexes (40×10^6 s^{-1}) than with coexisting free micelles (34×10^6 s^{-1}), as was the case for DPC in the PVP-SDS complexes (28 vs. 20×10^6 s^{-1}). This also indicates smaller micelles, as the diffusion controlled quenching rate constant depends on the distance between probe and quencher.

Fluorescence spectra of pyrene were measured in various samples. Typical I_1/I_3 values were 1.26 in SDS, 1.28 in PEO-SDS, and 1.63 in PVP-SDS, compared to 1.88 for aqueous pyrene. Values in PVP-SDS complexes tended to decrease with increasing ratio of surfactant to polymer as was reported by Zana *et al.* [188,189], indicating that the bound complexes are more polar than free micelles. Dipyme I_1/I_3 values also were higher in PVP complexes (1.98 ± .04) than in PEO complexes (1.82 ± .03). Measurements were made of fluorescence depolarization of anthracene in pure SDS solutions and in polymer-surfactant complexes. The measured residual polarization was much greater in the PVP-SDS complex, (p = 0.5% in SDS, 1.2% in PEO-SDS, 12.7% in PVP-SDS) indicating a more rigid probe environment. Spectra of dipyme showed similar trends in microviscosity, with the value of I_m/I_e increasing with polymer concentration and much greater in PVP-SDS complexes than in PEO-SDS.

Discussion

The aggregation numbers measured in PEO-SDS and PVP-SDS complexes increase with surfactant concentration and decrease with polymer concentration. The bound micelles are smaller than free micelles at the same surfactant concentration. Above the polymer saturation concentration the measured aggregation number is an average of the aggregation numbers of the coexisting populations of free and bound micelles. To better display this, the literature and experimental data for the PEO-SDS system are shown in a 3-D plot in Figure 5.1. The base plane is the PEO-SDS "phase diagram" oriented such that the binding saturation line (marked as a thick line on the base plane)

projects out of the page and all points to the left of the line are below saturation. The aggregation numbers are plotted on the z-axis with shading of the data points decreasing with aggregation number (i.e. the darkest symbols are bound micelles and the lightest symbols are free micelles). The sharp increase in aggregation number at saturation is evident.

Figure 5.1. 3-D Plot of PEO-SDS Aggregation Numbers

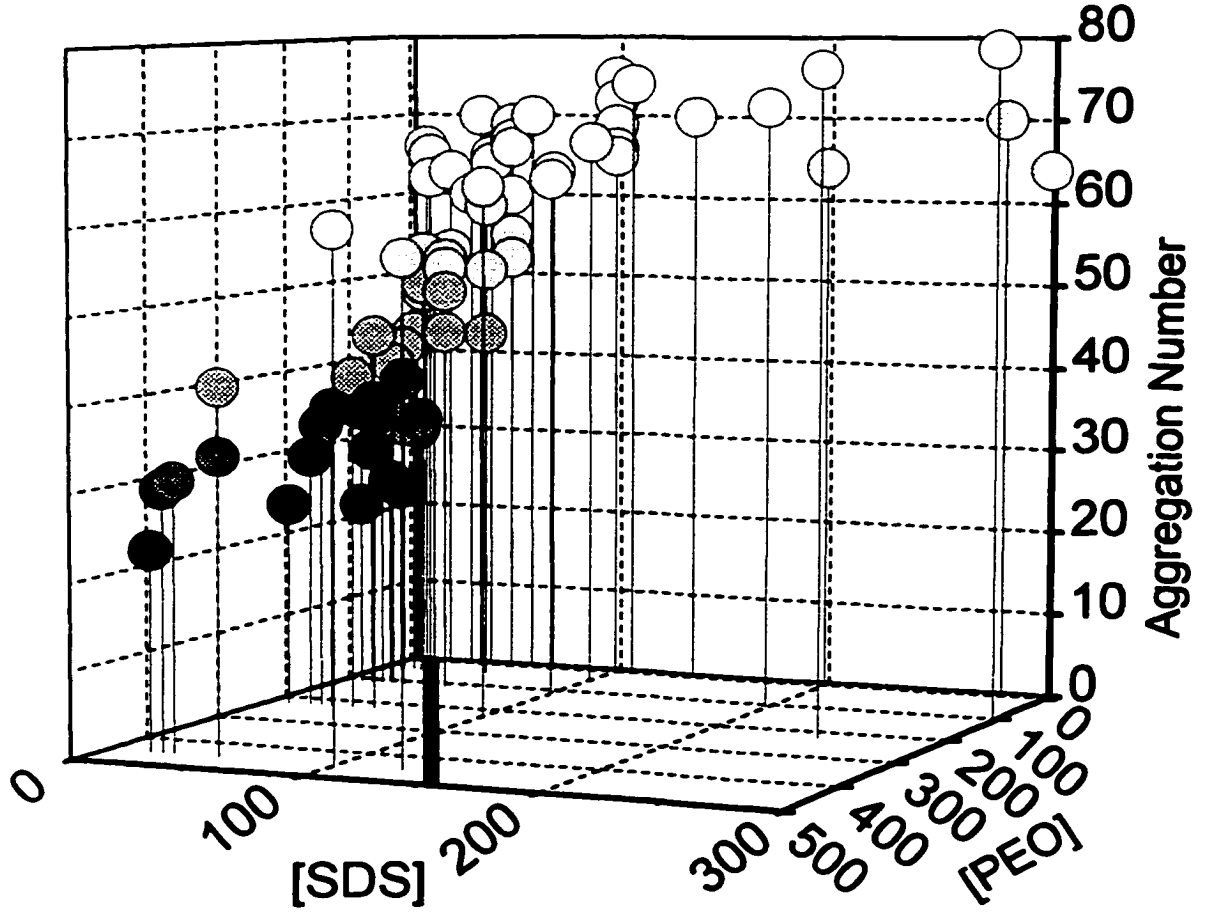

To compare the PEO and PVP systems, we plot our measured aggregation numbers against the inverse of the degree of saturation of binding (i.e. polymer concentration multiplied by saturation binding ratio divided by bound surfactant concentration). This is a useful representation as it allows the inclusion of aggregation numbers in the absence of polymer at the y-intercept, and normalizes the difference between saturation binding ratios of the two polymers (0.34 for PEO, 0.41 for PVP) such that both polymers are saturated at a value of one on the x-axis. This plot is shown as Figure 5.2. We see that below saturation, the aggregation number rises slowly from about 25 to 35, with no significant difference between PEO and PVP. Above saturation the aggregation numbers for PEO increase more rapidly toward those for free micelles, while the values for PVP remain relatively low. This suggests that the reported "saturation" value of 0.41 moles surfactant per mole polymer for PVP may actually be the concentration where free micelles begin to form, and binding to the polymer continues until a third critical point is reached, as reported by Fadnavis and Engberts [34].

Figure 5.2. Aggregation Numbers Versus Inverse of Degree of Saturation

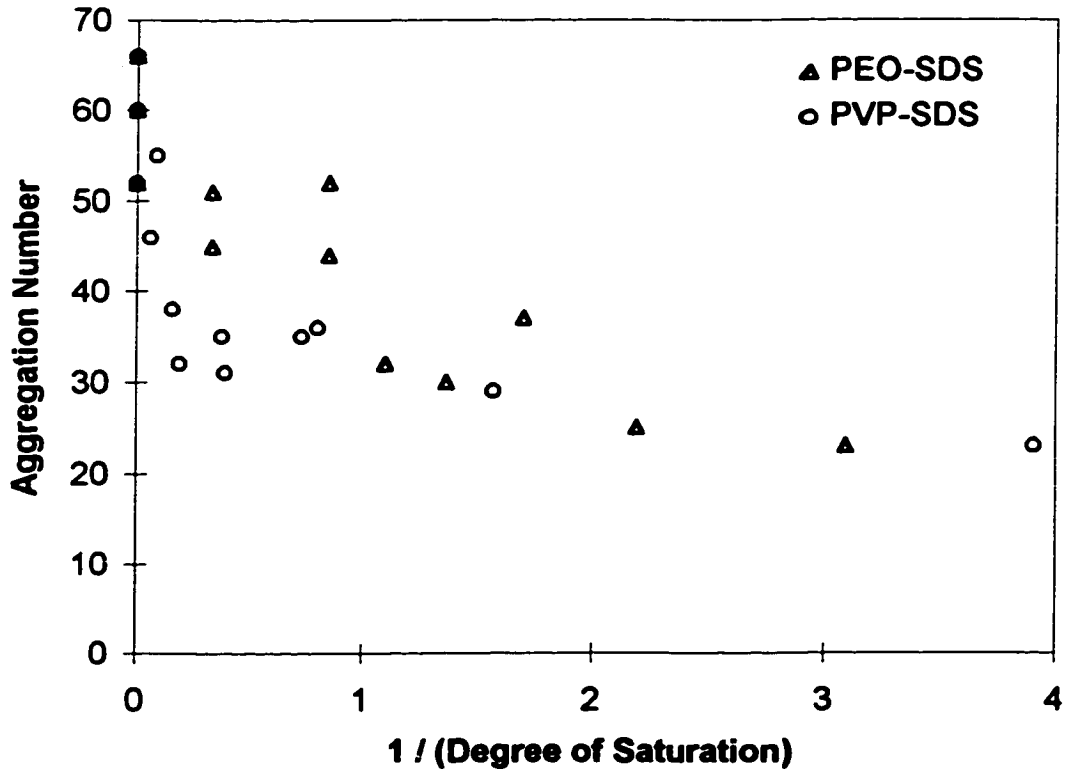

The aggregation numbers compare favourably with literature values, once polydispersity is taken into account. The relative error in our reported values is at least 10%, as in the literature: consider the two substantially different values (34, 42) for complexes of 50 mm SDS with 2% PEO, reported in different publications [192,189] from the same research group using the same method. Differences between our numbers obtained using benzophenone and DPC as quenchers are within error limits.

The increased microviscosity of the environment of the anthracene and dipyme probes correlates with the decrease in the diffusion controlled rate constant of the quenching of pyrene fluorescence by DPC. The aggregates bound to PVP are more rigid and more polar than those bound to PEO. The lower cac and higher binding ratio of surfactant to PVP at saturation suggests that micelles are bound more strongly than to PEO. Still, the measured values of N_s below saturation are similar for PEO-SDS and PVP-SDS complexes.

It is possible that the pyrrolidone ring is solubilized into the surface of the micelle, as has been proposed for the phenyl ring of polystyrene sulfonate [213]. The bulkiness of the pyrrolidone rings restricts the rotation of PVP, making the polymer stiffer than PEO, but the chain is capable of a conformation which places the amine and carbonyl groups on one face and the backbone and nonpolar parts of the ring on the other. The rings occupy space in the headgroup region, separating the headgroup charges to stabilize the smaller micelles. The polar moieties of the ring may contribute to the increase in the pyrene I_1/I_3 ratio. The presence of the rings increases the rigidity of the micelle surface as reported by the probes.

Conclusions From Fluorescence Experiments

Our results compare well with previous work in PEO-SDS and PVP-SDS systems. The measured aggregation numbers are small below the saturation of binding, then slowly increase near saturation because the method reports an average of the aggregation number of the coexisting bound and free micelles. Micelles of SDS bound to PVP have a more polar and rigid interface but are similar in size to those bound to PEO. The insertion of the pyrrolidone ring into the micellar surface may be responsible for this.

5.4. Size Exclusion Chromatography

We now discuss our results from size exclusion chromatographic investigations of a number of PEO samples of different molecular weights, and their interactions with SDS. We examined the binding to low molecular weight polyethylene glycols (PEG) to determine the lowest molecular weight which formed polymer surfactant complexes. This molecular weight cutoff point differed depending on whether the surfactant concentration was above or below the cmc. We also attempted to quantify the amount of surfactant bound, and the size and molecular weights of the complexes. Non-size-exclusion effects affected both the elution volumes of the complexes and the measured radii, molecular weights, and binding ratios.

Results

Refractometry

The refractive index increments for SDS and a wide variety of PEG and PEO samples were measured. The dn/dc of SDS was measured to be 0.125 ± 0.003 mL/g at 690 nm and 40 °C, in good agreement with literature values (0.119 [214] and 0.1179 [215]) measured at 633 nm and 25 °C. Contrary to the recent report of Chiu and Lin [215], we were unable to detect any variation in the dn/dc of SDS at the cmc (2.5 mg/mL at 40 °C) using 20 samples over the range 1.4 - 3.3 mg/mL. A difference between the values of dn/dc for free monomer and micelles would complicate the determination of the amount of bound surfactant based on the area of the surfactant void peak. An early study by Klevens [216] noted a change in the slope of plots of refractive index versus concentration at the cmc for solutions of a variety of surfactants. The slopes reported by Klevens show an average lowering of dn/dc above the cmc of 6.2% for the range of surfactants studied, but only 3.3% for sodium dodecyl sulfonate (the surfactant in his study most similar to SDS), values which would not have a large effect on our measurements.

Our measurements yield an average value and standard deviation of 0.135 ± 0.003

mL/g for the dn/dc of the higher PEGs and the PEOs at 690 nm and 40 °C. In agreement with the observations of Rempp [217] for PEG samples at 20 °C and 435.8 nm, dn/dc is independent of molecular weight at higher molecular weights, but drops off significantly below a molecular weight of about 1000. The data are shown in Figure 5.3 with the data of Rempp plotted for comparison (on different vertical axes for clarity).

Figure 5.3. Experimental (□) and Literature (Δ, [217]) dn/dc Values for Various Molecular Weight Samples of PEG and PEO

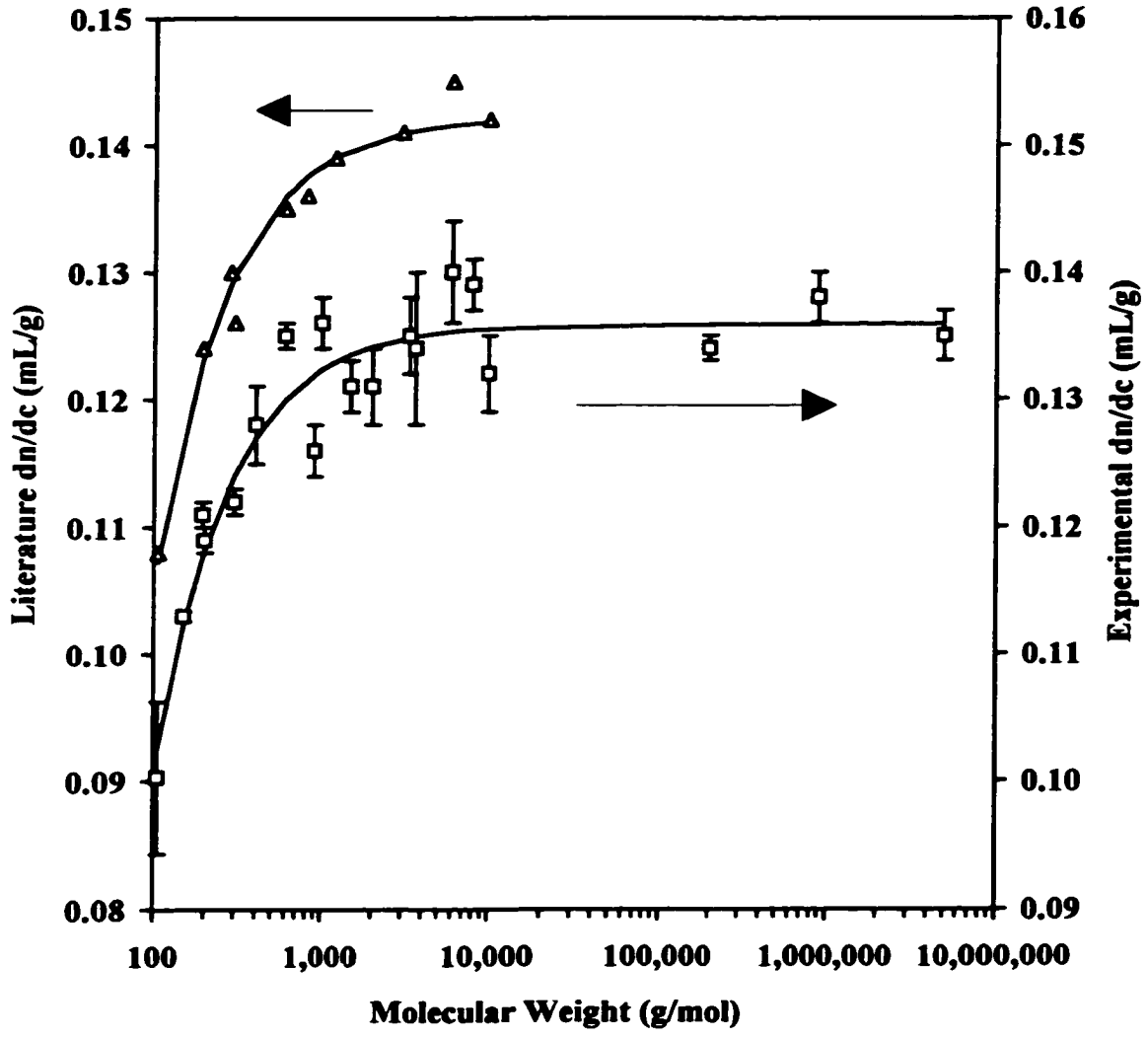

Size Exclusion Chromatography

SEC with deionized water as eluent was used to characterize a variety of PEG and PEO samples, both commercial grade and highly monodisperse standards. A plot of elution volume vs. log(M_n) in Figure 5.4 shows that the two columns combine to give good separation over four orders of magnitude of polymer molecular weight. The commercial PEG samples eluted as narrow peaks, however it was difficult to obtain precise molecular weight measurements of the lower molecular weight samples because the light scattering signals were too weak even at concentrations approaching the maximum response of the RI detector. Were such measurements of primary concern, a less sensitive RI cell (or detector) could be substituted to allow the use of higher sample concentrations to improve light scattering response. Instead, the molecular weight distributions of several of the lower glycols were determined by mass spectrometry. Values of M_n and M_w calculated from the relative intensities of oligomer peaks in ESI(+) and APCI(+) mass spectra are included in Table 5.2. The ESI(+) mass spectrum of PEG 1000 is shown as Figure 5.5, with the peaks representing $M + Na^+$ species. The molecular weights obtained by MS are in good agreement with the nominal values, and reveal even the commercial PEG samples to be highly monodisperse.

The commercial PEO samples displayed broad peaks of high polydispersity (>2), and both PEO 200k and 900k were bimodal. The high-mass peak may be an artifact of interpolymer aggregation. These highly polydisperse commercial PEO samples are not well suited to study of P-S interactions by SEC due to the uncertainty in measuring small changes in such a broad peak. The up to threefold increase in molecular weight expected on saturation by SDS is more reliably measured on a less disperse sample. It is noted that with such polydisperse polymers, one could have in the same solution complexes bearing only one micelle and complexes bearing hundreds of micelles. Equally, the interpretation of other types of binding measurements or structural studies with such PEO samples should take into account the high degree of polydispersity.

Figure 5.4. Polymer Elution Volumes Versus Nominal Molecular Weights in Several SDS Eluents.

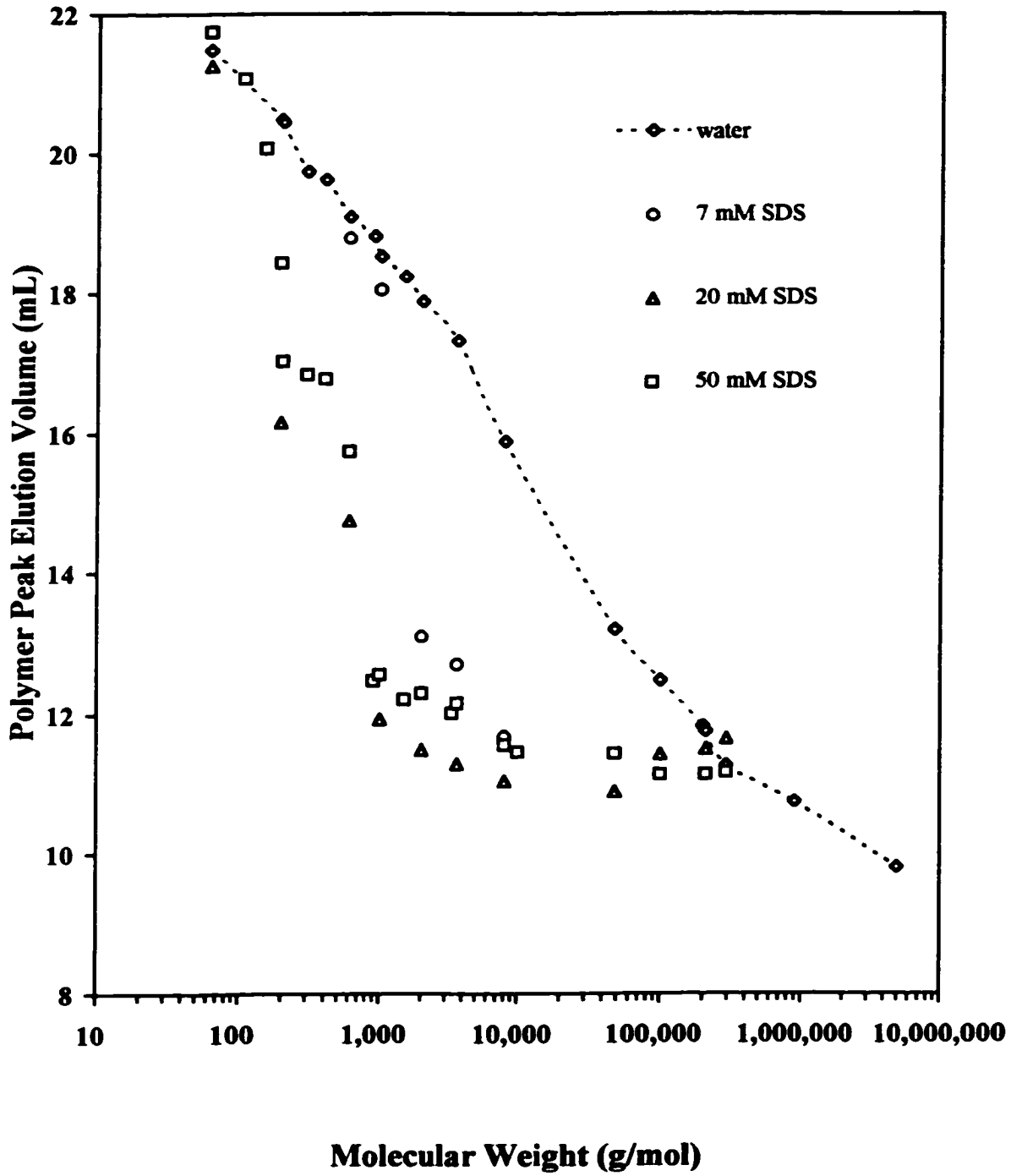

Figure 5.5. ESI(+) MS of PEG 1000 in Na^+ Ion Mode.

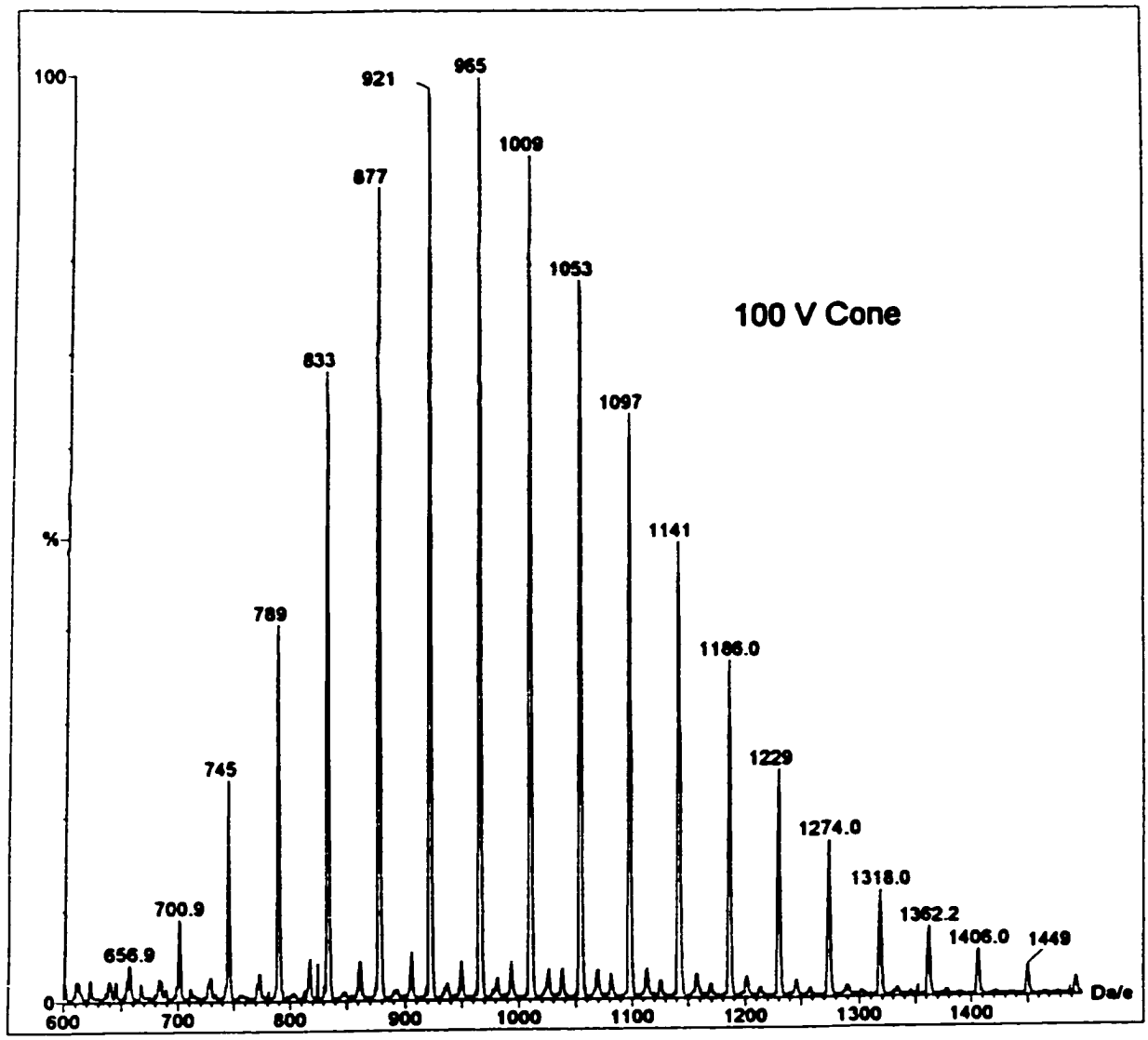

SEC was performed on the PEG samples and the highly monodisperse PEO standards with SDS in the eluent. SDS concentrations both below (7 mM) and above (10, 20 and 50 mM) the cmc were used. A sample chromatogram showing the complex peak and surfactant void of PEG 8000 in 20 mM SDS, run using the G5000 column only, is shown as Figure 5.6. Elution volumes of the complexes at the different eluent concentrations are reported in Figure 5.3.

The RI chromatograms for several surfactant-free samples injected into 7 mM SDS eluent (both columns) are shown in Figure 5.7. The surfactant void peaks in this eluent had very long elution times, and were not used to measure the amount of bound surfactant. The smaller oligomers (1000 and 600 g/mol) are not significantly shifted from their elution volumes in the absence of surfactant. The RI response indicates perhaps one bound SDS molecule per PEG chain, and the light scattering also indicates very little mass increase. The larger polymers (8000, 4000, and 2000 g/mol) are shifted toward lower elution volume from their uncomplexed behavior, indicating complexation. The RI signals of the complex peaks indicate an average binding ratio of 0.34 ± 0.03 moles of SDS bound per mole EO unit, comparable to the literature values in Table 5.1. The M_n values measured by the light-scattering detector are comparably higher than those measured for the unbound polymers. Results are given in Table 5.5.

Table 5.5. Measured Complex Molecular Weights and Binding Ratios in 7 mM SDS

Polymer	M_n g/mol	%RSD	Binding Ratio (mol SDS/mol EO)
PEG 600	800	11	0.04
PEG 1000	1900	10	0.05
PEG 2000	7200	3	0.32
PEG 3300-4000	8600	10	0.38
PEG 8000	17000	6	0.32

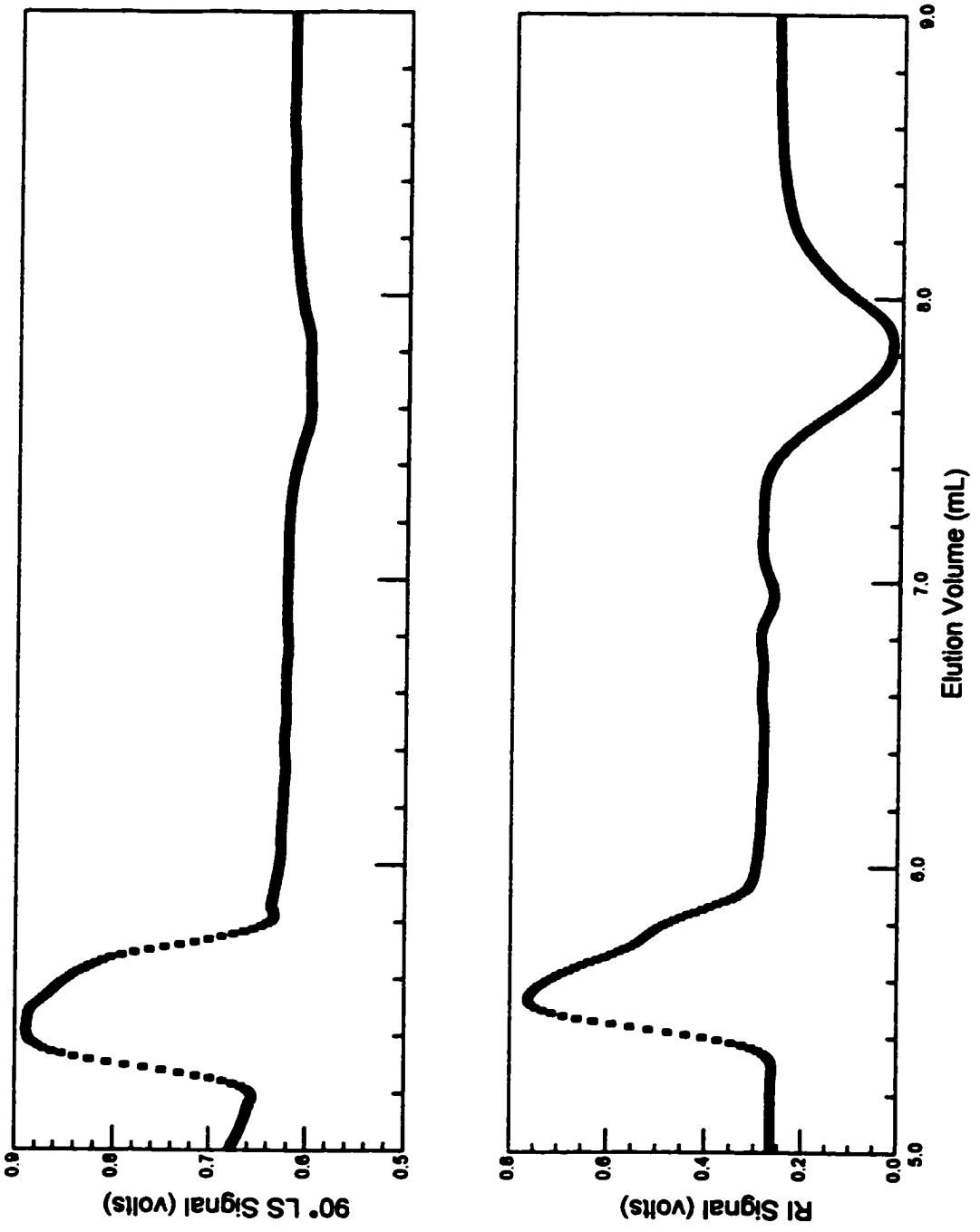

Figure 5.6. Chromatogram Exhibiting Complex Peak and Surfactant Void (PEG 8000 in 20 mM SDS).

Figure 5.7. Elution of PEG Samples in 7 mM SDS

(left to right): PEG 8000, PEG 4000, PEG 2000, PEG 1000, PEG 600.

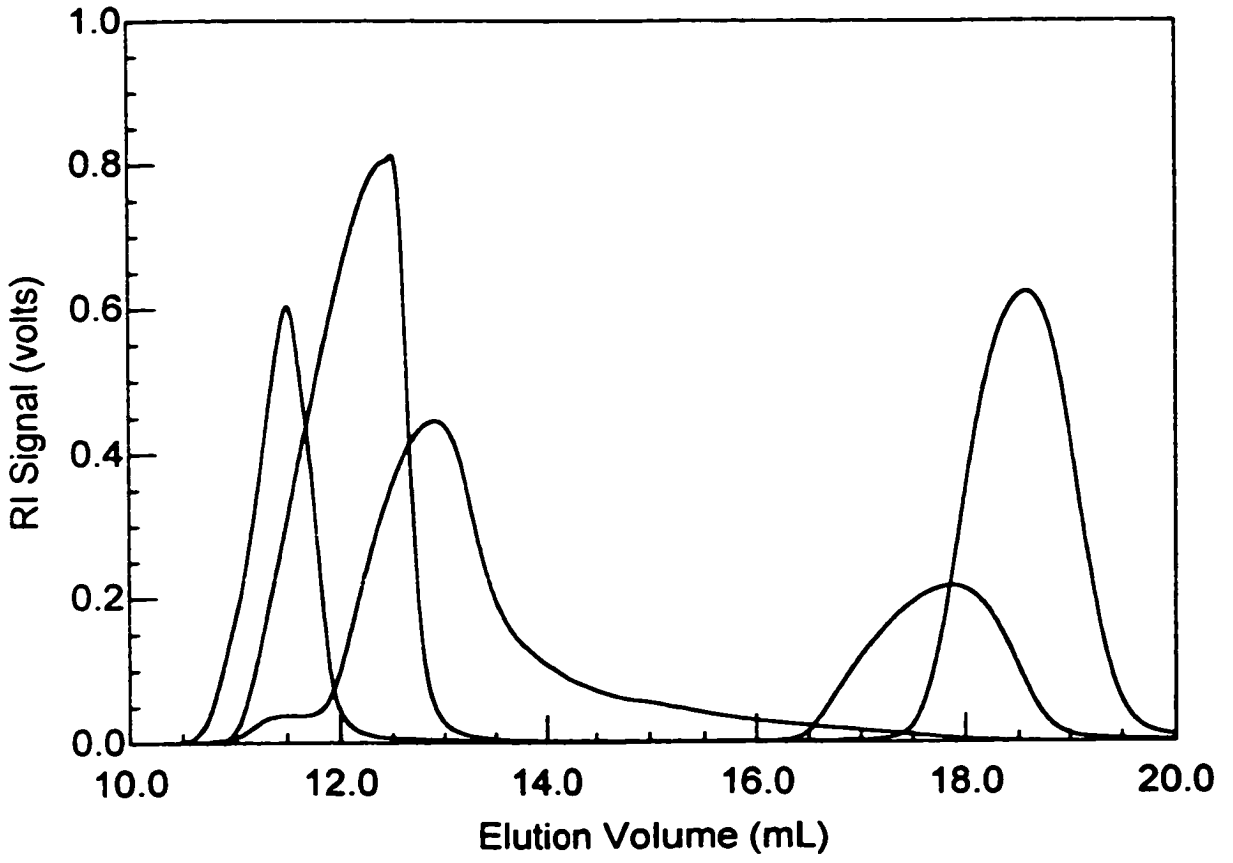

The binding ratios measured in micellar eluents tended to be slightly lower, which may be because the calculation was based on surfactant void volume. In 10 mM SDS the average measured binding ratio for a variety of polymer molecular weights was 0.28 ± 0.07 moles SDS per mole EO unit. The surfactant voids tailed strongly toward the complex peaks, which contributed to the error in the integration. Different amounts of PEO 240k were injected into 20 mM SDS (on the G5000 column only) to check the effect of injected mass on the binding ratio. A plot of mass surfactant bound versus mass polymer injected is shown in Figure 5.8. The intercept is zero within the limits of error, and the slope yields a binding ratio of 0.27 ± 0.02 moles SDS per mole EO unit. This approach is much more reliable than measuring the void area of a single chromatogram, as it would reveal lack of complex saturation as a curvature in the plot.

Figure 5.8. Measured Mass of Bound SDS Versus Injected Mass of PEO.

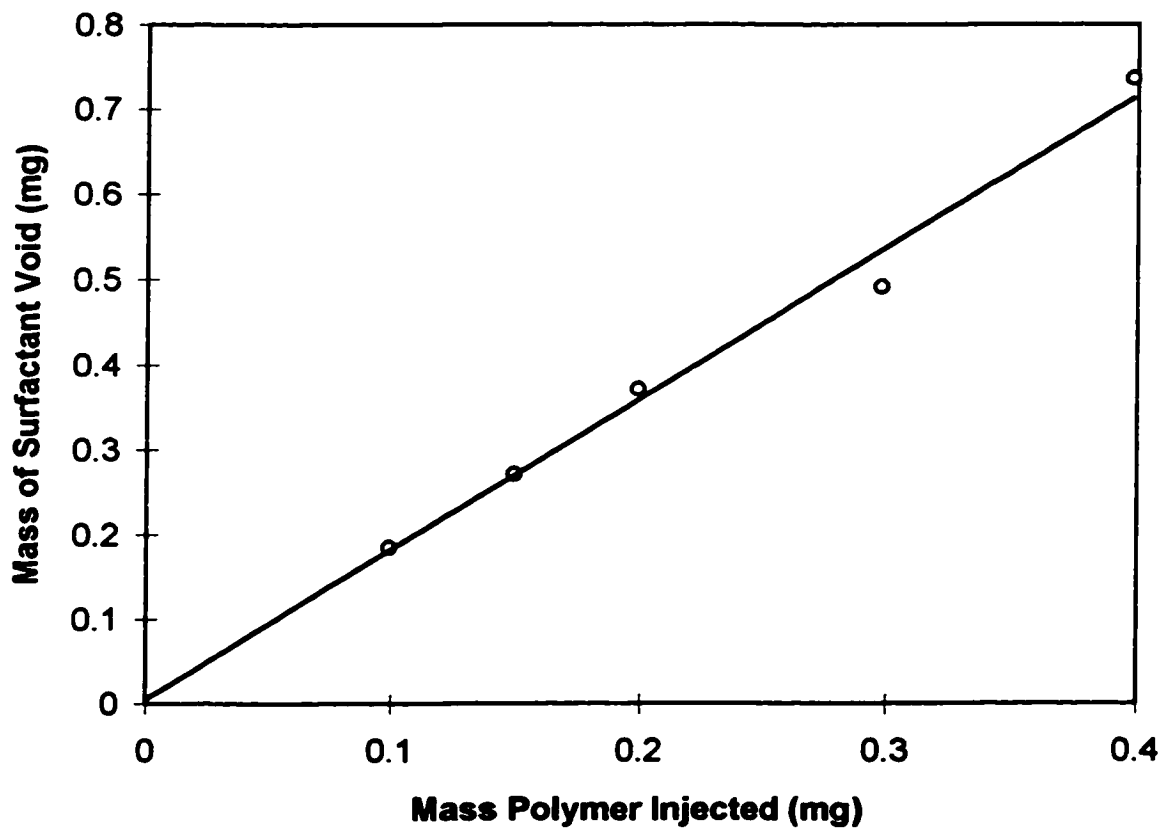

The voids in chromatograms run at 50 mM SDS often had a distorted shape, perhaps due to a superimposed peak. This perturbed the quantification of the void area such that it could not be used to calculate binding ratios. Figure 5.9 shows the RI elution profile of PEG 6000 in 50 mM SDS (both columns) as an example. Binding ratios and molecular weight measurements based on the complex peaks indicated little or no mass increase, even though the polymer peaks were largely shifted from their positions in the absence of surfactant.

The elution volume data for a range of polymer samples in 7, 20, and 50 mM SDS on the two-column setup are also shown in Figure 5.4 for comparison with the elution volumes without added surfactant. The elution peaks of complexes are shifted to lower elution volumes than the uncomplexed polymer, but approach a limiting elution volume of about 11 mL. Assuming that a saturated P-S complex, about three times the mass of the unbound polymer, would elute at the same volume as a polymer of that larger mass would predict a shift in elution volume of only about 1.4 mL, much less than we observe. A universal calibration plot of $[\eta]M$ versus V_e would likely yield unreasonably large values of molecular weight for the complexes.

For polymer samples of 200 to 600 g/mol average molecular weight, multiple peaks were observed, in some cases dropping below baseline. A sample chromatogram of PEG 600 in 20 mM SDS (both columns) is shown as Figure 5.10. Such patterns were observed only in the presence of micellar surfactant, not in pure water or 7 mM SDS. The patterns were similar when using the G3000 and/or G5000 column, indicating that this is not simply a pore size effect.

Figure 5.9. Typical Distorted Void Peak in 50 mM SDS Eluent

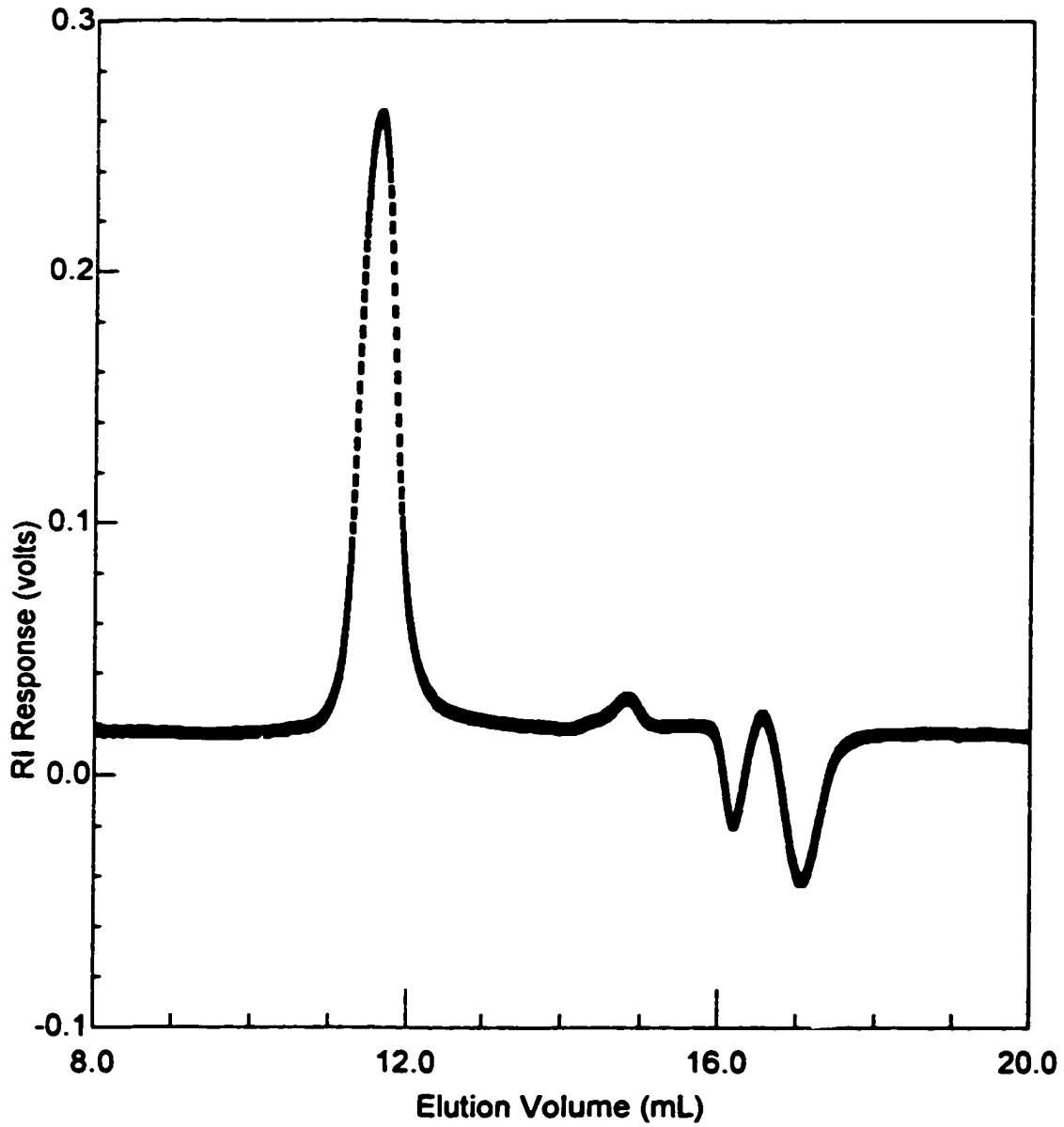

Figure 5.10. Multiple Peak Pattern of PEG 600 in 20 mM SDS

Curves are 90° LS (upper) and RI (lower) detector signals.

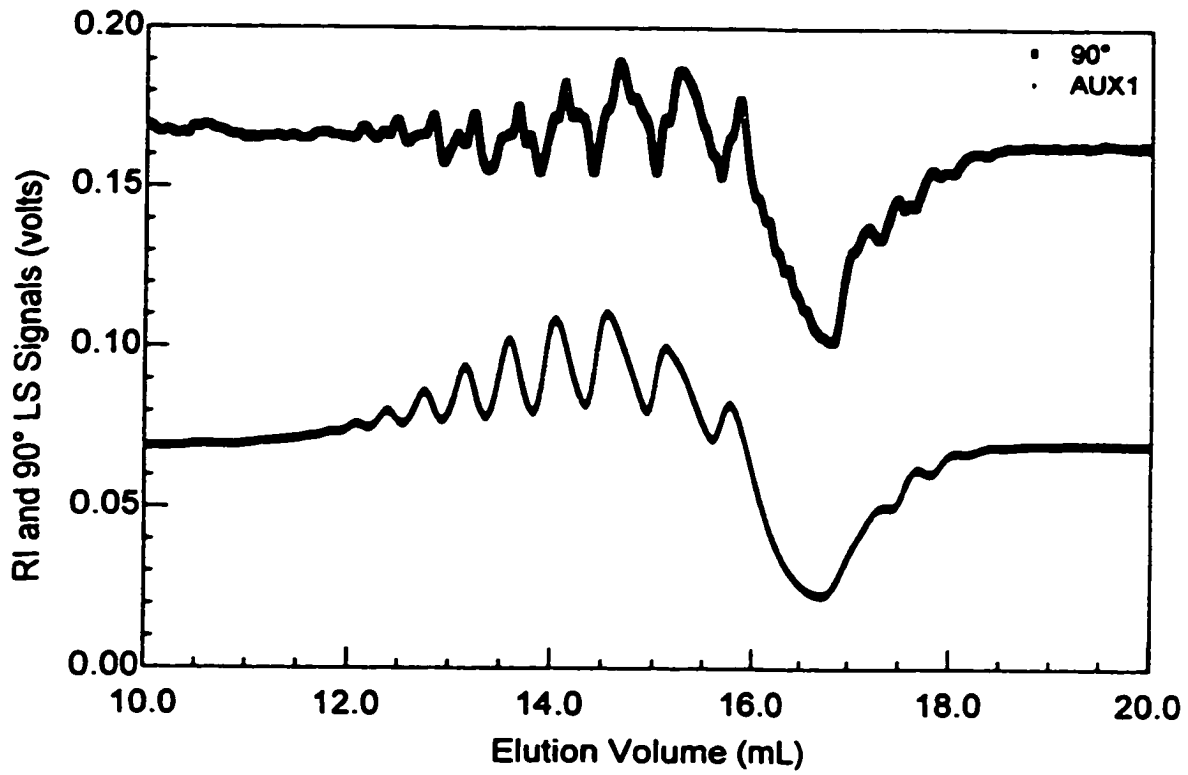

Discussion

Accurate dn/dc values for SDS and for the polymer samples are needed for the determination of analyte concentration by refractometry, and especially for the fitting of light scattering data to the Rayleigh equation, where the dn/dc enters as a square. Rempp [217] observed an increase of dn/dc in low molecular weight glycols to a reasonably constant value for masses between 1200 and 10,000 g/mol. Our samples span a broader range of molecular weight, confirming the constancy of dn/dc up to a molecular weight of 5,000,000 g/mol.

Candau *et al.* [218] noted that dn/dc values for solutions of polystyrene in several solvents are inversely proportional to molecular weight according to the relation

$$dn/dc_n = dn/dc_m + K_e / M_n \qquad (5.1)$$

where dn/dc_n is the measured dn/dc of a polymer sample of number-average molecular weight M_n, K_e is a parameter which represents the effect of the endgroups, and dn/dc_m has been interpreted as either the dn/dc of a polymer sample of infinite molecular weight, or that of the repeating unit. The lowering of dn/dc as the degree of polymerization decreases is due to the increased weighting of the effect of the polymer endgroups. The fit of our data for PEG and PEO to this equation is shown in Figure 5.3, yielding dn/dc_m = 0.1359 ± 0.0009 mL/g and K_e = -3.5 ± 0.3. A fit to the earlier data of Rempp [217] yields comparable values of dn/dc_m = 0.1422 ± 0.0009 mL/g and K_e = -3.7 ± 0.2. The errors reported are one standard deviation. In both fits the dn/dc of ethylene glycol was anomalously high and was omitted. We recognize that the PEO endgroups differ from those of the PEG samples, but this should not be a factor at high molecular weight. Several methoxy-terminated PEG samples of molecular weights less than 1000 g/mol were also measured and the dn/dc values were not significantly different from hydroxyl-terminated samples of similar molecular weight. We did not observe any anomalous increase of dn/dc proportional to the logarithm of molecular weight as was reported by Candau *et al.* [218] for polystyrene above 20,000 g/mol. The dn/dc values obtained from the fit were used in all further calculations.

The surfactant void, normally observed between 16 - 17 mL elution volume in

micellar eluent, as expected for a particle of 2 nm radius based on the elution volumes of PEG samples with the two column setup, was delayed in the premicellar eluent beyond the total mobile phase volume of the columns. The void in this eluent is a deficit in free surfactant concentration, which affects the equilibrium of the binding of surfactant to the column packing. Desorption of surfactant from the column packing results, which slows the elution of the void. In micellar eluents, the free surfactant concentration is buffered by the breakup of micelles rather than the desorption of surfactant from the stationary phase, and the void minimum elutes at a volume reasonable for a species the size of a micelle.

Figure 5.9 shows a change in the shape of the surfactant void observed in 50 mM SDS, which suggests a peak superimposed upon the void. This may be due to the dilution of the polymer concentration by band broadening as the complex elutes. Cann and Hinman [219] used a mass action argument to propose that this dilution would result in desorption of bound ligand (in this case, surfactant) from the macromolecule. This would result in a tailing of the complex peak, or a raised baseline between the complex and void peaks [220], and a peak of unbound ligand eluting just before the void. According to the model of Cann and Hinman, the magnitude of this effect should rise with the mobile phase ligand concentration, but diminish in large excess of ligand where the binding of larger amounts of ligand would be favored. Thus this effect may diminish in our case at higher surfactant concentration. This is in agreement with the observations of Veggeland and Austad [164], who suggest that the concentration of non-absorbed surfactant be kept above the cmc (i.e. free micelles should be present) to ensure saturation. While this appears to be necessary in micellar eluent, we observed saturated binding occurring online for surfactant-free polymer injections into premicellar eluent. Still, the relative concentrations of polymer and surfactant must be optimized when designing quantitative experiments to determine saturation of binding.

The elution volumes of complexes as displayed in Figure 5.4 are affected by the relative degrees of binding of the injected and eluted polymer, i.e. gain or loss of bound surfactant by the polymer during elution will affect the complex size and thus its elution velocity may not be constant over the length of the column. The observed 11 mL lower limit on exclusion volume for P-S complexes is probably due to ion exclusion [221], as we

believe that a surfactant layer is bound to the column packing which imparts a negative charge to the gel surface. The anionic complex is thus repelled by the gel and excluded from the pores. The observed limit is only slightly larger than the void volume of the column, suggesting that all of the pore volume of the G3000 column and some of the pore volume of the G5000 column is made inaccessible to the complexes. The fact that polymers in 50 mM SDS still show a substantial shift in elution volume proves that some degree of surfactant binding occurred in order to produce this ion exclusion effect. The fact that elution volumes of complexes in 50 mM SDS are somewhat higher than in 20 mM SDS is likely due to the higher ionic strength, reducing the double layer thickness and thus supressing the ion exclusion effect. In general, unless the surfactant used does not adsorb significantly on the column packing, or is nonionic, this ion exclusion effect will hamper the use of elution volume as a measure of complex size. The addition of sufficient supporting electrolyte should suppress this effect [222], but would also affect the free surfactant concentration and the binding ratio.

The multiple peak patterns observed in the elution profiles of the lower molecular weight PEGs are partly due to micellar chromatographic effects. In micellar liquid chromatography (MLC), a micellar mobile phase is used to enhance the separation of analytes [223]. The separation mechanism involves three partition equilibria, between the stationary, mobile, and micellar phases [224]. Hydrophobic analytes, which would otherwise be retained by the stationary phase, partition into the mobile hydrophobic environment of the micelles and are thus less retained. The technique has been used to measure micelle-water distribution coefficients for a variety of solutes [225].

From previous NMR experiments in our laboratory [18], it is known that the lower PEG oligomers have different apparent distribution coefficients into SDS micelles. The distribution coefficients are constant for PEG 4000 and above but lower for PEG 600 and 300, decreasing to zero for tetraethylene glycol (4EG). As with the decrease in dn/dc value for lower PEG oligomers, the decrease in distribution coefficient is due to the increased weighting of the effects of the endgroups on the molecular properties, with the hydroxyl endgroups favoring the aqueous environment. This suggests that there should be significant differences between the SDS micelle-water distribution coefficients of

individual oligomers of molecular weights perhaps as high as 1000 g/mol (DP = 22). This would permit separation by micellar chromatography, which would explain the multiple peaks shown in Figure 5.10.

We have applied the following equation, derived by Armstrong and Nome [224] in order to determine micelle-water distribution coefficients for the individual oligomers in the 600 g/mol PEG sample from their measured elution volumes.

$$\frac{V_s}{V_e - V_m} = \bar{v}[S]_m \frac{(K_{MW} - 1)}{K_{SW}} + \frac{1}{K_{SW}} \qquad (5.2)$$

In this equation K_{MW} and K_{SW} are the micelle-water and stationary phase-water distribution coefficients, $\bar{v}$ is the partial molar volume of micellar surfactant in the micelle (for SDS, 0.25 L/mol [226]), $[S]_m$ is the concentration of surfactant present in micelles (taken as the bulk concentration minus the cmc) and V_e, V_m and V_s are the peak elution, mobile phase, and stationary phase volumes. For a size exclusion column, we take V_m as the void volume, measured by the elution volume of a very large molecule which does not enter the gel pores, and V_s as the 'imbibed' volume of liquid in the pores, measured as the difference in elution volume between a very small molecule and a very large molecule. From a plot of $V_s/(V_e - V_m)$ versus $[S]_m$ at several concentrations of surfactant, the value of K_{MW} for each oligomer may be calculated from the ratio of the slope to the intercept. We determined distribution coefficients ranging from 20 to 68 for the 9th to 20th oligomers in the sample, consistent with the value of 45 ± 7 reported previously for the unseparated mixture [18]. We consider these results preliminary as we have no standard with which to confirm our assignments of oligomer numbers to the observed peaks.

Another contribution to some of the anomalous elution patterns may be a perturbation in the micelle size distribution in the injected samples due to the high oligoethylene glycol concentrations (0.3 - 1.5%) used. Previous work in our laboratory [227] showed that even though 4EG shows negligible partitioning into SDS micelles, acting only as a cosolvent, the average micelle aggregation number (N_s) and the critical micelle concentration (cmc) (and thus the free surfactant concentration in the presence of micelles or P-S complexes) of SDS decreased in the presence of this glycol. At the concentrations used in injected samples in the present study, the N_s and cmc would be

decreased by as much as 8%. The elution profiles of the pure glycol oligomers (for example, triethylene glycol in 50 mM SDS on the G5000 column, shown in Figure 5.11) show a trough and peak at the usual elution volume (16 - 17 mL on two columns, 7 - 8 mL on the G5000 column alone) of the surfactant void, even though the oligomer peak is not significantly displaced from its elution volume in pure water. Similar patterns appear with samples of mixed pure glycols EG through 4EG, and within the elution profile of PEG 200. As the sample loads onto the column, the larger micelles in the eluent will overtake the smaller micelles in the sample, creating a fluctuation in the mobile phase concentration of surfactant. As the micelles separate from the slower-moving glycol zone, the micelle size distribution will return to normal, but the concentration gradient will persist, resulting in the observed void and peak.

The effect of lower glycol oligomers on the cmc and aggregation number of SDS may also explain why 'negative peaks' are observed among the separated oligomers in the 200 to 600 g/mol mixtures. The baseline signal both in RI and LS detection should be suppressed in the presence of glycols due to lowering of free surfactant concentration and micelle size. Thus the peak pattern of the separated oligomers is superimposed upon a broad trough which interferes with the quantification of the RI and LS signals. Though no such distortions were observed with the higher molecular weight polymers, the free micelle concentration could experience some similar depression across the complex peak, since the free surfactant concentration in the presence of complex may be lower than the cmc. This would cause a slight distortion of the measured molecular weight averages and the quantitation of the complex peak. Veggeland and Austad [164] also expressed concern that some fraction of the missing surfactant was not bound to the complex but present in the counterion region of the complex due to the Donnan effect, which would cause the binding ratio to be overestimated slightly.

Figure 5.11. Perturbation of Micelle Background in RI Elution Pattern of 3EG in 50 mM SDS

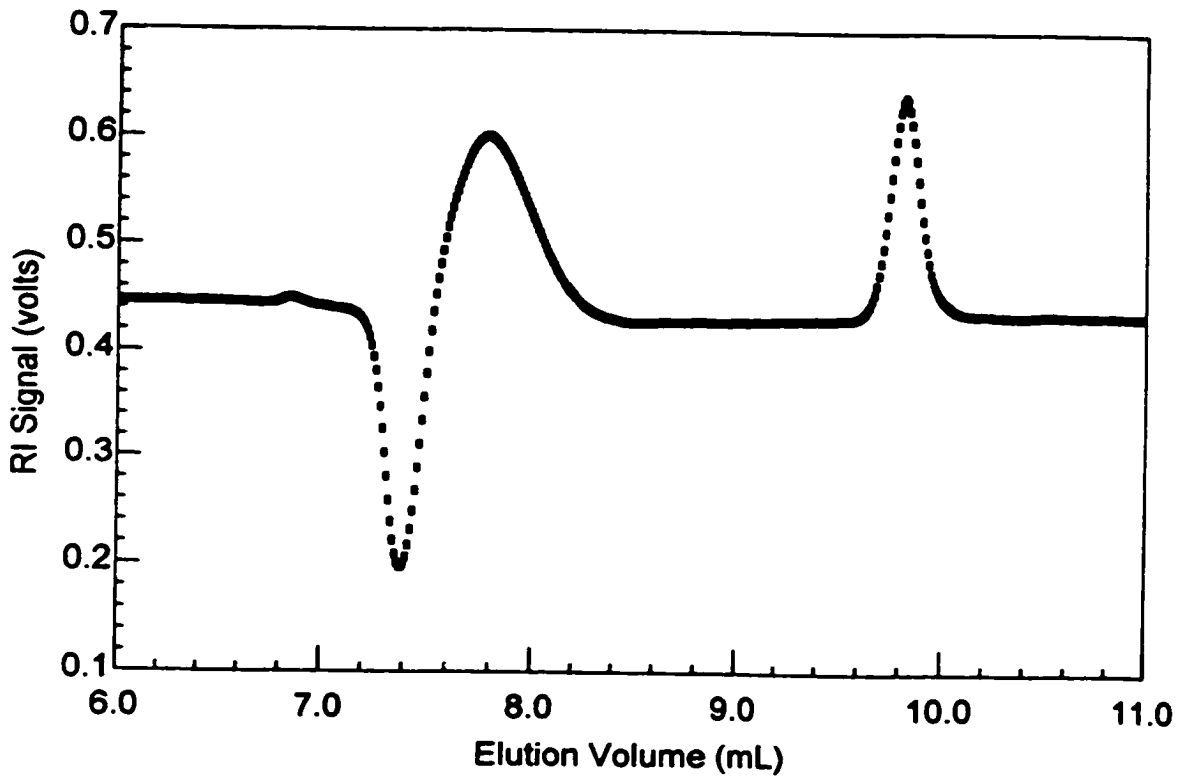

Conclusions From SEC Experiments

Size exclusion chromatography is a useful tool in the study of size and binding equilibria of polymer-surfactant complexes, but a number of difficulties are encountered in the quantitative interpretation of the results. Multi-angle laser light scattering detection provides additional information above that available from typical concentration detectors. However, the radius and molecular weight measurements are perturbed by fluctuations in the background scattering from micelles in the mobile phase. For light-scattering detection, the most promising mobile phase concentration is premicellar, between the cac of the polymer-surfactant complex and the cmc of the surfactant. There is the disadvantage that the surfactant void peak is delayed in premicellar eluent, eluting at volumes beyond the total column volume and thus lengthening run times. However, lack of micelles in the mobile phase minimizes fluctuations in background scattering, and eliminates the micellar chromatographic effects observed with smaller oligomers. In fact, the premicellar eluent clearly distinguishes between polymer samples which can and cannot nucleate micelle formation, i.e. polymers which produce a critical surfactant aggregation concentration lower than the surfactant cmc. The elution behavior of samples of molecular weight 600 and 1000 g/mol was unaffected by premicellar eluent even though these polymers were observed to interact with the micelles already present in eluents of higher concentration. We find that while a polymer of molecular weight 200 g/mol is sufficiently large to be solubilized by an existing micelle, a polymer larger than 1000 g/mol is needed to nucleate the formation of micelles at premicellar concentrations of surfactant.

This method should be applicable to study the interactions of any surfactant with any polymer of low polydispersity. Detailed investigation of a particular system requires the optimization of mobile phase composition, sample concentration and injection size, flow rate and pressure, etc. For the purposes of determining maximum binding ratios, choosing the correct mobile phase and sample concentrations is imperative. In practice, columns should provide optimum separation between the expected sizes of the P-S complex and the surfactant micelle [220]. The use of a polymer molecular weight at least an order of magnitude larger than the micelle molecular weight should provide adequate

separation. Also, the hydrophobicity of the column packing is important, as the reversible binding of surfactant to the packing can also affect the chromatography.

The demonstrated ability to distinguish aggregating and non-aggregating molecular weights of PEG suggests that this method should be sensitive enough to study weakly interacting systems (such as nonionic polymer-nonionic surfactant) to determine if there is any significant binding. Indeed, other studies of polymer-surfactant systems have demonstrated associative or dissociative behavior in HPSEC, depending on polymer structure and surfactant charge and headgroup [164-166]. Other systems may be amenable to more specific modes of detection such as UV or fluorescence, which may be used to independently detect polymer and surfactant amounts in the complex.

The results reported here clearly demonstrate three different types of PEG-SDS interaction depending on the PEG molecular weight. For very small oligomers (DP $\leq$ 4) the glycol acts as a cosolvent. It does not partition into or bind onto the micelles, but as a cosolvent causes a reduction of micelle size. Higher oligomers (DP up to at least 20) show increasing partition coefficients into the micelles, but are free to enter and exit the micelle. Polymers of greater size bind one or more surfactant micelles, and although individual surfactant monomers may migrate in or out of the complex, the polymer is never free of bound surfactant.

This work also points to the possibility of determining partition coefficients of such oligomers, or quantitative determination of oligomer distribution in mixtures, by micellar chromatography (with or without the additional size exclusion mechanism). Such separations are of interest for example in the structural analysis of mixed oligomeric polyglycol surfactants, whose surfactant properties are strongly dependent on the average and polydispersity of the number of glycol units in the molecules. A search of the literature indicates that while micellar chromatography has been in use for over twenty years to enhance separation of compounds [223] and to measure partition coefficients [228], it does not appear to have been used previously in the separation of oligomeric homopolymers. Our present detection system cannot precisely quantify the distribution of oligomers in the presence of fluctuating surfactant background, however better selectivity may be attainable by other detection methods such as FTIR, mass spectrometry, or UV or

fluorescence spectroscopy in the event that the polymer under analysis has a detectable chromophore.

5.5. Summary and Conclusions

The PEO-SDS and PVP SDS systems provide a well known testing ground for our fluorescence and chromatographic methods. Our aggregation numbers are smaller in the complexes (≈ 30) than in the free micelles (≈ 60) as has been widely reported. The aggregation number in the presence of both species is a weighted average which tends to be biased toward the smaller aggregates at high quencher concentrations. We also note the relatively high microviscosity of the PVP - SDS aggregates, which is attributable to the insertion of the pyrrolidone rings into the surface of the micelle, and the relative conformational rigidity of the polymer.

Refractometry, mass spectrometry and SEC were used to characterize PEO over a wide range of molecular weights. The refractive index increment of 0.1359 mL/g decreased at low molecular weight due to the increasing contribution from the endgroups of the polymer. Molecular weights were in good agreement with nominal values, and commercial PEG samples were noted to be highly monodisperse, while commercial PEO samples were broad and even bimodal, and not well suited for studies of surfactant binding by SEC.

Size exclusion chromatography equipment was adapted for use with surfactant eluent to study polymer-surfactant interactions. Multi-angle laser light scattering detection was used to measure molecular weights without reference to elution volume, which proved necessary due to non-size exclusion effects. The complex peak and surfactant void both provide the means to determine the amount of bound surfactant. Under optimized conditions, the SEC method yields the same saturation binding ratio as determined by other methods. We found best results using premicellar eluent, and recommend multiple injections of different quantities of polymer to ensure saturation of binding.

In the presence of free micelles, small oligomers of PEG were separated by micellar chromatography based on their partitioning between the micelle and water phases,

demonstrating that this method could be applied to determine distribution coefficients of various solubilizates, including fluorescence probes and quenchers. This also demonstrated that there are three classes of complexation of different oligomers of PEG with SDS: no interaction for very small oligomers, partitioning of intermediate oligomers in and out of micelles, and binding of micelles to larger oligomers which are then never free of bound surfactant.

CHAPTER 6. INTERACTIONS OF A CATIONIC SURFACTANT WITH ANIONIC POLYELECTROLYTES

In this chapter, we present a study of the interaction of the cationic surfactant dodecyltrimethylammonium bromide (DTAB) with the anionic polyelectrolyte sodium polyacrylate (NaPA) and partially hydrolyzed polyacrylamides (PAM-*co*-NaPA) of varying acrylate content. The time-resolved fluorescence quenching method was used to determine aggregation numbers, as well as rates of fluorescence decay and quenching by pyrene excimer formation or by added alkylpyridinium halide surfactant. We chose to study these systems because extensive literature data obtained using other techniques were available for comparison. Numerous binding isotherms for interactions of alkyltrimethylammonium and alylpyridinium halide surfactants with NaPA [229], partially hydrolyzed polyacrylamides [230], and other polyelectrolytes [231,232] had been measured previously in this research group, providing necessary data for the calculation of aggregation numbers from the fluorescence results. We also measured two isotherms for the binding of DTAB to NaPA specifically for this purpose, at desired conditions of polyelectrolyte concentration and added electrolyte.

At the commencement of our study, no aggregation number data had been published on these particular systems, which was our main reason for applying our fluorescence techniques to these systems. However, other researchers have since published studies which included the DTAB-NaPA system [233,234], to which we can compare our results. The agreement is good for the aggregation numbers and measured rate constants, but we find fault with their choice of quencher and some of their assumptions in handling the data, which will be discussed in Section 6.5.

6.1. Background

Mixtures of ionic surfactants with oppositely charged polyelectrolytes show strong cooperative binding, with critical aggregation concentrations typically two orders of magnitude lower than the surfactant cmc. The difference in the strength of the binding relative to that with nonionic polymers is ascribed to charge interactions, while the cooperativity is a result of hydrophobic interactions between nearest neighbour surfactant

molecules bound to the chain. The cooperativity may be modeled as a linear array of charge sites, with the following binding equilibria [235]:

$$S^+ + OO \underset{\longleftarrow}{\overset{K}{\longrightarrow}} OS \tag{6.1}$$

$$S^+ + OS \underset{\longleftarrow}{\overset{Ku}{\longrightarrow}} SS \tag{6.2}$$

where S^+ is a surfactant ion, OO represents two empty adjacent sites on the polymer, OS a single site bound and SS two adjacent sites bound. The binding constant K refers to isolated binding while the product Ku refers to binding to a site adjacent to another bound surfactant ion. The cooperativity parameter u refers to the aggregation of bound surfactants according to the equilibrium

$$2OS \underset{\longleftarrow}{\overset{u}{\rightleftharpoons}} OO + SS \tag{6.3}$$

A binding isotherm plotted as the fraction of occupied polymer charge sites β_c versus the logarithm of free surfactant concentration $[S]_f$ yields the equilibrium constants from the free surfactant concentration and the slope at the half-bound point on the isotherm ($\beta_c = 0.5$) from the expressions of Satake and Yang [236]

$$Ku = \left(\frac{1}{[S]_f}\right)_{\beta_c=0.5} \tag{6.4}$$

$$u = 16\left(\frac{d\beta_c}{d\ln[S]_f}\right)^2_{\beta_c=0.5} \tag{6.5}$$

Hayakawa *et al.* [229] reported a cooperativity parameter u of 15 and binding constant Ku of 26900 mol^{-1} kg for binding of DTAB to 1.0 mm NaPA in the absence of added salt. The binding constant of tetradecyltrimethylammonium bromide (TTAB) was an order of magnitude greater. The Gibbs energy of transfer of surfactant ions from bulk solution into the complex as given by

$$\Delta_{tr}G^\circ = kT \ln (Ku) \tag{6.6}$$

was determined, yielding a difference of 2.19kT between the binding of DTA^+ and TTA^+, typical for the transfer of two methylene groups from water to a micellar environment.

For the PAM-*co*-NaPA polymers, lower charge density results in less cooperative behaviour, and lower binding constants [230]. This is not a general rule for polymers of widely different structure, however, since hydrophobicity, flexibility and molecular structure also affect binding [235]. The model fits well to the lower end of the observed binding, but fails at high levels of bound surfactant, which may be attributed to electrostatic effects, particularly counterion condensation on the polymer. As well, since the model is based on pairwise interactions, it does not inherently predict the presence of a most favourable or modal value of the aggregation number, though at $\beta_c = 0.5$ the model predicts the average length of an unbroken series of occupied sites in an infinite array as $1 + u^{1/2}$, which has been used as an estimate of N_s.

The binding often leads to phase separation at dilute surfactant concentration, producing a coacervate rich in polymer and surfactant and a supernatant depleted in both. Addition of sufficient excess surfactant or supporting electrolyte can produce soluble complexes (and addition of water to concentrated samples in some cases results rather surprisingly in phase separation, due to the reduction of the concentration of supporting electrolyte, with further addition of water causing further concentration of the gel phase [237]). Thalberg *et al.* [238] reported phase separation in 1 mM NaPA at about 1.3 mM DTAB, with clearing at 1 M DTAB or with addition of 0.25 M NaBr. In the current research, we elected not to study the two-phase systems, and used this information to select sample concentrations in the dilute region below phase separation, as well as in the clear region with swamping electrolyte.

It is believed that the "beads and string" model of the complexes formed between surfactants and neutral polymers is also valid in surfactant-polyelectrolyte complexes. Fluorescence probing studies are an excellent method to test this theory, as they can detect the presence of numerous discrete aggregates bound per polymer chain. Evidence suggests that these structures persist even in highly condensed polymer-surfactant phases. This method has recently been applied to confirm the presence of discrete DTAB micelles in a crosslinked NaPA gel [239]. An X-ray scattering study of an FCC liquid crystal phase formed by a 1:1 DTA^+PA^- complex suggests a cylindrical structure with periodic fluctuations in diameter [240]. Although the authors do not interpret their model in this

manner, the periodicity of 4.1 nm and the average cylinder diameter of 2.1 nm are suggestive of a "beads and string" morphology even in this waterless state.

In recent years, several researchers have applied fluorescence techniques to study the structure of cationic surfactant-anionic polyelectrolyte complexes. Reported effects of polymer binding on surfactant aggregation numbers differ widely. Abuin and Scaiano [241] used a variety of photochemical techniques in a study of interactions of DTAB with poly(styrene sulfonate). They concluded from the quenching of xanthone triplets that the complexes contained numerous distinct clusters of less than 10 DTAB molecules each. Pyrene fluorescence spectra revealed a less polar micelle environment than in free DTAB micelles. Chu and Thomas [242] studied the poly(methacrylic acid)-C_nTAB system by steady-state and time resolved fluorescence of pyrene quenched by DPC as well as excimer formation. They did not correct for the concentration of free surfactant or quencher, which should halve the aggregation number of 100 to 120 surfactant molecules they reported for the single C_{10}TAB micelle bound to a polymer of average molecular weight 11,000. This still yields a higher aggregation number than the value of 36 reported for free C_{10}TAB micelles. The pyrene I_1/I_3 ratio decreased on formation of complexes and was used to measure cac values, which decreased with surfactant chain length. The fluorescence depolarization of 2-methylanthracene indicated a more fluid environment in the complex than in solutions of polymer or surfactant alone. A recent study using a fluorescent probe covalently bound to the anionic polysaccharide hyaluronan also reported a decrease in polarization above the cac for binding of DTAB [243]. Aggregation numbers in C_nTAB-hyaluronan complexes were reported to be rather insensitive to the binding ratio, due to the low charge density and stiffness of the polymer [244]. In the concentrated phase of a phase separated system the micelles were found to be larger than normal free micelles. Complexes of DTAB and CTAB with sodium polystyrenesulfonate reportedly have lower aggregation numbers and lower polydispersities than free micelles, attributed to the insertion of the hydrophobic portions of the polymer repeat units into the micellar surface [213]. The aggregation numbers were insensitive to the binding ratio or changing the surfactant counterion to chloride. On the other hand, complexes of DTAB with sodium polyvinylsulfate and sodium dextransulfate [245] were measured to have

larger aggregation numbers (>100) than in DTAB-NaPA complexes or free DTAB micelles (60) [234], attributed to the higher cooperativity of binding in these systems than in DTAB-NaPA. Aggregation numbers of DTAB bound to sodium carboxymethylcellulose increased with the linear charge density of the polymer toward the normal value for free micelles, again attributed to the increasing cooperativity of binding [246].

Several studies on cationic surfactant-polyacrylic acid (PAA) complexes have been reported recently. Chandar *et al.* [247] studied the interaction of DTAB with PAA and a pyrene-labeled PAA. The pyrene I_1/I_3 ratios indicated a lower micropolarity on formation of DTAB-PAA complexes, and were used to monitor the rise in cac with solution pH (and therefore in the degree of ionization of the polymer). Kiefer *et al.* [248] reported time resolved pyrene excimer quenching measurements of aggregation numbers in TTAB-PAA complexes at varying binding ratios and degrees of ionization of the polyelectrolyte. Their reported aggregation numbers reveal no trend with either variable, with an average value of 45 ± 13 which is lower than the value of 60 ± 2 reported for free micelles in 10 mM TTAB or 100 ± 13 reported in the presence of 10 mM NaBr. The change in I_3/I_1 with concentration of free surfactant closely resembled the binding isotherm, confirming the existence of a cac for the formation of hydrophobic regions. Choi and Kim [249] found that the cac for interactions of several alkyltrimethylammonium surfactants with PAA as evidenced by pyrene I_1/I_3 ratios decreased with polymer molecular weight and increased with polymer concentration. De Oliveira *et al.* [250] determined by TRFQ of pyrene by DPC a rather large aggregation number of 120 ± 10 for C_{10}TAB-PAA aggregates at pH 8.63. For aggregates formed with copolymers of increasing ethyl methacrylate content (but with degree of ionization fixed by lowering pH) aggregation numbers decreased to values similar to the value of 48 measured in free micelles. Fundin *et al.* [251] found that the aggregation number of CTAB-PAA aggregates increased with degree of binding (55-87) but was always less than in the free micelles (107). The CPC quenching rate constant was also smaller than in free micelles, even though the micelles were smaller, indicating a reduced mobility of quencher. The TRFQ studies of Hansson and Almgren on the DTAB-NaPA system [233,234] will be discussed in detail in Section 6.4.

This survey of literature data shows that fluorescence techniques can provide a variety of different types of information about polyelectrolyte-surfactant complexes. The reduced polarity sensed by pyrene in the aggregates compared to that in water has been widely reported and has been used to measure cac values with reasonable accuracy. However, fluorescence techniques, in particular measurements of microviscosity, have not been widely used on these apparently simple systems. Inconsistencies exist, especially in the reported aggregation numbers and their dependence on pH, binding ratio, etc., leaving much room in these systems for further use of fluorescence techniques.

6.2. Experimental

Materials

Poly(acrylic acid) (PAA, Aldrich, MW 250,000), in acid form, was purified by dialysis. It is obvious that pH will affect the degree of ionization of the polymer and thus the degree of binding, if not the aggregation number. We therefore added excess NaOH to our PAA sample to ensure complete neutralization. A concentrated PAA stock solution (0.1 m) was converted to the sodium salt (NaPA) by addition of NaOH solution to pH 11. Cetylpyridinium chloride (CPC, Aldrich) and tetradecylpyridinium bromide (TPB, product of an earlier synthesis from 1-bromotetradecane and pyridine [252]) were decolourized with charcoal and recrystallized from acetone. Dodecyltrimethylammonium bromide (DTAB, Aldrich) was recrystallized from an acetone/ethanol mixture. Pyrene (Py, Eastman, or K&K Laboratories, Hollywood, CA) was recrystallized from ethanol and then sublimed. Water was purified by a Millipore R/Q reverse osmosis filter system.

The following preparations and characterizations of a series of partially hydrolyzed polyacrylamides were performed by Sumita Ranganathan [230]. A polyacrylamide (carboxyl modified, low carboxyl content, MW 150,000) was obtained from Aldrich Chemical. Samples were hydrolyzed under chosen conditions of concentration, temperature and duration of exposure to NaOH solution, producing copolymers of desired carboxylate content. Polymers were precipitated from the aqueous reaction medium by addition of methanol, redissolved in water and freeze-dried. The degrees of hydrolysis

were determined by titrations (conductometric and pH) of samples of the copolymers which had been converted to the acid form on a cation exchange column. The original polymer was thus determined to have a carboxyl content of 16%. Molecular weights were determined using a Cannon-Fenske capillary viscometer, and were found to increase with degree of hydrolysis due to the fractionation effect of the polymer precipitation. Binding isotherms of DTAB to the copolymers and NaPA in 0.01m NaBr were determined using a surfactant selective electrode in the same manner as for the DTAB-NaPA binding isotherms presented here. The structures, viscosity-average molecular weights, and degrees of polymerization of the polymers are given in Figure 6.1.

Figure 6.1. Structures and Molecular Weight Properties of the PAM-*co*-NaPA Samples.

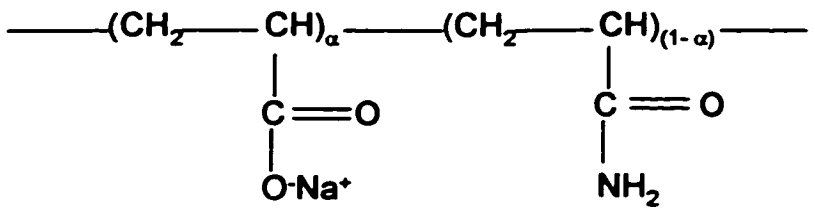

Polymer	α	M_v ($\times 10^3$ g/mol)	DP
PAM40	0.40	250	3100
PAM79	0.79	280	3100
NaPA	1.00	250	3400

Binding Isotherms

The DTAB-NaPA binding isotherm in the absence of added salt was measured by EMF titrations using a surfactant-sensitive electrode [253]. The electrode was prepared by affixing a plasticised poly(vinylchloride) (PVC) membrane containing a complex of DTAB with sodium dodecyl sulfate (SDS) to one end of a PVC tube which was then filled with a reference DTAB solution and placed in the sample cell. Two calomel electrodes were connected to the sample and reference cells via agar salt bridges and the potential difference between them was measured by a Keithley 614 electrometer. A Metrohm 645 Multi-Dosimat was used to titrate a 10 mm DTAB solution into a 1.1 mm polymer solution, keeping the polymer concentration (which was corrected for dilution in determining the degree of binding) within ±10% of 1.0 mm. A computerized autotitrator program allowed the voltage signal from the electrometer to stabilize to a set tolerance before recording the voltage and delivering the next aliquot. Comparison to a calibration curve measured in the absence of polymer yields the concentration of free monomeric surfactant in the polymer-surfactant solution. Using the known bulk surfactant concentration after each addition of titrant, the fraction of bulk surfactant bound to the polymer was calculated, and the binding ratio β

$$\beta = \frac{[\text{DTAB}]_b}{[\text{monomer}]} \tag{6.7}$$

where [monomer] is the polymer concentration expressed as moles monomer unit per kg solvent, was plotted versus the logarithm of the molal free surfactant concentration.

A second binding isotherm was similarly measured in the presence of 0.3 m NaCl by titrating a 30 mm DTAB solution into a 10 mm polymer solution. Samples for fluorescence measurements were then prepared at selected surfactant concentrations on the binding curves. In the case of the PAM-*co*-NaPA polymers, the degree of binding β_c is expressed in terms of mole bound surfactant per mole carboxylate unit (i.e. mole of negative charge groups), which is related to the binding ratio per total monomer concentration by the degree of hydrolysis α.

$$\beta_c = \frac{[DTAB]_b}{[COO^-]} = \frac{\beta}{\alpha} \qquad (6.8)$$

Obviously, for fully neutralized NaPA $\alpha = 1$ and the two binding ratios are identical. Binding isotherms measured previously in the presence of 10 mm NaBr [230] were used to calculate amounts of bound surfactant in fluorescence samples. Knowing the bulk polymer and surfactant concentrations, β_c is estimated, $[DTAB]_f$ is read from the plot, and the estimate is improved iteratively.

Fluorescence Probing Studies

Aggregation numbers were measured by time-resolved fluorescence using an FLI 3000 (Photochemical Research Associates) single photon counting apparatus with 256 data channels. Samples of polymer-surfactant mixtures containing hydrophobic fluorescence probes were prepared by slowly adding a dilute solution of DTAB into a similar volume of vigorously stirred dilute polymer stock, using a manually controlled Metrohm 645 Multi-Dosimat titrator. This method was required to avoid precipitation of saturated polymer-surfactant complexes which occurred on batch mixing or on addition of concentrated stocks. An aliquot of a stock solution of pyrene in ethanol was placed in a sample vial and the ethanol evaporated by a stream of nitrogen gas to leave a thin film of pyrene on the glass surface. Polymer-surfactant solution was then added and the sample mixed for a few days to ensure complete solubilization of the pyrene.

Due to the very low concentration of micelles expected (10^{-5} m), we chose pyrene excimer formation as the fluorescence quenching mechanism for NaPA samples, so that pyrene concentrations of that order could be used to maximize the intensity of the fluorescence signal. Due to suspicions of mobility of the pyrene probes between bound micelles, we later chose to investigate several cationic and nonionic quenchers in the systems with PAM-*co*-NaPA polymers. Due to the use of these very low pyrene concentrations, much longer collection times were required for the photon counting experiments.

The model equation for pyrene excimer quenching is of the same form (Infelta-Tachiya, Equation 3.12) as for added quenchers, with the pyrene concentration used as the

quencher concentration. In cases where only pyrene excimer quenching is being used, researchers tend to use a different symbol (e.g. P or Py) to denote pyrene concentrations, etc., and refer to an excimer decay constant k_E instead of the quenching rate constant k_q. Since we will be discussing both added quenchers and excimer quenching simultaneously in this chapter, we have chosen to use the symbol Q in all equations and to refer to pyrene as the quencher where appropriate in order to avoid repetition.

When calculating aggregation numbers, pyrene as quencher was assumed to be 100% micellized (i.e. $[Q]_b = [Q]_t$). The aqueous solubility of pyrene is only 0.7 μm, and its distribution coefficient between DTAB micelles and water is reported as 4×10^6 L mol^{-1} [113], such that at even at the low pyrene concentrations used in this study (5 μm and above) over 95% of the molecules should be solubilized. Failure of this assumption would result in an underestimation of the aggregation number.

The alkylpyridinium quenchers were also expected to be essentially completely solubilized because they are more hydrophobic than DTAB; both the cmc of the pure surfactant and the cac of the surfactant binding to NaPA are much lower for CPC and TPB than for DTAB. To verify this, we apply Clint's ideal mixing theory [254] for mixed micelles of two surfactants, which we will denote as Q and S, to estimate X_q, the mole fraction of Q in the mixed micelles,

$$X_q = \frac{[Q]_m}{[S]_m + [Q]_m} \tag{6.9}$$

which is not the same as a, the mole fraction of Q in the bulk.

$$a = \frac{[Q]_t}{[Q]_t + [S]_t} \tag{6.10}$$

Assuming ideal mixing, the free concentration of the first component surfactant $[Q]_f$ is related to the cmc of the pure surfactant $[Q]_{cmc}$ by

$$[Q]_f = X_q [Q]_{cmc}, \tag{6.11}$$

and for the other component surfactant of the mixture

$$[S]_f = (1-X_q)[S]_{cmc}. \tag{6.12}$$

To apply this theory to polyelectrolyte-surfactant complexes, we assume that the cac of the complex of any pure surfactant with a polyelectrolyte may be substituted for the

cmc (subscript cmc → cac), and bound concentrations for micellar concentrations (subscript m → b). This equivalence has been more rigorously derived in the literature [234]. We estimated cac values in our systems based on previously measured binding isotherms. Since binding isotherms of alkylpyridinium surfactants to the PAM-*co*-NaPA polymers were not available, we calculated $[Q]_{cac}$ by assuming that the ratio $[S]_{cac}/[Q]_{cac}$ was the same for the copolymers as for NaPA. $[CPC]_{cac}$ for binding to NaPA was estimated as 2 μm based on the values for DPC and TPB [252]. We thus estimated $[Q]_{cac}$ as 2.6 μm for CPC-PAM79 and 83 μm for TPB-PAM40.

The mole fraction of quencher in the mixed micelles is given by solving a quadratic equation in X_q [234], which is algebraically simpler than but identical to the equation in $[Q]_f$ given by Clint [254]

$$D X_q^2 + E X_q - [Q]_t = 0$$

$$X_q = \frac{-E + \sqrt{E^2 + 4D[Q]_t}}{2D} \qquad (6.13)$$

where $D = [S]_{cac} - [Q]_{cac}$ and $E = [S]_t + [Q]_t - D$. The fraction of the bulk concentration of quencher which is bound to the micelles may be calculated by rearranging Equation 6.11, with substitution of $[Q]_f = [Q]_t - [Q]_b$.

$$\frac{[Q]_b}{[Q]_t} = 1 - X_q \frac{[Q]_{cmc}}{[Q]_t} \qquad (6.14)$$

This calculation results in an expected bound fraction of 99% for CPC in the samples studied. For TPB, we estimate 94% of the quencher is bound in the samples at $\beta_c = 0.48$, and 74-84% (at increasing mole fraction of quencher) in the samples at $\beta_c = 0.14$. We then calculate aggregation numbers using the estimated mole fraction of quencher in the mixed micelle $N_a = \langle Q \rangle / X_q$, such that the resulting aggregation number is the total aggregation number of quencher and surfactant [234].

Samples were not deoxygenated because irreversible polymer-surfactant precipitates were formed when using the freeze-pump-thaw method. Samples could have been deoxygenated by other methods such as vacuum degassing or bubbling with inert gas, but these methods are less thorough, less reproducible, and may lead to loss of sample

due to foaming, or concentration of sample due to evaporation of solvent. A relatively constant, equilibrated oxygen level was deemed preferable to a reduced but uncertain level because the variation in the observed lifetime was of interest. We note that in the studies of Hansson and Almgren [233,234], samples were also in equilibrium with air.

Steady-state fluorescence spectra of some of these samples were recorded on a Perkin-Elmer MPF-66 fluorescence spectrophotometer. The peak intensities at ~374 and 385 nm were read in order to calculate I_1/I_3 ratios.

6.3. Results

Binding Studies

The binding isotherm of DTAB to 1.0 mm NaPA is shown in Figure 6.2. Surfactant concentrations of 0.3 mm and 0.5 mm were chosen for fluorescence samples. At these concentrations the fraction of the bulk amount of DTAB which was bound to the polymer $X_b = [S]_b / [S]_t$ was near the maximum value of 78%. The fraction of occupied polyelectrolyte charge sites β_c in the two samples was 22% and 38% respectively, so that the amount of bound polymer approximately doubles between the two samples. These samples exhibit binding of surfactant at concentrations well below the normal CMC of DTAB (15.5 mm in a salt-free solution [255]). Thus there are no free micelles present. At higher degrees of binding turbidity and precipitation became a problem.

The binding isotherm of DTAB to 10 mm NaPA in the presence of 300 mm NaCl is also shown in Figure 6.2. The curve is shifted to a higher free surfactant concentration and rises much more sharply than in the salt free case, indicating lower binding strength but higher cooperativity. The values of the binding constant Ku and cooperativity parameter u calculated from the isotherms using Equations 6.4 and 6.5 are shown in Table 6.1 and compared to previously determined values for NaPA [229] and the copolymers [230]. In general, Ku decreases and u increases with added salt, and both parameters increase with polymer charge density.

Figure 6.2. Binding Isotherms of DTAB to NaPA and PAM-*co*-NaPA [230]

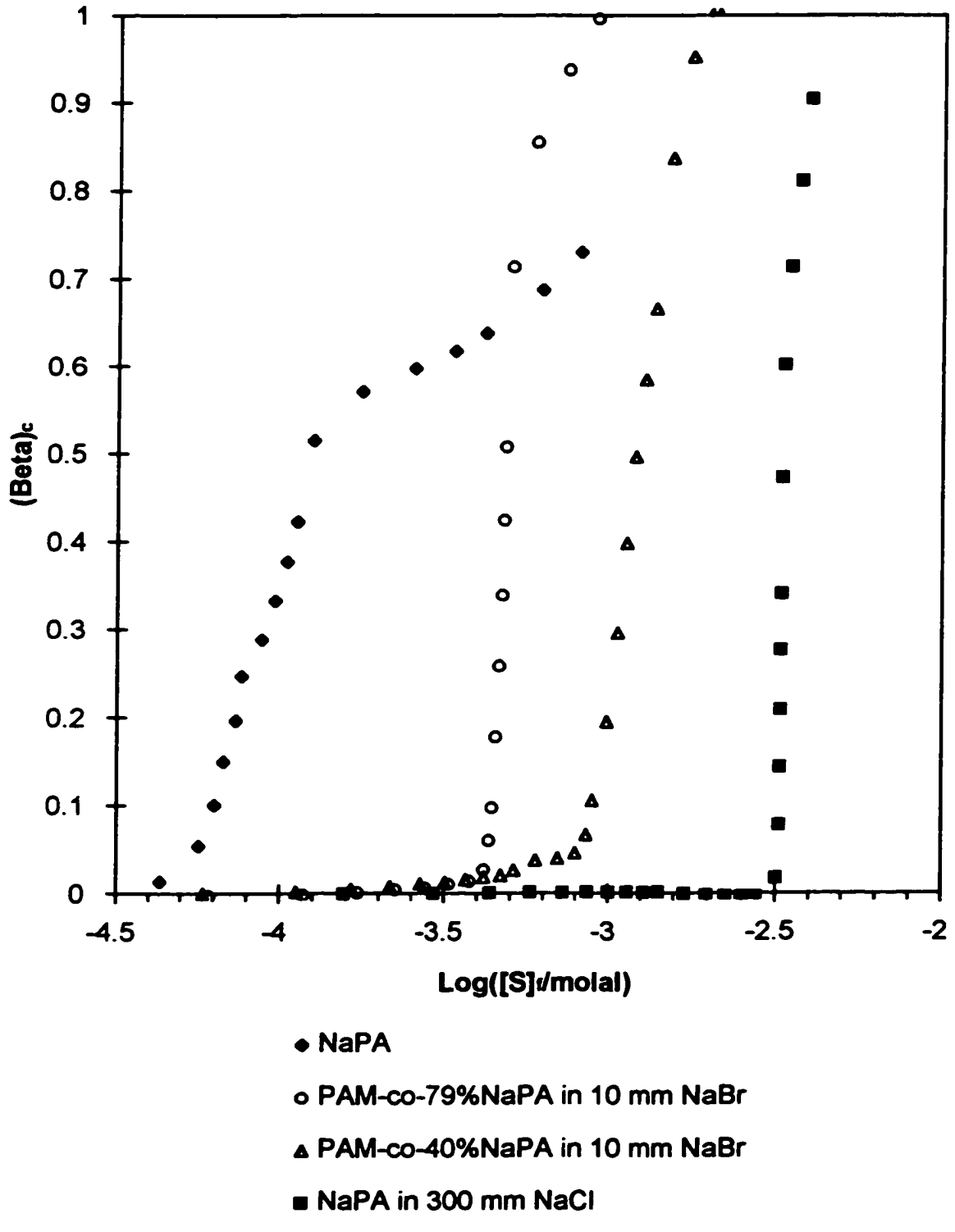

Table 6.1. Binding Constants Ku and Cooperativity Parameters u for DTAB-Polyacrylate Systems.

Polymer	Salt	Ku (mol^{-1} kg)	u	Reference
NaPA	none	26900	15	[229]
NaPA	none	8100	51	This Work
NaPA	10 mm NaCl	2690	500	[229]
NaPA	10 mm NaBr	2500	160	[230]
NaPA	300 mm NaCl	300	20000	This Work
PAM79	10 mm NaBr	2100	300	[230]
PAM40	10 mm NaBr	900	35	[230]

Our values of Ku and u for NaPA measured in the absence of salt are not in agreement with those reported by Hayakawa *et al.* [229], which we attribute to a slight excess of NaOH remaining after the neutralization of the polymer. Assuming that the relationship between log(Ku) and log([salt]) is linear as reported for several other cationic surfactant-anionic polyelectrolyte systems [232], we have estimated this excess ionic strength at 1.6 mm. Turbidity was still a problem even at this level of added salt, such that the samples prepared for fluorescence measurements had a rather low binding ratio (0.09).

Based on the available binding isotherms [230], also shown in Figure 6.2, samples of DTAB with PAM-*co*-NaPA polymers with 40% and 79% acrylate content were prepared in 10 mm NaBr for fluorescence quenching studies. In the samples with 40% acrylate copolymer, the quenching was by TPB or pyrene excimer formation, while several quenchers were compared in the 79% acrylate system before CPC was chosen. The compositions of all the P-S samples are summarized in Table 6.2.

Table 6.2. Compositions of DTAB/PAM-*co*-NaPA Samples Studied by TRFQ

	Polymer						quenching
α	[monomer]	[COO^-]	$[DTAB]_t$	X_b	β_c	[salt]	mechanism
1	1.0	1.0	0.50	0.78	0.38	0	excimer
1	1.0	1.0	0.30	0.75	0.22	0	excimer
1	8.7	8.7	4.0	0.19	0.087	300	excimer
0.79	0.39	0.31	0.60	0.20	0.40	10	various
0.79	0.57	0.45	0.60	0.22	0.30	10	CPC
0.40	6.0	2.4	2.3	0.49	0.48	10	TPB & excimer
0.40	4.1	1.6	1.2	0.20	0.14	10	TPB

All concentrations millimolal. Added salt NaCl for NaPA samples, NaBr for copolymer samples.

Fluorescence Measurements

Fluorescence decay curves were measured on the DTAB-polymer mixtures at varying quencher concentrations. Sample decay curves are shown in Figure 6.3. The complete results at each pyrene concentration for one of the excimer quenched DTAB-NaPA samples are given in Table 6.3 as an example. The fits to individual curves were generally good, as judged by regression correlation coefficients r^2 and plots of weighted residuals. The values of the fitted parameters, however, are inconsistent with the simple kinetic model of Equation 3.17. The values of A_2 are not constant within experimental error, but increase with quencher concentration, and do not approach the value of A_2 derived from a monoexponential fit to a decay curve measured at very low pyrene concentration. The values of A_4 also tend to increase slightly with pyrene concentration. The increase of A_3 with [Q] is not linear, and the value does not approach zero at very low concentrations of pyrene, such that the calculated aggregation numbers decrease with [Q].

Table 6.3: Fits of TRFQ Measurements on 0.30 mm DTAB-1.0 mm NaPA Samples.

[Py] (μm)	A_2 (10^6 s^{-1})	A_3	A_4 (10^6 s^{-1})	r^2	N_a
0.100	6.29 ± 0.11	-	-	0.9884	-
1.16	4.84 ± 0.17	0.351 ± 0.049	10.2 ± 1.7	0.9980	68 ± 9
1.77	4.75 ± 0.16	0.384 ± 0.043	11.2 ± 1.6	0.9946	48 ± 5
2.08	5.10 ± 0.12	0.370 ± 0.028	13.0 ± 1.4	0.9978	39 ± 3
2.44	5.23 ± 0.12	0.486 ± 0.029	12.3 ± 1.0	0.9971	45 ± 3
2.64	4.69 ± 0.27	0.533 ± 0.080	9.5 ± 1.6	0.9958	45 ± 7
3.78	4.88 ± 0.19	0.686 ± 0.055	10.3 ± 0.9	0.9937	41 ± 3
6.60	5.35 ± 0.17	0.835 ± 0.044	12.3 ± 0.9	0.9964	28 ± 1
9.43	5.62 ± 0.19	0.952 ± 0.046	13.2 ± 0.9	0.9968	23 ± 1
15.0	6.43 ± 0.14	1.353 ± 0.032	15.1 ± 0.5	0.9822	20 ± 1
20.0	6.29 ± 0.14	1.330 ± 0.034	14.8 ± 0.5	0.9821	15 ± 1

Figure 6.3. Sample Decay Curves in 2.34 mm DTAB - 6.0 mm PAM40 Samples

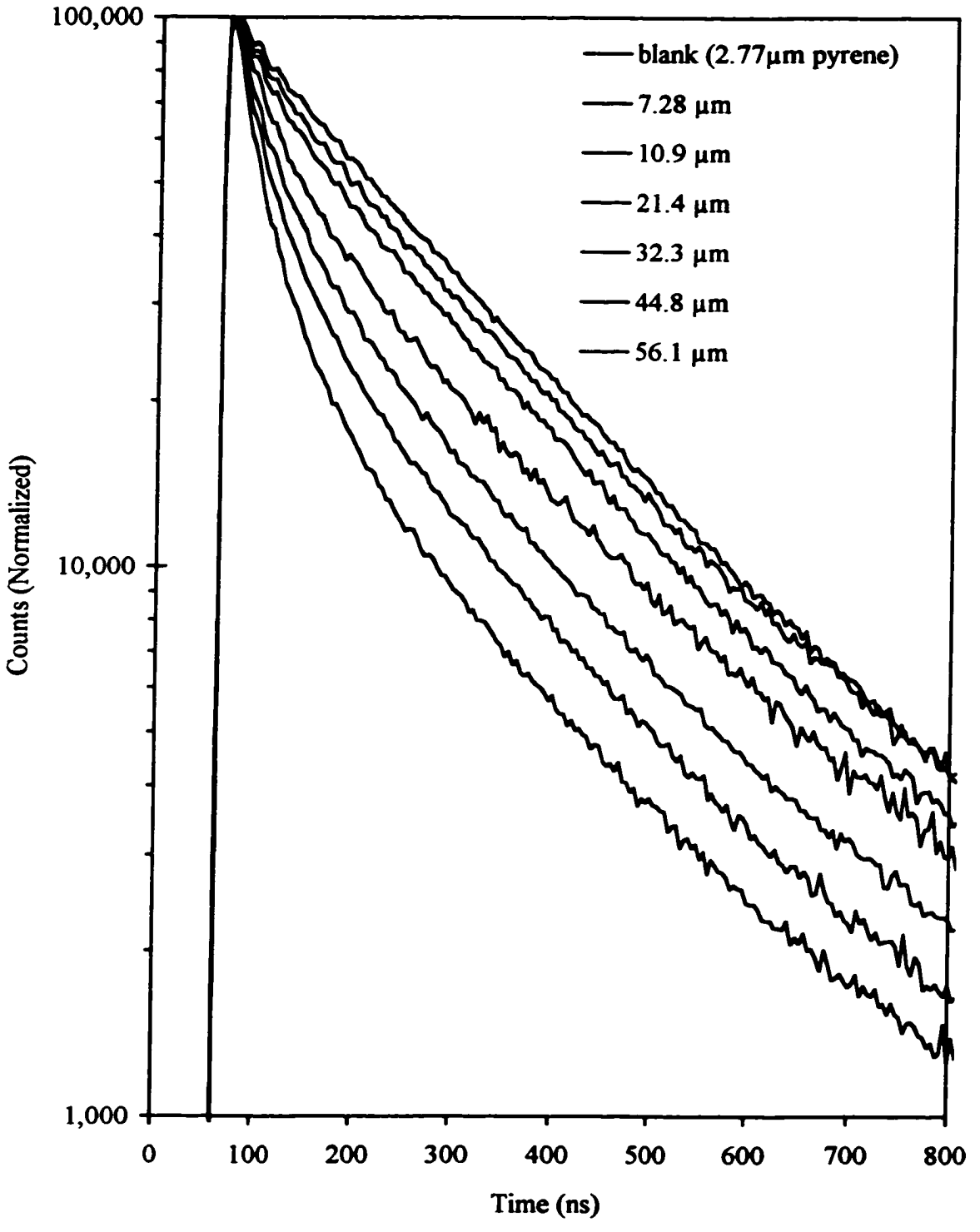

The fitted constants for all the samples, averaged over the different quencher concentrations studied, are given in Table 6.4. The fluorescence lifetime of pyrene $1/A_2$ is generally much higher than that measured in free DTAB micelles, indicating that the bound polyelectrolyte shields the micelles from bromide counterions which quench pyrene fluorescence. The ratio of A_4/A_2 (in Equation 3.18, the simplest kinetic case) is the relative efficiency of quenching over fluorescence decay, often referred to as $k_q\tau_0$. TPB gave the highest values of A_4 and thus of $k_q\tau_0$, but in general the quenching was inefficient, such that the use of steady state fluorescence quenching measurements to determine aggregation numbers in aerated samples of these polymer-surfactant systems would not be valid.

Table 6.4. Summary of Measured Rate Constants in Aerated P-S Samples.

System	unquenched τ_0 (ns)	quencher	A_4 (10^6 s^{-1})	$1/A_2$ (ns)	A_4/A_2
100 mm DTAB	116 ± 2	CPB	19 ± 3	128 ± 4	2.4
0.3 mm DTAB, 1 mm NaPA	159 ± 3	excimer	12 ± 2	190 ± 21	2.3
0.5 mm DTAB, 1 mm NaPA	171 ± 2	excimer	13 ± 2	176 ± 11	2.3
4mm DTAB, 9mm NaPA, 300mm NaCl	–	excimer	14 ± 2	178 ± 9	2.5
2.3mm DTAB, 6mm PAM40	191 ± 1	excimer	19 ± 5	203 ± 7	3.9
2.3mm DTAB, 6mm PAM40	191 ± 1	TPB	24 ± 3	199 ± 8	4.8
1.2mm DTAB, 4mm PAM40	168 ± 1	TPB	45 ± 19	146 ± 18	6.6
.6mm DTAB, .6mm PAM79	–	CPC	27 ± 4	128 ± 10	3.5

I_1/I_3 ratios measured on selected samples from the above series and at other compositions are tabulated in Table 6.5. The ratio was 1.46 in free DTAB micelles and was similar in most of the polymer-surfactant samples, even with high levels (0.3 m) of added electrolyte. A much higher value of 1.73 was measured in the 40% hydrolyzed polyacrylamide, which suggests that the micelles are less tightly bound by this polymer of lower charge density and are more open to penetration by water. The high value in NaPA in the absence of DTAB indicates minimal interaction of pyrene with the polymer alone, and the lack of hydrophobic regions in the absence of surfactant.

Table 6.5. I_1/I_3 Values Measured in Various DTAB-Polyacrylate Samples.

System	[Polymer] (mm)	Bulk [DTAB] (mm)	β_c	I_1/I_3 ± 0.03
Aqueous Pyrene	-	-	-	1.88
NaPA alone	1.0	-	-	1.80
PAM40 + DTAB	6.0	2.3	0.48	1.73
PAM79 + DTAB	0.57	0.60	0.30	1.41
NaPA + DTAB	0.96	0.20	0.14	1.45
NaPA + DTAB	0.70	0.20	0.18	1.45
NaPA + DTAB	1.0	0.30	0.22	1.46
NaPA + DTAB	2.0	1.0	0.44	1.42
NaPA + DTAB	0.30	0.15	0.53	1.47
NaPA + DTAB + 300 mm NaCl	8.7	4.0	0.09	1.47
DTAB alone	-	100	-	1.46

6.4. Discussion

There are at least two possible explanations for the nonideal behaviour of A_3 as a function of quencher concentration [256-258]. Either the quencher molecules migrate between micelles at a rate significant relative to the fluorescence quenching rate (i.e. k_- is significant) such that the more complex forms of the equations describing the values of the fitted constants are necessary, or the micelles are significantly polydisperse. These two possibilities were explored as described below.

The first possible cause of the deviation considered was mobility of the quencher in and out of the micelle on the timescale of the fluorescence. If the rate constant k_- for exit of a quencher from a micelle is significant compared to k_q, then from Equations 3.15 to 3.17 we can express the fit parameters as

$$A_1 = I(0),$$

$$A_2 = k_0 + \frac{<Q> k_- k_q}{A_4},$$

$$A_3 = <Q> \left(\frac{k_q}{A_4}\right)^2,$$

and $$A_4 = k_- + k_q. \qquad (6.15)$$

In theory k_0 can be measured using an unquenched sample at very low <Q>, however this is not required in order to extract the desired quantities from the data. Using the

measured A_i from a series of decay curves at varying [Q], one can solve for all of k_0, k_-, k_q, and <Q> [259]. The expressions for A_2, A_3 and A_4 above may be combined to give an expression of the form

$$A_2 = k_0 + DA_3 \tag{6.16}$$

where $$D = \left(k_- + k_q\right)\frac{k_-}{k_q} \tag{6.17}$$

Thus from a plot of A_2 vs. A_3, the intercept yields k_0 and the slope yields k_-

$$k_- = \frac{D}{\left(1+\frac{D}{A_4}\right)} \tag{6.18}$$

For this calculation, k_- is calculated from A_4 at each data point and then averaged. Then k_q and <Q> are calculated at each data point as follows

$$k_q = A_4 - k_- \tag{6.19}$$

$$< Q > = A_3\left(\frac{A_4}{k_q}\right)^2 \tag{6.20}$$

The equation for calculation of N_s from <Q> depends on the quenching mechanism.

$$N_s = <Q>\frac{[S]_b}{[Q]_b} \quad \{\text{excimer}\} \quad \text{or} \quad N_s = \frac{<Q>}{X_q} \quad \{\text{pyridinium}\} \tag{6.21}$$

We applied this model to the data from all our samples to see if the quencher molecules were significantly mobile. For the cationic quencher samples, only the 1.2 mm DTAB - 4.1 mm PAM40 series with TPB quencher showed any trend of A_2 increasing with A_3, yielding an exit rate constant of $(1.8 \pm 0.2) \times 10^6$ s^{-1} which is rather low compared to the quenching rate constant of $(44 \pm 18) \times 10^6$ s^{-1}. The resulting correction to <Q> had a negligible effect on the aggregation numbers. However, all but one of the pyrene excimer quenched samples exhibited an increase of A_2 with A_3, so we will concentrate our discussion on the mobility of pyrene.

A sample pyrene mobility plot is shown as Figure 6.4. The x- and y-error bars represent 95% confidence levels of the precision of the parameters as reported by the decay fitting software. These errors, while large, do not fully account for the scatter of

the data from the regression line. The calculated values of k_0 obtained from the regression intercepts are much lower than the experimental values derived from monoexponential fits to data from samples of very low pyrene concentration. The experimental value of k_0 is displayed in Figure 6.4 at $A_3 = 0$ for comparison, but is not included in the fit. The values of k_- calculated from the plot slopes were small (at most 12% of k_q), and in the case of the PAM40 sample k_- was definitely insignificant. The mobility appears to be more significant at lower degrees of binding, especially as evidenced by the lack of mobility of either pyrene or TPB in the PAM40 sample of higher binding ratio. The quality of the regressions is generally low as evidenced by the regression correlation coefficients r^2 shown in Table 6.6 along with the derived values of the rate constants and N_s.

Table 6.6: Results of Fits of Excimer Quenching Data to Mobility Model.

System	r^2	k_0 measured	k_0 fit	k_-	k_q	N_s
2 mm DTAB + 6 mm PAM40	0.049	5.24 ± .04	4.8 ± 0.4	.04 ± .08	15 ± 1	46 ± 14
0.3 mm DTAB + 1 mm NaPA	0.856	6.29 ± .13	4.2 ± 0.2	1.3 ± 0.5	11 ± 2	48 ± 21
0.5 mm DTAB + 1 mm NaPA	0.701	5.85 ± .08	4.8 ± 0.3	0.7 ± 0.2	13 ± 2	50 ± 12
DTAB + NaPA + 300 mm NaCl	0.749	-	3.6 ± 0.8	1.3 ± 0.5	13 ± 2	80 ± 30

Rate constants in units of 10^6 s^{-1}. Errors shown are one standard deviation.

The corrections to <Q> resulted in increases of up to 30% in the individual values of N_s. However, the corrected values of N_s still decrease with pyrene concentration and thus the reported standard deviations of the aggregation numbers averaged over all trials are too large to allow any conclusions about trends. Therefore, even though probe mobility may explain the observed trend in the fluorescence lifetime, this treatment of the data does not account for the variation in A_3 and thus does not yield a reliable estimate of the aggregation number.

Figure 6.4. Probe Mobility Plot for 0.30 mm DTAB - 1.0 mm NaPA Fluorescence Decay Data.

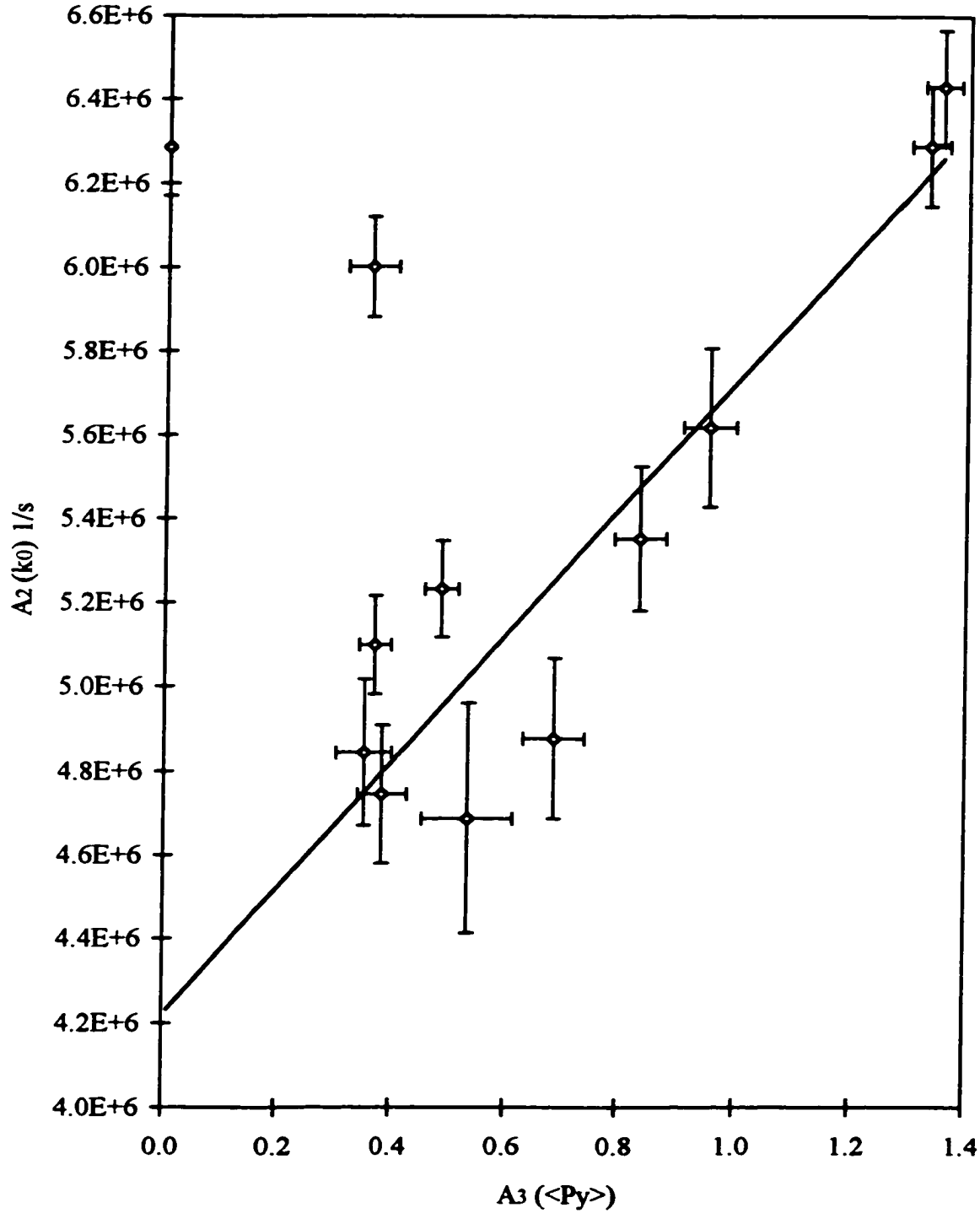

The notion of significant pyrene mobility in these systems is unexpected, given the low water solubility (0.7 μm) and high hydrophobicity of pyrene. The residence time of a pyrene molecule in free micelles of dodecyl surfactants has been reported as about 250 μs, one thousand times its fluorescence lifetime, while that of any particular dodecyl surfactant molecule is 6.1 μs [108]. This means that the aggregation number of a given micelle will fluctuate widely during the time a particular pyrene molecule resides in that micelle, but will be constant during the fluorescence lifetime of an excited probe. The probe remains in a given micelle long enough for that micelle to experience the full breadth of the micelle size distribution. If pyrene is indeed mobile in these systems, then this demonstrates a substantial change from the dynamics present in free micelles. Other researchers have measured similar small but significant values of k_- in polyelectrolyte-surfactant complexes [234,245]. The structure of the polymer-surfactant aggregate might favour the intermicellar transfer of solubilizates due to the proximity of the micelles aggregated on the polymer chain.

Several mechanisms for solubilizate transfer in free micelles have been discussed [260]. Transfer may occur through the bulk aqueous medium, but this should be insignificant for a probe as hydrophobic as pyrene with such a long residence time in the micelle. We see no reason for the rate of aqueous transfer in bound micelles to be greater than that in free micelles.

Solubilizates may also transfer by collision of micelles with mixing of their contents. The mean distance between micelles bound to a polymer is much shorter than for micelles free in solution, so this may make collisions more frequent. However, the measured exit rate was always greater at lower degrees of binding, both for pyrene and for TPB, contradictory to the expectation that rate of collision would increase with the number and thus proximity of bound micelles. Collisions are hindered by charge repulsions, which are reduced as the net micelle charge increases with increased polyelectrolyte binding. The greater mobility observed at lower binding ratios again is contrary to this trend.

Transfer may also occur by fragmentation of a micelle and coalescence of a solubilizate-containing fragment with another micelle. This may be enhanced in a

polymer-surfactant complex by the close proximity of the micelles and/or movement of the fragment along the polymer chain. The micelles are less strongly bound at lower binding ratios and thus more prone to fragmentation, while the strongly bound quenchers are less likely to fragment than pyrene. The aggregation number would exhibit a significant polydispersity if such fragmentation was widely present. This model appears most likely in the present case.

A second explanation for the nonideal trends in the fluorescence decay fitting parameters is that the micelles are significantly polydisperse in size [108]. Since the quenching rate within micelles is diffusion controlled, k_q depends on the average distance between solubilizates, which in turn depends on the size of the micelle. If the micelles are polydisperse in size, there will be a range of k_q and k_0 values and the decay could be represented as a sum of many equations of the Tachiya-Infelta form. As the probes and quenchers are evenly distributed across the volume of the micellar phase, the distribution favours the larger micelles. Thus the true number of micelles containing more than one pyrene molecule (or in the case of added quencher, one probe and at least one quencher) is less than that predicted by Poisson statistics. This results in an underestimated aggregation number as determined from the value of A_3.

The dependence of the measured quenching-average aggregation number N_q on quencher loading may be fitted to a quadratic truncation of a power series in $\Pi = [Q]_m/[S]_m$, with the fit parameters representing the weight average N_w, variance σ^2 and raw skewness Λ of the size distribution [261].

$$N_q = N_w - \frac{\sigma^2}{2}\Pi + \frac{\Lambda}{6}\Pi^2 - \ldots \qquad (6.22)$$

Skewness may be positive or negative, with positive skew indicating a mean value greater than the mode value. The skewness λ as standardised with respect to a Gaussian distribution is more readily compared between systems.

$$\lambda = \frac{\Lambda}{2\sigma^3} \qquad (6.23)$$

The results of fits to this model are summarized in Table 6.7 and Figure 6.5. The fits are of higher quality than for the mobility model, as evidenced by regression

coefficients greater than 0.9. Higher correlation cannot be expected due to the random scatter present in the data. The fits indicate broad polydispersities (the measured deviations are 60 - 80% of the mean aggregation numbers) with positive skew (mean > mode). The broad dispersity is in keeping with the results of the mobility model, which suggest smaller micelle fragments being transferred between larger micelles, though that model might suggest negative skew (mean < mode).

Table 6.7. Results of Fits of TRFQ Data to Polydispersity Model.

System	Quencher	β_c	r^2	N_w	σ	λ
DTAB/NaPA +.3 m NaCl	excimer	0.09	.985	131 ± 20	84 ± 20	0.15 ± 0.19
.3 mm DTAB/1mm NaPA	excimer	0.22	.945	53 ± 3	43 ± 4	0.22 ± 0.10
.5 mm DTAB/1mm NaPA	excimer	0.38	.903	66 ± 9	43 ± 15	0.16 ± 0.44
2.3 mm DTAB/6 mm PAM40	excimer	0.48	.944	54 ± 3	40 ± 6	0.40 ± 0.27
1.2 mm DTAB/4 mm PAM40	TPB	0.14	.962	94 ± 5	61 ± 5	0.16 ± 0.05
2.3 mm DTAB/6 mm PAM40	TPB	0.48	.978	113 ± 5	85 ± 7	0.29 ± 0.11
.6mm DTAB/.6 mm PAM79	CPC	0.30	.966	274 ± 18	210 ± 12	0.16 ± 0.04

The aggregation number appears to increase slightly with degree of binding (from 53 to 66 in NaPA by excimer quenching and from 94 to 113 in PAM40 by TPB quenching) and is greatly increased in the high salt case. Both of these trends are in keeping with general behaviour of ionic free micelles, whose aggregation numbers increase slowly as concentration is increased above the cmc and markedly in the presence of salt. The aggregation number reported by excimer quenching for micelles bound to PAM40 with $\beta_c = 0.48$ is nearly as low as that reported for micelles bound to NaPA at the lower degree of binding studied, $\beta_c = 0.22$, which suggests that the aggregation number increases with the ionic content of the polymer. A more systematic study at equal degrees of binding to polymers of different degrees of hydrolysis would be needed to prove this hypothesis.

Figure 6.5. Fits of TRFQ Data to Polydispersity Model.

a) Excimer Quenched Samples.

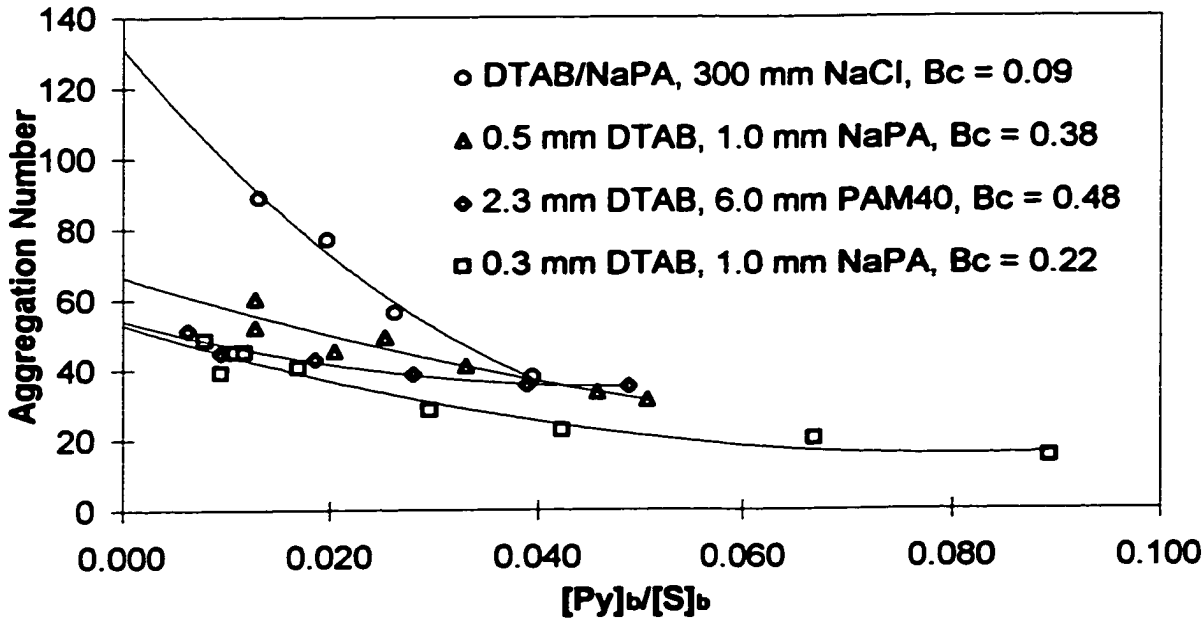

b) PAM-*co*-NaPA Samples.

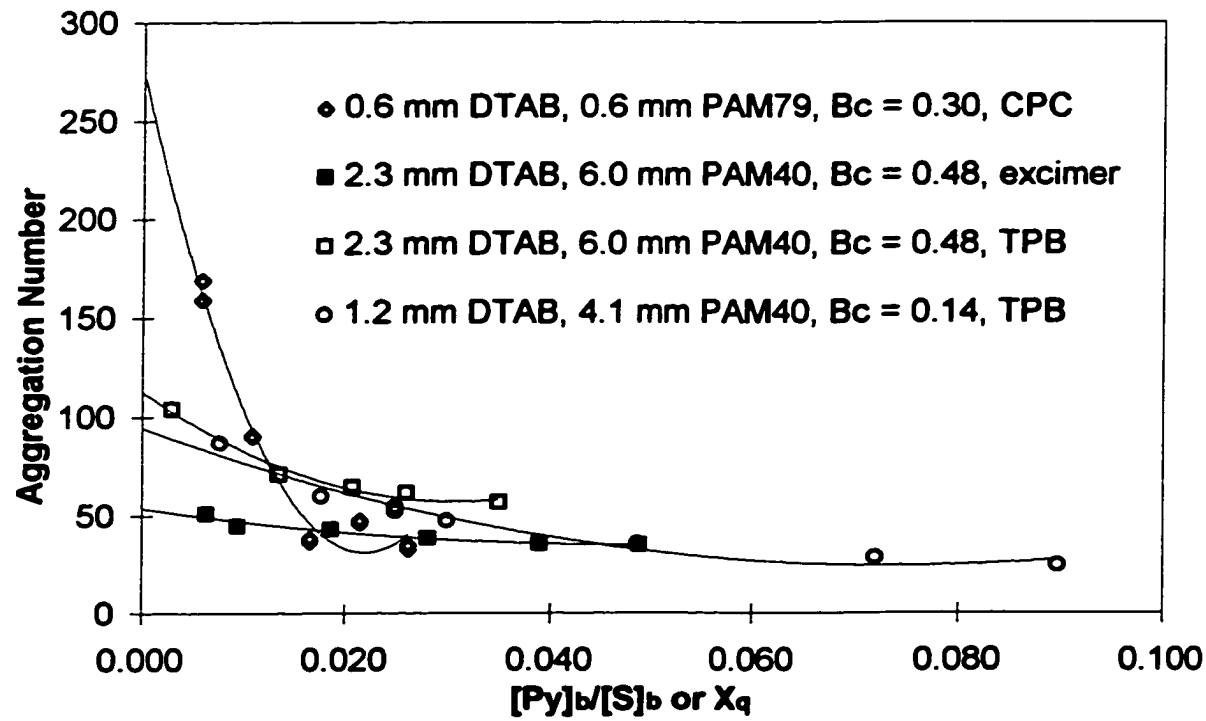

We find that the aggregation numbers calculated from measurements using cationic quenchers are much higher than those calculated from experiments using pyrene excimer formation. The aggregation number for 2.3 mm DTAB bound to 6 mm PAM40 is reported as 54 by excimer quenching but 113 by TPB quenching. We do not believe that this is due to incorrect assumptions regarding the amount of bound quencher. The estimation of 94% TPB bound in this system means that the aggregation number calculated from TPB quenching is overestimated by no more than 6%. To raise the aggregation number calculated from excimer formation to match that from TPB quenching requires that only 48% of pyrene is bound, which is too low a fraction even at the lowest concentrations of pyrene employed in this study. We find the aggregation numbers from excimer quenching measurements to be more reasonable, and believe that the cationic quenchers may perturb the binding in these systems, as will be discussed in Section 6.5.

Though the aggregation number increases with the fraction of polymer bound, so does the number of surfactant micelles bound per polymer chain. Assuming an average degree of polymerization of NaPA of 3400, the average number of discrete aggregates per polymer chain is 14 and 20 at the two DTAB-NaPA binding ratios 0.22 and 0.38 studied. In the high salt case at a very low binding ratio of 0.09, only two micelles are bound per polymer. The increase in the number of bound micelles with binding ratio is expectable, since there are not a small number of specific binding sites on the polymer which would nucleate a specific number of micelles. Such specific binding may occur in copolymers with hydrophobic and hydrophilic blocks, or proteins with a small number of charge sites.

Shirahama *et al.* [40] demonstrated by electrophoresis that in cases of highly cooperative binding, the presence of just a few bound surfactant ions on a polymer molecule makes further binding to that molecule much more favourable than binding to other polymer chains in the same solution. Entire chains can become saturated with bound micelles, and even bind excess surfactant such that the charge of the polyelectrolyte is reversed, before other chains in the same solution bind a significant number of surfactant ions. Based on the binding isotherm of the salt-free system, which indicates a value of the cooperativity parameter u of only 51, we conclude that all chains in the sample should display similar degrees of binding. However in the high-salt system the cooperativity of

the binding is quite high, and such effects as reported by Shirahama *et al.* may be possible.

6.5. Comparison to Literature

We will now compare our results to other published studies on DTAB-NaPA and similar systems. Hansson and Almgren [233] measured aggregation numbers of DTA^+ bound to NaPA using dodecylpyridinium bromide (DPB) as quencher, in both single phase and phase-separated systems. For the single phase systems, they used binding information from the isotherms of Hayakawa *et al.* [229]. To calculate aggregation numbers, they assumed that the quencher was distributed in the same way as the surfactant since the quencher was also a cationic surfactant and had a similar cmc. They supported this assumption with TRFQ measurements on polymer-free samples of 1.5 to 10 mm DTAB in 0.5 m NaBr, keeping the DPB/DTAB ratio constant at 0.01. They used reported aggregation numbers of 90 and 86 from light scattering measurements [262] and their own measurements of $<Q>$ and $[S]_{cmc}$ to calculate the concentration of micellized quencher,

$$[Q]_m = <Q> \frac{[S]_t - [S]_{cmc}}{N_s} \tag{6.24}$$

and compared this to ideal mixing theory [254], which gave excellent agreement with the Ns value of 86. The mole fraction of quencher in the mixed DPB/DTAB micelles (Equation 6.10) was essentially equal to the bulk mole fraction of 0.01 at high concentrations of micelles, but near the cmc it was as high as 0.016. Still, they concluded that even at low total surfactant concentrations, most of the surfactant in the locale of the polyelectrolyte is bound and thus the high concentration limit is the case. Algebraically, their assumption is

$$X_q = \frac{[Q]_b}{[Q]_b + [S]_b} = \frac{[Q]_t}{[Q]_t + [S]_t} = a \tag{6.25}$$

which when inverted and simplified becomes

$$\frac{[S]_b}{[Q]_b} = \frac{[S]_t}{[Q]_t} \tag{6.26}$$

This assumption results in the use of $[S]_t/[Q]_t$ instead of $[S]_b/[Q]_b$ (see Equation 6.21) to calculate N_s. As we have shown that existing binding isotherms combined with ideal

mixing theory may be used to calculate X_q for cationic surfactant quenchers, we feel that this is an unnecessary and possibly inaccurate assumption.

In their paper [233], Hansson and Almgren show fluorescence decay curves for the system 0.64 mm DTAB/ 0.50 mm NaPA/ 10 mm NaCl with and without 53 μm DPB quencher, presumably the highest concentration of quencher used. This corresponds to a bulk mole fraction of 0.077 for DPB in the mixed surfactant system (or 42% of DPB bound), much higher than the value of 0.010 used in the calculations used to verify their assumption. This is also equivalent to five bound quenchers per micelle, whereas it is generally advisable to keep the quencher occupancy less than two quenchers per micelle to avoid perturbing the system. Applying our Equations 6.13 and 6.14, we find that by ideal mixing theory 66% of the DPB molecules present should be bound in this case (note that because of the small difference between the cac values of DPB and DTAB, DPB is not 95-99% bound as is the case with TPB and CPC), corresponding to a mole fraction in the mixed micelles of 0.114, much larger than the bulk mole fraction. We therefore cannot agree that the amount of bound surfactant in these systems is sufficiently large to justify Hansson and Almgren's assumption that the mole fraction of quencher in the mixed micelle is equal to the mole fraction in the bulk mixed surfactant. According to our correction, the aggregation numbers as reported by Hansson and Almgren should be substantially larger than the true values.

Despite the differences in data treatment, we find good agreement between our results from excimer quenching and those of Hansson and Almgren from DPB quenching. In 0.25 mm DTAB and 0.5 mm NaPA ($\beta_c = 0.44$) these authors reported an aggregation number of 65, comparable to our value of 66 at $\beta_c = 0.38$. On addition of 10 mm of salt NaX to 0.64 mm DTAX (X = Cl, Br) and 0.5 mm NaPA ($\beta_c = 0.54$) the aggregation number was 65 for Cl^-, with a slight increase to 69 for Br^-. Our results in Table 6.7 predict a slight increase due to both the added salt and the higher degree of binding. Hansson and Almgren's aggregation numbers are similar to those reported earlier by the same research group for 50 mm DTAX micelles (57 for Cl^-, 65 for Br^-) [213]. In the phase separated systems, the aggregation numbers are only slightly larger in the gel phase than in the supernatant (N_s = 83 and 77 respectively for Br^-) and invariant of salt

concentration up to 0.4 m, but do depend slightly on the counterion (N_s = 70 and 65 respectively for Cl^-). The observation that the aggregation numbers in the phase separated region are higher than in the dilute samples is in keeping with our observations of increasing N_s at increasing degrees of binding. Hansson and Almgren did not perform any measurements at degrees of binding lower than 0.44, thus they did not observe any effect of binding ratio on N_s. Their results on phase separated samples are evidence that the "beads and string" structure persists in the condensed phase.

Hansson and Almgren later reported a more detailed study in this system, including a derivation which supports the validity of the ideal mixing model for mixed ionic surfactants in the field of an oppositely charged polyelectrolyte [234]. Their model accounts for three possible states of the surfactant: free monomers, monomers noncooperatively condensed in the vicinity of the polyelectrolyte due to counterion condensation, and monomers bound in surfactant micelles. They contend that the concentration of condensed surfactant cannot be easily measured, and since it should not increase above the cac, it is considered negligible. They arrive at an equation for the mole fraction of quencher in the mixed micelle X_q identical to our Equation 6.13, except that by neglecting the condensed surfactant the expression for D is reduced to $D = [S]_f - [Q]_f$ (where these concentrations refer to values obtained in the respective single surfactant systems). In practice this simplification should have little effect on the difference D. They estimated $[Q]_f$ based an empirical relation between the cmc data for DTA^+ and DP^+ for many systems of added salt or polyelectrolyte. They show that log $[Q]_{cac}$ is a linear function of log $[S]_{cac}$, with the constants so near unity that this does not differ significantly from our simpler assumption that $[Q]_{cac} / [S]_{cac}$ is a constant. In the end, Hansson and Almgren note that as long as the total concentration of mixed surfactant $[S]_t + [Q]_t$ is much greater than D, the mole fraction of quencher in the mixed micelles (X_q) may be approximated by the mole fraction of quencher in the bulk (a), which leads to the same approximations as used in their previous paper (our Equations 6.25 and 6.26). While this may hold in their experiments at high values of β_c with surfactant and quencher of equal hydrophobe length, we find that this is not so in our experiments at low values of β_c with more hydrophobic quenchers.

In order to test the ideal mixing model, Hansson and Almgren use CPC as quencher, assuming 100% of the quencher is bound, to measure aggregation numbers in samples of DTAB bound to 0.5 mm NaPA. Then they measure <Q> for DPC solubilized in otherwise identical samples and use the aggregation numbers from CPC quenching to calculate the mole fraction of bound DPC as $X_q = <Q> / N_s$. For all quenched samples the bulk mole fraction of quencher in the mixed surfactant was 0.010, i.e. the aggregation numbers were not investigated as a function of quencher concentration to check for polydispersity effects. We note that in our cationic-quenched samples (see Figure 6.5b) even though the weight average aggregation numbers were relatively high, the quencher average aggregation numbers at a = 0.010 ($X_q \approx 0.015$ to 0.030 depending on conditions) were similar to the weight average aggregation numbers (≈ 60) determined by pyrene excimer quenching. Hansson and Almgren report from CPC quenching an average aggregation number of 60 ± 4, insensitive to binding ratio ($\beta_c = 0.50$ and 0.66) or added NaBr (0 to 10 mm) [234]. This value is slightly smaller than those determined by DPB quenching in their previous paper (65 to 69) with the assumption of $X_q \approx a$ [233]. The experimental mole fractions of DPC in the mixed micelles are systematically about 10% lower than predicted, a reasonable agreement with theory.

Though ideal mixing theory may well be applicable to determine the mole fraction of quencher bound, we note that strongly bound cationic quenchers may perturb the system significantly. According to ideal mixing theory [254], the cmc of the mixed surfactant system will be intermediate between the cmcs of the individual pure surfactants

$$\frac{1}{cmc} = \frac{a}{[Q]_{cmc}} + \frac{1-a}{[S]_{cmc}} \tag{6.25}$$

where a is the bulk mole fraction of Q in the mixed surfactant system (Equation 6.10). Assuming this holds for surfactant-quencher mixed micelles bound to polyelectrolyte (i.e. cmc may be replaced by cac) then the cac of a system with added quencher will be perturbed from that in the absence of the quencher. In the case where the quencher is more strongly bound (has a lower cac) than DTAB, the cac of the mixture will be lower. and the bound amount of DTAB will be increased. The effect of the bound quencher on the amount of bound surfactant may be calculated as follows (from Equation 6.12).

$$[S]_b = [S]_t - (1 - X_q)\,[S]_{cac} \qquad (6.26)$$

Table 6.8 shows the results of ideal mixing theory calculations on hypothetical DTAB-NaPA systems with different quenchers (a = 0.010) at low and high values of β_c. We use isotherms reported by Malovikova *et al.* [252] for binding of cationic surfactants to 0.50 mm NaPA in 10 mm NaCl as sources of cac values for DTAB (.333 mm), DPC (.196 mm), TPB (.028 mm) and CPC (estimated ≈ .003 mm), and β_c values for DTAB.

Table 6.8. Ideal Mixing Theory Calculations on Model DTAB-NaPA Systems

quencher	β_c	$[S]_t+[Q]_t$	$[Q]_t$	D	E	X_q	$[S]_b$	β'_c
DPC	0.20	447	4.5	137	310	0.0145	114	0.232
DPC	0.50	620	6.3	137	483	0.0129	285	0.578
TPB	0.20	447	4.5	305	142	0.0299	119	0.246
TPB	0.50	620	6.3	305	315	0.0195	287	0.586
CPC	0.20	447	4.5	330	117	0.0351	121	0.251
CPC	0.50	620	6.3	330	290	0.0211	288	0.588

All concentrations $\times 10^{-6}$ molal.

The calculated mole fraction of bound quencher is always significantly higher than the bulk mole fraction of 0.01, the difference increasing with quencher hydrophobicity and decreasing with binding ratio. Thus X_q approaches a at high degrees of binding and low values of D. The concentration of bound surfactant in the mixed micelle system is greater than in the pure surfactant system (100 μm at β_c = 0.20 and 250 μm at β_c = 0.50) and again the difference is more pronounced at low degrees of binding and higher surfactant hydrophobicity. The binding ratio of mixed surfactant β'_c is therefore higher than for pure DTAB, following the same trends. Further calculations at different values of bulk mole fraction of quencher (a = 0.005 and 0.03) resulted in similar percentage increases in X_q, $[S]_b$ and β_c. Thus even a small quencher loading perturbs the binding isotherm. By comparison, in 100 mm DTAB (in the absence of polyelectrolyte), the addition of 2 mm CPB results in an increase in the concentration of micellized DTAB of only 0.3%, because the total concentration of surfactant is much greater than the cmc (i.e. in Equation 6.13, X_q = a when D is negligible). Thus we see that while a surface-active quencher does not significantly perturb a typical free micelle system, even a small amount of quencher affects the binding of a surfactant to a polyelectrolyte. Therefore we feel that the use of alkylpyridinium surfactants as quenchers in these systems should be avoided.

6.6. Conclusions

We have determined by time resolved pyrene excimer quenching measurements that DTAB micelles bound to NaPA or PAM-*co*-NaPA polyelectrolytes comprise about 60 surfactant molecules. The aggregation number increases slightly with the degree of binding and the charge density of the polymer. The aggregation numbers for bound micelles are similar to our results in 100 mm DTAB (60 ± 2) and slightly larger than that theoretically calculated for free DTA^+ micelles by packing considerations (N_s = 51) [263]. The bound micelles double in size in the presence of 300 mm NaBr. Surfactant aggregates are formed in these systems at DTAB concentrations far below the cmc (15.5 mm).

The pyrene fluorescence lifetimes ($1/A_2$) in P-S systems were higher than in free DTAB micelles (128 - 203 ns as compared to 116 ns), most likely due to a reduction in quenching by bromide counterions, which are displaced by the binding of polymer carboxylates at the micellar surface. This change in the conditions at the micelle surface is not reflected in the micropolarity as probed by pyrene I_1/I_3 measurements, which indicated no difference in polarity between P-S aggregates and free DTAB micelles. The quenching rate constant of TPB in PAM40 complexes increased with decreased degree of binding (and thus smaller micelle size) as expected, and the excimer quenching rate constant was higher in the smaller micelles bound to PAM40 than in micelles bound to NaPA. This suggests that the bound micelles are no more rigid than free DTAB micelles, which could be confirmed by microviscosity measurements.

The aggregation number rises only slightly with the degree of binding to the polymer, such that with increasing β_c micelles increase in number as well as size. The probes and quenchers exhibit greater intermicellar mobility than in free DTAB micelles, most likely due to a micellar fragmentation / coalescence mechanism which is enhanced by the close proximity of the bound micelles and is more pronounced at lower degrees of binding. However, this mobility is not sufficient to account for the changes in aggregation number with quencher concentration, which are due to a large micelle size polydispersity. There is a large scatter in the data, as evidenced in Figures 6.4 and 6.5 and by the error (generally 20-30%) in the final results. This points to the need for further work to confirm

these measurements, especially trials at carefully selected degrees of binding in order to allow better comparison between the polymers of different charge density.

Clearly, the application of surface active probes or quenchers in fluorescence investigations of interactions between oppositely charged polyelectrolytes and surfactants can lead to significant perturbations and must be used with care, if at all. We have shown that pyrene excimer quenching gives good results, with the added benefit of greater fluorescence intensity and thus shorter data collection times. If the use of surface-active quenchers is necessary, choosing surfactants and quenchers with very similar binding strengths and making samples with high degrees of binding minimizes the perturbation. The binding of C_nP^+ to NaPA is slightly stronger than that of C_nTA^+, such that the use of an alkylpyridinium quencher of chain length n (or perhaps n – 1) with an alkyltrimethylammonium surfactant of chain length n would minimize the perturbation. A better option would be to investigate the binding isotherms of the mixed surfactant systems with the polyelectrolytes, as in a recent study of the binding of tetradecylpyridinium chloride (TPC) and decylammonium chloride to poly(L-glutamate) [264]. Ideal mixing (Equation 6.25) accurately predicted the cac of the mixed surfactant, but only fit the shape of the measured isotherm below $\beta_c = 0.3$. A synergistic decrease observed in the free concentration of TPC in the presence of bound micelles was also exhibited by the calculated binding isotherms.

The strong binding in these systems leads to high viscosities and precipitation at very low concentrations. For size exclusion chromatographic studies with our current detector system, polymer concentrations at least ten times the levels used in the fluorescence work would be needed, concentrations at which phase separation occurs shortly after the onset of binding [238]. Therefore, we decided that to attempt such measurements would be inadvisable. Size exclusion studies could be applicable to systems which exhibit weaker binding and thus higher cac values and less tendency to precipitate, for example $C_{10}TA^+$ with the less hydrolyzed copolymers, or DTA^+ with polysaccharides of lower charge density.

CHAPTER 7. INTERACTIONS OF IONIC SURFACTANTS WITH HYDROPHOBICALLY MODIFIED POLYACRYLAMIDES

A series of hydrophobically modified polyacrylamides (HPAMs) with up to 2% incorporation of N-n-alkylacrylamide monomers with decyl, dodecyl and tetradecyl sidechains have been synthesized in our laboratory [265,37]. Hydrophobically modified polymers (HMPs) are of interest due to the interactions between the molecules in solution: the hydrophobic groups can form either inter- or intramolecular aggregates under different conditions. This is evidenced by marked changes in solution viscosity, or even gel formation or phase separation. These properties have lead to applications as thickening agents in latex coatings and paints and in subterranean petroleum recovery operations [266]. Rheology is one of the main methods which has been used to investigate these types of polymers. We decided to apply our fluorescence and chromatographic techniques to learn more about the aggregation of these polymers.

Our HPAM samples had been characterized previously by rheology [37], with molecular weights calculated assuming that the Mark-Houwink-Sakurada constants for polyacrylamide [267] would adequately describe the modified polymers. We chose to measure the molecular weights of the HPAMs using size exclusion chromatography, in order to verify the validity of using constants for polyacrylamide on modified polymers, as well as to determine the polydispersity of the molecular weights and to investigate the self-aggregation of the polymers. The effect of added surfactant on the inter- and intrapolymer interactions was also investigated by SEC. We applied our fluorescence probing methods to determine the size of the individual surfactant aggregates in the complex and to see if macroscopic changes in viscosity observed on the addition of surfactants were paralleled by changes in microviscosity within the aggregates.

7.1. Background

In this section we will summarize what is known about the properties of HMPs and their complexes with surfactants. In particular, we discuss previous studies on the HPAMs synthesized in our laboratory and how the methods used in this thesis supplement and expand on our understanding of these systems.

The binding of surfactants to neutral polymers is greatly dependent on the hydrophobicity of the polymer. Water-soluble polymers may be made more hydrophobic by the addition of alkyl side chains to a small percentage of the monomers (typically < 5 mol% monomer). It takes only a relatively low degree of substitution to render neutral polymers insoluble, however for polyelectrolytes, alternating copolymers with charge:hydrophobe ratios of up to 2:1, referred to as polysoaps [268], are quite soluble and have been widely studied.

The hydrophobic side chains of an HMP or polysoap can form intrapolymer micelle-like aggregates. For example, Hsu and Strauss measured an aggregation number of 24 by TRFQ for the intrapolymer aggregates of the hexyl side chains in a hydrolyzed copolymer of maleic anhydride and hexyl vinyl ether at low pH [259]. The aggregation number was independent of polymer concentration, and also remained the same as pH was varied over the range 4.5 to 5.8 in order to cause an uncoiling of the polymer. This uncoiling results in a decrease in the fraction of side chains micellized from 1.0 to 0.53, and by our calculation, a decrease in the average number of micelles per polymer chain (DP = 1700) from 40 to 20, but no change in micelle size. Intrapolymer aggregates appear to form at very dilute polymer concentrations, with no evidence of a critical concentration. The low micropolarity revealed by I_1/I_3 ratios of pyrene solubilized by our HPAMs [36] indicates that these polymers form hydrophobic microdomains at low polymer concentration, where the low viscosity suggests that the aggregates are intramicellar. The binding isotherms of tetradecyltrimethylammonium bromide with most HPAM samples exhibit noncooperative binding at very low surfactant concentrations [37,269], which suggests that individual surfactant molecules bind into hydrophobic microdomains already present in the polymer coil. This noncooperative part of the isotherm is absent for the least hydrophobic polymer (PAM-C10-0.5% at 2% polymer concentration), indicating that intramolecular aggregates form only if there are sufficient number and length of hydrophobes on a single polymer chain.

The increase of viscosity with concentration of a polymer solution is more pronounced above a point called the critical overlap concentration C^*, where the distance between polymer coils is small enough that intermolecular entanglements occur. In HMP

systems C^* is much lower than for unmodified polymers of the same chain length due to the favourable formation of intermolecular hydrophobic aggregates. Below C^* intramolecular aggregates dominate and the size of the polymer coil is less than that of an unmodified polymer of the same degree of polymerization. Interpolymer interactions lead to increased viscosity, gelling and phase separation. The balance between intra- and interpolymer interactions is affected by temperature, added surfactant or electrolyte, and shear rate.

The HPAMs investigated here form complexes with anionic or cationic surfactants, whereas unmodified neutral polymers generally show little affinity for binding of cationic surfactants. On addition of surfactant, mixed micelles are formed, with a noncooperative binding isotherm much like the addition of a charged surfactant to a micellar solution of a nonionic surfactant. The viscosity of the solution increases, with greater degrees of substitution and longer hydrophobes producing higher viscosities. Associative phase separation has been observed in the presence of salt, with the clearing temperature increasing with salt concentration [36]. The maximum viscosity is reached at a bulk mole ratio of two to four surfactant molecules per polymer hydrophobe. This is attributed to an uncoiling of the intrapolymer aggregates by the bound ionic surfactant and formation of interpolymer complexes whose micelles act as reversible crosslinks. By this stage the binding has become cooperative, with the bound surfactant molecules nucleating the binding of further charged surfactant. At higher mole ratios, the viscosity decreases as the micelles become more predominantly ionic surfactant micelles, and charge repulsion breaks up the interpolymer complexes in favour of micelles bound to one or a few hydrophobes on the same polymer chain.

A recent study on our hydrophobically modified polymers using flow microcalorimetry suggested a critical aggregation concentration for binding of SDS (3.6 mm) and TTAB (2.4 mm) which is independent of the polymer concentration or the hydrophobe length [270]. The cac was taken as the maximum in the measured differential enthalpy of mixing. Recall that the previously measured binding isotherms [37,269] do not exhibit a cac, but a noncooperative increase in binding starting at surfactant concentrations orders of magnitude lower than these values. We interpret this calorimetric

maximum as the onset of cooperative binding of added surfactant to aggregates which already contain a number of surfactant molecules. The cmc-cac difference is greater for SDS than for TTAB, indicating stronger binding of anionic surfactant as is typical with neutral polymers. The binding is found to be entropy driven, with a slight increase in the entropic term with increasing hydrophobe length.

Size exclusion chromatography can be applied to these polymers not only for characterization of the polymer molecular weight, but to investigate changes in the size of the polymer coil with the formation of intermolecular aggregates and polymer-surfactant aggregates. Fluorescence measurements reveal the size of the hydrophobic regions and how their polarity and microviscosity change as the bulk solution rheological properties change. These methods provide microscopic evidence to support the theories about the microscopic structure of the complexes which have been proposed based on macroscopic evidence.

7.2. Experimental

Materials

The hydrophobically modified poly(acrylamide)s were synthesized from mixtures of acrylamide (AM), N-n-alkylacrylamide (CnAM where n = 10, 12, 14), and acrylic acid (AA) monomers by Dr. Jochem Effing and Calvin Howley. Polymerization was performed under nitrogen atmosphere in t-butanol at 60°C with azobis(isobutyronitrile) as initiator [265,269]. Above a threshold molecular weight, the polymer became insoluble in the reaction solvent and precipitated. This precipitation is expected to provide a relatively reproducible molecular weight and relatively low molecular weight polydispersity. The polymers were purified by washing three times with acetone followed by freeze-drying from aqueous solution. The structures and nomenclature of the polymers are shown in Figure 7.1 and Table 7.1. The viscosity-average molecular weights (M_v) were determined with a Cannon-Fenske capillary viscometer [37], using published Mark-Houwink-Sakurada constants for poly(acrylamide) [267]. The average monomer molecular weight M_m is an average of the molecular weights of the monomers weighted according to the

feed mole ratios.

$$M_m = (1 - y - z)\, M_{AM} + y\, M_{CnAM} + z\, M_{AA} \quad (7.1)$$

Based on these values, the degree of polymerization DP and average number of hydrophobes per polymer chain $\bar{h}$ are calculated.

$$DP = M_v / M_m \quad (7.2)$$

$$\bar{h} = y\, DP \quad (7.3)$$

Figure 7.1. Structures of Hydrophobically Modified Polyacrylamides.

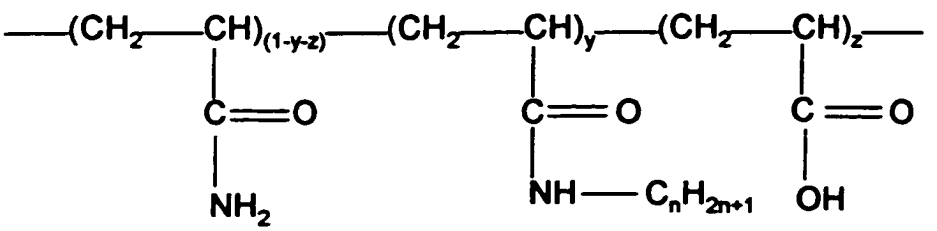

Table 7.1. Nomenclature and Characterization of HPAM Samples.

n	y	z	Name	M_m g/mol	M_v (±5%) (10^3 g/mol)	DP	$\bar{h}$
0	0	0	PAM	71.08	160	2300	0
10	0.005	0	PAM-C10-0.5%	71.78	170	2400	12
10	0.010	0	PAM-C10-1%	72.48	150	2100	21
10	0.015	0	PAM-C10-1.5%	73.18	220	3000	45
10	0.020	0	PAM-C10-2%	73.88	160	2200	43
10	0.020	0.05	PAM-C10-2%, 5%AA	73.93	180	2400	49
10	0.020	0.10	PAM-C10-2%, 10%AA	73.98	140	1900	38
12	0.005	0	PAM-C12-0.5%	71.92	210	2900	15
12	0.010	0	PAM-C12-1%	72.76	140	1900	19
12	0.015	0	PAM-C12-1.5%	73.60	160	2200	33
12	0.020	0	PAM-C12-2%	74.45	130	1700	35
12	0.020	0.05	PAM-C12-2%, 5%AA	74.49	190	2600	51
12	0.020	0.10	PAM-C12-2%, 10%AA	74.54	140	1900	38
14	0.005	0	PAM-C14-0.5%	72.06	200	2800	14
14	0.010	0	PAM-C14-1%	73.04	160	2200	22
14	0.015	0	PAM-C14-1.5%	74.02	110	1500	22
14	0.020	0	PAM-C14-2%	75.01	-	-	-

Tetradecyltrimethylammonium bromide (TTAB, Aldrich) and benzophenone (BzPh, Fisher) were recrystallized from acetone/ethanol mixtures. Cetylpyridinium chloride (CPC, Aldrich) and tetradecylpyridinium bromide (TPB, product of an earlier synthesis from 1-bromotetradecane and pyridine [252]) were decolourized with charcoal and recrystallized from acetone. Sodium dodecyl sulfate (SDS, Sigma, 99%), tetradecyltrimethylammonium chloride (TTAC, TCI America, 98+%), dimethylsulfoxide (DMSO, Caledon, 99.9%), *o*-chlorophenol (Aldrich, 98%) and 8-anilino-1-naphthalenesulfonic acid, ammonium salt hydrate (ANS, Aldrich, 97%) were used as received. Pyrene (Eastman, or K&K Laboratories, Hollywood, CA) was recrystallized from ethanol and then sublimed. Bis(1-pyrenylmethyl) ether (dipyme) was from the synthesis described in Chapter 3. Dye stocks were prepared in spectrophotometric grade solvents (ethanol or acetone, Aldrich). Type II deionized water (resistivity 1.5-2.5 MΩ·cm) from a Millipore Milli-R/Q reverse osmosis purifier was used throughout the research, with water for SEC samples filtered through 0.02 μm Anotop Plus 25 mm inorganic membrane syringe tip filters (Whatman).

Refractometry

Refractive index increments of the HPAMs were measured using an Optilab DSP interferometric refractometer (Wyatt Technology Corp.). A Rheodyne 7125 injector fitted with a 0.99 mL sample loop was used to inject 6 to 8 samples at increasing concentrations into the flow stream from a Tracor 995 HPLC pump at a typical flowrate of 0.7 mL/min, producing a series of plateaus in the detector response. DNDC for Windows version 5.00 software (Wyatt) was used to measure plateau values of the relative refractive index of each sample and to compute dn/dc values. The detector was thermostatted at 40°C and used a 690 nm light source.

Size Exclusion Chromatography

The size exclusion chromatography equipment used was as described in Chapter 4. A Progel-TSK PW_{XL} G5000 column (1000 Å pore size) column was used for SEC of the polymers alone, while the study in 20 mM SDS was performed using a G3000 (200 Å

pore size) and G5000 column in series to better separate the surfactant trough from the low mass tail of the complex peak. The detector system was a miniDAWN three-angle (nominally 45°, 90° and 135°) laser light scattering detector, followed by an Optilab DSP interferometric refractometer (both from Wyatt Technology Corporation), both equipped with 690 nm light sources. Data were collected and analyzed with ASTRA for Windows 4.2 software from Wyatt.

Fluorescence

Aggregation numbers were measured by time-resolved fluorescence as described in Chapter 3, using the FLI 3000 (Photochemical Research Associates) single photon counting apparatus with 256 data channels. Samples of polymer-surfactant mixtures containing hydrophobic fluorescence probes were prepared as follows. An aliquot of a stock solution of pyrene in ethanol was placed in a flask and the ethanol evaporated by a flow of nitrogen gas. Pyrene concentrations were kept on the order of 1/100 the expected concentration of micellar aggregates (10^{-6} m). A polymer-surfactant stock solution was added and the sample mixed for a few days to ensure complete solubilization of the pyrene. Samples of this stock were mixed with samples of aqueous quencher and polymer stocks and diluted with water to achieve desired concentrations. Some samples were deoxygenated by several freeze-pump-thaw cycles using specially designed bulbs to which stemmed 10 mm quartz fluorescence cuvettes (Hellma) were attached via a 7 mm Ace threaded o-ring collar.

Steady-state fluorescence spectra of pyrene and dipyme in polymer-surfactant samples were recorded on a Perkin-Elmer MPF-66 fluorescence spectrophotometer. The peak intensities at ~374 and 385 nm were read in order to calculate I_1/I_3 ratios, and I_e/I_m ratios were measured by integrating the areas under the excimer and monomer emission peaks. Temperature control was provided by a flow of water from a Lauda circulating bath. The fluorescence polarization measurements were performed on the same model spectrometer in the laboratory of Dr. Ram Palepu at St. Francis Xavier University, Antigonish, NS. Since ANS spectra show solvatochromism, excitation and emission wavelengths were optimized on each sample using a peak pick function; typical

wavelengths in P-S systems were 350 and 520 nm respectively. The excitation and emission polarizers were rotated between the 0° and 90° positions and spectra read at all four permutations. The reported emission wavelengths are the average of the maxima at the four polarizer settings.

7.3. Results

Refractometry

The dn/dc values at 40°C and 690 nm were measured for a number of HPAM samples, including copolymers with up to 2% of monomers bearing hydrophobes (hyd.), and terpolymers prepared with varying incorporation of acrylic acid monomer along with 2% hydrophobe. The measured values are presented in Table 7.2. The error in the measurements was typically 1 - 2%. No particular trend is noted in the values as a function of hydrophobe chain length or degree of substitution. The average value of dn/dc was 0.168 ± 0.008 mL/g. Several low values were measured in the 2% substituted polymers, which may be due to loss of sample from adsorption to filters, poor solubility, etc. The PAM-C14-1.5% and 2% samples were poorly water soluble and were not determined. The average dn/dc value excluding all data on 2% hydrophobe substituted samples was 0.173 ± 0.003 mL/g, which is comparable to the average (0.172 ± 0.020 mL/g) of four widely varying values reported in the literature for aqueous polyacrylamide under varying conditions [271] and should adequately describe all of the polymers. However, the measured dn/dc values have been used for all molecular weight calculations (the use of the average dn/dc changes the results by only about 10%).

Table 7.2. Refractive Index Increments (dn/dc, mL/g) of HPAMs (40°C, 690 nm)

Substitution	C10 hydrophobe	C12	C14
none (PAM)	0.170 ± 0.002	0.170 ± 0.002	0.170 ± 0.002
0.5% hyd.	0.173 ±0.002	0.173 ± 0.002	0.169 ± 0.002
1.0% hyd.	0.172 ± 0.003	0.170 ± 0.002	0.172 ± 0.002
1.5% hyd.	0.178 ± 0.003	0.177 ± 0.002	n.d.
2.0% hyd.	0.167 ± 0.003	0.158 ± 0.003	n.d.
2% hyd. + 5% AA	0.153 ± 0.003	0.178 ± 0.002	n.a.
2% hyd. + 10% AA	0.154 ± 0.002	0.160 ± 0.002	n.a.

n.d.: value not determined. n.a.: no such polymer available.

Size Exclusion Chromatography

The C10 and C12 modified HPAMs were studied by SEC using water as eluent. The average M_v value of all the samples was $(170 \pm 30)\times10^3$ g/mol, which was expected to be an intermediate value between the M_n and M_w values measured by SEC. The SEC measurements for PAM and PAM-C10-0.5% are consistent with these results, however the measurements for the more hydrophobic HPAMs yield higher than expected molecular weights as shown in Table 7.3 and Figure 7.2. This suggests that there is considerable interpolymer aggregation in these systems. The z-average radii reported in Table 7.3 are essentially equal except in the PAM-C10 samples with higher hydrophobe contents, which are perturbed by the presence of higher amounts of aggregate.

Table 7.3. Molecular Weights (10^3 g/mol) and Radii (nm) of HPAMs in Water

Polymer	M_n	M_v	M_w	M_w/M_n	R_z
PAM	100 ± 20	160 ± 10	270 ± 30	2.7	54 ± 7
PAM-C10-0.5%	150 ± 20	170 ± 10	350 ± 20	2.3	58 ± 5
PAM-C10-1.0%	410 ± 30	150 ± 10	790 ± 80	1.9	81 ± 5
PAM-C10-1.5%	660 ± 50	220 ± 10	890 ± 90	1.4	73 ± 6
PAM-C10-2.0%	610 ± 60	160 ± 10	830 ± 90	1.4	72 ± 6
PAM-C12-0.5%	370 ± 30	210 ± 10	570 ± 40	1.5	63 ± 5
PAM-C12-1.0%	330 ± 30	140 ± 10	450 ± 50	1.4	63 ± 6
PAM-C12-1.5%	420 ± 50	160 ± 10	490 ± 70	1.2	62 ± 9
PAM-C12-2.0%	220 ± 40	130 ± 10	250 ± 60	1.1	57 ± 6

The eluted mass for the more highly substituted polymer samples was low, and the chromatograms show substantial tailing, probably due to adsorption of sample to the column packing. A sample plot of molecular weight versus elution volume in Figure 7.3 indicates that the tail is comprised of material with a relatively uniform and relatively low molecular weight, indicative that adsorbed polymer is desorbing from the column and eluting in less aggregated form. The measured molecular weights of the C12 polymers are lower than the corresponding C10 polymers, likely due to increased adsorption of C12 aggregates to the column. The molecular weight polydispersity index M_w/M_n of PAM is not as narrow as the precipitation stage of the synthesis led us to expect, but is typical for a free radical polymerization. The substantial decrease of M_w/M_n with increasing hydrophobe substitution may be an artifact of the desorption of polymer from the column.

Figure 7.2. Molecular Weight Distributions of PAM-C10 Samples

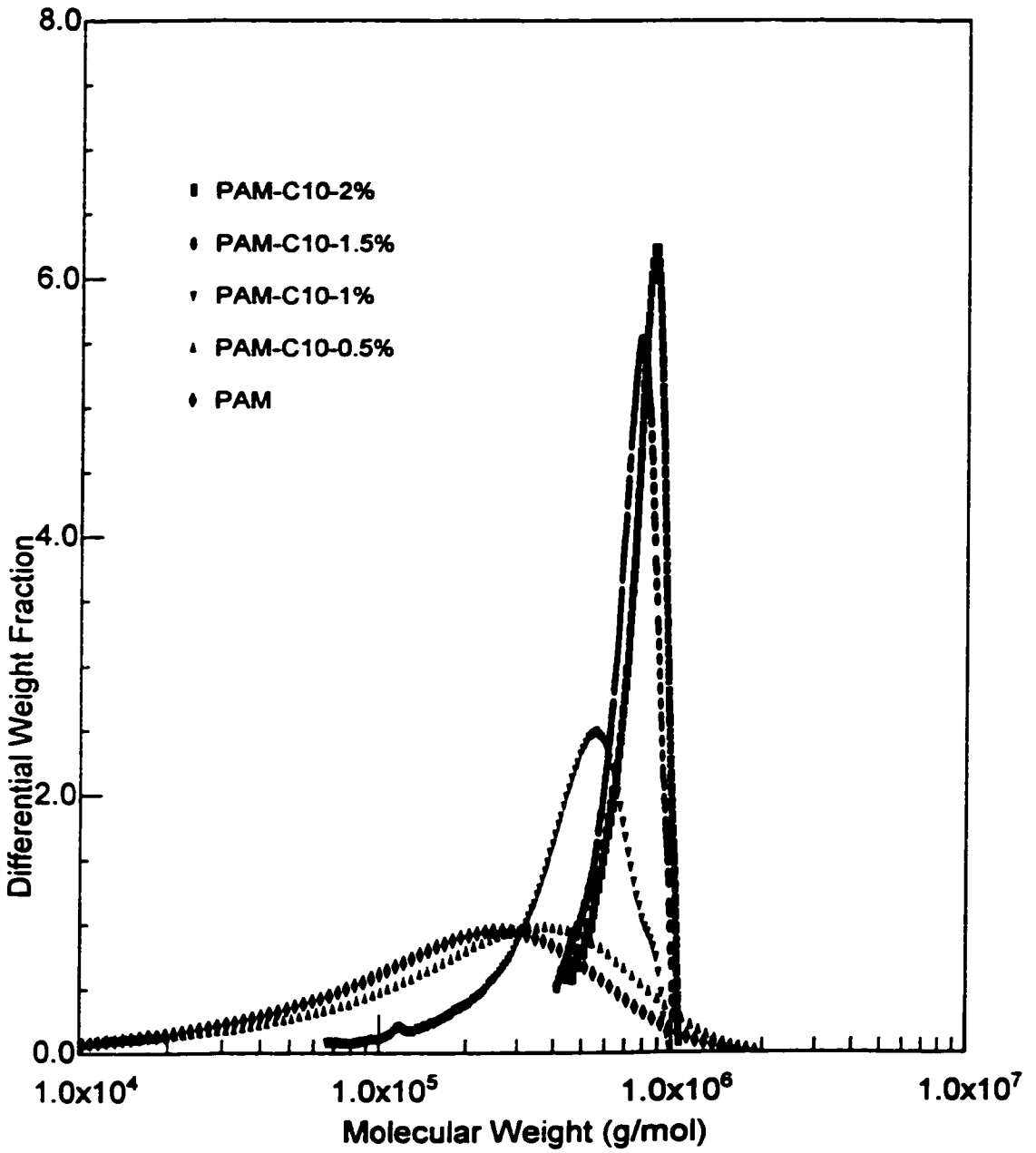

Figure 7.3. Tailing of Molecular Weight in the HPAM-C10-1% Sample

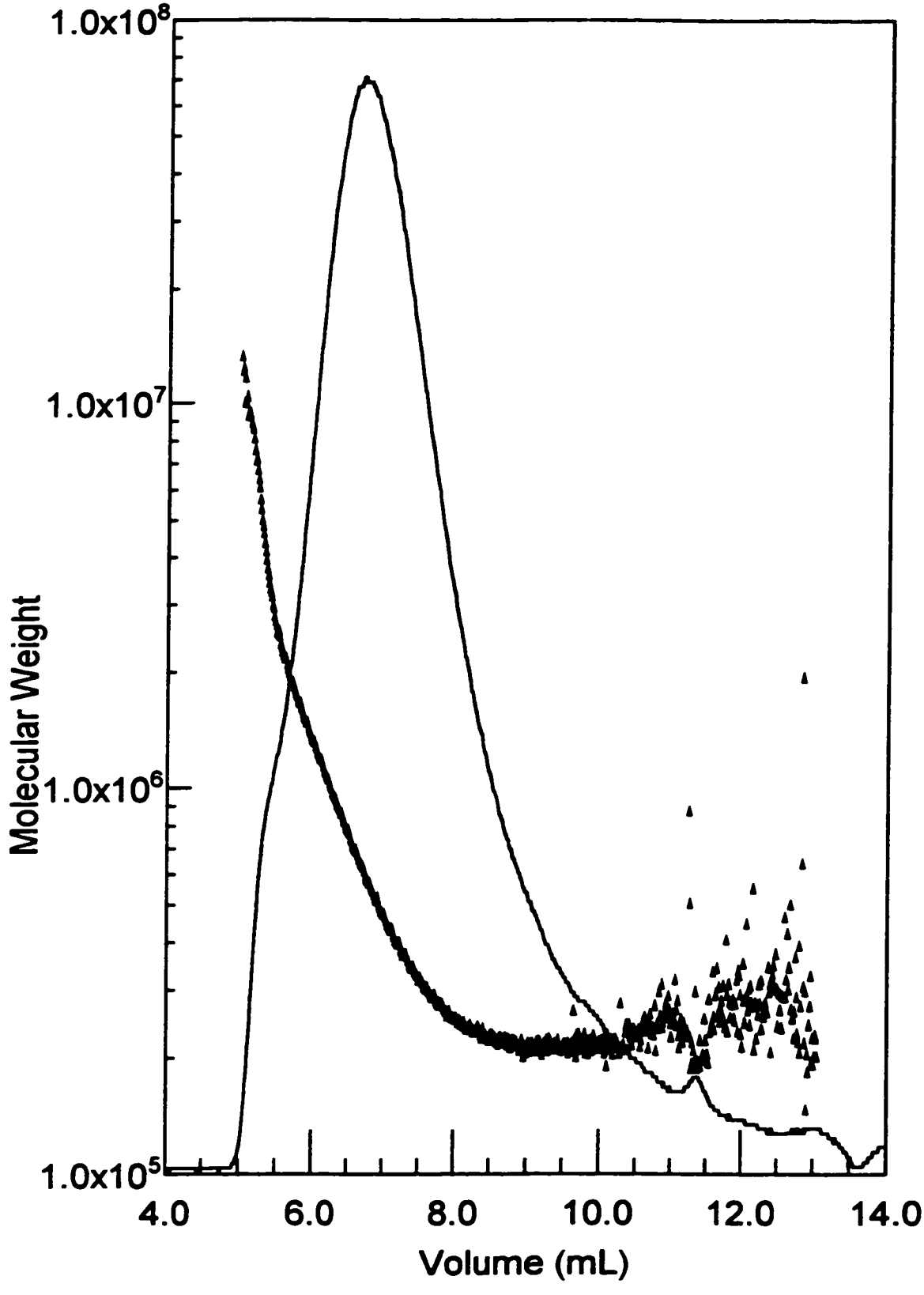

The C10-modified HPAM samples in 20 mM SDS were expected to be saturated with bound surfactant, and to form few intermolecular associations. Surprisingly, the samples clogged 0.2 μm syringe filters and had to be injected with only the 0.5 μm precolumn filter in place. The surfactant void peaks were multimodal (as discussed in Chapter 5) and difficult to quantitate. Thus the amount of bound surfactant was estimated from the mass of the complex peak, (assuming 100% polymer mass elution), and the estimated refractive index increment of the complex adjusted iteratively. Typically the binding amounted to 0.16 grams SDS per gram polymer (4 SDS molecules per 100 monomer units) and the adjusted dn/dc was 0.166 mL/g. As adsorption of sample is expected to be a problem, the true amount of binding could be several times higher than this. However, this corresponds to at least 2 surfactant molecules per hydrophobe, and thus the bound micelles are predominantly comprised of SDS.

The results of the SEC of HPAM-SDS complexes are summarized in Table 7.4. The complex radii were lower than in the absence of surfactant, suggesting decreased interpolymer aggregation. The molecular weights were somewhat higher for PAM and PAM-C10-0.5% than in the absence of surfactant, indicating the binding of surfactant to the polymers. The molecular weights for the more hydrophobic polymers, particularly M_n, tended to be smaller than the values in the absence of surfactant, suggesting some disruption of interpolymer aggregates by bound surfactant. The differential molecular weight plots shown in Figure 7.4 suggest a bimodality in the more hydrophobic polymers, with a shoulder at about 200k g/mol and the main peak near 700k g/mol. The main peak is interpreted as an interpolymer aggregate of on average 3 or 4 polymer chains linked by micelles, while the low molecular weight shoulder is believed to be due to later elution of single polymer chains bearing intramolecular micelles.

Table 7.4. SEC Molecular Weights (10^3 g/mol) and Radii of HPAMs in 20 mM SDS.

Polymer	M_n	M_w	M_w/M_n	R_z (nm)
PAM	180 ± 20	260 ± 20	1.5	27 ± 9
PAM-C10-0.5%	320 ± 20	460 ± 30	1.5	28 ± 8
PAM-C10-1.0%	270 ± 20	600 ± 40	2.2	39 ± 6
PAM-C10-1.5%	430 ± 30	930 ± 60	2.2	49 ± 4
PAM-C10-2.0%	280 ± 20	770 ± 40	2.7	39 ± 5

Figure 7.4. Molecular Weight Distributions of PAM-C10 Complexes in 20 mM SDS

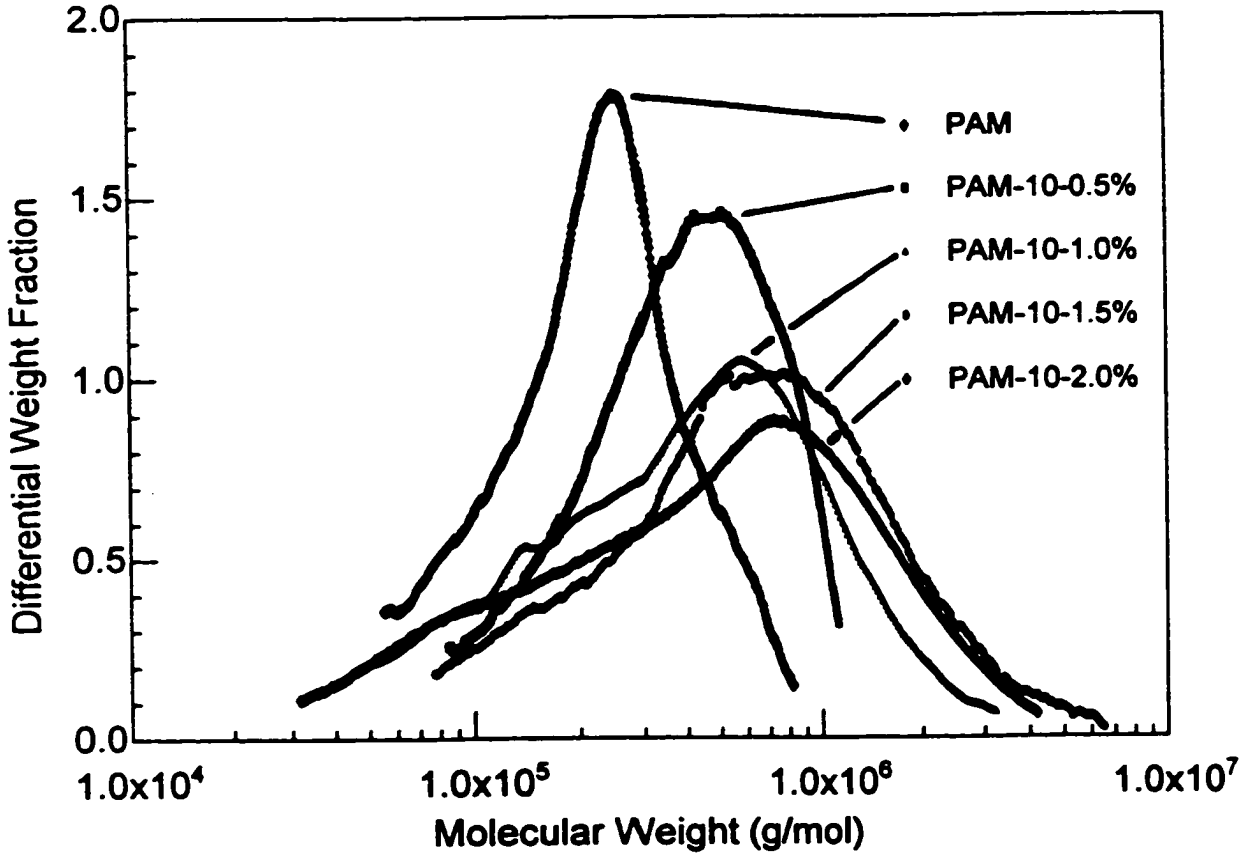

Fluorescence Methods

The interactions of PAM-C10-2% with SDS, TTAB and TTAC were studied by time resolved fluorescence quenching of pyrene with various quenchers. Although a TTAB binding isotherm was available [37], it was measured in the presence of 10 mm NaBr and did not extend to the higher degrees of binding which we studied. Therefore, the cac values for SDS and TTAB binding to PAM-C10-2% as measured by flow microcalorimetry [270] were used as estimates of the amount of free surfactant in order to calculate surfactant aggregation numbers. As the measured cac of TTAB (2.4 mm) is lower than the 2.0 mm bulk concentration of TTAC in our least concentrated set of samples, we note that little or no surfactant was actually bound in that case. This conclusion is supported by the lack of change in the I_1/I_3 ratio of pyrene in those samples (1.50) from that measured in the absence of surfactant (1.52) as compared to the increased polarity measured in the presence of 3 mm TTAB (1.65) or SDS (1.56). Binding ratios β_h are expressed per mole of HPAM hydrophobe. The SDS samples were quenched by benzophenone and TTAC samples by CPC. We assumed these quenchers to be 100% solubilized in the micelles, which may result in underestimates of N_s and N_h. TTAB samples were quenched by TPB, which we assumed to be distributed equally as TTAB. As in Chapter 6, the possibility of perturbation of the cac of a cationic surfactant by use of cationic quenchers is noted. We consider the error in these aggregation numbers to be about 30% due to the assumptions used.

The average number of micelles bound per polymer chain $\bar{m}$ was determined from the concentration of polymer chains [HPAM], calculated based on the viscosity average molecular weight of 160000 g/mol.

$$[\text{HPAM}] = \frac{\text{wt\%}}{0.1\ M_v} \tag{7.5}$$

$$\bar{m} = \frac{[Q]_b}{\langle Q \rangle [\text{HPAM}]} \tag{7.6}$$

We cannot be certain of the fraction of polymer hydrophobes which are contained in the bound micelles, but it is reasonable to assume all hydrophobes are micellized and calculate

a maximum value for the hydrophobe aggregation number N_h.

$$N_h = \bar{h}[HPAM]\frac{<Q>}{[Q]_b} \qquad (7.7)$$

The results of the quenching experiments are summarized in Table 7.5. The numbers given include data at temperatures up to 75 °C, for which the calculated aggregation numbers (assuming the same degrees of binding) did not change, but both the fluorescence decay and quenching rate constants increased. In the TTA^+ samples, the results suggest that the polymer forms one micelle at low degrees of binding, which after reaching a certain size breaks into two smaller micelles, which will then grow and divide, etc. The total aggregation number N_t of surfactant and hydrophobes in the HPAM-TTA^+ case approaches that measured in free TTA^+ micelles. A mixed micelle of ionic surfactant and uncharged cosurfactant has a lower surface charge density than a micelle containing ionic surfactant alone, allowing the micelle to be stable at a lower aggregation number of the ionic surfactant [272]. In the HPAM-SDS case, the surfactant aggregation numbers seem rather low, which we attribute to an incorrect assumption of 100% micellized quencher. Under the conditions investigated, there are certainly several micelles per polymer chain.

Table 7.5. TRFQ Aggregation Numbers in PAM-C10-2% - Surfactant Complexes

Surfactant	[S] (mm)	wt% HPAM	β_h	quencher	$\bar{m}$	N_s	N_h	N_t
TTAC	2.0	0.5	~0	CPC	1	~0	45	45
TTAB	3.0	0.5	0.46	TPB	1	23	50	73
TTAC	4.0	1.0	0.60	CPC	2	13	22	35
TTAC	8.0	1.0	2.1	CPC	2	43	21	64
SDS	6.0	0.5	1.8	BzPh	8	10	6	16

The pyrene fluorescence lifetimes and quenching rate constants measured in PAM-C10-2% systems are given in Table 7.6. Compared to the lifetime measured in the absence of surfactant, the lifetimes rise slightly in SDS complexes, decrease slightly in TTAC, and decrease markedly in the presence of bromide, all typical of pyrene lifetimes measured in surfactant micelles. The $k_q\tau_0$ values are all rather low, such that the use of static quenching methods to determine aggregation numbers in these systems would not be

valid. The quenching rate constants of all the quenchers are low, indicative of slow diffusion of the quencher within the micelles. The value of k_q is lowest for CPC in the 2 mm TTAC sample, where there is essentially no surfactant binding, and increases slowly with increasing TTAC binding ratio, suggesting a slow increase in the micelle fluidity.

Table 7.6. Fluorescence Rate Constants in PAM-C10-2% Systems

Polymer	Surfactant	τ_0	Quencher	k_q	$k_q\tau_0$
0.5%	–	206 ± 4	–	–	–
0.5%	3 mm SDS	239 ± 3	–	–	–
0.5%	6 mm SDS	212 ± 4	BzPh	14 ± 2	3.0
0.5%	3 mm TTAB	109 ± 6	TPB	19 ± 2	2.1
0.5%	2 mm TTAC	198 ± 2	–	–	–
0.5%	2 mm TTAC	201 ± 6	CPC	9 ± 1	1.9
1.0%	4 mm TTAC	181 ± 7	CPC	12 ± 1	2.5
1.0%	8 mm TTAC	209 ± 3	CPC	14 ± 1	2.5

These suspected changes in micelle fluidity are supported by the results of measurements of polarization of fluorescence of ANS in HPAMs, summarized in Table 7.7 and Figure 7.5. Glycerol provided a highly rigid environment for comparison, and yielded a polarization near the theoretical maximum of 0.5 for randomly oriented molecules in a rigid medium. In the absence of added surfactant, the polarization measured in the PAM-C10-2% sample was quite high and decreased with decreasing degree of hydrophobe incorporation in the polymer, indicating a more rigid microenvironment in the more hydrophobic polymers. The polarization in the PAM-C10-0.5% sample indicates a relatively fluid micelle, though not as fluid as SDS. The polarity of the intrapolymer aggregates as reported by the shift in emission wavelength decreases with increasing hydrophobicity. The emission wavelength and polarization in the PAM sample differ little from those in water, indicating minimal interaction of the dye with the unmodified polymer. On addition of surfactant, the rigidity of the probe environment decreases and the polarity increases, as shown in Figure 7.5. There is clearly no maximum in microviscosity at a ratio of 2 - 4 surfactants per hydrophobe as was seen [36] in the bulk viscosity. At high ratios of surfactant to hydrophobe, the rigidity approaches the lower value experienced in SDS micelles, but the polarity rises to a level higher than that measured in SDS.

Figure 7.5. Polarization and Solvatochromism of ANS Fluorescence in HPAM-SDS Samples

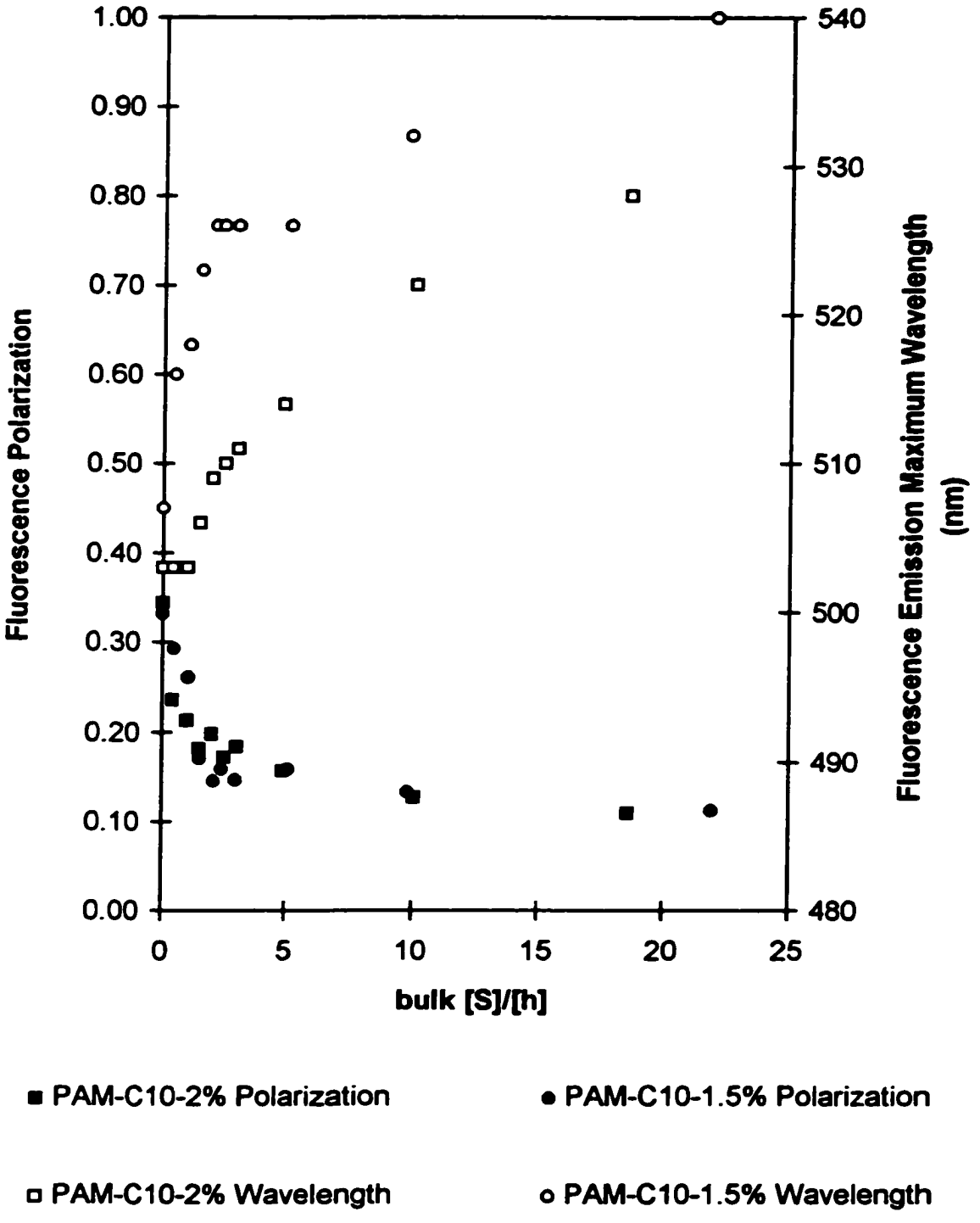

Table 7.7. Fluorescence Polarization of ANS in HPAM and Other Samples

System	λ_{max} (nm)	p
glycerol	507	0.41
0.10% PAM-C10-2%	503	0.34
0.10% PAM-C10-1.5%	507	0.33
0.10% PAM-C10-1%	508	0.30
0.10% PAM-C10-0.5%	524	0.18
0.10% PAM	540	0.11
100 mm SDS	515	0.10
water	555	0.10
ethanol	486	0.016

The fluorescence spectra of dipyme in HPAM-SDS samples show similar trends. The results as plotted over a range of temperatures average out the scatter in the data and more clearly exhibit the small changes in spectral properties observed at different surfactant to hydrophobe ratios. The actual trends with temperature are weak and depend on too many factors to allow any conclusions to be drawn. The plots of the intensity ratio of monomer to excimer fluorescence shown in Figure 7.6 indicate a decreasing rigidity of the micelles with increasing bulk surfactant to hydrophobe ratios, and at the highest ratios the rigidity approaches the value measured in SDS micelles. There is little difference between the results for the three different hydrophobe lengths, though the PAM-C14-2% sample with the least amount of added surfactant appears to be significantly more rigid than the polymers with shorter hydrophobes. There is again no evidence of a peak in microviscosity at 2 to 4 surfactants per hydrophobe as was seen [36] in the bulk viscosity. The I_1/I_3 ratios shown in Figure 7.7 indicate an increase in the polarity of the probe environment with increasing surfactant to hydrophobe ratio, with the polarity at the highest s/h ratios being slightly higher than in free SDS micelles. The samples containing 2 mm SDS are below the reported cac for the complex and thus represent the low polarity present when there is little or no surfactant binding.

Figure 7.6. Monomer/Excimer Fluorescence Intensity Ratios of Dipyme in HPAM-SDS Samples

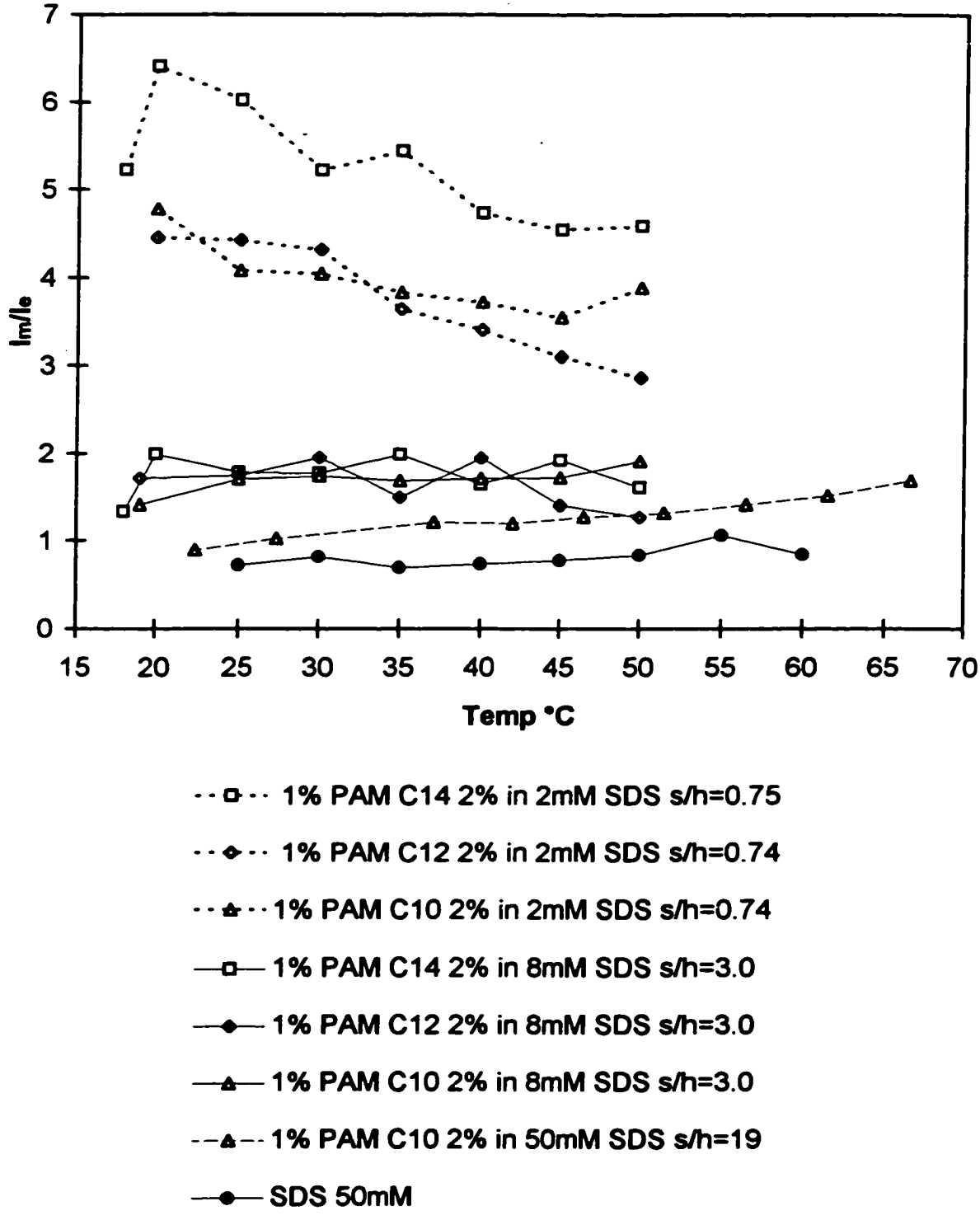

Figure 7.7. Vibronic Peak Fluorescence Intensity Ratios of Dipyme in HPAM-SDS Samples

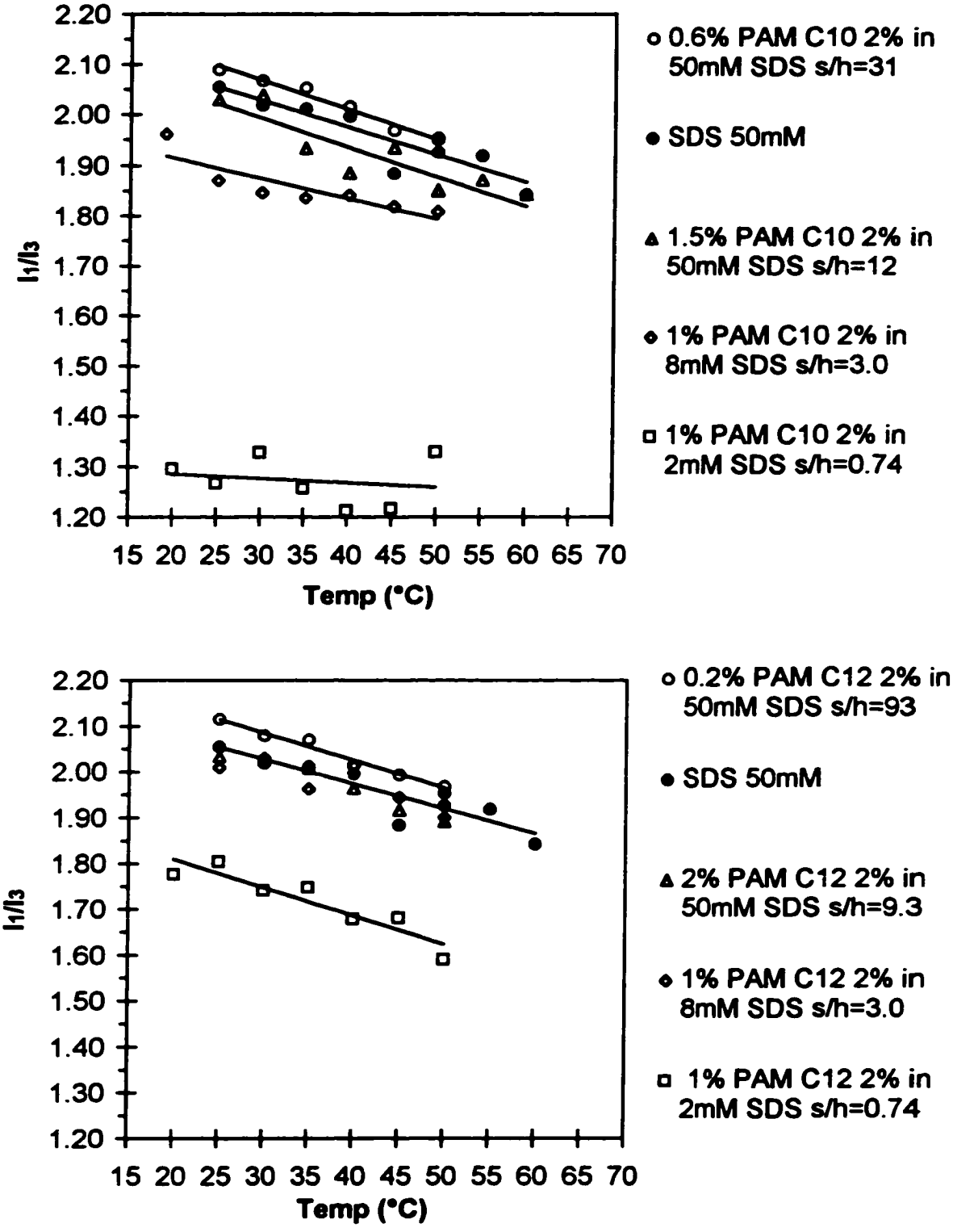

7.4. Discussion

It had been previously noted that the viscosity of solutions of anionic surfactants (SDS [36] or sodium 4-(2-decyl)benzenesulfonate [265]) with 3 wt% PAM-10-2% rose markedly with increasing surfactant concentration, to a maximum at a ratio of about 2 surfactant molecules per hydrophobe, then decreased at higher surfactant concentrations. It was our goal to investigate the size exclusion chromatography of the HPAMs in the presence of surfactant at varying surfactant/hydrophobe ratios. We would expect to see increasing interpolymer aggregation at low surfactant concentration, followed by breakup of the interpolymer complexes to give swollen or elongated single-chain polyelectrolytic complexes at higher s/h ratios. However, the rheological properties of the solutions hamper a more systematic investigation. At the polymer concentrations necessary for good detector response (2 mg/mL), we experienced loss of sample with the more hydrophobic polymers, due to adsorption to the column packing, and excessive column pressure due to the viscosity of the samples.

This is probably compounded by the shear thickening behaviour of the polymers [37], which results in a maximum viscosity at shear rates of 50 - 200 s^{-1}. Shear is believed to uncoil the intrapolymer aggregates, allowing increased formation of interpolymer aggregates. To estimate the shear rate under SEC conditions, we apply the Kozeny-Carman equation for a model of a packed bed as flow through multiple capillaries [273]

$$< v > = \frac{\varepsilon^2 d_p^2 \Delta P}{270(1-\varepsilon^2)\eta L} \qquad (7.8)$$

where <v> is the flow velocity, ΔP is the pressure drop over the length of the capillary L, η is the solution viscosity, d_p the particle diameter of the packing and ε the porosity ratio of the packed bed (typically 0.4). Typical conditions for pure water eluent flowing through our G5000 column (ΔP = 300 psi = 2×10^6 kg m^{-1} s^{-2}, L = 0.3 m, η = 1 cP = 10^{-3} kg m^{-1} s^{-1} and $d_p = 10^{-5}$ m) yield an estimate of <v> of 1.1×10^{-3} m s^{-1}. The shear rate dv/dr in a channel of radius r_c is maximum at the wall (where $r = r_c$) and zero at the center (where r = 0); the flow velocity is zero at the wall and at the center reaches a maximum of

$$v_{max} = 2 < v > = \frac{\Delta P r_c^2}{4L\eta}. \tag{7.9}$$

Then the maximum shear rate is given by

$$-\left(\frac{dv}{dr}\right)_{max} = \frac{r_c \Delta P}{2L\eta} = \frac{2v_{max}}{r_c} = \frac{4 <v>}{r_c}. \tag{7.10}$$

Assuming a channel radius of 2 μm, we find that shear rates of up to 2200 s^{-1} are achievable in the column. With viscous polymer samples, this maximum shear rate will be divided by a factor equal to the relative viscosity of the sample, which under our conditions may be 5 or more. At this level of shear the samples exhibit much higher viscosities than at the zero shear limit. The shear developed in the narrower channels (0.2-0.5 μm) of filters may be higher still. Therefore, the observed intermolecular aggregation of the more hydrophobic polymers may not be present in the sample at rest, but is induced or at least enhanced by the shear experienced while on column.

Attempts were made to find chromatographic conditions which would avoid intermolecular aggregation of the polymers, in order to verify the molecular weights and polydispersities of the unaggregated chains. Added electrolyte has been shown to increase interpolymer interactions, resulting in phase separation [36]. HPAMs proved to be poorly soluble in most organic solvents, with DMSO and *o*-chlorophenol being the only solvents found to be useable near room temperature. The samples dissolved at room temperature with little residual turbidity, and remained soluble after heating to about 50 °C and cooling to room temperature. Samples in *o*-chlorophenol tended to precipitate at temperatures above 70 °C. The relatively high refractive index of DMSO (n_D^{20} = 1.479) resulted in small negative values of dn/dc (-0.027 ± 0.008 mL/g for PAM), making quantitation difficult. We were unable to maintain a stable RI baseline using DMSO eluent, which was believed to be due to the hygroscopicity of the solvent. Attempts to maintain the dryness of the eluent with molecular sieves and/or helium blanketing, or to maintain a stable water content by addition of 1% deionized water, failed. Use of *o*-chlorophenol as eluent was attempted but abandoned mainly due to the odor, corrosiveness and toxicity of the solvent. We then considered organic additives which might reduce aggregation in aqueous eluent. Recently, preliminary studies with 10% isopropanol have shown some

promise.

As a result of shear thickening behaviour, comparison of complex sizes measured under chromatographic conditions to fluorescence measurements at zero shear is complicated. We note that fluorescence quenching measurements cannot provide conclusive evidence of interpolymer crosslinks, as knowing the average number of hydrophobes per micelle says nothing about whether or not they belong to the same polymer chain. Measurements which indicated an average of significantly less than one micelle per polymer (leading to values of N_h greater than the number of hydrophobes on one polymer chain) could indicate aggregation of two or more polymer molecules to form one micelle. Our observations of hydrophobe aggregation numbers slightly higher than the average number of 43 hydrophobes per polymer chain are not significant within the experimental error.

The intrapolymer aggregates have much higher microviscosities than the mixed aggregates formed with added SDS. This is sensed by both the restricted rotational motion of ANS and the restricted conformational folding of dipyme, two very different motions which need not report the same trend in an anisotropic environment such as that provided by a micellar surface. This suggests that the hydrophobes are not loosely collected but are very tightly locked together. Perhaps the amide groups of the polymer form a hydrogen-bonded shell on the micelle surface. It takes at least a 1:2 ratio of bound surfactant molecules to polymer hydrophobes to significantly break up this hard surface, resulting in multiple bound micelles per polymer which have a fluidity approaching that of ordinary surfactant micelles. The polarity sensed by the probes increases during this process, likely due to increased exposure to the sulfate headgroups of SDS and to increased water penetration.

7.5. Conclusions

The application of size exclusion chromatography to the study of hydrophobically modified polymers and their interactions with surfactants is hampered by the effects of adsorption of sample to the column and the high levels of shear created in the flow stream. We might be able to overcome these difficulties by working at reduced pressure (i.e.

reduced flow rate) and lower concentrations (i.e. lower viscosity), or by finding a solvent system which inhibits intermolecular associations and a column of more favourable hydrophilicity. Our experiments clearly indicate intermolecular associations both in the presence and absence of added surfactant, at least under shear, but have not revealed the true molecular weight distributions of the polymer samples. The interpolymer aggregates are somewhat disrupted, but not completely, in favour of bound surfactant micelles. A dramatic decrease of polymer radius occurs as the polymer coils about the bound micelles, even in the case of the unmodified PAM.

Time resolved fluorescence quenching measurements suggest a stepwise growth and division of the bound micelles with increasing binding ratio. The single intramolecular aggregate is eventually broken into several hydrophobic regions. More precise information about the amount of surfactant and quencher bound in these systems is necessary to verify the reported aggregation numbers, which tend to be lower than those measured for free micelles due to the stabilization provided by solubilized polymer hydrophobes. The intrapolymer aggregates exhibit high microviscosity, increasing with degree of hydrophobe substitution and decreasing with degree of surfactant binding. The micropolarity in the aggregates conversely decreases with degree of hydrophobe substitution and increases with degree of surfactant binding, i.e. the more rigid aggregates are also more nonpolar. The ability to tailor these properties could have an impact on the use of these types of polymers in such applications as drug delivery systems, where the rigidity and hydrophobicity of the intrapolymer aggregates affects the solubilization capacity and the rate of release of the drug.

CHAPTER 8. SUMMARY AND FUTURE WORK.

This thesis reports the development and application of two methods for the study of polymer-surfactant interactions. A wide variety of methods reveal different aspects of the structure of polymer-surfactant complexes, as reviewed in Chapter 2. Time resolved fluorescence quenching, discussed in Chapter 3, is an established method used extensively in micellar systems. Polymer-surfactant systems are more likely to exhibit complex morphology and kinetics which make the data analysis more difficult. An available single photon counting instrument required new software which could fit the measured decay curves to the various forms of the Tachiya-Infelta model for quenching of probe fluorescence in a compartmentalized system. We first obtained the program CONVOL from Zana and coworkers, and wrote software to convert our data to a readable format. This was used with some success, but the desire for a more user-friendly program with more flexibility for background correction, more complex model equations, and fixed variables led us to write our own software. The FLIFIT program, written in the MATLAB language and employing an available regression subroutine, improved the fitting of data in our more complex experimental systems and can be easily upgraded to test new model equations. This method was used to measure aggregation numbers in several polymer-surfactant systems.

Size exclusion chromatography, described in Chapter 4, had previously seen little use in the study of polymer-surfactant interactions. We developed equipment to filter and degas surfactant eluent, and used multi-angle laser light scattering detection in order to measure the size and molecular weight of polymer-surfactant complexes without reference to elution volume. In Chapter 5, our study of the PEO-SDS system showed this to be an important adaptation, as the elution of the complexes was perturbed by ion exclusion effects from surfactant adsorbed to the column packing. Observed elution volumes of most complexes were much less than predicted, such that the molecular weights as estimated by elution volume would be greatly overestimated. We found best results for samples in eluent of surfactant concentration below the cmc, as background scatter from the free micelles in the eluent was not necessarily constant and thus difficult to correct for. Multiple injections of different amounts of polymer confirmed the saturation of binding

and improved the determination of binding ratio. This method should be able to give evidence of binding in weakly interacting systems, such as mixtures of neutral polymers with cationic or nonionic surfactants. Other specific detection systems including UV could be applied to distinguish sample components, e.g. to independently quantify polymer and surfactant in the complex peak.

Fluorescence and size exclusion chromatography studies of the well-known PEO-SDS and PVP-SDS systems are presented in Chapter 5. These systems show quite strong binding despite the nonpolarity and relative hydrophilicity of the polymers. From fluorescence quenching we calculate relatively low aggregation numbers for polymer-bound micelles, rising at surfactant concentrations above the saturation point of the polymer to values approaching those measured in the absence of polymer. The rise in aggregation number is due to the coexistence of populations of free and bound micelles with different mean sizes. Our measurements agree with literature values, once the effect of this size polydispersity is taken into effect. These measurements, along with decay and quenching rates, pyrene spectra, and depolarization of fluorescence of anthracene indicate that the PVP-SDS aggregates are more rigid and more polar than PEO-SDS aggregates or free micelles. This is attributed to the relative rigidity of the PVP chain, and insertion of the hydrophobic portions of the pyrrolidone rings into the micellar surface.

The size exclusion chromatography study of the interactions of PEO with SDS by also presented in Chapter 5 was our main test of this new method. The increased molecular weight of the complex compared to the polymer is measurable, but quantification is often difficult due to desorption of surfactant during elution and perturbations of the background signals. The extra data provided by the dual detector system was vital in our understanding of several non-size-exclusions effects which perturbed the elution of the samples. Under optimized conditions, we measure binding ratios comparable to those reported in the literature by other methods. The interaction of oligomeric poly(ethylene glycol)s with SDS is seen to depend on the degree of polymerization: no interaction with glycols up to a DP of about 4, partitioning of glycols of DP up to 15 to 20 in and out of micelles, and binding of surfactant to larger polymers such that the polymer is never free of bound surfactant. In the intermediate range of DP,

the oligomers do not nucleate the formation of micelles in eluent of surfactant concentration below the cmc. The partitioning of mixtures of glycols into the micelles results in a micellar chromatographic separation of individual oligomers, by which we made a preliminary determination of their partition coefficients.

A study of the interactions of a cationic surfactant, DTAB, with anionic sodium poly(acrylate) and poly(acrylamide-*co*-acrylate) polyelectrolytes is presented in Chapter 6. The strong tendency toward precipitation of the charge neutralized complexes and the low concentrations necessary to maintain solubility precluded the use of size exclusion chromatography, though other oppositely charged polymer-surfactant systems with weaker interactions could be considere for future work. Fluorescence measurements indicate that the aggregation numbers of bound micelles are similar to those of free DTAB micelles, but show slight increases with the degree of binding and the charge density of the polymer. The micelles are highly polydisperse in size, and the uncharacteristically significant mobility of probes and quenchers at low degrees of binding suggests that the transfer of small micelle fragments between aggregates is facilitated by the proximity of the micelles and the connectivity of the polymer chain. The small decreases of the quenching rate constants with increasing micelle size suggest no increase in rigidity of the micelles as more polymer carboxylates bind to the surface. Microviscosity measurements would be useful to confirm this hypothesis.

The use of cationic alkylpyridinium quenchers in some of the cationic surfactant - anionic polyelectrolyte samples yielded higher aggregation numbers than excimer quenching. Treatment of this mixed surfactant system by ideal mixing theory predicts the amount of bound quencher based on the total concentrations and cac values of the quencher and surfactant. However, the quencher perturbs the binding of the surfactant, lowering the cac and increasing the binding of the surfactant significantly. This effect is more pronounced for large difference between surfactant and quencher cac values and at low degrees of binding, resulting in greater perturbation in these P-S systems than in the absence of polyelectrolyte. Though ideal mixing appears to adequately predict the perturbation, we recommend the use of nonionic quenchers or excimer formation for studies on dilute systems. Because of the perturbed data in most of our copolymer

samples, further investigations at carefully chosen degrees of binding are warranted.

Finally, we present the results of a study of the binding of surfactants to hydrophobically modified polyacrylamides in Chapter 7. Size exclusion chromatography of the polymers yielded higher molecular weights than those calculated earlier from capillary viscometric measurements. The polymers form intermolecular aggregates which inflate the observed molecular weight distribution. Some decrease in aggregation was observed in 20 mM SDS, evidenced by slightly decreased molecular weights and substantially reduced radii of the complexes. So far, efforts to characterize these polymers in a non-aggregated state have failed. The shear experienced on-column causes uncoiling and increased intermolecular interactions of the polymers, which might be reduced by reduced flow rates and concentrations. Further investigation in a surfactant below its cmc, or of different charge or chain length, or some other inhibitor of aggregation, may yield solely intramolecular complexes.

Static fluorescence investigations indicate that the intrapolymer aggregates are rigid and nonpolar, with the addition of surfactant decreasing both of these traits. The polyacrylamides may form a hydrogen-bonded shell around the aggregates, which is weakened as surfactant binding is increased. Fluorescence quenching measurements suggest a growth of the intrapolymer micelle to a total aggregation number of surfactant and polymer hydrophobes somewhat larger than a free surfactant micelle, followed by division into two small micelles per chain, further growth, and so on. Accurate information (from binding studies, etc.) about the fractions of surfactant, hydrophobes and probes incorporated in the micelles is necessary to verify these observations. More systematic study may also reveal the maximum number of bound micelles per polymer chain, which should be limited to the number of hydrophobes per chain.

APPENDIX. TRFQ FITTING SOFTWARE

```
function [parms,summary,others] = flifit

% FLIFIT  An interface to read PRA 3000 FLI decay datafiles
%         from the MCACGA data acquisition program
%         and fit to user-defined model equations using
%         a Levenberg-Marquardt nonlinear least-squares algorithm
%         leasqr.m (which also calls dfdp.m),
%         courtesy of The Mathworks, Inc. (www.mathworks.com)
%         and Sean Brennan (bren@slac.stanford.edu).
%
%         Input commands allow user selection of files and fitting
%         function (choices monoexpo, biexpntl, micellar, mobility)
%         and any desired parameters may be fixed during the fit.
%
%         Note that time units are ns and concentrations are mM for all
%         parameters. For example, kq as displayed has units E9 s^-1,
%         and k+ is E12 M^-1 s^-1.
%
%         A figure is displayed at each iteration showing the current
%         fit curve superimposed on the data points (set verbose = [0 0]
%         to disable this), then is replaced by the final fit curve
%         and a residuals plot.
%
%         Returns three matrices: fitted parameters, modelled curve,
%         and other scalar results including chi^2 and r^2.
%
%         Output to disk of a file of results remains to be implemented.
%
% Last modified 26 Nov 1997 Andrew P. Rodenhiser
% Except comments added 22 June 1998

% PARAMETERS: (other than temp/self explanatory)
%
% verbose: tells leasqr.m how much screen output to produce (boolean)
%          verbose(1) controls text output, (2) controls graphical output
% decay: the experimental fluorescence decay curve
% decaymax, decaymaxch: maximimum value and associated channel number
% descr: the title info string read from the flamp file
% dtv: vector read from flamp which includes the ns/channel timescale
% flamp: the experimental flash lamp profile
% flampn: flamp normalized to unit area for use in convolution
% x: the vector of time values in each channel, from 0 to 254*dtv(2)
% func: 8-character name of fitting function (without .m extension)
% a: vector of initial fitting parameter estimates
% dp: vector of coefficient increments in x used to determine
%     partial derivatives of func wrt a(i).  default = .001.
%     Setting dp(i)=0 causes a(i) to be fixed during the fit.
% fsc: the first channel of decay used in the fitting procedure.
%      Earlier channels are weighted zero for fitting purposes.
% wt: weighting of the decay data for the fit.
%     default is decay^(-0.5), and zeros for channels before fsc.
% fit: the calculated fitted decay curve
% acalc: the calculated fit parameters
% kvg: (boolean) Has convergence been reached?
% iter: number of iterations required to reach convergence
% cora: correlation matrix of acalc
```

```
% cova: covariance matrix of acalc
% covr: diagonalized covariance matrix of stdres
% stdres: standardized residuals of fit
% Zconf: matrix that defines the confidence region
% r2: coefficient of multiple determination
% stdev: standard deviations of acalc
% chisq: Chi squared statistic of the fit

% set verbose (if not preset) for leasqr.m to select level of screen output

if ~exist('verbose')
 verbose=[0 1];
end
global verbose

% open and read decay curve, replacing any zeroes with ones
% Assumes 256 channel MCA: a variable should be implemented
% to permit selection of 1024 channel files.
% Note that as data is read 5 per line, 256th data point is lost.

clc;
[decayfile,decaypath]=uigetfile('*.dcy','Select Decay File');
fid=fopen([decaypath decayfile]);
d=fscanf(fid,'%g %g %g %g %g',[5,51]);
fclose(fid);
decay=(reshape(d,255,1))';
decay=max(ones(size(decay)),decay);
[decaymax,decaymaxch]=max(decay);

% open and read flamp curve including file descriptor and dt

[flampfile,flamppath]=uigetfile('*.flm','Select Flamp File');
fid=fopen([flamppath flampfile]);
descr=fgetl(fid);
dtv=fscanf(fid,'%g %g %g %g',[4,1]);  % dtv(2) is dt (ns/channel)
for i=1:9
 line=fgetl(fid);       %skip blank lines in file
end
d=fscanf(fid,'%g %g %g %g %g',[5,51]);
fclose(fid);
flamp=(reshape(d,255,1))';
flamp=max(ones(size(flamp)),flamp); % avoid zero elements
[flampmax,flampmaxch]=max(flamp);

% Normalize flamp to unit area for use as convolution function.
% This variable must be global in order to be read by the fitting function
% within the leasqr routine, which is not designed to pass this variable.

global flampn;
norm=sum(flamp);
flampn=flamp./norm;

% normalize flamp to the same max counts as decay
% (for display purposes only)

flamp0=flamp*decaymax./flampmax;

% scale x by the ns/channel value read from the flamp file
```

```
clc;
disp(descr);
disp(' ');
disp(sprintf('The current timescale is %5.3f ns/ch.',dtv(2)));
dt=input('Enter the correct value, or enter "0" to accept the current value.
');
if dt ~= 0
 dtv(2)=dt;
end
x=dtv(2)*[0:254];

% Plot flamp0 and decay
% Position variables are optimized to a 640x480 screen size to view
% both the main window and the figure.

disp(' ');
disp('Displaying the raw data curves');
hold off;
clf;
set(gcf,'Position',[4 4 632 210]);
set(gcf,'MenuBar','none');
axes('position',[.07 .18 .9 .7]);
semilogy(x,decay,'g.',x,flamp0,'r-');
axis([0 300*dtv(2) .5*min(flamp0(9:255)) 2*decaymax]);
ylabel('Counts');
title(descr);
xlabel('Time (ns)');
text(30*dtv(2),2*min(flamp0(9:255)),'green = decay red = flamp');

% An optional background subtraction could be implemented here.
% Setting the background variable to fixed has the same effect.

% initialize parameter estimates, trial function,
% least squares weighting of data points, and
% dp increment for partial derivative calculation

disp(' ');
disp('Enter name of desired fitting function.')
func=input('Choose from: monoexpo, biexpntl, micellar, mobility?  ','s');

% Calculate initial parameter estimates for the fit.
% These are approximations of order-of-magnitude accuracy.

a(1)= 1.2*decaymax;
a(2)= (x(200)-x(150))./log(decay(150)./decay(200)); %decay slope
dtmp=sort(decay);
a(3)= mean(dtmp(1:10));  % est. bgnd as min value of decay file
if func=='biexpntl'
 a(5)=a(3);
 a(4)=a(2);
 % extrapolate long time decay back to time zero for Io estimate
 a(3)=decay(150)*exp((x(decaymaxch)-x(200))./(x(150)-x(200)));
 % estimate slope in early channels as fast decay lifetime
 a(2)= (x(90)-x(decaymaxch))./log(decay(decaymaxch)./decay(90));
 a(1)= a(1) -a(3);
elseif func=='micellar'
 a(5)=a(3);
```

```
 a(4)=5./a(2);   % assume kqTo=5
 a(3)=0.5;       % typical <Q>=.5
elseif func =='mobility'
 a(8)=a(3);
 a23=input('Provide fixed values for [ (To) ([Q]) ]: ');
 a(2)=a23(1);
 a(3)=a23(2);
 a(7)=2*a(3);          % typical <Q>=.5
 a(6)=1./a(2)./a(7);   % guess k+ = inverse of [M]*To
 a(5)=.2./a(2);        % assume kq/k- = 25
 a(4)=5./a(2);         % assume kqTo = 5
end

% Other functions such as triexptl can be implemented later
% Calculations for parameter estimates must be added here
% Warning: fit functions must have an 8-character filename!

% User may now improve any parameter estimates as desired

clc;
cpe=length(a);
while cpe ~= 0,
 disp('Current parameter estimates:');
 disp(sprintf('%.4g ',a));
 disp(' ');
 disp('Enter the number of any parameter whose estimate you wish to change');
 cpe=input('Otherwise, enter "0" to accept the estimates.  ');
 if cpe ~=0,
  a(cpe)=input(sprintf('Enter a new estimate for parameter a(%1d):  ',cpe));
 end
 clc;
end

% fix any parameters as desired

dp=.001*ones(size(a));
if func == 'mobility',
 dp(2) = 0; dp(3) = 0;
end
clc;
disp('Enter a 1/0 (true/false) vector selecting which parameters you wish to
be');
disp('adjusted during the fit.  For example, [1 1 0] will fix the
background');
disp('for a monoexpo fit, [1 0 1 1 1] will fix the lifetime for a micellar
fit.');
disp('The mobility fit defaults to fixed To and [Q], you must specify
otherwise.');
disp(sprintf('Ensure that you enter %1d elements.', length(a)));
dpc=input('Otherwise, enter "0" to adjust all parameters.  ');
if size(dpc)==size(a)
 dp=min(dp,dpc);
 fixed=find(dpc==0);
 clc;
 if length(fixed)>1
  disp(sprintf('You have chosen to fix parameters %1d %1d %1d.', fixed));
  disp(sprintf('Their current values are %.4g ', a(fixed)));
  disp('Enter a vector of new values if you wish to change these values.');
```

```
  else
   disp(sprintf('You have chosen to fix parameter %1d.', fixed));
   disp(sprintf('The current value is %.4g.', a(fixed)));
   disp('Enter a new value if you wish to change it.');
  end
  n='n';
  newv=input('or type "n" to accept.  ');
  if ~isstr(newv)
   a(fixed)=newv;
  end
end

% weight the fit as 1/sqrt(y) and set points before flampmax to zero weight

clc;
disp(sprintf('The flash max channel is %2d ',flampmaxch));
disp(sprintf('The decay max channel is %2d ',decaymaxch));
fsc=input('Enter the channel number at which to start the fit: ');
wt=decay.^(-0.5);
wt(1:fsc-1)=zeros(1,length(1:fsc-1));

% prepare figure for iterative plot

hold off;
clf;

% fit the data

clc;
disp(sprintf('Attempting to fit to %8s function.',func));
[fit,acalc,kvg,iter,cora,cova,covr,stdres,Zconf,r2]=...
  leasqr(x',decay,a,func,.001,20,wt,dp);
% last two variables (dfdp,options) left as default

% display the decay and fit curves for visual comparison

hold off;
clf;
subplot('position',[.07 .18 .4 .65]),semilogy(x,decay,'g.',x,fit,'r-');
axis([0 300*dtv(2) .5*min(fit(9:255)) 2*max(decaymax,max(fit))]);
title(descr);
ylabel('Counts');
xlabel('Time (ns)');
text(80*dtv(2),2*min(fit(9:255)),'green = raw   red = fit');

% plot residuals

subplot('position',[.57 .18 .4 .75]), plot(x,stdres');
axis([0 300*dtv(2) min(stdres) max(stdres)]);
xlabel('Time (ns)');
ylabel('Weighted Residuals');

% calculate fit quality

stdev= sqrt(diag(cova));
chisq=sum(stdres.^2)./(length(decay)-(fsc-1)-length(stdev));
% deg. freedom = #nonzeroweighted decay points - #variable parameters
```

```
%pad stdev with zeros for any fixed variables to make it length(a)

unfixed=zeros(size(a));
unfixed(find(dp))=stdev;
stdev=1.96*unfixed';
% reports RSD=1.96*stdev according to
% t-distribution for ~220pts (approximately an infinite dataset)

% Create output matrices

summary=[flamp' decay' fit stdres covr];
parms=[a' dp' acalc stdev];
others=[dtv(2) kvg iter chisq r2];

% Show us what you got

clc;
disp('Fit Results:');
disp(' ');
disp(descr);
disp(' ');
disp(cora);
disp(Zconf);
disp('       Estimated    dP    Calculated   Standard Deviation');
for i = 1:length(a),
 disp(sprintf('a(%d) %9.5g %7.3f %12.4g %12.4g',...
  i,a(i),dp(i),acalc(i),stdev(i)));
end
disp(' ');
disp('Timescale  Convergence  #Iterations  Chi^2      r^2');
disp(sprintf('%8.3f %10d %10d %11.5f %11.5f',dtv(2),kvg,iter,chisq,r2));
if func=='micellar'
 disp(sprintf('kq*To = %6.2f',acalc(2)*acalc(4)));
elseif func=='mobility'
 disp(sprintf('kq*To = %6.2f',acalc(2)*acalc(4)));
 disp(sprintf('kq/k- = %6.2e',acalc(4)./acalc(5)));
 disp(sprintf('k+[M]/k- = %6.2e',(acalc(6)*acalc(7)./acalc(5))));
end

% Output of a results file is still to be implemented.
% Dialog box for output filename will be displayed using command   uiputfile
% Results are currently returned as matrices parms, summary, others
%   which may be written to a file by the user if desired.
% User can also print the final graph using command   print -dwin

end
```

```
function [f,p,kvg,iter,corp,covp,covr,stdresid,Z,r2]= ...
leasqr(x,y,pin,func,stol,niter,wt,dp,dfdp,options)
%function[f,p,kvg,iter,corp,covp,covr,stdresid,Z,r2]=
%                    leasqr(x,y,pin,{func,stol,niter,wt,dp,dfdp,options})
%
% Version 3.beta
% Levenberg-Marquardt nonlinear regression of f(x,p) to y(x), where:
% x=vec or mat of indep variables, 1 row/observation: x=[x0 x1....xm]
% y=vec of obs values, same no. of rows as x.
% wt=vec(dim=1 or length(x)) of statistical weights.  These should be set
```

```
%   to be proportional to (sqrts of var(y))^-1; (That is, the covaraince
%   matrix of the data is assumed to be proportional to diagonal with diagonal
%   equal to (wt.^2)^-1.  The constant of proportionality will be estimated.),
%   default=1.
% pin=vector of initial parameters to be adjusted by leasqr.
% dp=fractional incr of p for numerical partials,default= .001*ones(size(pin))
%   dp(j)>0 means central differences.
%   dp(j)<0 means one-sided differences.
% Note: dp(j)=0 holds p(j) fixed i.e. leasqr wont change initial guess: pin(j)
% func=name of function in quotes,of the form y=f(x,p)
% dfdp=name of partials M-file in quotes default is prt=dfdp(x,f,p,dp,func)
% stol=scalar tolerances on fractional improvement in ss,default stol=.0001
% niter=scalar max no. of iterations, default = 20
% options=matrix of n rows (same number of rows as pin) containing
%   column 1: desired fractional precision in parameter estimates.
%     Iterations are terminated if change in parameter vector (chg) on two
%     consecutive iterations is less than their corresponding elements
%     in options(:,1).  [ie. all(abs(chg*current parm est) < options(:,1))
%      on two consecutive iterations.], default = zeros().
%   column 2: maximum fractional step change in parameter vector.
%     Fractional change in elements of parameter vector is constrained to be
%     at most options(:,2) between sucessive iterations.
%    ie. abs(chg(i))=abs(min([chg(i) options(i,2)*current param estimate])).],
%     default = Inf*ones().
%
%          OUTPUT VARIABLES
% f=vec function values computed in function func.
% p=vec trial or final parameters. i.e, the solution.
% kvg=scalar: =1 if convergence, =0 otherwise.
% iter=scalar no. of interations used.
% corp= correlation matrix for parameters
% covp= covariance matrix of the parameters
% covr = diag(covariance matrix of the residuals)
% stdresid= standardized residuals
% Z= matrix that defines confidence region
% r2= coefficient of multiple determination

%  {}= optional parameters
% ss=scalar sum of squares=sum-over-i(wt(i)*(y(i)-f(i)))^2.

% All Zero guesses not acceptable
% Richard I. Shrager (301)-496-1122
% Modified by A.Jutan (519)-679-2111
% Modified by Ray Muzic 14-Jul-1992
%       1) add maxstep feature for limiting changes in parameter estimates
%          at each step.
%       2) remove forced columnization of x (x=x(:)) at beginning. x could be
%          a matrix with the ith row of containing values of the
%          independent variables at the ith observation.
%       3) add verbose option
%       4) add optional return arguments covp, stdresid, chi2
%       5) revise estimates of corp, stdev
% Modified by Ray Muzic 11-Oct-1992
%      1) revise estimate of Vy.  remove chi2, add Z as return values
% Modified by Ray Muzic 7-Jan-1994
%       1) Replace ones(x) with a construct that is compatible with versions
%          newer and older than v 4.1.
%       2) Added global declaration of verbose (needed for newer than v4.x)
```

```
%       3) Replace return value var, the variance of the residuals with covr,
%          the covariance matrix of the residuals.
%       4) Introduce options as 10th input argument.  Include
%          convergence criteria and maxstep in it.
%       5) Correct calculation of xtx which affects coveraince estimate.
%       6) Eliminate stdev (estimate of standard deviation of parameter
%          estimates) from the return values.  The covp is a much more
%         meaningful expression of precision because it specifies a confidence
%          region in contrast to a confidence interval..  If needed, however,
%          stdev may be calculated as stdev=sqrt(diag(covp)).
%       7) Change the order of the return values to a more logical order.
%       8) Change to more efficent algorithm of Bard for selecting epsL.
%       9) Tighten up memory usage by making use of sparse matrices (if
%          MATLAB version >= 4.0) in computation of covp, corp, stdresid.
% Modified by Sean Brennan 17-May-1994
%          verbose is now a vector:
%          verbose(1) controls output of results
%          verbose(2) controls plotting intermediate results
% Modified by Andrew P. Rodenhiser 19 Nov 1997
%          plotcmd changed to a semilog plot with properly scaled axes
%          and y and f plotted in different colours.
%
% References:
% Bard, Nonlinear Parameter Estimation, Academic Press, 1974.
% Draper and Smith, Applied Regression Analysis, John Wiley and Sons, 1981.
%
%set default args

% argument processing
%

plotcmd='plot(x(:,1),y,''+'',x(:,1),f); shg';
%if (sscanf(version,'%f') >= 4),
vernum= sscanf(version,'%f');
if vernum(1) >= 4,
  global verbose
%  plotcmd='plot(x(:,1),y,''+'',x(:,1),f); figure(gcf)'; altered by APR
  plotcmd=['semilogy(x(:,1),y,''g.'',x(:,1),f,''r-'');' ...
    'axis([0 max(x) .5*min(f) 2*max(y)]);figure(gcf)'];
end;

if(exist('verbose')~=1), %If verbose undefined, givem everything
      verbose(1)=1;    %This will tell them the results
      verbose(2)=1;    %This will replot each loop
end;

if (nargin <= 8), dfdp='dfdp'; end;
if (nargin <= 7), dp=.001*(pin*0+1); end; %DT
if (nargin <= 6), wt=ones(length(y),1); end;  % SMB modification
if (nargin <= 5), niter=20; end;
if (nargin == 4), stol=.0001; end;
%

y=y(:); wt=wt(:); pin=pin(:); dp=dp(:); %change all vectors to columns
% check data vectors- same length?
m=length(y); n=length(pin); p=pin;[m1,m2]=size(x);
if m1~=m ,error('input(x)/output(y) data must have same number of rows ')
,end;
```

```
if (nargin <= 9),
  options=[zeros(n,1) Inf*ones(n,1)];
  nor = n; noc = 2;
else
  [nor noc]=size(options);
  if (nor ~= n),
    error('options and parameter matrices must have same number of rows'),
  end;
  if (noc ~= 2),
    options=[options(noc,1) Inf*ones(noc,1)];
  end;
end;
pprec=options(:,1);
maxstep=options(:,2);
%

% set up for iterations
%
f=feval(func,x,p); fbest=f; pbest=p;
r=wt.*(y-f);
sbest=r'*r;
nrm=zeros(n,1);
chgprev=Inf*ones(n,1);
kvg=0;
epsLlast=1;
epstab=[.1 1 1e2 1e4 1e6];

% do iterations
%
for iter=1:niter,
  pprev=pbest;
  prt=feval(dfdp,x,fbest,pprev,dp,func);
  r=wt.*(y-fbest);
  sprev=sbest;
  sgoal=(1-stol)*sprev;
  for j=1:n,
    if dp(j)==0,
      nrm(j)=0;
    else
      prt(:,j)=wt.*prt(:,j);
      nrm(j)=prt(:,j)'*prt(:,j);
      if nrm(j)>0,
        nrm(j)=1/sqrt(nrm(j));
      end;
    end
    prt(:,j)=nrm(j)*prt(:,j);
  end;
% above loop could ? be replaced by:
% prt=prt.*wt(:,ones(1,n));
% nrm=dp./sqrt(diag(prt'*prt));
% prt=prt.*nrm(:,ones(1,m))';
  [prt,s,v]=svd(prt,0);
  s=diag(s);
  g=prt'*r;
  for jjj=1:length(epstab),
    epsL = max(epsLlast*epstab(jjj),1e-7);
    se=sqrt((s.*s)+epsL);
```

```
    gse=g./se;
    chg=((v*gse).*nrm);
%   check the change constraints and apply as necessary
    ochg=chg;
    for iii=1:n,
      if (maxstep(iii)==Inf), break; end;
      chg(iii)=max(chg(iii),-abs(maxstep(iii)*pprev(iii)));
      chg(iii)=min(chg(iii),abs(maxstep(iii)*pprev(iii)));
    end;
    if (verbose(1) & any(ochg ~= chg)),
      disp(['Change in parameter(s): ' ...
         sprintf('%d ',find(ochg ~= chg)) 'were constrained']);
    end;
    aprec=abs(pprec.*pbest);       %---
    if (any(abs(chg) > 0.1*aprec)),%---  % only worth evaluating function if
      p=chg+pprev;                       % there is some non-miniscule change
      f=feval(func,x,p);
      r=wt.*(y-f);
      ss=r'*r;
      if ss<sbest,
        pbest=p;
        fbest=f;
        sbest=ss;
      end;
      if ss<=sgoal,
        break;
      end;
    end;                           %---
  end;
  epsLlast = epsL;
  if (verbose(2)),
    eval(plotcmd);
  end;
  if ss<eps,
    break;
  end
  aprec=abs(pprec.*pbest);
%  [aprec chg chgprev]
  if (all(abs(chg) < aprec) & all(abs(chgprev) < aprec)),
    kvg=1;
    if (verbose(1)),
      fprintf('Parameter changes converged to specified precision\n');
    end;
    break;
  else
    chgprev=chg;
  end;
  if ss>sgoal,
    break;
  end;
end;

% set return values
%
p=pbest;
f=fbest;
ss=sbest;
kvg=((sbest>sgoal)|(sbest<=eps)|kvg);
```

```
if kvg ~= 1 , disp(' CONVERGENCE NOT ACHIEVED! '), end;

% CALC VARIANCE COV MATRIX AND CORRELATION MATRIX OF PARAMETERS
% re-evaluate the Jacobian at optimal values
jac=feval(dfdp,x,f,p,dp,func);
msk = dp ~= 0;
n = sum(msk);           % reduce n to equal number of estimated parameters
jac = jac(:, msk);  % use only fitted parameters

%% following section is Ray Muzic's estimate for covariance and correlation
%% assuming covariance of data is a diagonal matrix proportional to
%% diag(1/wt.^2).
%% cov matrix of data est. from Bard Eq. 7-5-13, and Row 1 Table 5.1

if vernum(1) >= 4,
  Q=sparse(1:m,1:m,(0*wt+1)./(wt.^2));  % save memory
  Qinv=inv(Q);
else
  Qinv=diag(wt.*wt);
  Q=diag((0*wt+1)./(wt.^2));
end;
resid=y-f;                                    %un-weighted residuals
covr=resid'*Qinv*resid*Q/(m-n);                 %covariance of residuals
Vy=1/(1-n/m)*covr;  % Eq. 7-13-22, Bard         %covariance of the data

jtgjinv=inv(jac'*Qinv*jac);
covp=jtgjinv*jac'*Qinv*Vy*Qinv*jac*jtgjinv; % Eq. 7-5-13, Bard %cov of parm
est
d=sqrt(abs(diag(covp)));
corp=covp./(d*d');

covr=diag(covr);                  % convert returned values to compact storage
stdresid=resid./sqrt(diag(Vy));  % compute then convert for compact storage
Z=((m-n)*jac'*Qinv*jac)/(n*resid'*Qinv*resid);

%%% alt. est. of cov. mat. of parm.:(Delforge, Circulation, 82:1494-1504, 1990
%%disp('Alternate estimate of cov. of param. est.')
%%acovp=resid'*Qinv*resid/(m-n)*jtgjinv

%Calculate R^2 (Ref Draper & Smith p.46)
%
r=corrcoef(y,f);
r2=r(1,2).^2;

% if someone has asked for it, let them have it
%
if (verbose(2)), eval(plotcmd); end,
if (verbose(1)),
  disp(' Least Squares Estimates of Parameters')
  disp(p')
  disp(' Correlation matrix of parameters estimated')
  disp(corp)
  disp('Covariance matriix of Residuals  ' )
  disp(covr)
  disp( 'Correlation Coefficient R^2')
  disp(r2)
  sprintf('95%% conf region: F(0.05)(%.0f,%.0f)>=
delta_pvec''*Z*delta_pvec',n,m-n)
```

```
  Z
%   runs test according to Bard. p 201.
  n1 = sum((f-y) < 0);
  n2 = sum((f-y) > 0);
  nrun=sum(abs(diff((f-y)<0)))+1;
  if ((n1>10)&(n2>10)), % sufficent data for test?
    zed=(nrun-(2*n1*n2/(n1+n2)+1)+0.5)/(2*n1*n2*(2*n1*n2-n1-n2)...
      /((n1+n2)^2*(n1+n2-1)));
    if (zed < 0),
      prob = erfc(-zed/sqrt(2))/2*100;
      disp([num2str(prob) '% chance of fewer than ' num2str(nrun) ' runs.']);
    else,
      prob = erfc(zed/sqrt(2))/2*100;
      disp([num2str(prob) '% chance of greater than ' num2str(nrun) '
runs.']);
    end;
  end;
end;

% A modified version of Levenberg-Marquardt
% Non-Linear Regression program previously submitted by R.Schrager.
% This version corrects an error in that version and also provides
% an easier to use version with automatic numerical calculation of
% the Jacobian Matrix. In addition, this version calculates statistics
% such as correlation, etc....
%
% Version 3 Notes
% Errors in the original version submitted by Shrager (now called version 1)
% and the improved version of Jutan (now called version 2) have been
corrected.
% Additional features, statisitcal tests, and documentation have also been
% included along with an example of usage.  BEWARE: Some the the input and
% output arguments were changed from the previous version.
%
%     Ray Muzic     rfm2@ds2.uh.cwru.edu
%     Arthur Jutan  jutan@charon.engga.uwo.ca
```

```
function prt=dfdp(x,f,p,dp,func)
% numerical partial derivatives (Jacobian) df/dp for use with leasqr
% --------INPUT VARIABLES---------
% x=vec or matrix of indep var(used as arg to func) x=[x0 x1 ....]
% f=func(x,p) vector initialsed by user before each call to dfdp
% p= vec of current parameter values
% dp= fractional increment of p for numerical derivatives
%      dp(j)>0 central differences calculated
%      dp(j)<0 one sided differences calculated
%      dp(j)=0 sets corresponding partials to zero; i.e. holds p(j) fixed
% func=string naming the function (.m) file
%      e.g. to calc Jacobian for function expsum prt=dfdp(x,f,p,dp,'expsum')
%----------OUTPUT VARIABLES-------
% prt= Jacobian Matrix prt(i,j)=df(i)/dp(j)
%=============================
m=length(x);n=length(p);      %dimensions
ps=p; prt=zeros(m,n);del=zeros(n,1);       % initialise Jacobian to Zero
for j=1:n
      del(j)=dp(j) .*p(j);    %cal delx=fract(dp)*param value(p)
           if p(j)==0
```

```
            del(j)=dp(j);     %if param=0 delx=fraction
            end
        p(j)=ps(j) + del(j);
        if del(j)~=0, f1=feval(func,x,p);
            if dp(j) < 0, prt(:,j)=(f1-f)./del(j);
            else
            p(j)=ps(j)- del(j);
            prt(:,j)=(f1-feval(func,x,p))./(2 .*del(j));
            end
        end
        p(j)=ps(j);     %restore p(j)
end
return
```

```
function y = monoexpo(x,a)

% FUNCTION y = MONOEXPO(x,a)
%           accepts x (dt*[0:254], the time axis)
%           and a (current fit parameters)
%           and uses global (flampn) to convolute
%           a monoexponential decay with background
%           subtraction to be compared against the
%           experimental decay curve

global flampn;
y=a(1)*exp(-x/a(2))+a(3);
y=conv(y,flampn);
y=y(1:255)';
end

% 17 Nov 1997 Andrew P. Rodenhiser
```

```
function y = biexpntl(x,a)

% FUNCTION y = BIEXPNTL(x,a)
%           accepts x (dt*[0:254], the time axis)
%           and a (current fit parameters)
%           and uses global (flampn) to convolute
%           a biexponential decay with background
%           subtraction, to be compared against the
%           experimental decay curve

global flampn;
y= a(1)*exp(-x/a(2)) + a(3)*exp(-x/a(4)) + a(5);
y=conv(flampn,y);
y=y(1:255);
end

% 20 Nov 1997 Andrew P. Rodenhiser
```

```
function y = micellar(x,a)

% FUNCTION y = MICELLAR(x,a)
%           accepts x (dt*[0:254], the time axis in ns)
%           and a (current fit parameters) and uses
```

```
%          global (flampn) to convolute a micellar
%          compartmentalized fluorescence decay using the
%          Infelta-Tachiya model with background subtraction,
%          to be compared against the experimental decay curve
%
% a(1) = Io, intensity at time zero
% a(2) = To, fluorescence lifetime (in ns units)
% a(3) = <Q>, quencher occupancy ratio [Q]/[M]
% a(4) = kq, quenching rate constant (in reciprocal ns)
% a(5) = background correction
%
% 25 Nov 1997 Andrew P. Rodenhiser

global flampn;
y= a(1) *exp( -x/a(2) -a(3)*(1- exp( -a(4)*x ))) +a(5);
y=conv(flampn,y);
y=y(1:255);
end
```

```
function y = mobility(x,a)

% FUNCTION y = MOBILITY(x,a)
%
%          Accepts x (dt*[0:254], the time axis)
%          and a (current fit parameters) and uses
%          global (flampn) to convolute a micellar
%          compartmentalized fluorescence decay using
%          the full Infelta-Tachiya model with quencher
%          mobility and background subtraction, to be
%          compared against the experimental decay curve.
%
% a(1) = Io, intensity at time zero
% a(2) = To, probe decay lifetime in ns units (fixed)
% a(3) = [Q], quencher concentration in mM (fixed)
% a(4) = kq, quenching rate constant (in reciprocal ns)
% a(5) = k-, quencher exit rate constant (reciprocal ns)
% a(6) = k+, second-order quencher entry rate (reciprocal mM*ns)
% a(7) = [M], micelle concentration in mM
% a(8) = background correction
%
% 23 Nov 1997 Andrew P. Rodenhiser

global flampn;
c(5) = a(7) +a(5) ./a(6);
c(4) = a(5) +a(4);
c(1) = a(4) *a(3) ./(c(4) * c(5));
c(2) = 1 ./a(2) +c(1) *a(5);
c(3) = a(4) *c(1) ./c(4);
y= a(1) *exp( -x *c(2) -c(3) *(1 -exp( -c(4) *x))) +a(8);
y=conv(flampn,y);
y=y(1:255);
end
```

REFERENCES

1. C. Tanford, The Hydrophobic Effect: Formation of Micelles and Biological Membranes, 2nd Ed., Wiley-Interscience, New York, 1980.
2. C. Tanford, Proc. Natl. Acad. Sci. USA, 76 (1979) 4175.
3. H. Morawetz, Macromolecules in Solution, 2nd Ed., High Polymers Vol. XXI, Wiley-Interscience, New York, 1975.
4. D. Eagland, in F. Franks, Ed., Hydration Phenomena in Colloidal Systems, Water Science Reviews Vol. 4, Cambridge University Press, Cambridge, 1989.
5. J.E. Glass, in J.E. Glass, Ed., Water Soluble Polymers: Beauty With Performance, Advances in Chemistry Series Vol. 213, ACS, Washington, 1986, Chapter 1.
6. T.C. Amu, Polymer 23 (1982) 1775.
7. F.E. Bailey Jr. and R.W. Callard, J. Appl. Polym. Sci. 1 (1959) 56.
8. J. Brackman, Langmuir 7 (1991) 2097.
9. S. Saito, J. Biochemistry 154 (1957) 21.
10. M.N. Jones, J. Colloid Interface Sci. 23 (1967) 36.
11. H. Arai, M. Murata and K. Shinoda, J. Colloid Interface Sci. 37 (1971) 223.
12. K. Shirahama, K. Tsuji and T. Takagi, J. Biochem. (Tokyo) 75 (1974) 309.
13. J.A. Reynolds and C. Tanford, J. Biol. Chem. 245 (1970) 5161.
14. B. Cabane, J. Phys. Chem. 81 (1977) 1639.
15. B. Cabane and R. Duplessix, J. Phys. (Paris) 43 (1982) 1529.
16. B. Cabane and R. Duplessix, Colloids Surfaces 13 (1985) 19.
17. Z. Gao, R.E. Wasylishen and J.C.T. Kwak, J. Phys. Chem. 93 (1989) 2190.
18. Z. Gao, R.E. Wasylishen and J.C.T. Kwak, J. Phys. Chem. 95 (1991) 462.
19. E.D. Goddard and K.P. Ananthapadmanabhan, in J.C.T. Kwak, Ed., "Polymer-Surfactant Systems", Surfactant Science Series Vol. 77, Marcel Dekker, New York, 1998, Chapter 2.
20. R. Nagarajan, J. Chem. Phys. 90 (1989) 1980.
21. Y.J. Nikas and D. Blankschtein, Langmuir 10 (1994) 3512.
22. K. Shirahama, in J.C.T. Kwak, Ed., "Polymer-Surfactant Systems", Surfactant Science Series Vol. 77, Marcel Dekker, New York, 1998, Chapter 4.
23. G. Brown and A. Chakrabarti, J. Chem. Phys. 96 (1992) 3251.
24. T. Wallin, Ph.D. Thesis, Lund University 1998.
25. S. Karaborni, K. Esselink, P.A.J. Hilbers, B. Smit, J. Karthäuser, N.M. van Os and R. Zana, Science 266 (1994) 254.

26. M. Laradji, O.G. Mouritsen, S. Toxvaerd and M.J. Zuckermann, Phys. Rev. E 50 (1994) 1243.

27. A.C. Balazs, K. Huang and T. Pan, Colloids Surfaces A, 75 (1993) 1.

28. S. Karaborni, K. Esselink, P.A.J. Hilbers and B. Smit, J. Phys.: Condens. Matter 6 (1994) A351.

29. P. Linse, L. Piculell and P. Hansson, in J.C.T. Kwak, Ed., "Polymer-Surfactant Systems", Surfactant Science Series Vol. 77, Marcel Dekker, New York, 1998, Chapter 5.

30. E.D. Goddard, Colloids Surfaces 19 (1986) 255.

31. R. Zana, Ed., Surfactant Solutions: New Methods of Investigation, Surfactant Science Series Vol. 22, Marcel Dekker, New York 1987.

32. S.G. Cutler, P. Meares, and D.G. Hall, J. Electroanal. Chem. 85 (1977) 145.

33. K. Shirahama and N. Ide, J. Colloid Interface Sci. 54 (1976) 450.

34. N. Fadnavis and J.B.F.N. Engberts, J. Am. Chem. Soc. 106 (1984) 2636.

35. C. Botré, F. De Martiis and M. Solinas, J. Phys. Chem. 68 (1964) 3624.

36. J.J. Effing, I.J. McLennan and J.C.T. Kwak, J. Phys. Chem. 98 (1994) 2499.

37. C. Howley, M.Sc. Thesis, Dalhousie University, 1996.

38. L. Piculell and B. Lindman, Adv. Colloid Interf. Sci. 41 (1992) 149.

39. L. Piculell, B. Lindman and G. Karlström, in J.C.T. Kwak, Ed., "Polymer-Surfactant Systems", Surfactant Science Series Vol. 77, Marcel Dekker, New York, 1998, Chapter 3.

40. K. Shirahama, K. Kameyama and T. Takagi, J. Phys. Chem. 96 (1992) 6817.

41. J. François, J. Dayantis and J. Sabbadin, Eur. Polym. J. 21 (1985) 165.

42. B.H. Lee, S.D. Christian, E.E. Tucker and J.F. Scamehorn, Langmuir 7 (1991) 1332.

43. W. Guo, H. Uchiyama, E.E. Tucker, S.D. Christian and J.F. Scamehorn, Colloids Surfaces A 123-124 (1997) 695.

44. P.L. Dubin, D.R. Rigsbee, L.-M. Gan and M.A. Fallon, Macromolecules 21 (1988) 2555.

45. J. Lang and R. Zana, in R. Zana, Ed., Surfactant Solutions: New Methods of Investigation, Surfactant Science Series Vol. 22, Marcel Dekker, New York, 1987, Chapter 8.

46. C. Tondre, J. Phys. Chem. 89 (1985) 5101.

47. A. D'Aprano, C. La Mesa and L. Persi, Langmuir 1997 13 5876.

48. G. Olofsson and G. Wang, in J.C.T. Kwak, Ed., "Polymer-Surfactant Systems", Surfactant Science Series Vol. 77, Marcel Dekker Inc., New York, 1998, Chapter 8.

49. Z. Gao and J.C.T. Kwak, in K.L. Mittal and D.O. Shah, Eds., Surfactants in Solution, Volume 11, Plenum Press, New York, 1991, 261.

50. O. Söderman and P. Stilbs, Prog. Nucl. Magn. Reson. Spectrosc. 26 (1994) 445.

51. P. Stilbs, in J.C.T. Kwak, Ed., "Polymer-Surfactant Systems", Surfactant Science Series Vol. 77, Marcel Dekker Inc., New York, 1998, Chapter 6.

52. M.I. Gjerde, W. Nerdal and H. Høiland, J. Colloid Interf. Sci. 183 (1996) 285.

53. K. Shirahama, M. Tohdo and M. Murahashi, J. Coll. Interf. Sci. 86 (1982) 282.

54. Y. Wang, D. Lu, H. Yan and R.K. Thomas, J. Phys. Chem. B 101 (1997) 3953.

55. F.M. Witte, P.L. Buwalda and J.B.F.N. Engberts, Colloid Polym. Sci. 265 (1987) 42.

56. E.A. Ponomarenko, A.J. Waddon, D.A. Tirrell and W.J. MacKnight, Langmuir 12 (1996) 2169.

57. E.A. Ponomarenko, A.J. Waddon, K.N. Bakeev, D.A. Tirrell and W.J. MacKnight, Macromolecules 29 (1996) 4340.

58. D.C. Duffy, P.B. Davies and A.M. Creeth, Langmuir 11(1995) 2931.

59. D.J. Neivandt, M.L. Gee, C.P. Tripp and M.L. Hair, Langmuir 13 (1997) 2519.

60. F.M. Winnik and S.T.A. Regismond, in J.C.T. Kwak, Ed., "Polymer-Surfactant Systems", Surfactant Science Series Vol. 77, Marcel Dekker, New York, 1998, Chapter 7.

61. R. Zana, in J.C.T. Kwak, Ed., "Polymer-Surfactant Systems", Surfactant Science Series Vol. 77, Marcel Dekker, New York, 1998, Chapter 10.

62. H. Maeda, H. Kato and S. Ikeda, Biopolymers 23 (1984) 1333.

63. M. Henriquez, E. Abuin and E. Lissi, J. Colloid Interface Sci. 179 (1996) 532.

64. K. Hayakawa, in J.C.T. Kwak, Ed., "Polymer-Surfactant Systems", Surfactant Science Series Vol. 77, Marcel Dekker, New York, 1998, Chapter 11.

65. C. Reichardt, Chem. Rev. 94 (1994) 2319.

66. J. Kido, M. Hiyoshi, C. Endo and K. Nagai, J. Colloid Interface Sci. 142 (1991) 326.

67. W. Sui, G. Li, G. Xu , C. Ma and J. Tang, Colloids Surfaces A 123-124 (1997) 473.

68. T. Isemura and A. Imanishi, J. Polym. Sci. 33 (1958) 337.

69. R. Zana, A. Kaplun and Y. Talmon, Langmuir 9 (1993) 1948.

70. M. Goldraich, J.R. Schwartz, J.L. Burns and Y. Talmon, Colloids Surfaces A 125 (1997) 231.

71. N. Kamenka, A. Kaplun, Y. Talmon and R. Zana, Langmuir 10 (1994) 2960.

72. M. Swanson-Vethamuthu, P.L. Dubin, M. Almgren and Y. Li, J. Colloid Interface Sci. 186 (1997) 414.

73. P.L. Dubin, D.R. Rigsbee and D.W. McQuigg, J. Colloid Interface Sci. 105 (1985) 509.

74. P.L. Dubin, S.S. Thé, D.W. McQuigg, C.H. Chew and L.M. Gan, Langmuir 5 (1989) 89.

75. D.W. McQuigg, J.I. Kaplan and P.L. Dubin, J. Phys. Chem. 96 (1992) 1973.

76. P.L. Dubin, J.H. Gruber, J. Xia and H. Zhang, J. Colloid Interface Sci. 148 (1992) 35.

77. J. Xia, P.L. Dubin and Y. Kim, J. Phys. Chem. 96 (1992) 6805.

78. Y. Li, P.L. Dubin, H. Dautzenberg, U. Lück, J. Hartmann and Z. Tuzar, Macromolecules 28 (1995) 6795.

79. B. Cabane, in R. Zana, Ed., Surfactant Solutions: New Methods of Investigation, Surfactant Science Series Vol. 22, Marcel Dekker, New York 1987, Chapter 2.

80. B. Chu, F. Yeh, E.L. Sokolov, S.G. Starodoubtsev and A.R. Khokhlov, Macromolecules 28 (1995) 8447.

81. J. Ruokolainen, G. ten Brinke, O. Ikkala, M. Torkkeli and R. Serimaa, Macromolecules 29 (1996) 3409.

82. D. Süss, Y. Cohen and Y. Talmon, Polymer 36 (1995) 1809.

83. N.J. Turro, M. Gratzel and A.M. Braun, Angew. Chem. Int. Ed. Engl., 19 (1980) 675.

84. R. Zana, in R. Zana, Ed., Surfactant Solutions: New Methods of Investigation, Surfactant Science Series Vol. 22, Marcel Dekker, New York, 1987, Chapter 5.

85. N.J. Turro, Modern Molecular Photochemistry, Benjamin / Cummings, Menlo Park, California, 1978.

86. C.A. Parker, Photoluminescence of Solutions, Elsevier, Amsterdam, 1968.

87. B. Katušin-Razem, M. Wong and J.K. Thomas, J. Am. Chem. Soc. 100 (1978) 1679.

88. T. Suzuki and K. Obi, Chem. Phys. Lett. 246 (1995) 130.

89. A. Nakajima, Bull. Chem. Soc. Jpn. 44 (1971) 3272.

90. K. Kalyanasundaram and J.K. Thomas, J. Am. Chem. Soc. 99 (1977) 2039.

91. D.S. Karpovich and G.J. Blanchard, J. Phys. Chem. 99 (1995) 3951.

92. K.P. Ananthapadmanabhan, E.D. Goddard, N.J. Turro and P.L. Kuo, Langmuir 1 (1985) 352.

93. G. Weber, in D. M. Hercules, Ed., Fluorescence and Phosphorescence Analysis, Interscience, New York, 1966.

94. M. Shinitzky, A.C. Dianoux, C. Gitler and G. Weber, Biochemistry 10 (1971) 2106.

95. M. Grätzel and J.K. Thomas, J. Am. Chem. Soc. 95 (1973) 6885.

96. F. Perrin, Ann. Phys. (Paris) 12 (1929) 169.

97. Th. Förster, Angew. Chem. Int. Ed. 8 (1969) 333.

98. F.M. Winnik, Chem. Rev. 93 (1993) 587.

99. F. Hirayama, J. Chem. Phys. 42 (1963) 3163.

100. K. Zachariasse and W. Kühnle, Z. Physik. Chem. Neue Folge 101 (1976) 267.

101. H. Evertsson and S. Nilsson, Macromolecules 30 (1997) 2377.

102. D. Georgescauld, J.P. Desmasèz, R. Lapouyade, A. Babeau, H. Richard and M.A. Winnik, Photochem. Photobiol. 31 (1980) 539.

103. T. Nivaggioli, B. Tsao, P. Alexandridis and T.A. Hatton, Langmuir 11 (1995) 119.

104. F.M. Winnik, M.A. Winnik, H. Ringsdorf and J. Venzmer, J. Phys. Chem. 95 (1991) 2583.

105. F.M. Winnik, H. Ringsdorf and J. Venzmer, Langmuir 7 (1991) 905.

106. N.J. Turro and A. Yekta, J. Am. Chem. Soc. 100 (1978) 5951.

107. P.P. Infelta, Chem. Phys. Lett. 61 (1979) 88.

108. M. Almgren and J.E. Löfroth, J. Chem. Phys. 76 (1982) 2734.

109. P.P. Infelta, M. Gratzel and J.K. Thomas, J. Phys. Chem. 78 (1974) 190.

110. M. Tachiya, Chem. Phys. Lett. 33 (1975) 289.

111. M.A.J. Rodgers and M.E. da Silva e Wheeler, Chem. Phys. Lett. 43 (1976) 587.

112. A. Yekta, M. Aikawa and N.J. Turro, Chem. Phys. Lett. 63 (1979) 543.

113. M. Almgren, F. Grieser and J.K. Thomas, J. Am. Chem. Soc. 101 (1979) 279.

114. M.H. Gehlen, M. Van der Auweraer and F.C. De Schryver, Langmuir 8 (1992) 64.

115. A.V. Barzykin and I.K. Lednev, J. Phys. Chem. 97 (1993) 2774.

116. M. Tachiya, J. Chem. Phys. 76 (1982) 340.

117. M. Tachiya, J. Chem. Phys. 78 (1983) 5282.

118. J.C. Dederen, M. Van der Auweraer and F.C. De Schryver, Chem. Phys. Lett. 68 (1979) 451.

119. M. Van der Auweraer, J.C. Dederen, E. Geladé and F.C. De Schryver, J. Chem. Phys. 74 (1981) 1140.

120. L.J. Cline Love and L.A. Shaver, Analytical Chemistry 48 (1976) 364A.

121. D.W. Marquardt, J. Soc. Indust. Appl. Math. 11 (1963) 431.

122. V. Brückner, K.-H. Feller and U.-W. Grummt, Applications of Time-Resolved Optical Spectroscopy, Elsevier, Amsterdam, 1990.

123. M.G. Badea and L. Brand, Methods in Enzymology 61 (1979) 378.

124. M.M. Villegas and S.L. Neal, J. Phys. Chem. A 101 (1997) 6890.

125. A.E.W. Knight and B.K. Selinger, Aust. J. Chem. 26 (1973) 1.

126. Instruction manuals, FLI 3000, Photochemical Research Associates, London, Ontario, 1985.

127. A.E. McKinnon, A.G. Szabo and D.R. Miller, J. Phys. Chem. 81 (1977) 1564.

128. D.V. O'Connor, W.R. Ware and J.C. Andre, J. Phys. Chem. 83 (1979) 1333.

129. A. Grinvald and I.Z. Steinberg, Anal. Biochem. 59 (1974) 583.

130. N. Boens, H. Luo, M. Van der Auweraer, S. Reekmans, F.C. De Schryver and A. Malliaris, Chem. Phys. Lett. 146 (1988) 337.

131. S. Reekmans, N. Boens, M. Van der Auweraer, H. Luo, and F.C. De Schryver, Langmuir 5 (1989) 948.

132. M.H. Gehlen, N. Boens, F.C. De Schryver, M. Van der Auweraer and S. Reekmans, J. Phys. Chem. 96 (1992) 5592.

133. H. Luo, N. Boens, M. Van der Auweraer, F.C. De Schryver and A. Malliaris, J. Phys. Chem. 93 (1989) 3244.

134. W.R. Ware, in V. Ramamurthy, Ed., Photochemistry in Organized and Constrained Media, VCH Publishers, New York, 1991.

135. A. Siemiarczuk and W.R. Ware, Chem. Phys. Lett. 160 (1989) 285.

136. A. Siemiarczuk, W.R. Ware and Y.S. Liu, J. Phys. Chem. 97 (1993) 8082.

137. P.R. Bevington, Data Reduction and Error Analysis for the Physical Sciences, McGraw-Hill, New York, 1969.

138. A.J. Shusterman, P. G. McDougal and A. Glasfeld, J. Chem. Educ. 74 (1997) 1222.

139. H. Bouas-Laurent, personal communication.

140. H. Bouas-Laurent, J.-P. Desvergne, A. Castellan, J. Parrot, M. Webb and G. Bourgeois, Bull. Soc. Chim. France 3 (1987) 449.

141. H. Determann, Gel Chromatography, 2nd Ed. (E. Gross and J. M. Harkin, Trans.) Springer-Verlag, New York, 1969.

142. W.W. Yau, J.J. Kirkland and D.D. Bly, Modern Size Exclusion Liquid Chromatography, John Wiley & Sons, New York, 1979.

143. Gel Filtration Theory and Practice, Pharmacia Fine Chemicals, Rahms, Lund, Sweden, 1979.

144. T. Provder (Ed.), Size Exclusion Chromatography: Methodology and Characterization of Polymers and Related Materials, ACS Symp. Ser. 245, ACS, Washington, 1984.

145. H.G. Barth, in J.E. Glass (Ed.), Water Soluble Polymers: Beauty with Performance, Adv. Chem. Ser. 213, ACS, Washington, 1986, Chapter 2.

146. P.L. Dubin (Ed.), Aqueous Size-Exclusion Chromatography, Journal of Chromatography Library Vol. 40, Elsevier, Amsterdam, 1988.

147. M. Potschka and P.L. Dubin (Eds.), Strategies in Size Exclusion Chromatography, ACS Symp. Ser. 635, ACS, Washington, 1996.

148. J. Porath and P. Flodin, Nature 183 (1959) 1657.

149. J.C. Moore, J. Polym. Sci. A 2 (1964) 835.

150. H.G. Barth and F.E. Regnier, in T. Provder (Ed.), Size Exclusion Chromatography, ACS Symp. Ser. 245, ACS, Washington, 1984, Chapter 13.

151. G. Chauveteau, in J.E. Glass (Ed.), Water Soluble Polymers: Beauty with Performance, Adv. Chem. Ser. 213, ACS, Washington, 1986, Chapter 14, p. 230.

152. P. Munk, Introduction to Macromolecular Science, John Wiley & Sons, New York 1989, Chapter 3.

153. A. Rudin, The Elements of Polymer Science and Engineering, Academic Press, Orlando, 1982, Chapter 3.

154. H.R. Allcock and F.W. Lampe, Contemporary Polymer Chemistry, 2nd. Ed., Prentice-Hall, New Jersey, 1990, Chapter 15.

155. H. Benoit, Z. Grubisic, P. Rempp, D. Decker and J-G. Zilliox, J. Chim. Phys. 63 (1966) 1507.

156. Z. Grubisic, P. Rempp and H. Benoit, J. Polymer Sci. B 5 (1967) 753.

157. T.K. Korpela and J.-P. Himanen, in P.L. Dubin, Ed., Aqueous Size-Exclusion Chromatography, Journal of Chromatography Library Vol. 40, Elsevier, Amsterdam, 1988, Chapter 13.

158. K.S. Birdi, in P.L. Dubin, (Ed.), Aqueous Size-Exclusion Chromatography, Journal of Chromatography Library Vol. 40, Elsevier, Amsterdam, 1988, Chapter 15.

159. J.P. Hummel and W.J. Dreyer, Biochim. Biophys. Acta. 63 (1962) 530.

160. T. Sasaki, K. Kushima, K. Matsuda and H. Suzuki, Bull. Chem. Soc. Jpn. 53 (1980) 1864.

161. W.A. Wan-Badhi, W.M.Z. Wan-Yunus, D.M. Bloor, D.G. Hall and E. Wyn-Jones, J. Chem. Soc. Faraday Trans. 89 (1993) 2737.

162. D.M. Bloor, W.M.Z. Wan-Yunus, W.A. Wan-Badhi, Y. Li, J.F. Holzwarth, and E. Wyn-Jones, Langmuir 11 (1995) 3395.

163. V. Szmerekova, P. Kralik, and D. Berek, J. Chromatogr. 285 (1984) 188.

164. K. Veggeland and T. Austad, Colloids Surfaces A 76 (1993) 73.

165. K. Veggeland and S. Nilsson, Langmuir 11 (1995) 1885.

166. K. Taugbøl, T.van Ly and T. Austad, Colloids Surfaces A 103 (1995) 83.

167. T. Provder, H.G. Barth and M.W. Urban (Eds.), Chromatographic Characterization of Polymers: Hyphenated and Multidimensional Techniques, Adv. Chem. Ser. 247, ACS, Washington, 1995.

168. P. Schiebener, J. Straub, J.M.H. Levelt Sengers and J.S. Gallagher, J. Phys. Chem. Ref. Data 19 (1990) 677.

169. J. Brandrup and E. Immergut (Eds.), Polymer Handbook, 3rd. Ed., John Wiley & Sons, New York 1989.

170. L. Hagel, Anal. Chem. 50 (1978) 569.

171. P.J. Wyatt, Anal. Chim. Acta 272 (1993) 1.

172. Optilab DSP Interferometric Refractometer Hardware Manual, Wyatt Technology Corporation, Santa Barbara CA, 1995.

173. P.J. Wyatt, J. Liq. Chrom. 14 (1991) 2351.

174. Astra For Windows 4.2 Software Manual, Wyatt Technology Corporation, Santa Barbara CA, 1996.

175. B.H. Zimm, J. Chem. Phys. 16 (1948) 1093.

176. B.H. Zimm, J. Chem. Phys. 16 (1948) 1099.

177. P. Debye, J. Phys. Colloid Chem. 51 (1947) 18.

178. W.H. Stockmayer, L.D. Moore Jr., M. Fixman and B.N. Epstein, J. Polym. Sci. 16 (1955) 517.

179. H. B. Bull and H. Neurath, J. Biol. Chem. 118 (1937) 163.

180. T. Isemura and Y. Kimura, J. Polymer Sci. 16 (1955) 92.

181. I. Blei, J. Colloid Sci. 14 (1959) 358.

182. I. Blei, J. Colloid Sci. 15 (1960) 370.

183. M.J. Schwuger, J. Colloid Interface Sci. 43 (1973) 491.

184. N.M. van Os, J.R. Haak and L.A.M. Rupert, Physico-Chemical Properties of Selected Anionic, Cationic and Nonionic Surfactants, Elsevier, Amsterdam, 1993, 27-32.

185. K. Shirahama, Colloid & Polymer Sci. 252 (1974) 978.

186. M.L. Smith and N. Muller, J. Colloid Interf. Sci. 52 (1975) 507.

187. T. Gilányi and E. Wolfram, Colloids & Surfaces 3 (1981) 181.

188. R. Zana, J. Lang and P. Lianos, Polym. Prepr. (Amer. Chem. Soc., Div. Polym. Chem.), 23 (1982) 39.

189. R. Zana, J. Lang and P. Lianos, in P.L. Dubin (Ed.), Microdomains in Polymer Solutions, Plenum Press, New York 1985, 357.

190. R. Zana, P. Lianos and J. Lang, J. Phys. Chem. 89 (1985) 41.

191 E.A. Lissi and E. Abuin, J. Colloid Interface Sci. 105 (1985) 1.

192. W. Binana-Limbele and R. Zana, Colloids & Surfaces 21 (1986) 483.

193. F.M. Witte and J.B.F.N. Engberts, Colloids & Surfaces 36 (1989) 417.

194. F. Tokiwa and K. Tsuji, Bull. Chem. Soc. Jpn. 46 (1973) 2684.

195. N. Kamenka, I. Burgaud, C. Treiner and R. Zana, Langmuir 10 (1994) 3455.

196. G. Olofsson and G. Wang, Pure Appl. Chem. 66 (1994) 527.

197. K. Ballerat-Busserolles, G. Roux-Desgranges and A.H. Roux, Langmuir 13 (1997) 1946.

198. M. Murata and H. Arai, J. Colloid Interface Sci. 44 (1973) 475.

199. K. Kale, G.C. Kresheck and J. Erman, in K.L. Mittal and E.J. Fendler (Eds.), Solution Behavior of Surfactants, Plenum, New York, 1982, 665.

200. M.L. Fishman and F.R. Eirich, J. Phys. Chem. 75 (1971) 3135.

201. D.P. Norwood, E. Minatti and W.F. Reed, Macromolecules 31 (1998) 2957.

202. S. Saito, J. Colloid Sci. 15 (1960) 283.

203. E. Ruckenstein, G. Huber and H. Hoffmann, Langmuir 3 (1987) 382.

204. C. Maltesh and P. Somasundaran, J. Colloid Interface Sci. 154 (1993) 14.

205. G.N. Arkhipovich, S.A. Dubrovskii, K.S. Kazanskii, N.V. Ptitsina and A.N. Shupik, Eur. Polym. J. 18 (1982) 569.

206. R.C. Weast, Ed., Handbook of Chemistry and Physics, 50th Ed., CRC, Cleveland, 1969, C-194.

207. B.N. Jewett, M.Sc. Thesis, Department of Chemistry, Dalhousie University 1997.

208. B.N. Jewett, L. Ramaley and J.C.T. Kwak, J. Am. Soc. Mass Spectrom., submitted.

209. P. Lianos and R. Zana, J. Colloid Interface Sci. 84 (1981) 100.

210. G.G. Warr, F. Grieser and D.F. Evans, J. Chem. Soc., Faraday Trans. 1 82 (1986) 1829.

211. M. Almgren and S. Swarup, J. Colloid Interface Sci. 91 (1983) 256.

212. Y. Croonen, E. Geladé, M. Van der Zegal, M. Van der Auweraer, H. Vandendriessche, F.C. De Schryver and M. Almgren, J. Phys. Chem. 87 (1983) 1426.

213. M. Almgren, P. Hansson, E. Mukhtar and J. van Stam, Langmuir 8 (1992) 2405.

214. N. Nishikido, M. Shinozaki, G. Sugihara, M. Tanaka and S. Kaneshina, J. Colloid Interface Sci. 74 (1980) 474.

215. Y.C. Chiu and Y.W. Lin, Colloids Surfaces A 106 (1996) 23.

216. H.B. Klevens, J. Phys. Colloid Chem. 52 (1948) 130.

217. P. Rempp, J. Chim. Phys. 54 (1957) 421.

218. F. Candau, J. François and H. Benoit, Polymer 15 (1974) 626.

219. J.R. Cann and N.D. Hinman, Biochemistry 15 (1976) 4614.

220. T.K. Korpela and J.-P. Himanen, J. Chromatogr. 290 (1984) 351.

221. B. Stenlund, Adv. Chromatogr. 14 (1976) 37.

222. P.A. Neddermeyer and L.B. Rogers, Anal. Chem. 40 (1968) 755.

223. D.W. Armstrong, J. Chromatogr. 122 (1976) 17.

224. D.W. Armstrong and F. Nome, Anal. Chem. 53 (1981) 1662.

225. J.P. Foley, Anal. Chim. Acta 231 (1990) 237.

226. P. Mukerjee, J. Phys. Chem. 66 (1962) 1733.

227. D.G. Marangoni, A.P. Rodenhiser, J.M. Thomas and J.C.T. Kwak, Langmuir 9 (1993) 438.

228. D.G. Herries, W. Bishop and F.M. Richards, J. Phys. Chem. 68 (1964) 1842.

229. K. Hayakawa, J.P. Santerre and J.C.T. Kwak, Macromolecules 16 (1983) 1642.

230. S. Ranganathan, M.Sc. Thesis, Dalhousie University, Halifax 1994.

231. K. Hayakawa and J.C.T. Kwak, J. Phys. Chem. 86 (1982) 3866.

232. T. Shimizu, M. Seki and J.C.T. Kwak, Colloids Surfaces 20 (1986) 289.

233. P. Hansson and M. Almgren, Langmuir 10 (1994) 2115.

234. P. Hansson and M. Almgren, J. Phys. Chem. 99 (1995) 16684.

235. K. Hayakawa and J.C.T. Kwak, in D.N. Rubingh and P.M. Holland, Eds., Cationic Surfactants: Physical Chemistry, Surfactant Science Series Vol. 37, Marcel Dekker, New York, 1991, Chapter 5.

236. I. Satake and J.T. Yang, Biopolymers 15 (1976) 2263.

237. P. Ilekti, L. Piculell, F. Tournilhac and B. Cabane, J. Phys. Chem. B 102 (1998) 344.

238. K. Thalberg, B. Lindman and K. Bergfeldt, Langmuir 7 (1991) 2893.

239. P. Hansson, Langmuir 14 (1998) 4059.

240. M. Antonietti and J. Conrad, Angew. Chem. Int. Ed. Engl. 33 (1994) 1869.

241. E.B. Abuin and J.C. Scaiano, J. Am. Chem. Soc. 106 (1984) 6274.

242. D.-Y. Chu and J.K. Thomas, J. Am. Chem. Soc. 108 (1986) 6270.

243. S. de Fátima Santos, F. Nome, D. Zanette and W.F. Reed, J. Colloid Interface Sci. 164 (1994) 260.

244. K. Thalberg, J. van Stam, C. Lindblad, M. Almgren and B. Lindman, J. Phys. Chem. 95 (1991) 8975.

245. P. Hansson and M. Almgren, J. Phys. Chem. 99 (1995) 16694.

246. P. Hansson and M. Almgren, J. Phys. Chem. 100 (1996) 9038.

247. P. Chandar, P. Somasundaran and N.J. Turro, Macromolecules 21 (1988) 950.

248. J.J. Kiefer, P. Somasundaran and K.P. Ananthapadmanabhan, in I. Noda and D.N. Rubingh, Eds., Polymer Solutions, Blends, and Interfaces, Elsevier, Amsterdam 1992, 423.

249. L.-S. Choi and O.-K. Kim, Langmuir 10 (1994) 57.

250. V.A. De Oliveira, M.J. Tiera and M.G. Neumann, Langmuir 12 (1996) 607.

251. J. Fundin, P. Hansson, W. Brown and I. Lidegran, Macromolecules 30 (1997) 1118.

252. A. Malovikova, K. Hayakawa and J.C.T. Kwak, in M.J. Rosen, Ed., Structure / Performance Relationships in Surfactants, ACS Symp. Ser. 253, 1984, Chapter 15.

253. K. Hayakawa, A.L. Ayub and J.C.T. Kwak, Colloids Surfaces 4 (1982) 389.

254. J.H. Clint, J. Chem. Soc. Faraday Trans. I 71 (1975) 1327.

255. D.G. Marangoni and J.C.T. Kwak, Langmuir 7 (1991) 2083.

256. M.Tachiya, in G.R. Freeman, Ed., Kinetics of Nonhomogeneous Processes, John Wiley & Sons, New York, 1987, Chapter 11.

257. M. Almgren, in M. Grätzel and K. Kalyanasundaram, Eds., Kinetics and Catalysis in Microheterogeneous Systems, Surfactant Science Series Vol. 38, Marcel Dekker, New York, 1991, Chapter 4.

258. M. Almgren, Adv. Colloid Interface Sci. 41 (1992) 9.

259. J.-L. Hsu and U.P. Strauss, J. Phys. Chem. 91 (1987) 6238.

260. A. Malliaris, J. Lang, J. Sturm and R. Zana, J. Phys. Chem. 91 (1987) 1475.

261. G.G. Warr and F. Grieser, J. Chem. Soc. Faraday Trans. I, 82 (1986) 1813.

262. E.W. Anacker, R.M. Rush and J.S. Johnson, J. Phys. Chem. 68 (1964) 81.

263. E. Roelants and F.C. De Schryver, Langmuir 3 (1987) 209.

264. J. Liu, N. Takisawa and K. Shirahama, J. Phys. Chem. B 102 (1998) 6696.

265. J.J. Effing, I.J. McLennan, N.M. van Os and J.C.T. Kwak, J. Phys. Chem. 98 (1994) 12397.

266. J.E. Glass, Ed., Polymers in Aqueous Media: Performance Through Association, Adv. in Chem. Ser. 223, ACS, Washington 1989.

267. D. Hunkeler, X.Y. Wu and A. Hamielec, Polym. Prepr. 34 (1993) 1071.

268. P.L. Dubin and U.P. Strauss, J. Phys. Chem. 74 (1970) 2842.

269. C. Howley, D.G. Marangoni and J.C.T. Kwak, Colloid Polym. Sci. 275 (1997) 760.

270. Y. Wang, B. Han, H. Yan and J.C.T. Kwak, Langmuir 13 (1997) 3119.

271. J. Brandrup and E.H. Immergut, Eds., Polymer Handbook, 2nd. Ed., Wiley-Interscience, New York, 1975, p. IV-280.

272. D.G. Marangoni, A.P. Rodenhiser, J.M. Thomas and J.C.T. Kwak, in P.M. Holland and D.M. Rubingh, Eds., Mixed Surfactant Systems, ACS Symp. Ser. 501, ACS, Washington, 1992, p. 194.

273. J.C. Giddings, Unified Separation Science, Wiley-Interscience, New York, 1991, Ch. 4.